Loughborough University

This item was submitted to Loughborough's Institutional Repository (https://dspace.lboro.ac.uk/) by the author and is made available under the following Creative Commons Licence conditions.

creative commons

COMMONS DEED

Attribution-NonCommercial-NoDerivs 2.5

You are free:

- to copy, distribute, display, and perform the work

Under the following conditions:

Attribution. You must attribute the work in the manner specified by the author or licensor.

Noncommercial. You may not use this work for commercial purposes.

No Derivative Works. You may not alter, transform, or build upon this work.

- For any reuse or distribution, you must make clear to others the license terms of this work.
- Any of these conditions can be waived if you get permission from the copyright holder.

Your fair use and other rights are in no way affected by the above.

This is a human-readable summary of the Legal Code (the full license).

Disclaimer

For the full text of this licence, please go to:
http://creativecommons.org/licenses/by-nc-nd/2.5/

Architecture and Control of Large Power Networks with Distributed Generation

by

W.G Garlick

A DOCTORAL THESIS SUBMITTED IN PARTIAL FULFILMENT

OF THE REQUIREMENTS FOR THE AWARD OF

DOCTOR OF PHILOSOPHY

OF LOUGHBOROUGH UNIVERSITY

23 March 2009

©2009 William George Garlick

Abstract

The architecture of the UK's passive power network has taken over one hundred years to evolve through a process of demand and technology led development. In the early years of electrical power, distribution systems were islands of distributed generation, often of different voltages and frequencies. Increasing demand for electrical power and the need to reduce distribution costs eventually led to the standardisation of frequency and voltages and to the connection of the island systems into a large network. Today's power networks are characterised by their rigid hierarchical structure and unidirectional power flows.

The threat of climate change is driving the demand for the use of more renewable energy. For electricity production, this is achieved through generation using more wind, biomass, tidal and solar energy. This type of generation is often referred to as "Distributed Generation" (DG) because it is not a centralised facility connected to the high voltage transmission grid but a distributed source connected to the lower voltage distribution network. The connection of DG to the distribution network significantly alters the power flow throughout the network, and costly network reinforcement is often necessary. The advancement in the control of electrical power has largely been facilitated by the development of semiconductor power electronic devices and has led to the application of "Flexible Alternating Current Transmission Systems (FACTS), which include such devices as "Static Var Compensators" (SVC) and Static Compensators (STATCOM), for the control of network voltages and power flows.

Providing a secure power network is a demanding task, but as network complexity is expected to grow with the connection of high levels of DG, so the problem of integration, not just connection, of each successive generator becomes more protracted. A fundamental change to the network architecture may eventually become necessary, and a new, more active network architecture, perhaps based on power cells containing local generation, energy storage and loads, has been proposed by some researchers.

The results of an historic review of the growth of power networks, largely in the UK, forms the basis of a case to replace the conventional power transformer with an Active Transformer that will provide a more controllable, flexible and robust DG connection and

will facilitate greater network management and business opportunities, and new power flow control features.

The Active Transformer design is based on an a.c. link system and an a.c.-a.c. high-frequency direct resonant converter. This thesis describes a model of the converter, built in MATLAB and Simulink®, and used to explore control of the converters. The converter model was then used to construct a model of the Active Transformer, consisting of a resonant, supply-side converter, a high frequency transformer and a resonant, load-side converter. This was then used to demonstrate control of bi-directional power flow and power factor control at the Grid and Distribution Network connections.

Issues of robustness and sensitivity to parameter change are discussed, both for the uncompensated and compensated converters used in the Active Transformer. The application of robust $\mathscr{H}_\infty$ control scheme proposed and compared to a current PI control scheme to prove its efficacy.

Untitled

Born of a million yesterdays
was I, wise man, and you,
gleanings from time's unnamed byways
humbling, wise man, but true.

And all that's left of yesterday
to me, wise man, and you
just images, how stored away
I ask, wise man, you too?

Those bubbles snatched from yesterday
are mine, wise man, and yours
until they burst, then who's to say
what kills, wise man, or cures?

True wealth we gleaned from yesterday
if mine, wise man, or thine,
illumination's brightest ray
in us, wise man, will shine.

Festus Pragnell (of West Tytherley, 1879 –1966)

Table of Contents

Acknowledgements

At the end of my career in Electrical Engineering, I have had a rare opportunity and privilege to undertake a research project that combined two subjects of special interest to me, power and control engineering. For this opportunity I very grateful and have many people to thank.

Professor Glyn James, now Emeritus Professor in Mathematics at Coventry University, first lifted the veil on the mathematics of control systems during my M.Sc. studies and kindled the idea that if life and opportunity permitted, someday I would like to return to University to further my M.Sc. studies. I would like to express my special gratitude to Professor Roger Goodall, Loughborough University, whose practical, sound engineering approach to classical design and application of control systems inspired me many years ago whilst I was working in industry and has continued to do so ever since. Without his help my project would not have been possible. My grateful thanks I give to Derek Grieve, Technical Director Converteam, a colleague and a friend for many years, for his keen and long support of industrial research, and who with EPSRC has financially supported my research project for three years. My supervisors, Dr Argyrios Zolotas and Professor David Infield made me feel very welcome at Loughborough. Their guidance and encouragement has ably supported me, and kept me smiling every day of three of the most enjoyable years of my career.

I give my grateful thanks to my parents for their belief in the importance of good education and training and for their never ending encouragement to succeed.

There is however, one person who has stood beside me, loved and supported me throughout all the years that I have studied electrical engineering subjects, both in the early years as a junior engineer and more recently as a research student, my wife Shirley. Words can not really express the gratitude that I feel, but thank you Shirley for the wonderful opportunity and experience that you have given me to indulge myself in research. It has been a tremendously enriching and rewarding experience and I hope that someday I will be able to give you a similar opportunity.

List of Tables

List of Figures

Glossary and Acronyms

Abbreviations and units are in accordance with "*Units and Symbols for Electrical Electronic Engineering*", An IEE Guide, June 1997.

$\triangleq$	Equal by definition
$\overset{s}{=}$	transfer function with state space realisation
µ	micro
abc-dq0	d-q Transform
a.c.	alternating current
B.E.S.A	British Engineering Standards Association
BEA	British Electricity Authority
C	Capacitance
CNA	CASE for New Academics
CASE	Co-operative Awards in Science and Engineering
CEB	Central Electricity Board
CEGB	Central Electricity Generating Board
CHP	Combined Heat and Power
d.c.	direct current
DFIG	Doubly-Fed Induction Generator
DG	Distributed Generation
DGCG	Distributed Generation Co-ordination Group
DMS	Distribution Management System
d-q	direct-quadrature
DSO	Distribution System Operator
DTI	Department of Trade and Industry
e	the base of natural logarithms
EC	European Commission
EPSRC	Engineering and Physical Sciences Research Council
ETH	Swiss Federal Institute of Technology
EU	European Union
F	Farad
FACTS	Flexible a.c. Transmission System
FSIG	Fixed Speed Induction Generator
G(s)	Open loop transfer function
GTO	Gate turn-off thyristor

GWh	Gigawatt hour
H	Henry
$\mathcal{H}_\infty$	the "Hardy space" set of transfer functions with bounded ∞-norm or the set of stable and proper transfer functions.
HVDC	High Voltage Direct Current
Hz	Hertz
I_A, I_B, I_C	3-phase line or phase currents
I_d, I_q, I_0	I_A, I_B, I_C transformed by the abc-dq0 Transform
Iff	if and only if
I.E.E.	Institution of Electrical Engineers
IGBT	Insulated Gate Bipolar Transistor
ITAE	Integral of time multiplied by absolute error
K	constant
K_a, K_b, K_c	constant coefficients representing the fraction of the input voltage appearing at the output of the converter
kV	kilovolt
kW	kilowatt
L	Inductance
Ls	Series line inductance
MVA	Mega Volt Amps
MW	Megawatt
Ofgem	Office of Gas and Electricity Markets
ol	open loop
OLTC	On-LoadTap Changer
P	Real Power
PI	Proportional Integral
PWM	Pulse Width Modulation
Q	Reactive power
R	Resistance
R&D	Research and Development
RES	Renewable Energy System
R_L	Load resistance
RTD	Research and Technological Development
s	Laplace transform
S_p^T	System sensitivity function
S_a, S_b, S_c	coefficients representing the switching functions in a three-phase bridge
SCADA	Supervisory Control And Data Acquisition
S_d, S_q, S_0	S_a, S_b, S_c transformed by the abc-dq0 Transform

SiC	Silicon carbide
SISO	Single input single output
SSS	Solid State Substation
SST	Solid State Transformer
STATCOM	Static Compensator
SV	Space vector
SVC	Static VAr Compensator
SVM	Space Vector Modulation
$T_{(s)}$	Closed loop transfer function
TSO	Transmission System Operator
UK	United Kingdom
UMIST	University of Manchester Institute of Science and Technology
V^*_{tank}	nominal value of V_{tank}
VAr	Volt-Amperes reactive
$V_A\ V_B\ V_C$	Phase voltages in a 3-phase system
$V_{AN}\ V_{BN}\ V_{CN}$	Line-neutral voltages in a 3-phase system
$V_d\ V_q\ V_0$	V_A, V_B, V_C transformed by the abc-dq0 Transform
VSC	Voltage Source Converter
V_{tank}	Voltage across a resonant circuit
V_{tank_avg}	Average voltage across a resonant circuit
WS	Work stream
δ	damping factor
ΔI_i	Change in line currents, where i=A,B,C
ΔV_{tank}	Change in V_{tank}
ΔV_{tank_avg}	Change in V_{tank_avg}
ω	angular frequency
Ω	Ohms
ω_0	Resonant angular frequency of the supply voltage
ω_r	Resonant angular frequency of the tank circuit

Other symbols and acronyms are defined as they appear.

Chapter 1.

Introduction

"The purpose of my research is not to change the world, but to understand it."

1.1. Project sponsorship

The "Architecture and Control of Large Power Networks with Distributed Generation" project was sponsored under the EPSRC scheme, Co-operative Awards in Science and Engineering (CASE) for New Academics (CNA), grant reference CASE/CNA/04/63, and the industrial support was provided by Converteam Ltd., Rugby, formerly ALSTOM Power Conversion Limited. The CNA scheme provides a means for new academics to build links with an industrial organisation at an early stage in their career through co-supervision of a CASE student. In the case of this project, the collaborators shared a common interest in the:

i) effects on contemporary power networks of the introduction of large scale renewable energy generation
ii) development, architecture and control of power networks
iii) application and control of high power electronic systems.

1.2. Overview

1.2.1 Power networks

The architecture of the UK's power network has taken over one hundred years to evolve through a process of demand and technology led development. In the early years of electrical power, distribution systems were islands of distributed generation, often of different voltages and frequencies. Increasing demand for electrical power and the need to

reduce distribution costs eventually led to the standardisation of frequency and voltages and to the connection of the island systems into a large network.

Contemporary power networks are largely passive, with unidirectional power flow, and through much of their development have been centrally controlled. Global warming and the need to reduce carbon emissions are driving the power generation industry towards the use of more renewable energy and distributed generation and consequently, towards the need for a change of network architecture. Today, distributed generation is defined as an electric power source connected directly to the distribution network or to the customer side of the network [1].

With the increasing application of distributed generation, power networks, which are already large-scale, will evolve into even more complex systems. The transition to an intelligent network via an enhanced network architecture and control characterised by bi-directional power flow and power management, will become more necessary.

This research project has sought to define a potential means to control a future flexible network architecture, such as one based on a matrix of independent, asynchronous, power hubs or cells, that will improve operability and controllability of the whole network and facilitate the integration of future tranches of distributed generation.

In the past, the advancement in the control of electrical power has largely been facilitated by the development of semiconductor power electronic devices such as thyristors, Gate Turn-Off thyristors (GTOs), and Insulated-Gate Bipolar Transistors (IGBTs). Their ability to switch high voltages or currents has led to the design of converters and inverters that have been used in the design of Static VAR Compensators (SVCs), HVDC transmission systems, Static Compensators (STATCOMS) and other Flexible A.C. Transmission System (FACTS) apparatus. These systems have significantly improved the performance of modern power networks. Therefore, it is not unreasonable to assume that the development of intelligent or active networks will require greater control measures and that these will be based on power electronic devices and converters. The difficulty with today's semiconductor devices is that they are of limited voltage capability and must be

connected in large, series strings to achieve the high voltage operation needed for cost effective, direct connection to distribution and transmission systems.

1.3. Scope of research

1.3.1 Active Transformer

In the longer term, where a significant proportion of the UK's generation may be connected to distribution networks, there are important issues of power flow and stability of networks for national security of supply [2], and for sound technical reasons this cannot be achieved through piecemeal development [3] as has been demonstrated by the reports of dynamic stability problems in NE America in August 2003 [4] and operational difficulties in Denmark [5]. These issues highlight the need for greater control of power networks.

An Active Transformer is intended to replace a conventional power transformer, initially in a distribution network, in order to provide greater power management opportunities through additional robust control features. The use of fast acting current control will also limit network fault currents, thus reducing or postponing the need to upgrade circuit breaker capacity as power levels increase.

The Active Transformer will have fast acting current control that may also be configured to limit or interrupt network fault currents. Designed for 20 kHz operation, the power circuit components will be smaller than their equivalent 50 Hz design and will provide a smaller overall footprint than the conventional power transformer. The use of direct a.c. conversion will reduce the number power semiconductors required in each converter by half compared to an equivalent d.c. link design.

The Active Transformer is a novel concept and a simplified schematic diagram is shown in Figure 1. It is essentially a high-frequency, a.c. link converter system. The system consists of a grid-side converter, a high frequency transformer and a distribution-side converter. The converters are similar in design, current sourced, 50 Hz 3-phase resonant, direct converters. The grid converter is controlled as a 3-by-2 matrix converter, essentially

a 50 – 20 kHz frequency changer. The distribution-side converter operates as a 20 kHz -3-phase 50 Hz frequency changing converter. Input grid current and phase angle, grid-side converter output voltage (at 20 kHz) and distribution-side converter output current and phase angle are controlled. When controlling current flow from grid to distribution side, the grid converter current control determines which of the 8 possible converter switch configurations will produce current in the line inductors that is closest to the demanded value over the next half cycle of converter output. A voltage control loop is used to control the mean of the peak converter output voltage. Having a symmetrical design, the Active transformer is able to operate and control current in either direction.

The proposed application of the Active Transformer is as an interface between the supply Grid and a Distribution Network cell as a means of providing improved network management and control. In a future decentralised distributed power network an Active Transformer may also be used to control bi-directional power flow between a distribution power cell and another power cell, or a large wind farm. A future network of power cells will be characterised by high penetration levels of distributed generation, variable cell loads will be satisfied firstly, by the locally connected wind or other renewable energy generation, which is will be variable, and secondly, by power drawn from energy storage, the transmission grid or an adjacent network via the active transformer to automatically achieve a local balance between power supply and demand while maintaining cell voltages at supply standards. At times of excess power generation capacity in the cell, and rather than balancing the cell load/generation by generation curtailment, real and/or reactive power could be traded and exported via the active transformer. The Active Transformer may also provide a means of controlling and stabilising distribution network voltages and limiting, or isolating, fault currents in either direction should the need arise. An "islanded network" control capability may also be achieved although the distribution side converter would use a different method of control from the one described in this research. What ever the application, the key to the exploitation of the Active Transformer is its versatility and controllability.

A number of control approaches were investigated during this research and an effective control solution is demonstrated. Robust control techniques, such as $\mathscr{H}_\infty$ control via loop-

shaping (which effectively deal with system uncertainty of the load conditions) and multi-objective performance criteria [6][7], were applied.

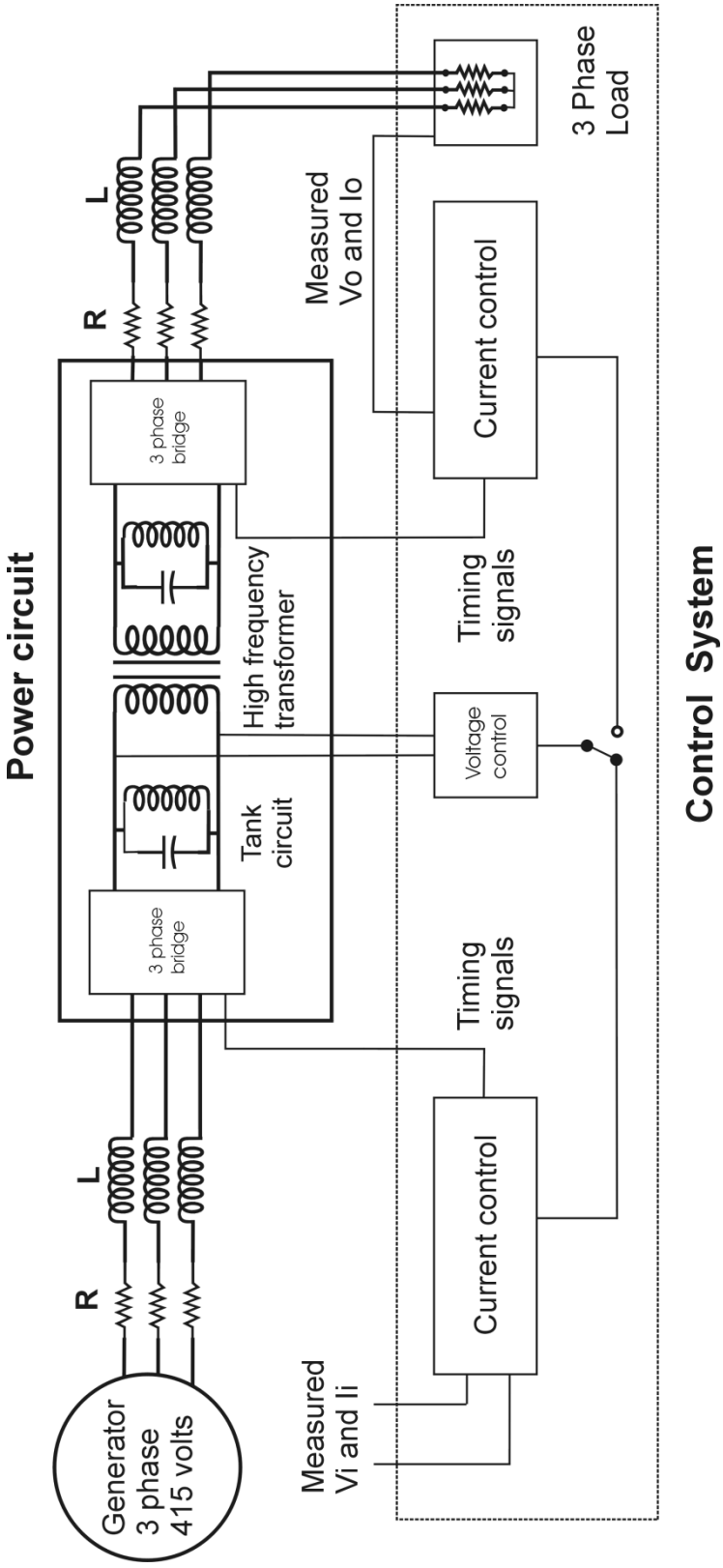

Figure 1 Active transformer schematic diagram

1.4. Project Scope and Aims

The research aims were to:

i) review the architecture of the UK power network and investigate changes that may result from the introduction of large amounts of distributed generation to make a case for an advanced power flow controller
ii) demonstrate, using simulation techniques, the key features of the Active Transformer that may replace, in a future decentralised network, the conventional, high-power 50 Hz transformers that are widely used throughout the UK's transmission and distribution systems
iii) apply modern techniques to the control of the Active Transformer to ensure robust and stable operation under network operating conditions
iv) Analyse rigorously of robustness of the current and proposed control schemes.

The many possible power flow control features of the Active Transformer may be used to enhance power system performance. The operation and control of the Active Transformer was investigated through modelling and simulation of the converters and the control system in order to verify its robustness and suitability for use in very large and complex power systems.

1.5. Work addressed in this thesis

1.5.1 General

The research described in this thesis reviewed the evolution of transmission and distribution networks from the late 19th century, and explained that the introduction of significant amounts of distributed generation may bring about a future fundamental change to power network architecture. Three options for change currently being researched were reviewed. Their potential application makes a case for the conventional power transformer to be replaced by an Active Transformer as part of an evolutionary process towards more active networks. The objective of the proposed change was to provide a more controllable,

flexible and robust interface that will facilitate greater network management and business opportunities, and new power flow control features.

The Active Transformer is based on high-frequency converter technology and an a.c. link. The research in this thesis takes a proven converter design, enhances its control with the use of modern robust techniques and uses it in a model of an Active Transformer. The model was then subjected to testing in a simulated network environment.

1.5.2 Thesis organisation

This thesis is laid out as follows:

i) Chapter 2 describes the background and motivations to the research and some of the subsequent developments and initiatives in the United Kingdom (UK).

ii) Chapter 3 is a brief historical review of power network development and a brief look at some of the current developments currently being researched. This review makes the case for a more controllable interface between transmission and distribution systems or between more localised power cells.

iii) Chapter 4 is a brief review of literature dealing with the control of converters.

iv) Chapter 5 focuses on a previously designed PI controller design and records additional analysis to highlight issues on its of robustness performance.

v) Chapter 6 develops a Simulink® model of a direct, high-frequency converter based on the work from Nottingham University as the basis for the design of a controller that uses modern robust control techniques. The results of simulations are compared with those from Nottingham to verify the clarity of the Simulink® model.

vi) Chapter 7 proposes an alternative controller design based on the $\mathcal{H}_\infty$ loop-shaping and a design procedure. It presents the results of simulations using the Nottingham University converter design.

vii) Chapter 8 contains a description of the Active Transformer model and presents the results of simulations including demand and load changes. A demonstration of power flow reversal and phase angle control are also shown.

viii) Chapter 9 contains conclusions and discussions on the overall thesis results, and suggests possible further work.

The following information is included in Appendices:

i) Appendix A The d-q Transform
ii) Appendix B Power system modelling
iii) Appendix C MATLAB® m-files
iv) Appendix D Derivation of converter state-space equations
v) Appendix E Simulink® converter model diagrams
vi) Appendix F Copies of published papers

1.6. List of published papers

i) W.G. Garlick, A.C. Zolotas, "Modelling of a direct converter with H_∞ voltage control," submitted to ICSE 2009 conference, Coventry, 8-10 September 2009.

ii) W. G. Garlick, A. C. Zolotas, D. Grieve, R. M. Goodall, "The Architecture and Control of Large Power Systems with Distributed Generation," CIGRE 2008 Session, Paris, 24 – 29 August 2008.

iii) W. G. Garlick, A. C. Zolotas, D Infield, "A novel architecture for power networks with distributed generation - concept outline," UKACC, Control 2006, paper 223, September 2006.

1.7. Thesis contributions

This thesis addresses a number of the issues concerning the application of power electronic converters in a future, active power network and makes contributions in the following areas:

i) the novel idea of replacing a conventional power transformer with an Active Transformer

ii) design, development and modelling of an H_∞ controller as an alternative to a classical PI controller used in a resonant converter

iii) a rigorous analysis of robustness issues and the use of uncertainty modelling to identify controller design limitations

iv) development of an Active Transformer model and simulations to demonstrate forward and reverse current flow and independent control of real and reactive power flows.

The work reported in [45] is the design and laboratory demonstration of a direct, current-sourced resonant converter that uses classical PI voltage control. However, research described in this thesis identifies stability problems with the converter at light loads and develops an alternative H_∞ controller to address stability at light loads. The revised converter/controller design is used in the design of an Active transformer that was intended to replace a conventional network power transformer. Modelling and simulations techniques are then employed to demonstrate its operation.

Chapter 2.

Background to research

"But, as I have said, things have changed, and they have not changed yet as much as they are going to change in the future. The question that we have to deal with must be considered in the light of what electricity will be ten, fifteen, or twenty years hence."[1]

2.1. Motivation

The European Council's (EC) Decision 2002/358/EC of 25 April 2002 [8] ratified the Kyoto Protocol to the United Nations Framework Convention on Climate Change and agreed to an overall 8% reduction of greenhouse gas emissions compared to 1990 levels by the year 2012. A target was also fixed for Member States of the European Union and that for the United Kingdom (UK) was 12.5%.

The Directive of the European Parliament and Council on the Promotion of Electricity Production from Renewable Energy Sources in the Internal Electricity Market [9] established targets for the increase in the generation of electricity from renewable energy sources (RES). The Directive stated that "the increased use of electricity produced from renewable energy sources constitutes an important part of the package of measures needed to comply with the Kyoto Protocol to the United Nations Framework Convention on Climate Change ...". The Directive required electricity generated from RES in the EU to rise from 14% in 1997 to 22% in 2010.

[1] *Mr S. Z. De Ferranti in his opening speech at an Extraordinary meeting of the I.E.E. held in association with the American Institute of Electrical Engineers held on 16 August 1900 at the US National pavilion in the Paris Exhibition.*

The European commission defined the need for R&D for Distributed Generation [10]:

> *"To pave the way to a sustainable energy future based on a large share of DG, there is a clear need to prepare the European electricity system for the large-scale integration of both renewable and other distributed energy sources. To this end research on the key technologies will allow a transition towards interconnected grids using common European planning and operational systems.*
>
> *The research will assist in removing barriers relating to finance, policies, technologies and technology standards and RTD actions aimed at the adaptation of technical grid infrastructures, the establishment of necessary institutions and the harmonisation of related regulatory frameworks and market conditions need to be undertaken.*
>
> *The challenges that need to be addressed to achieve a broad and sustainable future European energy service network can be summarised as: power reliability and quality; power system technologies; enabling technologies and the commercial and regulatory challenge."*

In the 2003 Energy White Paper [11], 'Our energy future – creating a low carbon economy', the UK government sets out it's policy on renewable energy and confirmed the EU target that, by 2010, 10 per cent of electricity should come from renewable sources. The paper also included the aspiration that, by 2020, 20% of the UK's electricity supply should be met by renewable energy.

Increased usage of renewable energy and technologies will contribute to greater diversity in energy supply. The increased importance attached to this form of energy production was highlighted by The Prime Minister, Tony Blair. In the White Paper, he stated:

> *"However, our energy system faces new challenges. Energy can no longer be thought of as a short-term domestic issue. Climate change - largely caused by burning fossil fuels - threatens major consequences in the UK and worldwide,*

most seriously for the poorest countries who are least able to cope. Our energy supplies will increasingly depend on imported gas and oil from Europe and beyond. At the same time, we need competitive markets to keep down costs and keep energy affordable for our businesses, industries, and households.

This white paper addresses those challenges. It gives a new direction for energy policy. We need urgent global action to tackle climate change. We are showing leadership by putting the UK on a path to a 60% reduction in its carbon dioxide emissions by 2050. And, because this country cannot solve this problem alone, we will work internationally to secure the major cuts in emissions that will be needed worldwide."

Figure 2 Kentish Flats wind farm under construction

2.2. United Kingdom developments and initiatives

Figure 2 shows an example of the UK Department of Trade and Industry (DTI)'s and The Crown Estate's first round of wind farm development at the Kentish Flats in the Thames

estuary where 30, 3 MW wind turbines were under construction and are now producing electrical power. As part of the UK's programme to further the development of renewable energy sources, in December 2003, the Department of Trade and Industry (DTI) and The Crown Estate announced the second round of 12 successful wind farm developers, who have been offered 15 site leases, with a potential generation capacity ranging from 64 to 1200 MW, the largest being further than 12 miles offshore. Existing power distribution networks were not designed to accept extensive distributed generation and added to their size and distance offshore, the proposed increase in generation presents new technical challenges for their connection to the power network. Often the closest connection will be at the end of a long and weak distribution cable and therefore fault levels and stability are significant reinforcement issues.

To focus attention on the issues surrounding the connection of distributed generation the DTI and the Office of Gas and Electricity Markets (Ofgem) created, and jointly chaired, the Distributed Generation Co-ordination Group (DGCG). The Group was concerned with a wide range of issues related to the connection and operation of distributed electricity generation in Great Britain, [2] and [12]. The issues included the consideration and making of recommendations as to any research and development action that may be helpful to achieving Government targets for the generation of electricity from renewable energy sources.

A key objective of DGCG Workstream 3 (WS3), was to establish how to facilitate the connection to the distribution networks of distributed generation, without driving reinforcement costs high and without impairing the quality of supply to load customers. The problems and the solutions that the group proposed were categorised in terms of managing fault levels, voltage levels and network power flows. Identification of STATCOMs and Active Network Voltage Control solutions were identified as long term solutions requiring significant additional research and development.

The integration of large wind farms into power networks will hold new challenges for Transmission and Distribution System Operators, (TSOs and DSOs). In the UK the responsibility for balancing the supply and demand of electrical power currently resides

with the TSO. With low levels of wind power penetration, a number of researchers have suggested that wind generation behaves more like negative load than generation and perhaps it should be treated accordingly in analysis. Power system engineers are used to dealing with an aggregate load that has a high degree of randomness and uncertainty so perhaps they may start to think about accepting the uncertainty of wind generation and continue to balance the net load [13].

Distribution systems generally have few or no control mechanisms, only protection mechanisms. So, with large amounts of distributed generation comes the need for more certainty in the control, meeting of statutory requirements for voltage limits and the despatch of distributed generation. Only when distributed generation can be "dispatched" will their benefits be fully realised.

In 2004, as part of DGCG Workstream 5 (WS5) Long-term network concepts and options, the DGCG asked the I.E.E. to investigate Technical Architecture options. The results of the I.E.E.'s investigation were presented in a report [14]. This report summarised the current status in the UK as:

> "*It has become abundantly clear that unless a common framework for future network design is adopted, the chance of being able to integrate in a cost efficient, safe and reliable way, many of the enabling technologies to allow future flexibility could be severely limited and, at worst, be excluded from the UK. This will not only damage our competitiveness as a country but will reduce our ability to take advantage of innovative solutions in the future."*

The report presented a vision that the current technical architecture would change from a centralised plant model to an "active network model". The term "active network" is taken to mean an enlarged distribution network containing integrated monitoring, control and communication systems. A number of projects were identified including: automation for active networks and future network scenarios, tools and methodologies.

This research project develops a novel active network solution that addresses directly the problems identified by DGCG Workstream outcomes.

2.3. Comparisons with a conventional power transformer

Conventional power transformers can exceed 1000MVA and weigh 100s of tonnes. They are used to transfer the incoming high voltage to the next voltage level, for example, an incoming high voltage of 400 kV would be transformed down to 220 kV. They are connected to the grids via high voltage bushings and cables. Power transformers are designed for operation at relatively low frequencies and therefore require a large soft iron core for high efficiency. The highest-voltage transformers are contained in large, insulating oil filled, steel tanks and have extensive monitoring and cooling systems. As a result of their construction, materials and the need for high-voltage insulation and isolation, power transformers are very large and heavy.

HV and LV windings are galvanically isolated. For high voltage windings at voltages greater 145 kV, paper insulated layer windings of transposed copper conductors are preferred. The low and high voltage windings are cylindrically wound to form a compact integrated system. The advantages of this type of construction are: high short circuit strength, compact dimensions, few conductor joints. The cylindrical windings are arranged concentrically and separated by axial oil ducts to improve cooling effectiveness.

In order to alter the voltage ratio to meet the requirements of the power system, the transformer may be fitted with a tapped winding. The voltage ratio can therefore be changed either by a no-load tap changer (NLTC) after switching off the transformer, or under load with an on-load tap changer (OLTC). Motor drives are used to operate the OLTC switches, which may be controlled locally or remotely at a control centre. No-load tap changers are normally set manually.

The type of cooling system most frequently used is natural cooling (ONAN). The heat loss is absorbed by the transformer oil and given off to the surrounding air via radiators. With ONAF cooling the radiators are additionally cooled by fans. The cooling system may also consist of separate radiator banks, or water coolers.

Types of cooling:

i) natural air cooling with radiators (ONAN)
ii) radiators additionally cooled by fans (ONAF)
iii) cooling by separate radiator banks
iv) water instead of air as cooling medium.

At this early stage of development, a practical Active Transformer has not be designed and therefore its physical characteristics are not known and can not be directly compared to those of a contemporary power transformer. However, some characteristics may be compared in a general way. Noting that, ideally, transformers are designed for the smallest size, highest efficiency and lowest cost, materials that produce low size designs invariably produce low efficiency and high cost designs. Whereas, a design with high efficiency is usually large and has a high cost.

The windings are likely to be cylindrical or toroidal but made from a low-loss high frequency conductor, such as Litz wire. Some design compromises will be necessary for operation at 20 kHz, but a smaller, less dense core material, such as amorphous iron or ferrite that is efficient at these frequencies will be a key design requirement. The core configuration may well be similar to conventional 50 Hz transformer designs to minimise stray field loss although a toroidal design, perhaps with an air core would eliminate saturation effects and reduce the transformer size. More novel solutions, such as planar or superconducting transformers, may also be feasible.

Power frequency transformers suffer a degradation or breakdown of their insulation systems when exposed to high frequency transient events such as lightning strikes or converter switching transients. The effects of high frequency operation will reduce the breakdown voltage of transformer mineral oil, for a gap of 4 mm, from 80 kV to 30 kV. Therefore, the insulation system of the Active Transformer will be designed to withstand the high operating frequency continuously with the use of improved dielectrics. The type of insulation used will be a balance between the thermal and electrical insulation designs. Encapsulating the windings in silicone rubber may be one solution that meets the electrical requirements but the cooling system design will be difficult using the conventional

methods above. Because of the likely difficulties in balancing cooling and insulation, a superconducting design has the advantage of direct cooling using liquid nitrogen that has good high frequency dielectric properties.

The overall effect of using a high frequency design, see Table 1, should lead to a smaller, lighter transformer that may enhance application options, but as with all power electronic applications, the cost will be a critical factor.

Table 1 Comparison of conventional and high-frequency transformers

Conventional 50 Hz power transformer		**High frequency power transformer**	
Advantages	Disadvantages	Advantages	Disadvantages
Simple construction	Very large and heavy transportation difficult	Small and light weight transportation easier	Complex construction
Established and proven design	Voltage transformation	No voltage transformation	Unproven design
Basic materials – copper & iron	Insulation – paper & oil	Potentially solid insulation	High frequency conductors
High efficiency	Saturation effects	No saturation effects if air-cored	Lower efficiency
Lower manufacturing cost	On-load tap changing	Fixed windings possibly cables	Higher cost likely

2.4. Application scenario

An example of a future distribution network application of the Active Transformer is shown in Figure 3. The key difference between the network shown and a contemporary distribution network is where and how generation and load are balanced. In a contemporary network, balancing is undertaken against an aggregated load at the large central generators. Future networks will be de-centralised and included high levels of distributed, renewable energy, generation, for example > 40% of the load, energy storage as well as convention loads. The balancing of generation and load may therefore be best undertaken locally to avoid excessive voltage variations using the control of power from local generators and energy storage. The presence of energy storage will facilitate the management and timing of power export as well as network support functions. The Active transformer provides the means by which a decentralised network may be managed.

In a conventional network, with high levels of distributed generation, excess generation in a network will cause a local variation in voltage. If the excess generation is sufficiently large to exceed the local load, the local voltage will increase to balance generation and load power by reverse power flow through the grid transformers. Current monitoring and protection systems, and indeed, the transformer tap changers, may well be defeated in this situation leading to costly network and equipment failure.

In a conventional substation of two in-feed transformers, the network protection and monitoring is usually designed for power flow in one direction only and the network would not be fully protected against continuous reverse powers. In the application scenario shown, the Active Transformer is connected in parallel with a conventional power transformer and is able to control the flow and direction of power flow through itself and hence, through the fixed transformer. Thus, in the case where the network load exceeds the local generation the network controller balances the power flow through the Active Transformer and the conventional transformer. When local generation exceeds the local load the power flow, the network management may choose to store or export power, or a combination of both in any ratio. In choosing to export power the flow through the Active Transformer would be reversed and adjusted to maintain the load-side voltage and power balanced. In each of these modes of operation, the impedance presented to the grid and distribution networks may be adjusted, thereby controlling active and reactive power independently, supporting the grid and the network in much the same manner as STATCOM.

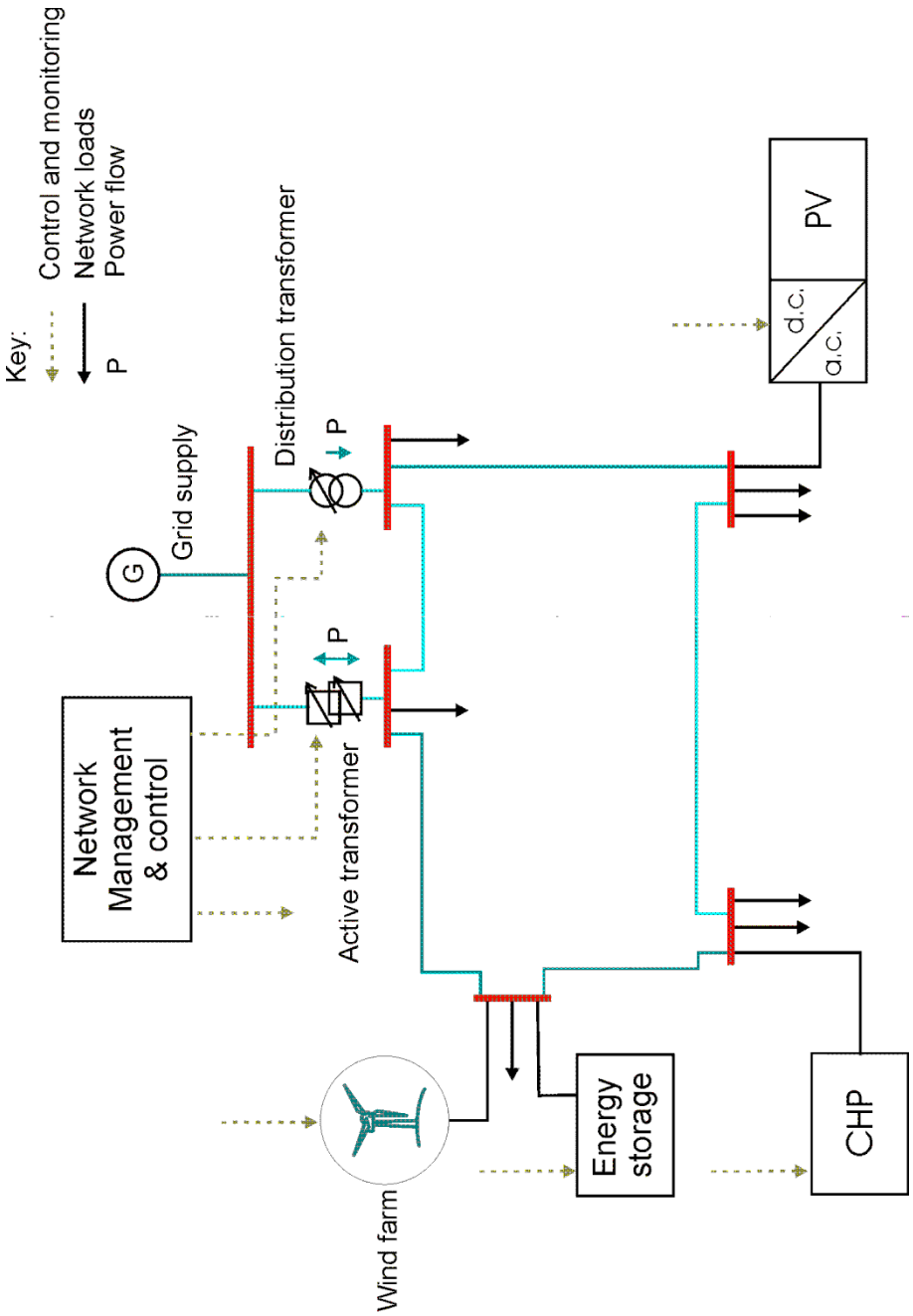

Figure 3 Example application network

Chapter 3.

Network Architecture

"What I am seeing today is the dream of my life realised. I don't know what electricity is, and cannot define it – I have spent my life on it – I do not know the limits of electricity but it will go far beyond anything we conceive today."[2]

3.1. Historical Review, 1880 - 1948

There are few comprehensive studies of the development of the British Electrical Network but "Electricity before Nationalisation: A study of the Development of the Electricity Supply Industry in Britain to 1948" [15] by Leslie Hannah is essential reading. The study was commissioned by the Electricity Council of Great Britain, which gave the author free access to a considerable collection of documentation. Hannah's study does not focus on a technical history, but more on the central policy-making relevant to the development of the national network. However, the work does describe the changing nature of electricity supply network, from one with numerous inefficient stand-alone systems with no standards to larger, more integrated networks where control was divided between private companies and municipal authorities by legislation. Hannah thus gives a good overview of the network development and the processes of change that are important in understanding the network that we have today and how it may change in the future. What became clear very quickly was that the change process was led by consumer demand for electricity; technical innovation and development often lagged behind the demand for more power. A change process that is not unfamiliar today.

[2] *Lord Kelvin – from his speech on the opening of Neptune Bank Power Station on Tyneside in 1901.*

The Institution of Electrical Engineers (I.E.E.) was founded in 1871 and incorporated in 1883. The Journals of the I.E.E. provide a rich source of history of the UK's electrical network. Not only do they provide insights into technical developments but also record, sometimes at great length, transcripts of presentations made to I.E.E. meetings and transcripts of subsequent discussions. For example, Volume XIX No. 88 1890, contains the text of a paper, "The treatment, regulation, and control of electricity supply by the Legislature and the Board of Trade [16]" read by Major P. Cardew. Cardew compared the requirements of the first legislative action, The Electricity Act 1882, and the Amending Act 1888. Although the author advised that "the scientific interest of the paper is very small", it did highlight safety and modes of supply issues, e.g. parallel and series systems and the use of overhead wires, which were significant issues in the development of the early distribution systems. Legislation also laid down the first standards of supply declaring that:

"pressure at the consumer's terminals, which is not to vary more than 4 percent each way from the mean or a total variation of 8 percent, and the variation of which may be tested for the consumer on his application by the electrical inspector".

This requirement may be compared to today's standard of ±6%. Many of the major technical problems of the day were discussed at I.E.E. meetings. For example, an extraordinary meeting of the I.E.E. was held in association with the American Institute of Electrical Engineers on 16 August 1900 in the US National Pavilion at the Paris Exhibition [17]. This was a grand setting for a discussion on the relative advantages of alternating and continuous current for a general supply of electricity. The meeting underlined the fact that the technology of the electrical supply apparatus was international, but that the supply systems were designed to meet national and even local requirements. The meeting also focused of the interference effects of electricity, electrolysis, and the damage caused to traction and telephone cables. However, during the meeting Sir William Preece raised the topic of standardisation of frequency and gave examples in the UK of 50 Hz, 67 Hz, and in the City of London, 97-100 Hz, but, regrettably, little debate was recorded.

The invention of the incandescent lamp by Joseph Swan in 1878 initiated a luxury market in electrical lighting powered by generators installed in individual premises. On 18 December 1878 Swan demonstrated his incandescent electric light bulb to an audience at the Newcastle Chemical Society. Unfortunately, it burned out after only a few minutes. On 19 January 1879, the incandescent electric light bulb once again successfully demonstrated during a lecture to an audience at the Athenaeum in Sunderland. His invention quickly led to a demand for lighting to be supplied from public supply mains in order to minimise the cost of installing generators on individual properties. Electrical power networks began their development to meet a growing commercial need for electrical power in the later quarter of the 1800s. The demand was small by today's standard, 1-2 GWh [18] and in competition with the gas supply industry. The network architecture was simple; power flowed from a generator to a distributed load. The early years from 1881 to 1920 are characterised by small-scale, local generation and a sense of pioneering as the boundaries of scientific and technical knowledge were being expanded.

The first public electricity supply system was introduced in 1881 at Godalming. It was used for street lighting and used water-wheel hydropower from the river Wey [19]. The Electric Lighting Act 1882 enabled the Government to grant licences to municipalities, companies or persons to install electricity supply systems and, importantly to dig up streets in order to bury cables. Previously, the cables for some distribution systems had been laid in gutters! It also empowered local authorities to buy any supply company's system at "written-down" values after 21 years. This was a sure way to dampen investment. During the next few years proposed developments using overhead cables were often blocked by municipalities in order to protect their own gas supply industry. Fortunately however, the barriers to development were reduced by the Electric Lighting Act 1888 that allowed the Board of Trade to overrule objections and grant licenses to independent electricity supply companies and extend take-over periods from 21 to 42 years.

By the late 1880s most of the electricity supply development had led to d.c. systems with a wide range of voltages and only a few a.c. systems with frequencies varying from 25 to 100 Hz. The challenge then was, not as it is now, to seek economies of scale by using larger generators and creating larger networks. Sebastion de Ferranti's plan for a large

electricity supply system for London was ambitious. It used 10 kV transmission at 83.5 Hz over a distance of 11 km to central London loads. In 1889, the first generating station had 4 small generators and two new 2 MW 10 kV generators. Unfortunately, the 10 kV cables proved to be unreliable, which delayed the project and allowed other companies to meet the demand. 25 Hz supplies became the standard for industrial motors and for conversion to d.c. but, to avoid problems of flicker, lighting supplies were of higher frequencies, often 100 Hz, which made them unsuitable for higher power industrial applications. In 1899 Charles Mertz, aided by William McLellan and R.P. Sloan, designed the Neptune Bank power station and adopted the 3-phase distribution system established by Westinghouse in the USA, to facilitate the use of higher voltages for industrial motors and lower voltages for domestic lighting. Metz compromised on the supply frequency and chose 40 Hz and 6.6 kV, meeting both power and lighting demands, and this became the standard frequency in the North East coast area. With the addition of further power stations of a similar design and a rapidly expanding customer base, the north east of the UK pioneered a unique integrated regional power network and soon began to show the benefits of large-scale interconnected operation [15].

The Electricity Lighting Act 1909 authorised two or more municipalities to set up joint boards to create larger systems. Progress of interconnecting local supply schemes was slow, with the exception of the Newcastle Electricity Supply Company who by the technical ingenuity and imagination of Merz and McLellan, expanded their network from 16 km^2 to 3600 km^2 by 1914 and in so doing created the largest interconnected power system in Europe. Changes in the rest of the UK followed more slowly with some linking of small-scale systems, often along non-standard lines, to achieve some of the economies offered by Merz and McLellan networks. But it wasn't until the onset of war in 1914 that the efficacy of the act really became clear: inefficient small generating plants were not affordable and the lead set by Merz and McLellan had indeed been the right one. With interconnection came the opportunity for greater operational control of power from multiple generators, which improved availability, but made the protection and control requirements more complex. Thus the interconnection of power systems produced

vertically integrated networks and unidirectional power flow. The passive network was born.

By 1920 the transmission of electrical power by overhead line was rare except in parts of the North East of the UK as a result of difficulties in obtaining wayleaves and objections based on aesthetic and environmental grounds. Overhead lines were substantially cheaper to install than underground cables and their use often meant the difference between a successful and an unsuccessful network. Following the Electricity Act 1919, an increasing number of high voltage transmission lines were approved at voltages ranging from 6.6 kV to 66 kV. The question of standard voltages and frequency across the whole country was again raised in an I.E.E. paper, "Electrical Standardisation, 1926" [20], in a year when the British Engineering Standards Association (B.E.S.A.) issued many British Electrical Standards for electrical equipment and apparatus.

A major advance in the integration of power systems came with the Electricity (Supply) Act 1926 that established the Central Electricity Board (CEB) with a duty to:

i) concentrate generation in "selected" stations
ii) interconnect existing regional systems into a national "Grid" by building a high voltage transmission network
iii) standardise frequency throughout the country
iv) supply local distributors from the selected stations.

This was the birth of today's network architecture. The CEB started work in 1927 and the 132 kV 50 Hz Grid, Figure 4, was completed in 1934 enabling full commercial operation in January 1935 with the CEB directing the operation of 140 generating stations. The network became known as the "National Grid" because of its grid-iron type structure running North-South and East-West and connecting nine areas. The grid-like structure or architecture was not initially designed as a long distance transmission system but as an economic means of interconnection of the different regions. The capacity of the inter-regional tie-lines was only 50 MW and it was the main rings of the grid in industrial areas that made a significant contribution to the economy of scale. In effect, the National Grid at

this time was a network of inter-regional interconnections with some ties being able to carry limited power between regions to support maintenance and fault outages.

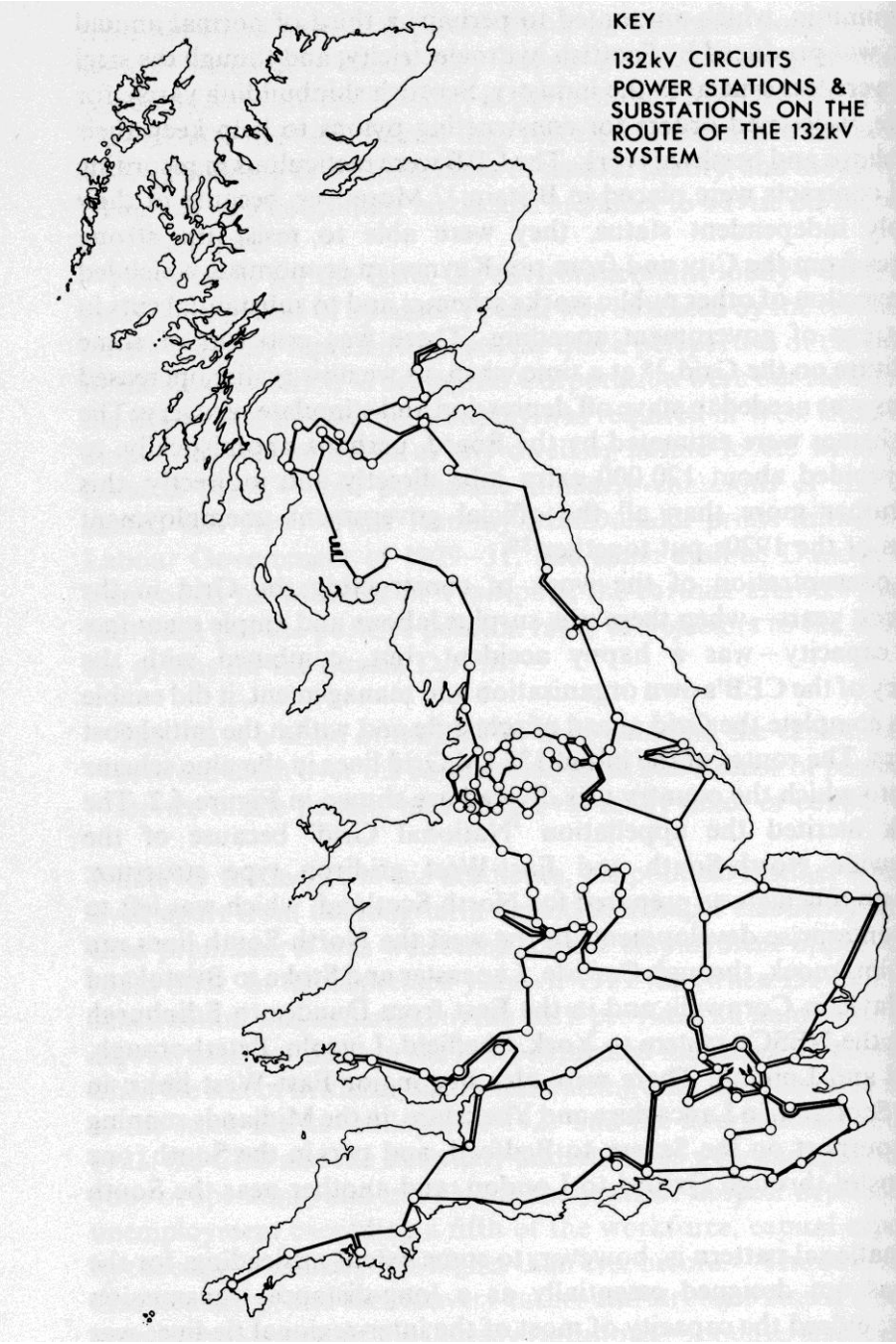

Figure 4 The National Grid in 1933[3]

[3] L. Hannah, "Electricity before Nationalisation", published by The Macmillan Press Ltd., 1979, page 120.

In 1936 the whole of the grid system was operated experimentally as one machine, the largest number of generating stations ever run in parallel. Following this, the northern and southern regions of the UK were regularly run as two systems. In 1938 a National Grid Control Centre was established and subsequently, the whole system was run as a synchronised network for long periods of time.

3.2. Contemporary Networks, 1948 – today

"The North American interconnected power system is the largest and most complex machine ever devised by man[4].

3.2.1 Overview

At the end of the Second World War engineers had the task of rebuilding much of the European power networks that had been ravaged by war. On 1 April 1948 the Electricity Act 1947 brought all former company and municipal electricity suppliers into full public ownership. The British Electricity Authority (BEA) was formed and was then responsible for 14 generating divisions, and the transmission and the sale of electricity to 14 regional boards. Contemporary power networks have a well-established and recognisable design that results from their history under this centralised industry in which a central body, in the UK - the Electricity Council, provided the technical focus and architectural design [18].

In the 1950s increasing demand for power led to the construction of a new high voltage "supergrid" operating at 275 kV. The Electricity Act 1957 formed the Central Electricity Generating Board (CEGB), which was given the responsibility for generation, transmission and wholesale selling of electricity. Twelve area boards were created and responsible for distribution retailing. These changes moved the network towards a more decentralised structure reversing the direction set under the 1947 Act. With the introduction of nuclear

[4] Charles Steinmetz, paraphrased by Prabha Kundur in "Power System Stability and Control."

power, in the early 1960s the "Supergrid" was upgraded to 400 kV and our current network is largely based on those developments.

During this period the growing complexity of the network and the use of system diagrams and centralised operational control boards, to visualise its structure and connectivity, has perhaps added to the idea of power network architecture. The development of power networks has been largely incremental and conservative following the traditional practices and standards developed by engineers, some who have long since retired. In the United Kingdom a common set of standards and guidance documents were developed to ease integration and network expansion. These standards now form part of the transmission and distribution Grid Codes [21] [22]. As networks matured, and deregulation introduced, these "codes" have replaced the original "Network Architects" such that there is no longer a recognisable person or agency that can claim design authority for the network, transmission and distribution, as a whole. The regulatory framework and market forces effectively decide the extent of network design changes.

Although electrical power networks have grown in size and structure, they all have similar characteristics [23], which in effect describe their architecture:

i) they are built around three-phase systems operating at constant voltages
ii) primary sources of energy are converted to electrical energy by synchronous machines
iii) power is transmitted to consumers over considerable distances via complex networks of subsystems and cables.

In addition, in many networks:

iv) generation, transmission, and distribution are vertically integrated and centrally controlled.

The difference between distribution and transmission networks is usually based on a legal definition as part of the electricity market regulation. Anything that is not defined as a transmission network in the legislation can be regarded as a distribution network.

A "transmission" network is the backbone of the system. It connects all the major generating stations and loads, and operates at voltages usually in excess of 230 kV, although there are some indications that the connections to some of the larger offshore wind farms will be designated as "transmission" connections at 132 kV. "Distribution" networks transfer power to the loads at appropriate voltage levels from the transmission network via a series of voltage changing substations.

3.2.2 Distributed Generation

In the literature there are many types and definitions of generation [24] that are not centralised e.g. embedded generation, distributed or dispersed generation. This thesis will follow the general definition proposed in [1]:

> *"Distributed generation is an electric power source connected directly to the distribution network or on the customer side of the meter."*

It should be noted [1] defines the rating, source, area of power delivery and technology of distributed generation as "not relevant", as these will depend upon the local distribution network conditions.

From the previous sections it is clear that contemporary distribution networks are designed and operated to accept bulk power from the transmission system and to distribute to consumers, i.e. unidirectional power flow for the connection of loads. Unlike the largest power stations, which are connected to high-voltage electricity transmission systems, distributed generation is often connected to regional distribution networks at lower voltages. Distribution networks were not designed to include power generation but, with the introduction of distributed generation, the direction of power flow in the network will change because generated power is largely independent of the load demand and indeed, may exceed local load requirements. The direction of power flows, particularly under fault and light loading conditions, is an important consideration for the design of protection schemes [25] [26]. Short circuit current profiles on distribution feeders will differ from those on more conventional networks and will certainly have an impact on protection co-ordination and circuit breaker interruption requirements and may prove difficult to evaluate

reliably. Because of differing local network conditions and load requirements, the bespoke connection of DG has led to networks with different design and operating restrictions and to the abundance of one-off constraint management and DG connection schemes.

Distributed generators are mostly, though not exclusively, those generating power from environmentally friendly renewable energy sources, such as on-shore/off-shore wind, tidal and biomass energy, or from combined heat and power (CHP) plants. It is anticipated that electrical power generated from renewable energy will, over the next twenty years, become a significant part of the total generating capacity of the European Union (EU). For example, the installed capacity of wind energy in Europe, between 1995 and 2004, increased from 2.5 GW to 34 GW [27]. In the UK the amount of distributed generation is relatively small and from an operational point of view it has been "connected to" rather than "integrated with" the grid on the basis that once the connection has been designed it will be fit for purpose. In some quarters this is called a "fit and forget" strategy [28] . A DG connection strategy, as opposed to an integration strategy, reinforces the essentially passive nature of the power network, which means that DG is often regarded as a negative load precluded from contributing to network ancillary functions that are traditionally assigned to the larger generators.

The connection of large wind farms, particularly those proposed for large offshore sites, into existing power networks presents new management and control challenges for network engineers. In the past, network expansion has not been without its problems. The control and stability of power flow and voltage were issues of electrical power distribution that grew out of the developing network of interconnected distribution systems in 1920 [29] and in 1988 [30]. Thus it is not surprising to find that there are similar concerns today as networks continue to grow and develop to meet an increasing demand for more electrical power in a deregulated environment.

These concerns are forcing Distribution Network Operators to consider a more active role for distributed generation in the supply of ancillary services such as voltage control, reactive power support, post-fault network restoration, black-start facilities frequency control and support [31] [32]. The need for a fault ride-through capability for wind

generation is particularly relevant to an increased contribution to ancillary services. Fault ride-through requirements differ throughout the world but in the UK the requirement is quite significant; the Grid Code requires ride-through down to 0% of rated voltage for 140 ms compared to Spain where the requirement is 20% and 500 ms [24]. When a fault on the network occurs, most network operators disconnect distributed generation to maintain safe conditions for repair activities, to simplify the network for ease of restoration and to facilitate auto-reclosing circuit breakers. There is an ongoing debate about fault ride-through requirements but what appears to be accepted is that there is a need for distributed generation to stay connected to the network and contribute to post-fault recovery conditions.

The current approach [33] is to examine each proposed connection and assess its compliance with the Grid and Distribution Codes. Load flow studies are undertaken in support of the connection using critical scenarios representing conditions of minimum/maximum load and maximum embedded generation output, which may then determine the need for any special network support or control measures. These measures are generally costly and not undertaken lightly.

In the USA, the Public Service Company of New Mexico successfully integrated a 204 MW wind farm with the transmission grid. The connection was to a "certified control area" and achieved 10.5% and 18.2% of the company's on-peak and off-peak control area load respectively. At the time this was the largest penetration of wind energy in the USA. However, due to the small size of the control area, the company had experienced difficulty in meeting standards for further DG connections and had a queue of connection requests for a further 1 GW of wind energy generation.

Control technologies, such as HVDC and Static Compensators (STATCOMs), are sometimes specified as network support measures to assist with DG connection. These are based on power electronic devices and may prove to be the only feasible and economic way for DG connections to comply with current Codes in the near term. Development of these control technologies for distribution network applications is currently being undertaken in industry where the equipment is manufactured. HVDC can offer some

significant benefits not normally available to network operators [34]. They allow power flow control and frequency decoupling and considerably increase the potential for meeting the Grid Code requirements. Further, the reduced operational power losses and cabling requirements for longer connections provide some cost advantage over an a.c. connection. Recently, small wind farms have been successfully connected using "HVDC Light"; e.g. 8MW scheme at Tjaereborg, Denmark, this scheme uses voltage source converters (VSC) with IGBT devices.

3.2.3 Wind turbine generators

Wind turbines and wind farms continue to increase in size and electrical capacity with no indication of this trend coming to an end. The size of wind farms grows as offshore and large onshore sites are developed. In response to the growing capacity of wind generation, transmission system operators are proposing to demand that wind turbines contribute to the operation of the power system.

Conventional fossil fuel, nuclear and large hydro generating stations all use synchronous generators, while DG use a variety of generator technologies, such as squirrel cage induction generators or wound rotor asynchronous generators either fully or partially coupled to the grid via voltage source converters. However, wind turbine designers often view the electrical generator, and any power electronic converters, primarily as a means of obtaining the required dynamic response of the drive train. In response to more stringent network connection regulations concerning large wind farms, variable speed wind turbines employing doubly-fed induction generators (DFIG) are now used and need to perform both drive-train and network control functions. These generators are of proven technology[33] and use power converters connected to a wound rotor of an induction generator, but at a reduced power rating, typical 0.25 to 0.35 p.u. compared to a fully-fed solution. The present design of these DFIG systems has difficulty in meeting the Grid Code [35].

A wind turbine employing a DFIG has the capability to provide reactive power, voltage and frequency support to the network by virtue of the capability to vary the power and reactive power production and the potential ability to "ride through" a.c. system faults. On the other hand, the manufacturing cost of a DFIG wind turbine is higher that an equivalent

fixed speed induction generator (FSIG) wind turbine and has a reduced reliability due to its power electronic equipment. To meet the 'ride-through' requirement of the grid connection codes, the DFIG has to be modified from its present design and is dependent on the addition of hardware and control software modifications. This enhancement potentially increases the cost of the offshore installations and may also impact on reliability, availability and maintenance issues.

In a recent paper [36], Strbac el al. used a simplified network model to assess the cost benefits of wind generation assuming different levels of wind penetration of the UK power network. To deal with the unpredictable nature of demand, system operators commit about 600 MW to the dynamic control of frequency and hold 2400 MW reserve capacity to manage demand over a 3 – 4 hour period. The cost of this management is included in the current cost of power, which for domestic users is 6p/kWh. Strbac's analysis demonstrates that in order to maintain network security wind generation cannot replace conventional plant on a MW for MW basis and calculates that the net additional cost would be 0.28p/kWh. The application of energy storage for standing reserve was found to be economic, particularly for generating systems with limited flexibility. The paper also studies the cost of accommodating significant amounts of wind generation without the capability to ride-through network faults and concludes that it would lead to a considerable increase in system costs, higher than the cost of providing fault ride through for DFIG generators.

The technical impact of DG on the Portuguese transmission system operation at different levels is reviewed by Peças Lopes el al. [37]. The work emphasises the need to move away from the "fit and forget" DG policy towards full integration into the power system and operation through active management of distribution networks. The need for operational changes is in the areas of co-ordination of protection and operation of ancillary services.

3.2.4 Summary of contemporary networks

The construction of a large wind farm takes a short time compared to the time needed to construct a large coal-fired or nuclear power station. In some cases this may lead to the

wind farm development in weak areas being faster than the process of planning approval and for network support measures to be constructed, causing operational delays or restrictions. For the connection of new larger scale distributed generation, e.g. large wind farms or biomass projects, system stability and fault current capability need to be assured via a formal analytic impact assessment. Modelling plays a significant role in this exercise. It is already a complex task, but as the power network grows with each new connection so the problem of assuring stability and fault capability becomes more and more protracted and will generate pressure for a change of network architecture. The network operator's ability to increase the capacity of the contemporary network is thus limited and a more flexible, active network will be needed to assure future electrical supplies and network development.

3.3. Future Networks

Throughout the 130-year history of the electricity supply network in the UK there has been a dependence upon a steady development of technology to meet a growing demand for electrical power. The industry has always been conservative in its adoption of new technology and radical change, tending to err on the side of caution to maintain a robust, cost efficient and reliable supply.

Power network capacity has expand through a demand led change and technical advance process from an abundance of small-scale isolated systems to the large-scale, bulk power transfer, complex network that we have today. We can see that this history represents two significant changes of network architect:

i) isolated to interconnected systems
ii) interconnected systems to a bulk power transmission system.

These changes did not happen quickly, without cost implications or without much legislative, commercial and technical debate. However, radical change happened in the past and will continue, much as Lord Kelvin and Mr Ferranti predicted. The drivers for change are clear, and arguments for integration and connection are heard regularly, both of which usually involve little change to the basic network architecture. But should the

debate also include interconnection along the American and European lines as a means to network expansion? Perhaps the first step towards an interconnected architecture appeared when the Cross-Channel link was constructed in 1961.

So what may the UK network architecture be in the future? Will the current architecture expand until it cannot accept any further change, will it collapse unable to maintain stability and control due to demands of a low-carbon economy? Or will we see a gradual change, perhaps reverting to the interconnected networks of late 1920s and early 1930s? My personal view is the latter case will eventually dominate and it is this view that has driven my research.

One of the major limitations of the contemporary network architecture is a lack of flexibility. For example, generation schedules may be exchanged daily at a pedestrian pace, and generators have to meet their agreed power schedule. There is no automatic response to power flow fluctuations in local or distribution network other than at an aggregated level. This is significant when changes of power flow are tightly linked to the trade between energy converters and users in a deregulated market where the production of power from large wind farms is not accurately predicable.

A fundamental change to the network architecture and its control is therefore to be considered. Research is currently being undertaken on network architectures. Given the past history of slow architectural change, no change to the network, except for a more sophisticated SCADA architecture taking on an active control role, is a short-term solution. Network architecture is being researched at University of Manchester Institute of Science and Technology, (UMIST) based on a distribution cell [38] and on an energy hub at ETH Zurich [39]. Both schemes seek to divide power networks into small cells that incorporate electrical generation, storage and loads. The cells are managed and controlled centrally by a dedicated controller. However, given the experience in New Mexico, the capacity and topology of the cell will need to be carefully designed.

3.3.1 SCADA Active Control

There are high barriers to change in the electricity network architecture, including load management and the time taken from fault identification to corrective action being taken. The existing architecture, perhaps with expanded capacity, may be used in an active manner with a revised SCADA architecture and system configured for active control. This would make it possible to monitor the network and issue signals or dispatch generators to balance network states thus facilitating additional distributed generation and avoiding network reinforcement.

A feasibility study, [40], undertaken by Scottish Power Systems Ltd. to investigate SCADA based active network control concluded that there were fundamental limitations to the speed of operation, reliability and resilience of existing SCADA systems. Active control involves taking regular measurements from the network, performing assessments to compare with predetermined references, output of a control command and reporting control action complete. To convert the existing network into a more active network it is import to consider stand-alone generation and future network development. Therefore, embedding more logic into the distribution network requires reliable and secure communications. An active SCADA scheme would be based on a layered architecture as shown in Figure 5. High bandwidth communications will be a prime requirement of this approach to active network control.

Each layer of the scheme is important. The Active Unit is autonomous, effecting local control and ensuring local integrity of voltage and fault level. The Active Cell co-ordinates the control of a group of Active Units and utilises bi-directional communications passing data and commands to Unit and Network controllers. The Active Transformer may be used in a control role at this level to balance load/demand and enhance management opportunities from detailed data. The Active Network would consist of Active Cells and Units adjusting network targets to balance generation/load with adjacent networks or provide a range of ancillary services such as network frequency control.

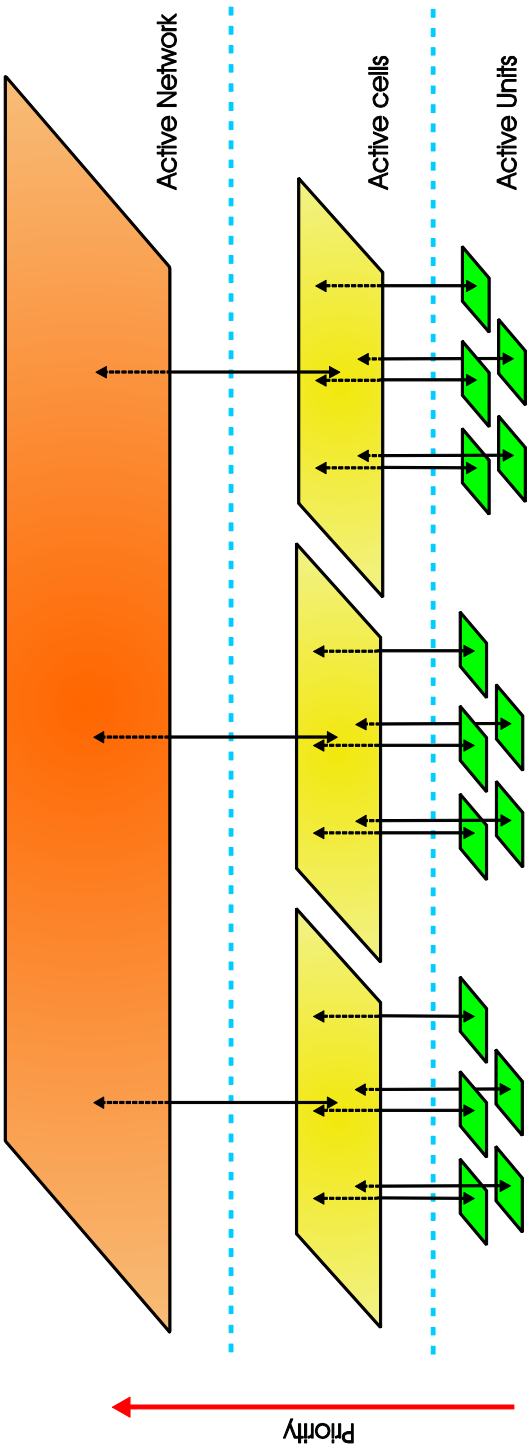

Figure 5 SCADA active control schematic

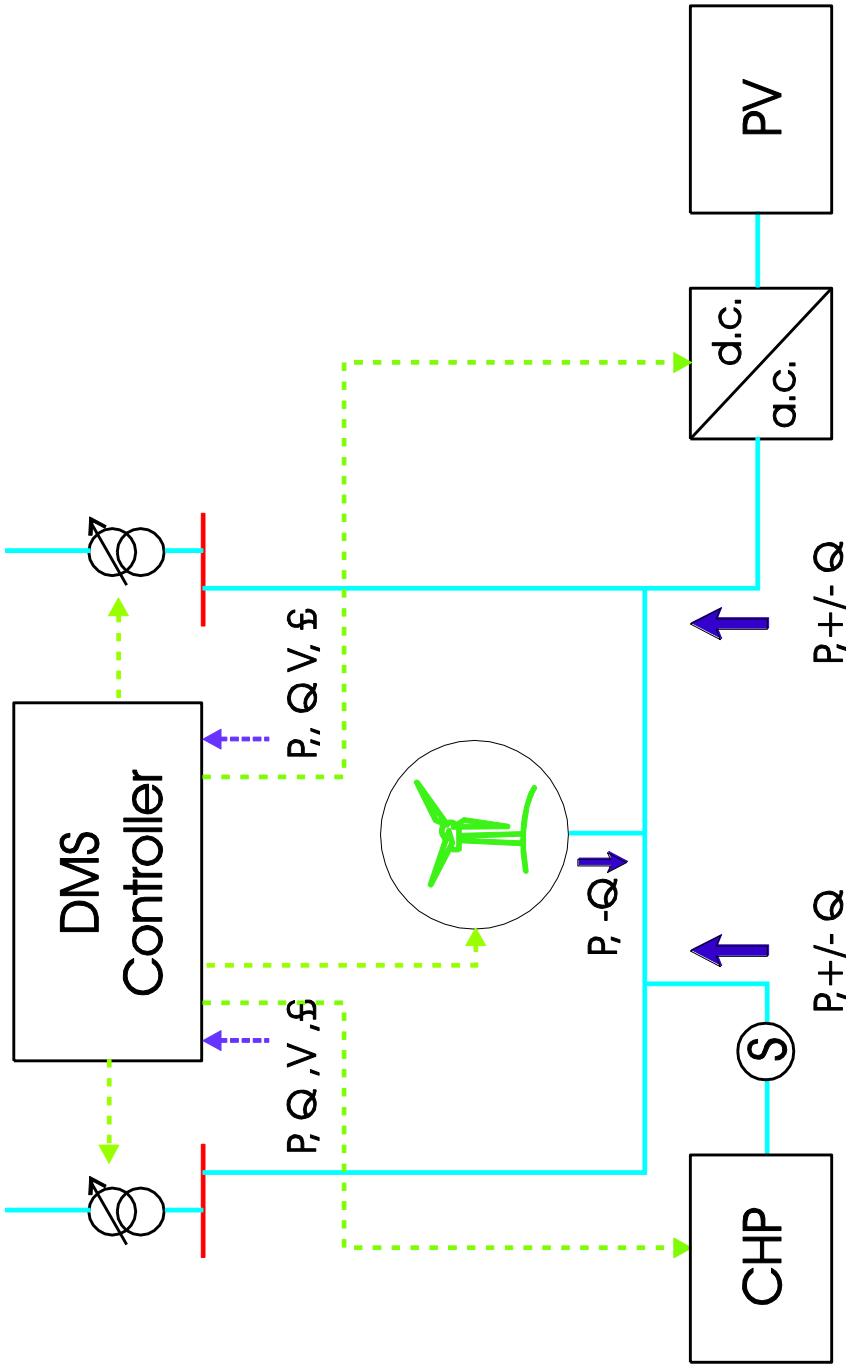

Figure 6 Active distribution network

Active management is shown to be beneficial achieving a three-fold increase in the distributed generation connections compared with connections to a passive network. The use of active network control effectively changes a "connection strategy" into an "integration strategy", as discussed previously, for distributed generation. A Distribution Management System (DMS) controller is proposed and five levels of design are considered. Control is hierarchical and requires appropriate levels of communications between the network and the active elements.

The Grid and Distribution Codes define the quality of supply that users can expect. These codes determine the design and cost of the distribution network and hence, over many years, techniques have been developed to make the maximum use of the network to supply users within the required voltages. Some supply transformers are fitted with on-load tap changers (OLTC) that are adjusted to maintain voltages within the limits set by the codes, for example, to compensate for voltage drop due to line resistance. At maximum load, network voltages are adjusted so that remote users receive an acceptable voltage, during periods of low load, the voltage at user terminals is just below the maximum allowed.

If an embedded generator is now connected to the end of such a circuit, then the power flowing in the circuit will change and hence the voltage profiles will vary. In some instances, a voltage rise can be limited by reversing the flow of reactive power (Q) either by using an induction generator or by under-exciting a synchronous machine and operating at leading power factor. This can be effective on higher voltage overhead circuits, which tend to have a higher reactance/resistance ratio. However, on low voltage cable distribution circuits the dominant effect is that of the real power and the network resistance and so only relatively small generators are connected to low voltage networks.

Thus, for the cases where significant amounts of generation are to be integrated into the distribution network, which may also include energy storage, active control over the local supply is required in order to maintain the quality of supply. A power module or cell, Figure 6, is thus formed and the network architecture and its dynamics have been changed. A local balance of generation, storage and load will be the factors that determine the size of the cell and the degree/sophistication of control and communications required to meet

the supply codes. This should be more readily achieved within a cell than having to rebalance the whole of the electricity network each time new DG is added to the network.

3.3.2 Energy Hub

At the Swiss Federal Institute of Technology, Zurich, a novel project entitled *Vision of Future Energy Networks* [39] is researching a green field approach to future power systems using "energy hubs", where the boundary conditions of contemporary power systems are disregarded in order to achieve greater overall system performance. The project examines the use of multiple energy carriers and the use of distributed energy resources, conversion and storage. Potential applications are suggested as:

i) power plants, co- and tri-generation
ii) industrial plants, steel works, paper mills, refineries
iii) big buildings airports, hospitals, shopping malls
iv) bounded geographical areas, rural and urban districts, towns and cities
v) island power systems, trains, ships, aircrafts.

Energy converters and storage devices are integrated into energy hubs, Figure 7, which are supplied by various energy sources and deliver power to loads consuming different forms of energy. This approach combines the transmission of different energy carriers in one device, which is called an energy inter-connector. Electricity and gaseous (e.g. hydrogen) energy carriers can be transported together in an underground transmission element. The whole energy system, Figure 8, is then designed using energy hubs, inter-connectors, and conventional elements.

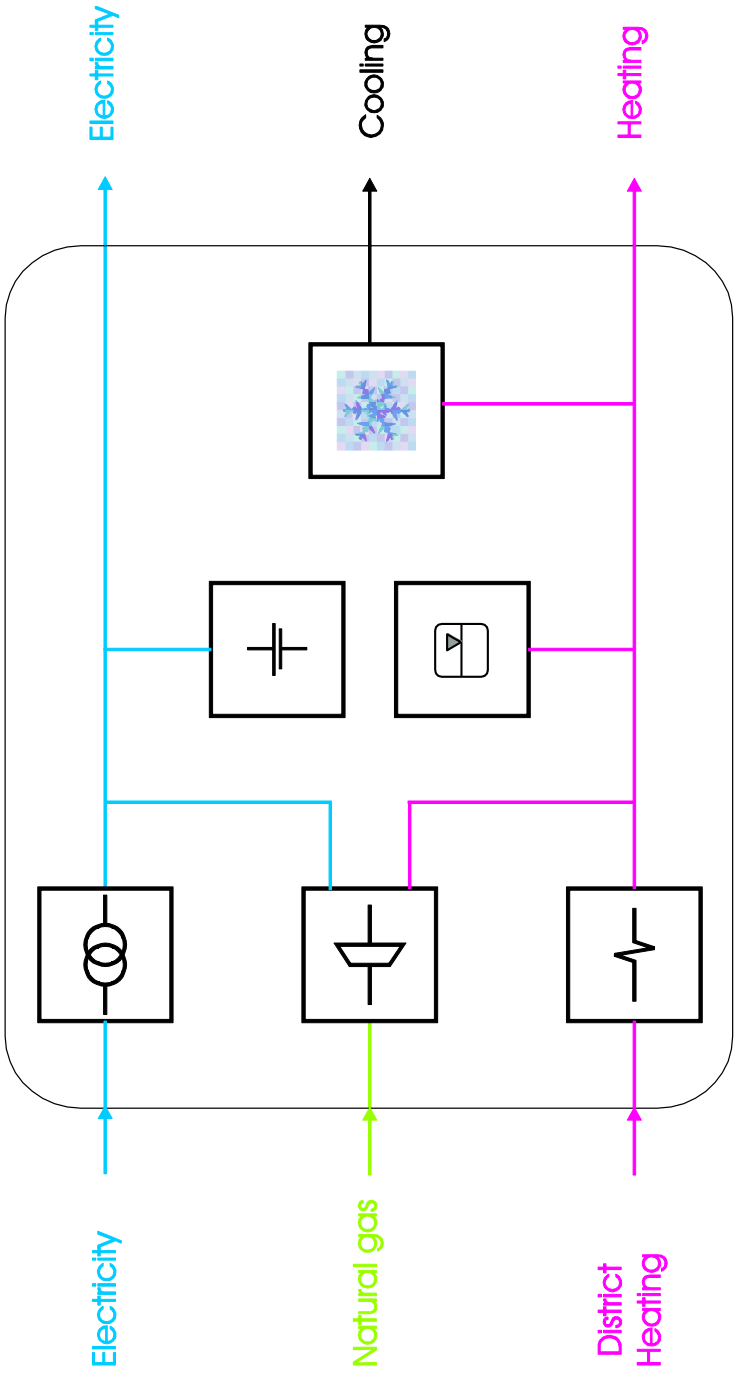

Figure 7 Energy Hub

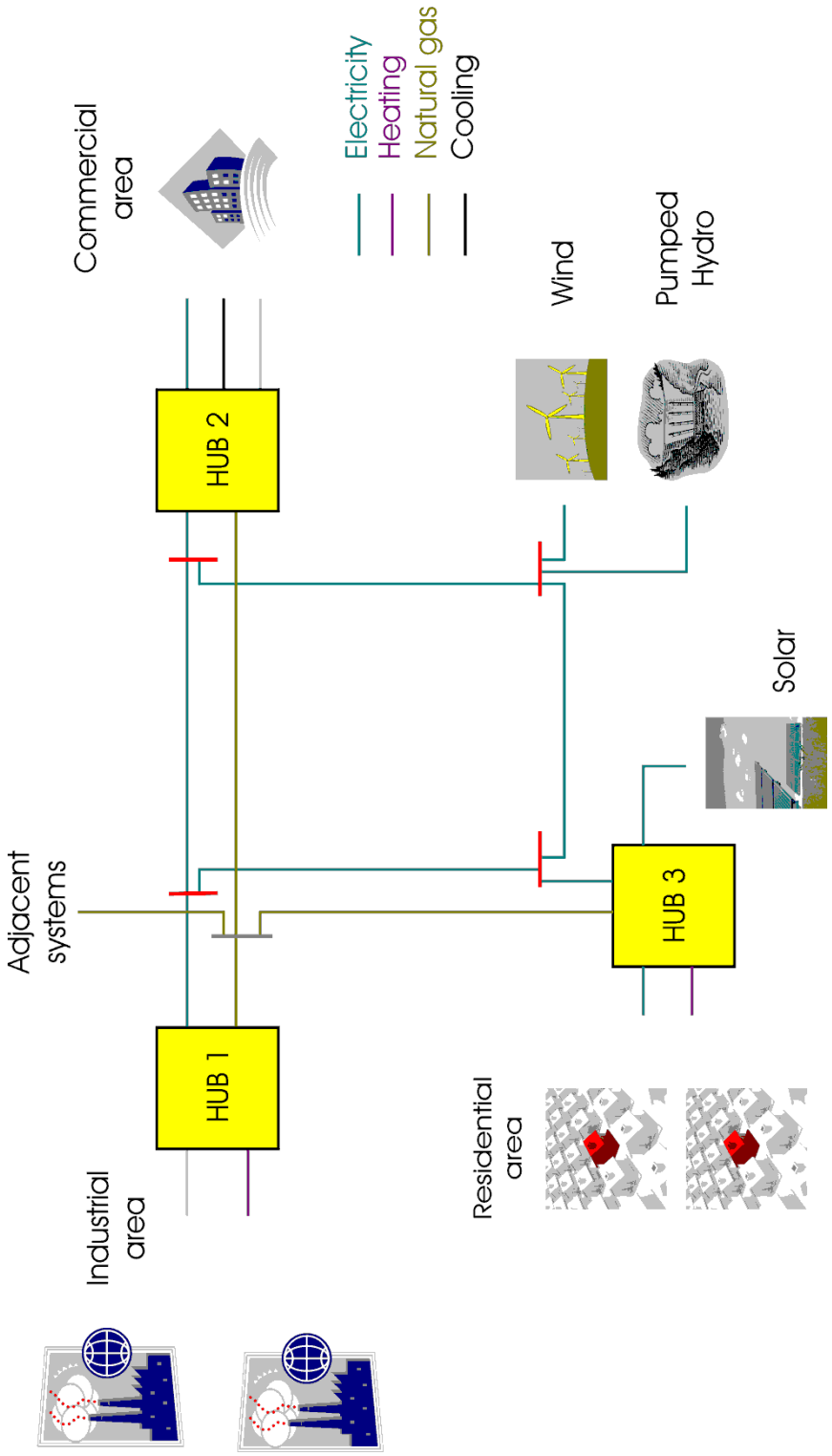

Figure 8 Sketch of a system of interconnected hubs

Direct connections are used to deliver energy or power from an input to an output without any conversion or change of quality, e.g., electric voltage, hydraulic pressure. Electric cables, overhead lines, and pipelines are examples of this type of element. Besides that, converter elements are used to transform power into other forms or qualities. Examples are steam and gas turbines, reciprocating internal combustion engines, Stirling engines, electric machines, fuel cells, electrolysers and thermoelectric converters. The use of energy storage is also proposed using technologies such as supercapacitors, superconducting devices, batteries, hydro reservoirs, flywheels, compressed air storage or reversible fuel cells. The project uses modelling to study the power flows within and without the hubs and therefore does not give much detail about the energy interfaces.

3.4. Summary

In the early electrical power networks, operational control was effected using geographical system diagrams of the whole network. As the networks grew in size and complexity, hand dressed-diagrams were commonly used for large systems and these were considered to be superior to automatic diagrams [41]. As network complexity grew, new methods were needed to ensure network security and availability. Calculating boards, such as the General Electric Company's a.c. network analyser [42], were used to ascertain fault MVA and current levels. Remote supervisory equipment was installed by some progressive operators to enable voltage regulation and switching to be done from a central control room and these methods has led to the idea of network architecture.

With the introduction of nuclear power, in the early 1960s the "Supergrid" was upgraded to 400 kV and the current passive network is largely based on those developments. Connection type strategies for additional generation are unlikely to meet all future integration needs and a fundamental change to the network architecture and its control is needed to facilitate further network development and robust integration of large renewable energy generation. If the use of significant amounts of DG are to displace large central generation and its ancillary facilities in the UK, then the present legislative framework, as well as the network architecture, must change to enable DG to contribute to the network

support activities. Whatever solution or solutions are eventually used to fully integrate distributed generation, their capital cost and reliability will be significant considerations.

The use of SCADA systems to implement active control strategies will be a short term solution but, based on the continued growth of demand for renewable power generation, a greater degree of freedom will eventually be required for network control. Distribution cells and energy hubs are two schemes currently being researched and both use a conventional power transformer as the connection to the rest of the network.

Chapter 4.

Literature Review

4.1. Introduction

Power electronic equipment is widely used in transmission and distribution systems to solve grid problems and improve power quality. Contemporary equipment uses silicon semiconductor devices as switches. New generations of power semiconductors will have a significant impact on the design and application of power electronic equipment for power networks, e.g. transformers with inbuilt voltage source converters for power flow control, [44].

The idea of an "Active Transformer" arose some years ago in a discussion between me and Dr Colin Oates at AREVA Technology Centre. The discussion was centred on the results of some modelling of a converter for a device described as a "solid-state sub-station" (SSS). At that time my interests were in machines, which to indicate a high level integration with power electronics, were classed as "active motors" and "active generators". The extension of this class to transformers, being stationary machines, was logical and so the idea of the "active transformer" was born. Dr Oates subsequently registered two patents in the USA. In some papers similar devices are called "solid state transformers" (SSTs).

4.2. Converters Topologies

There are many possible converter topologies that could be used within an Active Transformer and [45] provides a good review of the main candidates that have potential applications at high frequencies, powers and voltages. A summary of the review is given here.

The Active Transformer can provide voltage transformation, bi-directional power flow and galvanic isolation. Using high frequency conversion will minimise the size and weight of the transformer, however, the cost of the transformer is likely to be higher. Four possible

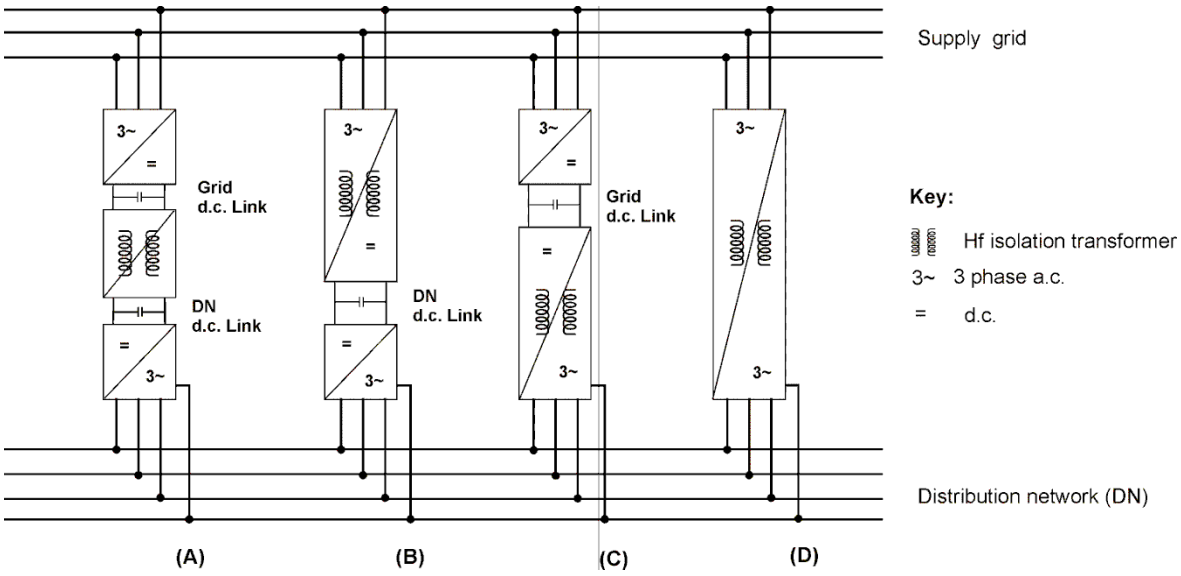

Figure 9 Power converter configuration

converter configurations are shown in Figure 9. The first example is a three stage conversion with grid-side and DN-side d.c. links. The second example is a two stage conversion with a DN-side d.c. link. The third example is a two stage converter with a grid-side d.c. link. In these examples the d.c. link may be resonant thus facilitating zero voltage or current switching to minimise switching losses in the converter and harmonic distortion. The fourth example is a single stage a direct a.c/a.c. resonant conversion. All four use a high frequency transformer for galvanic isolation, and, reduced size compared with a conventional power transformer.

The fourth configuration, direct a.c./a.c. resonant conversion, is preferred for the following reasons:

i) the power semiconductor device count is the lowest therefore minimising device cost
ii) d.c. link capacitors are not required

iii) resonant operation minimises switching losses and reduces harmonic distortion.

iv) semiconductor devices can be connected in series to achieve high operating voltages without complex arrangements for voltage sharing, such as active gate control as proposed by Palmer [46].

4.3. Power converter switching strategy

4.3.1 Background

The choice of converter topology, and the devices used to implement a direct a.c./a.c. resonant converter, will largely determine the device switching strategy employed. Converter control techniques are briefly reviewed in [45] and cover pulse density, delta-M and sigma-delta M techniques. However, the choice is that of sliding mode control, which is a form of "switching-law" or boundary control and has been used by researchers at Nottingham University successfully in several other applications with proportional-integral voltage control. Its simplicity and ease of application that subsequently leads to good robustness, are the key reasons for its use in the Active Transformer. It possible disadvantage is its coarseness of control.

Other control techniques are also available for direct a.c-a.c. converter control and two of these are compared in [47]. The authors contrast the Venturi and Space Vector Modulation (SVM) methods for their relative performance under balanced/unbalanced supply conditions, input/output current harmonics and converter losses. These converters may be used in frequency and voltage changing applications and it is noted that the maximum voltage at the output was 86% of the supply because the output can not be greater than the minimum peak-to-peak line voltage. SVM is a simpler method for the control of input power factor and results in lower switching losses but the Venturi method compensates for unbalanced supply conditions and produces a similar harmonic content. However, the authors do not address robustness, stability limits or direct resonant converters.

4.3.2 Semiconductor devices

While it is possible to connect a large number of devices in series with contemporary silicon semiconductor technology, the cost of a transmission voltage or large distribution voltage converter is likely to be prohibitive except in very exceptional circumstances. Direct-on-line high voltage converter topology is however, more suited to silicon carbide devices (SiC) currently under development, which operate at much higher voltages (20-30 kV) than silicon (5-7 kV), and may be available in suitable ratings in the next five to ten years.

Low power SiC devices are finding widespread use in the automotive and telecommunications industries. Devices based on diamond semiconductors are also being developed and these would undoubtedly operate at higher voltages than even silicon carbide and therefore could considerably reduce the device count needed for very high voltage converters, however, commercially available power devices are even further away than SiC devices.

4.3.3 Pulse width modulation

Pulse width modulation (PWM) is a well established converter control technique and many schemes have been devised for particular applications. Different PWM techniques (ways of determining the modulating signal and the switch-on switch-off instants from the modulating signal) exist. Popular examples are sinusoidal PWM, hysteric PWM and the relatively new space-vector (SV) PWM. There are many excellent textbooks that describe conventional PWM strategies, reference [48] was found to be particularly useful and readable and although it briefly mentioned soft-switching resonant converters as a current area of research interest, disappointingly, it did not consider them further.

4.3.4 Space-vector pulse width modulation

SV PWM refers to a way of determining the switching states, or sequence, of a three-phase converter bridge. It is often applied to voltage sourced converters used in the control of rotating machines where the control of both voltage and frequency are important. It has

been shown to generate less harmonic distortion in the output voltages and/or currents in the windings of the motor load and provides more efficient use of d.c. supply voltage, in comparison to direct sinusoidal modulation technique [49].

SVM applies the d-q transform, Appendix A, to the supply phase voltages or currents. This is the same as an orthogonal projection of the phase variable on to the two-dimensional d-q plane and results in eight stationery or basic space vectors, six non-zero and two zero or null vectors. The angle between any two adjacent vectors is 60°. The objective of the SVM method is to control an output voltage or current by approximating it to a combination of switching states equivalent to the basic state vectors. Any output vector can be derived from the application of the adjacent basic vectors for a defined duration. The only criterion necessary is that the period of change must be small with respect to the period of the required output voltage/current. In practice, this is a normal condition of PWM techniques.

4.4. Advanced control methods

4.4.1 Introduction

The design of converters generally has to cope with a significant level of uncertainties, not just in component parameters, but also in the environmental conditions, often unpredictable, such as wide variations in temperature, load and supply voltages. The conventional approach is to use a PI controller, over design and over rate the converter for its particular application to ensure performance is maintained over a wide range of conditions. Substantial test regimes are then used to verify performance, which tend to be costly and lengthy.

So, in considering the choice of controller for the Active Transformer, the key factors affecting the design are that it:

i) is a non-linear system
ii) has high levels of load uncertainty
iii) has complex control requirements.

Some of the disadvantages and limitations of classical linear design methods are shown in the results of Chapter 5. Modern design techniques aim to produce controllers that are robust by design and attempt to overcome these limitations and the disadvantages of over design. A complete design of the current-sourced converter used in the Active Transformer will require a multivariable control strategy to cater for the complex control requirements, i.e. line current, input phase angle and output voltage, but the key requirement at this stage of the design process is for a robust controller design that caters for the uncertainty of the load. A further more general requirement is that the controller design method must be relatively straightforward to apply if it is to be accepted in the power electronics industry. The candidate control methods are discussed below.

4.4.2 Review of candidate strategies and methodologies

Current sourced converters are often used in high power converter applications. A drive system application, [50], used a multivariable PI controller where high performance was required. In this paper the state matrices were derived in state-space form, which is the modern method. The controller design used a tuning strategy and recommended the use of the inverse d.c. gain matrix of the open loop system as the matrix for the integral controller. The results presented, without feed forward, showed an acceptable response to a step change, but with some overshoot that was much reduced when feed forward was introduced.

For current-sourced resonant converters, although not widely used in power electronics applications because choosing suitable weights may be difficult, an alternative to PI strategies are optimal control strategies. These techniques have several forms, but each uses a quadratic performance index to reduce a signal or transfer function to a minimum at every control step and should, in practise, lead to stable, high dynamic system responses with a classical 60° phase margin guaranteed, [51]. For supply-side converter applications, such as in the Active Transformer, it has good robustness against supply variations.

A robust control system [52] is one that exhibits the required performance in the presence of significant uncertainty. A control system is robust when:

iv) there are low sensitivities to environmental effects

v) it is stable over the required range of parameters (uncertainty), i.e. the concept of robust control

vi) its performance continues to meet specification in the presence of defined parameter variation, i.e. the concept of robust performance.

There are many methods for the design of converter controllers. Methods applicable to the design of the Active Transformer are:

a) Signal based methods.

In this approach, time domain formulations result in the minimisation of a norm of a signal, such as an error signal or system output. The Linear Quadratic Gausian (LQG) method is such an example where the input signal is assumed to be stochastic and the expected value of the system output is minimised against a quadratic cost function (2-norm). It is a simple method to apply, however, the system dynamics are required to be linear and, importantly, known. In practise, all states are not known and therefore a state estimator is used with optimal state feedback. Frequency dependent weights may be added to the signals leading to the so called $\mathcal{H}_2$ control that aims to minimise the r.m.s. the controlled value. Because of the use of a state estimator, the LQG method often leads to complex transfer functions that do not guarantee satisfactory robustness of the controller, once the estimator is included in the loop. It is criticised for the representation of uncertain disturbances by white noise as being unrealistic. In the Active transformer, the uncertainty is in the load. The converter transfer function used in the design of the voltage loop includes a term containing the load. The variation in load is not known, and therefore, neither is the transfer function known. Therefore, signal based methods, such as the LQG, are not as attractive for the design of the controller for the Active Transformer. Where uncertainty is addressed, an $\mathcal{H}_\infty$ procedure is a more direct and natural approach than $\mathcal{H}_2$ control.

b) $\mathcal{H}_\infty$ *mixed-sensitivity methods*

Mixed-sensitivity is the name given to methods that shape closed-loop transfer functions, e.g. the sensitivity transfer function $S = (I + GK)^{-1}$ along one or more other closed-loop transfer functions, such as the complementary sensitivity transfer function *T*. For example, in a regulation type control problem, the aim is to reject a disturbance at the system output, and it is assumed that measurement noise can be ignored. The disturbance is usually a low frequency and will be rejected when the maximum singular value of *S* is made small at the same low frequencies. This is achieved by a scalar low-pass filter, ω_1(s), with bandwidth equal to that of the disturbance and the control designed minimising$\|\omega_1 S\|_\infty$. For the Active Transformer converter, which has a right-hand plane zero, the controller requires infinite gains and is therefore not a practical control solution. For a more practical situation $\left\|\begin{bmatrix}\omega_1 S \\ \omega_2 KS\end{bmatrix}\right\|_\infty$ may be applied, where ω_2 is a scalar high-pass filter, with a crossover frequency approximately equal to the desired closed-loop bandwidth. This method is usually restricted to less complex systems with control channels of quite different bandwidths. The mixed-sensitivity approach is often cumbersome to apply to complex systems, due to the choice of appropriate weights and a more flexible design procedure is required.

c) $\mathcal{H}_\infty$ *loop shaping methods.*

$\mathcal{H}_\infty$ mixed-sensitivity methods incorporated the formulation of the control problem in closed-loop. By contrast, the $\mathcal{H}_\infty$ loop-shaping method, [52], provides robust stability in an open-loop shaping method to achieve closed-loop specifications, and in fact this ides is based on the well known classical loop-shaping concepts. The classical loop-shaping method is to shape the frequency response of the open-loop transfer function to give the desired bandwidth. In the $\mathcal{H}_\infty$ approach, the multivariable system specification includes the magnitude of the singular values, which are the values of the transfer functions between specific inputs and an outputs, or directions, as a function of frequency. The

designer then seeks a controller to give the required loop shape. The key benefit of the $\mathcal{H}_\infty$ loop-shaping design procedure is that it makes the system robust at all frequencies and guarantees stability. The control problem aims simply to minimise the peaks of the maximum singular values of the open-loop frequency response of a shaped system, which is the original system transfer function embraced with suitable pre- and post-weighting functions. The shaped system is then robustly stabilised with respect to a general class of coprime factor uncertainty using $\mathcal{H}_\infty$ optimisation.

To avoid the limitations of LQG and mixed-sensitivity approaches, for many industrial applications, the flexibility and simplicity of the $\mathcal{H}_\infty$ loop-shaping method is preferred because it is based on classical loop-shaping ideas that are well understood.

4.4.3 Choice of controller

Power converters operate in a sensitive environment where the consequence of a failure, whether due to a fault or poor design, is often catastrophic for the converter. Consequently converter designers are usually very conservative in their designs, which give them a high degree of robustness. The application of advanced modern control schemes in high power or high voltage converters is, until recently, quite rare. A back-to-back HVDC scheme has some similarities in application to the Active transformer in that it connects two isolated power networks and controls the flow of power between them. It comprises of two notionally independent converters and a d.c. link as opposed to an a.c. link used in the Active Transformer.

A good example of an application is given in [53], which applies mixed-sensitivity $\mathcal{H}_\infty$ design to the control of an HVDC back-to-back converter scheme. A major difference between the converters used in the HVDC scheme and the Active Transformer is the converter topology. In conventional HVDC schemes the converters are supplied from a step down transformer and use thyristor technology and series bridges at power frequencies to achieve the required performance and reliability. Power frequency operation necessitates large transformers, wound components and link capacitors. The Active

Transformer, on the other hand, uses direct high frequency resonant conversion, silicon carbide technology and high frequency techniques that aim to significantly reduce device costs and minimise the overall converter size.

In the HVDC scheme the $\mathcal{H}_\infty$ controller design objectives were robust stability, disturbance rejection and tracking performance over a wide variation of a.c. system short circuit currents (SCL). Good disturbance rejection is necessary for the recovery from a.c. faults and reduces the risk of commutation failures. There are two controllable inputs, phase-lock-loop (PLO) oscillators, that control the timing of the firing pulses on each side of the d.c. link. The PLO frequency is varied to control the d.c. link current, I_{dc}, and link voltage, V_{dc} independently.

Multiplicative uncertainty modelling of the SCL was used and a tuning procedure from [52] used to determine the weights for an $\mathcal{H}_\infty$ mixed-sensitivity design approach that shaped the sensitivity (S) and complementary (T) sensitivity functions of the closed loop plant. Weights were applied to S and T to provide adequate tracking and disturbance rejection, and noise rejection respectively. Extensive simulation confirmed that the $\mathcal{H}_\infty$ controller was stable for all SCR conditions and was "superior" in rejecting disturbances of I_{dc}.

The application of $\mathcal{H}_\infty$ mixed-sensitivity to the design of the HVDC controller gives good confidence in the application of $\mathcal{H}_\infty$ methods in a high power environment. But a concern over the untried complexity of the resonant converter control compared to that of the conventional HVDC bridge and the desire to use simple methods that extend the use of classical control methods, and the novelty in proposing an alternative untried design method for this application makes the choice of $\mathcal{H}_\infty$ loop-shaping the preferred method.

4.5. Patents

In his patent [54] Oates details an electrical substation, described as a "solid state substation" (SSS), based on a high frequency d.c. link power converter that overcomes some of the limitations of tap-changing conventional power transformers and permits a degree of control usually provided by a Static VAr Compensator (SVC). It is also

suggested that "the input switching network may include a resonant circuit" and a high voltage resonant matrix converter is described in his companion patent [55]. Both d.c. and a.c. supplied converters are described. The resonant configuration enables high voltage operation by overcoming the problems of synchronising the switching of large numbers, 50 or more, of series semiconductor devices needed to construct a suitable converter.

The combination of high frequency resonant converters and a high frequency transformer that Oates outlines in his two US patents can be considered more generally as an "active transformer". This is a novel power system device and no prior research or application was initially found in power systems or networks. The matrix topology of the a.c. supplied converter in [55] perhaps implies the use of space-vector control techniques. In [56] the technique is referred to as "hysteresis-band control" and is perhaps similar to what Oates had in mind.

4.6. Discussion on previous work relating resonant converters

Work in [45] provides a comprehensive and readable investigation of the design of direct, high-frequency power conversion with the analysis, design, construction and test of a 5 kW direct converter. Oates is acknowledged for his contribution at the beginning of the research but the work is focused on the design of a supply converter that could be used as the front-end of a "solid-state Transformer" (SST) or the "Solid State Substation" (SSS) as both are descriptions of similar applications, rather than a complete SST or SSS. The converter design aims to control input current using a predictive current technique to achieve unity power factor and conventional PI control of output voltage.

Depending largely on their application and topology, there are many ways in which power converters may be modelled for design purposes. For example, detailed component models are used for circuit analysis and design where the timing and rating of components is critical. Block diagram or transfer function models, often of a simplified or representative nature, are used for system and controller design where the converter's response to an environmental change is more important.

The thrust of the afore mentioned work was the practical demonstration of the feasibility of the direct current-sourced converter using predictive current control and hence a popular circuit-based modelling tool, SABER®, was used for the detailed analysis and design of a demonstration 5 kW converter to verify the design. The design aim of the converter control was to maintain a steady tank voltage level, and keep the input phase currents at a defined magnitude and phase related to the supply voltage. However, the Active Transformer essentially consists of a 3-phase to 1-phase supply converter connected in series with a load or output converter, of a similar design, but configured to supply a 3-phase output from a high frequency single phase supply.

The results of the test of a 5 kW converter demonstrate its feasibility and the control method, up to a point. The analysis and design of the voltage controller is based on a linearised model operating at a full load condition and this is valid for only small perturbations around the operating point. In practice however, the design should have been tested for a wider variety of loads, particularly as power converters are well known to have stability problems at low loads, which would have shown the possibility of unstable operation with light loads. In the case of the intended application on a power network, the load is likely to be constantly varying or uncertain, and may range from 10 to 120%. The linearised transfer function used for the design of the voltage control loop also indicates closed loop poles that move towards the right-hand half of the s-plane (RHP) for light loads. However, the test results reported did not show any instability as a result of this movement, perhaps because the loop gain also reduces for smaller loads and the two effects tend to cancel each other to some extent. The possibility for instability still remains. Further analysis of PI voltage controller is discussed in Chapter 5.

Chapter 5.

Linear Modelling and Classical Control Design

5.1. Introduction

The challenge for the converter control system designer is that results of the often used small signal analysis method are very dependent upon the model, and the frequency domain behaviour is well known to be dependent upon the load. The design then proceeds with an analysis based on worst case conditions, which is problematic when the model is variable and inevitably leads to over design or a lack of robustness. It may also be argued that, because of the presence of non-linear switching functions in a power converter, that non-linear techniques, though more complex, require much more effort for success. The next chapter will review sliding mode control, a non-linear method used for current control in a resonant converter.

However, small-signal designs do provide a systematic way to address the design and they do provide a good insight in to the controller performance. As we shall see in the following sections, this approach has been used to good effect in the design of the voltage controller.

This chapter describes the converter PI voltage control system. It was based on a classical PI controller design using the traditional root-locus method. These methods and techniques are still popular with converter designers because, with conservative circuit designs and component specification, they lead to quite robust converters able to achieve satisfactory performance under a wide range of operational conditions. However, a potential for instability often remains with load shedding to light loads, and this was

verified by further analysis. In an attempt to overcome the problem, the controller was redesigned using a robust PI method. The results of an analysis of the two designs were compared and contrasted.

5.2. Review of PI converter control

5.2.1 Control of line currents

A block diagram of a resonant converter control system is shown in Figure 10, [45]. It describes a means of controlling the three-phase input currents, i.e. choose a switching sequence for the 3-phase bridge to generate the error vector that takes the output voltage or input currents closer to their desired values. The converter has eight possible switch states, Table 2, but states 7 and 8 have similar outcomes and, therefore, there are only seven possible control outcomes for line currents.

Table 2 Coefficients Ka, Kb and Kc as a function of switch state

Switch state	**Upper switches**			**Lower switches**			$\mathbf{S_a}$	$\mathbf{S_b}$	$\mathbf{S_c}$	$\mathbf{K_a}$	$\mathbf{K_b}$	$\mathbf{K_c}$
	S_{a1}	S_{b1}	S_{c1}	S_{a2}	S_{b2}	S_{c2}						
1	1	0	0	0	1	1	1	0	0	-⅔	⅓	⅓
2	1	1	0	0	0	1	1	1	0	-⅓	-⅓	⅔
3	0	1	0	1	0	1	0	1	0	⅓	-⅔	⅓
4	0	1	1	1	0	0	0	1	1	⅔	-⅓	-⅓
5	0	0	1	1	1	0	0	0	1	⅓	⅓	-⅔
6	1	0	1	0	1	0	1	0	1	-⅓	⅔	-⅓
7 (zero vector)	1	1	1	0	0	0	1	1	1	0	0	0
8 (zero vector)	0	0	0	1	1	1	0	0	0	0	0	0

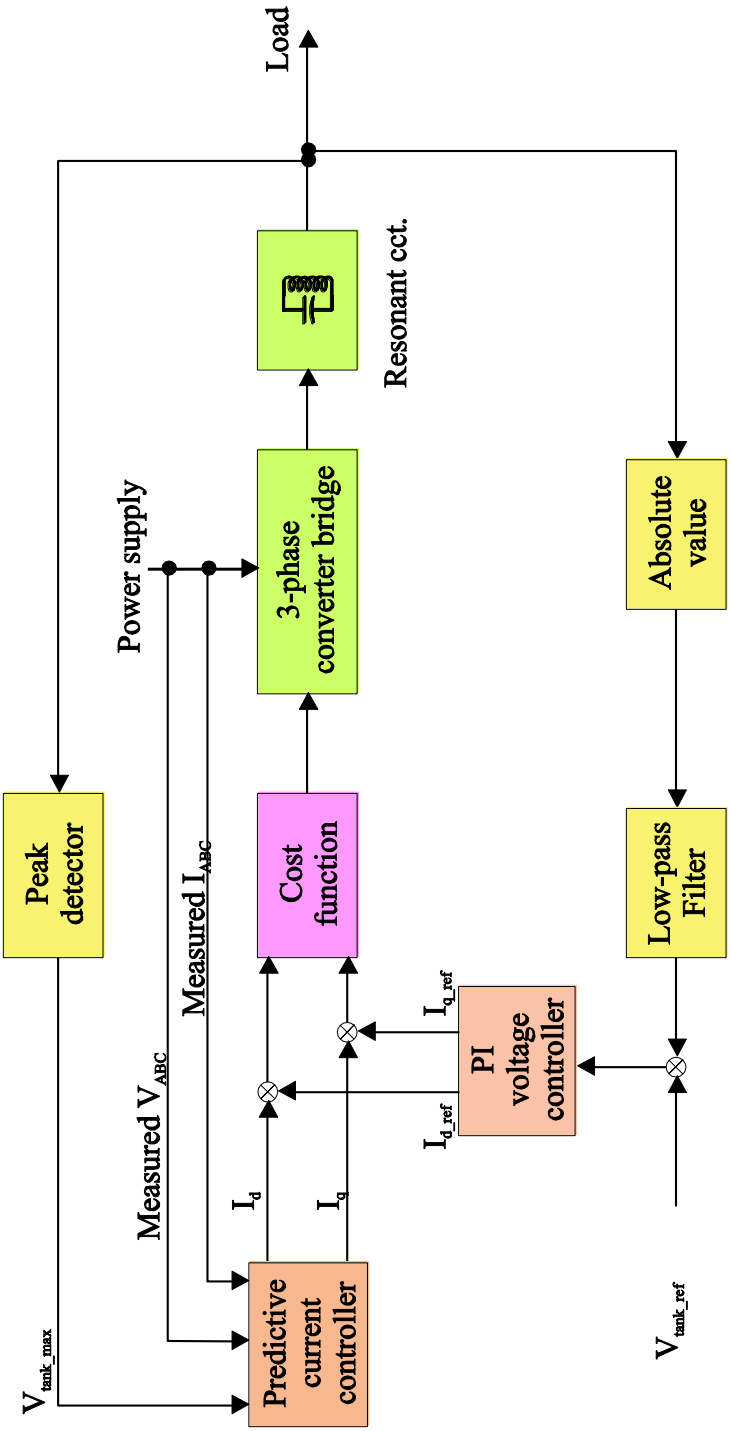

Figure 10 Converter block diagram

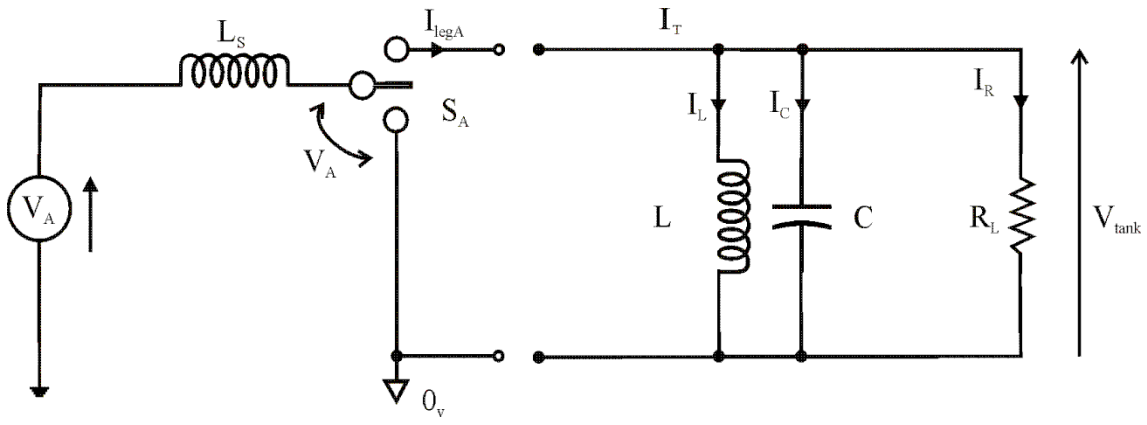

Figure 11 Representation of phase A

A representation of the converter, phase A, is shown in Figure 11, from which the converter state equations, (1)(2)(3), are derived for a 3-phase supply system:

$$(1) \quad d/dt \begin{bmatrix} I_A \\ I_B \\ I_C \end{bmatrix} = -1/L_S \begin{bmatrix} S_a \\ S_b \\ S_c \end{bmatrix} V_{tank} + 1/L_S \begin{bmatrix} V_{AN} \\ V_{BN} \\ V_{CN} \end{bmatrix} + 1/L_S \begin{bmatrix} V_N \\ V_N \\ V_N \end{bmatrix}$$

$$(2) \quad dV_{tank}/dt = \frac{1}{C} \begin{bmatrix} S_s & S_b & S_c \end{bmatrix} - \begin{bmatrix} I_A \\ I_B \\ I_C \end{bmatrix} - \frac{1}{RC} V_{tank} - \frac{1}{C} I_L$$

$$(3) \quad \frac{dI_L}{dt} = \frac{1}{L} V_{tank},$$

that completely described the behaviour of the converter. The state equations in the dq0 co-ordinate system are:

$$(4) \quad d/dt \begin{bmatrix} I_d \\ I_q \end{bmatrix} = -1/L_S \begin{bmatrix} I_d \\ I_q \end{bmatrix} V_{tank} + 1/L_S \begin{bmatrix} S_d \\ S_q \end{bmatrix} + 1/L_S \begin{bmatrix} V_d \\ V_q \end{bmatrix}$$

$$(5) \quad dV_{tank}/dt = \frac{1}{CS_q} \begin{bmatrix} S_d & S_q \end{bmatrix} - \begin{bmatrix} I_d \\ I_q \end{bmatrix} - \frac{1}{RC} V_{tank} - \frac{1}{C} I_L$$

$$(6) \quad \frac{dI_L}{dt} = \frac{1}{L} V_{tank}$$

The afore mentioned model is not directly employed for control system design, instead an expression for the input inductor current has been derived for designing the "predicted current controller". Thus, integrating (1), the change in current through the line inductors over the next half cycle of the output voltage was:

$$(7) \qquad \Delta I_i = \frac{1}{L_s \omega_r} \left(V_{in}\pi + 2K_i V_{tank\_m} \right); \quad i = A, B, C$$

This result was then added to the instantaneous value of line-inductor currents to provide a prediction of the line current at the next zero crossing of the output voltage. A simple error-squared cost function is used to determine the switching state that produces the minimum line current error and this result is then the next switch-state of the converter.

5.2.2 PI voltage controller

A linearised, small-signal, low frequency model of the converter is used as the basis of the voltage control design, deriving the converter transfer function from a balance of the instantaneous power at the converter input to the instantaneous power delivered to the output of the converter and considering a small perturbation of the input currents, in the dq0 plane, applied at the nominal full-load operating point.

$$(8) \qquad G(s) = \Delta V_{tank\_avg}(s) / \Delta I_d(s)$$

$$(9) \qquad G(s) = \frac{-\frac{3}{2} L_s I_d^* s + (\frac{3}{2} V_d - 3R_s I_d^*)}{C_{eq} V_{tank\_avg}^* s + \frac{2V_{tank\_avg}^*}{R_{eq}}}$$

This is a fairly common initial approach to the design of a converter controller, but in this case it has two potential problems that affect the converter's performance. Firstly, by inspection it can be seen that, if R_{eq}, which is essentially the load resistance, increases, the open loop pole, moves closer to the origin of the s-plane. There is a risk that the complex closed loop poles, which from the compensated root locus design were placed in the left half of the s-plane, will move towards the right half plane as the load varies and hence, the system will become unstable. Secondly, V_{tank_avg} will be derived from the measurement of

the peak tank voltage and the measurement circuit will have some dynamics that must be taken into account in the controller design. This aspect is dealt with further in Chapter 7.

The benefits of power electronic converters come from their flexibility to operate over a wide range of loads and conditions. Hence their design and operation is not normally restricted to a small region close to a fixed point, such as full load. Therefore, the PI controller designed at full load must be sufficiently robust to meet practical applications and realistic load conditions.

Power converters, that are not robustly designed, are well known to have stability problems, particularly when lightly loaded. The following analysis demonstrates the stability problem and evaluates the value of the load resistance that would cause unstable operation.

For ease of analysis, the uncompensated open loop converter transfer function is depicted as (gain, pole, zero designations):

$$G(s) = K_0 \frac{(s+a)}{(s+p)}$$

The values for K_0, a, p are teken from [45], i.e.:

K_0 = *-46.79*

a = *-9251.70*

p = *13,333.52*

Using the transfer function $G(s) = -46.79 \frac{(s-9251.7)}{(s+13{,}333.52)}$, the PI controller can be then designed using MATLAB® SISOTOOL feature, with traditional design requirements of damping factor ξ=0.7 and a cut-off frequency f_n =500 Hz. The resulting coefficients were:

Kp = 0.002, (proportional)

Ki = 100, (Integral)

The PI controller transfer function is:

(10) $$G_c(s) = K_p\,(s + \frac{K_i}{K_p}) / s$$

The compensated open loop transfer function is:

(11) $$Gol(s) = G_c(s)\,G(s)$$

(12) $$Gol(s) = K_0\,\frac{(s+a)}{(s+p)} \times K_p\,\frac{(s + K_i/K_p)}{s}$$

(13) $$Gol(s) = K_0 K_p\,\frac{(s+a)(s + K_i/K_p)}{s(s+p)}$$

And the closed loop transfer function is given by:

(14) $$T(s) = \frac{G_c(s)\,G(s)}{1+G_c(s)\,G(s)} \; or \; \frac{Gol(s)}{1+Gol(s)}$$

(15) $$T(s) = \frac{K_0 K_p\,(s + K_i/K_p)\,(s+a)}{s\,(s+p) + K_0 K_p\,(s + K_i/K_p)\,(s+a)}$$

Re-arranging coefficients:

(16) $$T(s) = \frac{K_0 K_p\,(s + K_i/K_p)(s+a)}{(1+K_0 K_p)\,(s^2 + (\frac{p + K_0 K_i + K_0 K_p a}{1+K_0 K_p})\,s + \frac{a K_0 K_i}{1+K_0 K_p})}$$

Thus, the point of marginal stability occurs when:

(17) $$(p + K_0 K_i + K_0 K_p a) = 0$$

Substituting in the values from above gives:

(18) $$p = -865 \cdot 774 + 4679$$

(19) $$p = 3813 \cdot 226$$

However:

$$p = \frac{2V^*_{\tan k\_avg}}{R_{eq}C_{eq}V^*_{\tan k\_avg}}$$

And thus:

$$R_{eq} = \frac{2V^*_{\tan k\_avg}}{pC_{eq}V^*_{\tan k\_avg}}$$

Using the afore mentioned :

$C_{eq} = 1.85\mu F$

$R_{eq} = \frac{8R_L}{\pi^2} ohms$

gives

$R_{eq} = 2/3813.226 \times 1.85 \times 10^{-6} ohms$

$R_{eq} = 283.35 ohms$

while $R_L = 349 \cdot 57 ohms$.

Thus, load resistances greater than 350 ohms may result in unstable operation. Compared to the full load resistance of 100 ohms, this result is approximately 28% of full load and well within the normal range of operation of the converter and would be an unacceptable restriction of performance. This system, with an expected wide range of loads, may not be considered adequately robust.

5.3. Additional analysis

5.3.1 Effect on gain and the position of the zero

The load resistance changes in the transfer function produce a pole movement towards the origin of the s-plane, i.e. towards a pure integrator. Further examination of the converter voltage transfer function reveals that when a change in load resistance occurs, a change in supply current I_d also occurs simultaneously, leading to a change of system gain and system zero position. The position of the zero is in the right half of the s-plane and thus defines the system as non-minimum phase. The load resistance increases (towards a light

load), and I_d reduces, hence the system gain also falls towards zero. The position of the system zero moves away from the s-plane axis towards infinity as the load resistance increases. The reduction in gain helps to stabilise the system at light loads but the effect of the zero moving increases the speed of the system and hence increases the likelyhood for an oscillatory response to a step change of input. The combined effects of the pole, gain and zero changes on the stability and performance of the converter may be seen by examining the uncompensated frequency response, Figure 12, for a range of converter loads. The controller gains remain unchanged from those determined at the 100 % load design point, that is, the plant transfer function changes as R_L changes from 50 to 1000 Ω but the controller gains remain constant.

The pole and zero movements are clearly seen in magnitude response, Figure 12, which gives, at 50 Ω, the asymptotic break frequency of the system zero at 3 krads/s and the pole at 30 krads/s. These move to 100 krads/s and 1.2 krads/s respectively at 1 kΩ load with 25 dB increase in low frequency gain and a similar decrease in high frequency gain. At 1 kΩ load the system response is similar to an integrator so that when the control loop is closed with a PI controller, the closed loop system now has a double integrator response, the classical configuration of an oscillator.

Although the magnitude responses are always positive, never crossing the 0 dB line, and would normally indicate an infinite phase margin, in practise, the phase changes caused by the movement of positive zero in the system are difficult conditions for the design of a classical PI controller. From the step response plots, Figure 13, the system remains stable, but oscillatory, largely due to the reduction in gain, effected by a reduction in input current I_d associated with the change in load. However, the system performance becomes increasingly degraded and oscillatory such that it no longer meets the original settling time requirement. It can then be claimed that, relative to achieving the specification, the system is not classified as robust and hence leads to a need for further system robustness.

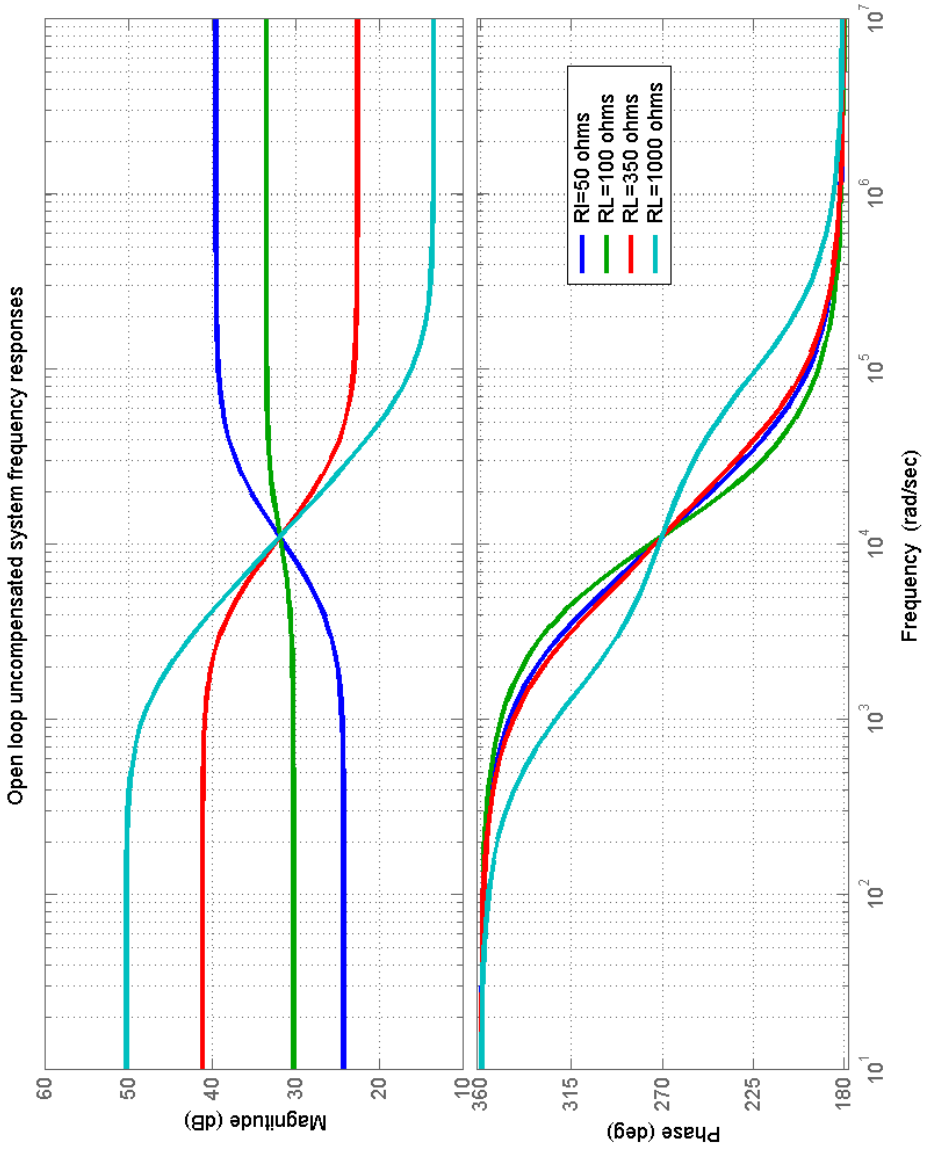

Figure 12 Uncompensated system frequency responses with variation of R_L

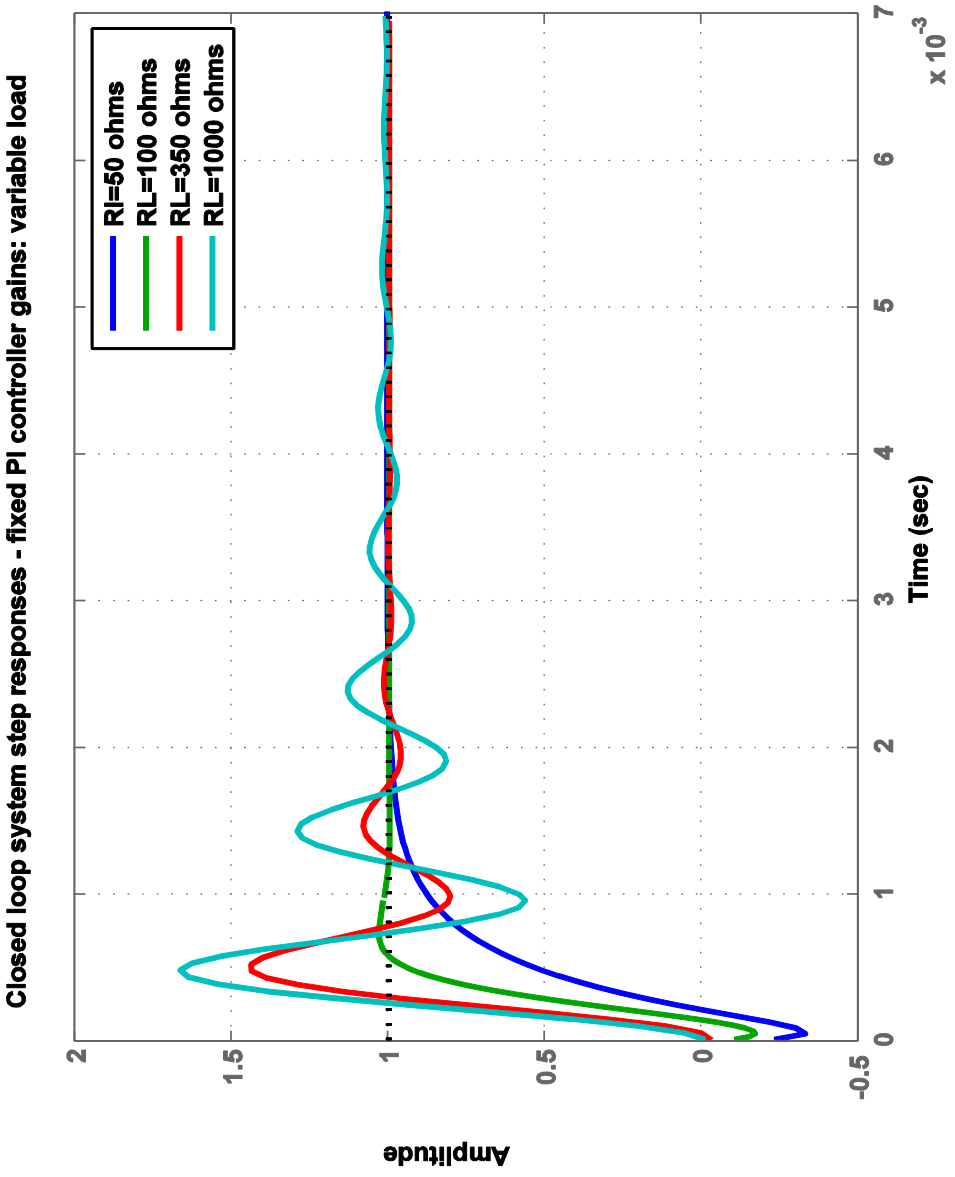

Figure 13 System step responses: R_L 50 – 1000 ohms

5.3.2 Sensitivity analysis

Another approach to the analysis of robustness is to consider the variations in the system sensitivity. The sensitivity of a control system to parameter changes is of high importance and a prime advantage of closed loop systems is their ability to the system sensitivity. The closed loop transfer function, *T(s)* of the system *G(s)* with feedback *K(s)*, , is given by:

(20) $$T(s) = \frac{G(s)}{1 + GK(s)}$$

Thus, if $GK(s) \gg 1$, then $T(s) = {}^{1}/_{H(s)}$ and is insensitive to changes in *G(s)*.

System sensitivity is defined as the ratio of the change in the system transfer function to the change of a process transfer function (or parameter) for a small incremental change,[57]:

(21) $$S_G^T = \frac{1}{1 + GK(s)}$$

but, *GK(s) =Gol*

from Equation (13), $Gol = K_0 K_p \frac{(s+a)(s+K_i/K_p)}{s(s+p)}$

(22) $$S_G^T = \frac{1}{1 + K_0 K_p \frac{(s+a)(s+K_i/K_p)}{s(s+p)}}$$

(23) $$S_G^T = \frac{s(s+p)}{s(s+p) + K_0 K_p (s+a)(s+K_i/K_p)}$$

(24) $$S_G^T = \frac{s(s+p)}{s(s+p) + K_0 K_p (s+a)(s+K_i/K_p)}$$

(25) $$S_G^T = \frac{s^2 + 1.333 \times 10^4}{(1 + K_0 K_p) s^2 + (p + K_0 K_p (a + K_i/K_p)) s + a K_0 K_i}$$

$$(26) \quad S_G^T = \frac{s^2 + 1.333 \times 10^4}{0.9064\ s^2 + 9250\ \ s + 4.329 \times 10^7}$$

Note that the system sensitivity *S* may be reduced by increasing the value of *GK(s)* over the frequencies of interest. A Bode plot of $20\log|S_{(j\omega)}|$ is shown in Figure 14. Where $|S_{j\omega}| < 1$ feedback control will improve performance in terms of reducing |error|.

From Figure 14 we can see that at low frequencies, up to 3.38 krads/s, the gain is less than 1 and therefore a feedback system will attenuate these frequencies. At frequencies greater than 3.38 krads/s the gain is greater than 1 and therefore signals, particularly high frequency noise will be amplified. A peak of 4.09 dBs occurs at 7.85 krads/s and this may be particularly troublesome as it is within the range of harmonic signals expected at the converter input.

Therefore, the peak of the sensitivity response in, max $|S_{j\omega}|$, is a measure of the worst-case performance degradation, or a measure of robustness, but for both stability and performance max $|S_{j\omega}|$ should be close to or less than unity. It can then be claimed that, relative to achieving a sensitivity function less than 1, the system is not classified as robust and hence again shows the a need for further system robustness.

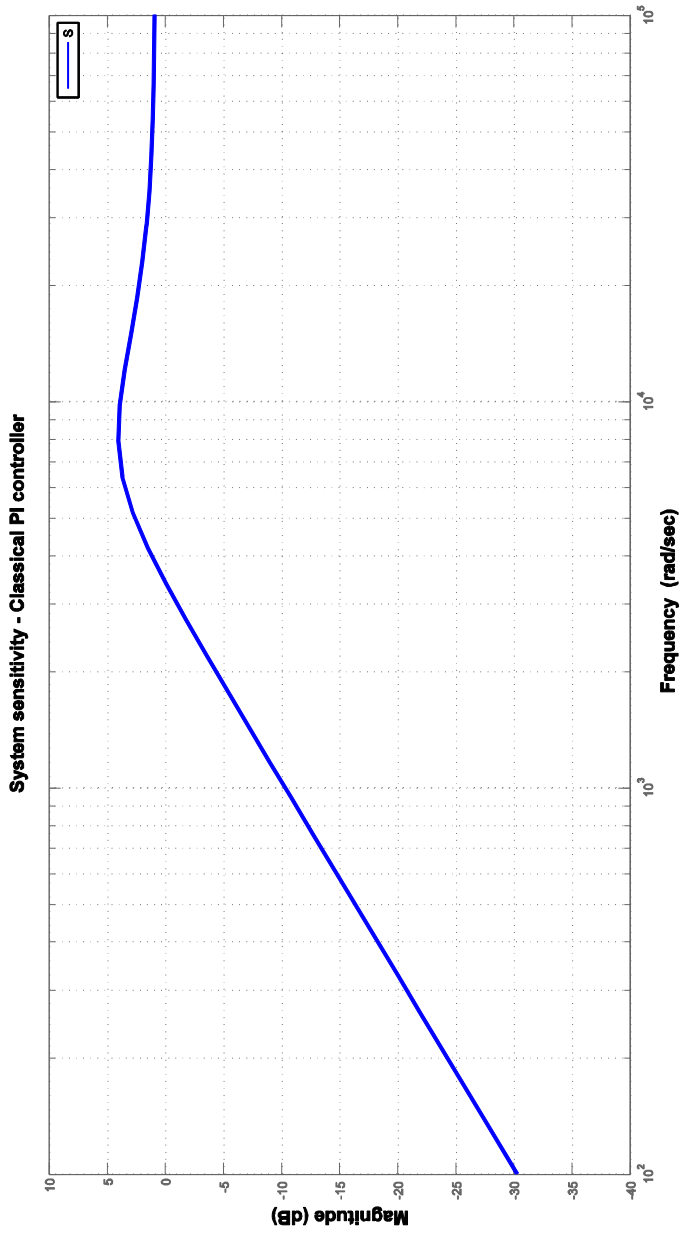

Figure 14 Sensitivity (Bode magnitude) plot

5.4. Summary

Analysis of the resonant converter voltage loop transfer function showed that instability could occur for loads above 350 Ω. A sensitivity analysis also indicated a lack of adequate robustness.

A linearised, small-signal, low frequency model of the converter is used as the basis for a classical PI design for the voltage control loop. The converter load is an uncertain quantity and is expected to vary between 10 and 110% in a random manner. The load resistance changes produce a pole movement towards the origin of the s-plane, i.e. towards a pure integrator; a change of system gain and a change system zero position in the right half of the s-plane (RHP). The nature of these changes means that the converter transfer function has variable and uncertain parameters and the analyses in this chapter demonstrated that the design of a classical PI controller with fixed gains was problematic and unlikely to result in a robust design.

The design of a robust controller using advanced control techniques is presented in Chapter 7.

Chapter 6.

Non-linear Converter Modelling and Simulation

"For comparison with scant experimental data, the use of a low order model produces a more reliable guide to system performance"[5]

6.1. Introduction

One of the aims of this project has been to understand and improve the control of the converter in order to facilitate its use when connected to a power network as an Active Transformer. Within the normal duration of study, the design and building of a demonstration Active Transformer would not have been practicable as it takes many years of development and testing before new equipment, even in demonstrator form, is permitted to be connected to the power network. Equally, to build a reasonable laboratory demonstration, a converter (rated at 150 kW, or greater, with some simple load to represent a grid connection) to verify controller action would not readily have been achievable within the period of research. A small laboratory model of the Active transformer, would also have taken too long to build and set to work and left insufficient time to verify controller action.

Modelling is a cost effective precursor to a practical demonstration of all high power converter designs and applications. The design of large converters follows an incremental process that starts with a simple computer model in order to explore design options and

[5] L.W. Taylor, "How complex should a model be?" Proceedings of JACC 1970, Session Paper 18D, page 441.

gain an overall appreciation of the design problems and constraints. Design issues associated with the scaling up of the Active Transformer are largely concerned with the power circuit layout and its physical construction, when such issues as:

i) voltage insulation
ii) voltage isolation
iii) stray inductance and capacitance
iv) timing and switching
v) ratings, losses and cooling
vi) component temperatures
vii) protection

become more significant. In the case of the Active Transformer, it was the performance of the control system that was to be investigated and this, at least in this early design stage, requires a simplified converter model. In the view of the author, it was more important to be able to compare the results of alternative controller models with published work than to address any scaling issues at this early stage in the development cycle.

The approach adopted in this project was achievable and thus the values of the principle power circuit components used are similar to those used in [45]: The principle component values are:

i) line inductors L1-L3 3.75 mH and 1mΩ in series
ii) resonant inductor La 84.4 µH and 1mΩ in series
iii) resonant capacitor C 0.75 µF
iv) full load resistance 100 ohms
v) 20 kHz transformer 1:1 turns ratio

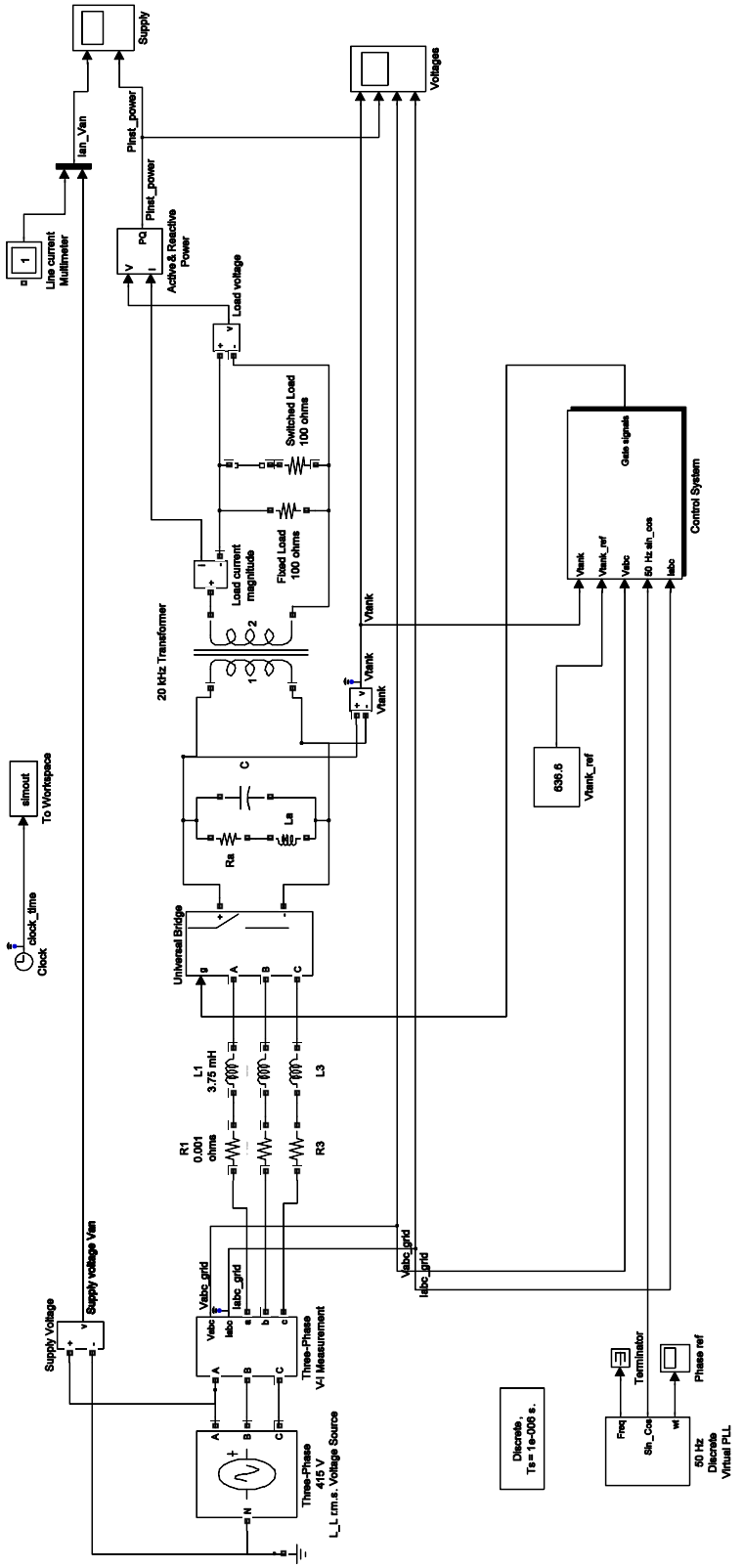

Figure 15 Simulink® converter model

6.2. Converter design

A schematic diagram of the supply converter is shown in Figure 15. Key design variables are the bridge model, tank circuit voltage and the supply current ripple.

6.2.1 Bridge model

Simulink® offers a selection of bridge models, including some containing detailed power semiconductor device models. At this stage in the development process, a sophisticated converter model using SiC power devices, assuming that they were available, was unnecessary and would not have been helpful in understanding the operation of an Active Transformer. A simple functional, lossless model was all that was needed to explore control issues and therefore a universal bridge model, containing ideal switches, was chosen.

6.2.2 Tank circuit

The tank circuit provides a means of storing energy in a similar manner to the capacitors in a d.c. link converter. As with the d.c. link voltage, a design aim is to maintain the tank voltage constant. The resonant circuit is normally a lossy device and with high Quality factors (Q) comes high resonant circulating currents, approximately Q×load current. It is therefore important to keep Q, hence the tank losses, as low as practicable in order to have high converter efficiency. Q must also be high to store sufficient energy to maintain robust oscillation. Thus there is a balance to be achieved between converter efficiency and tank voltage robustness. The tank circuit component values were calculated using the standard formulae for a parallel resonant circuit with a load resistance defined at the maximum rating of the converter. A reasonable balance was achieved with Q = 10, and hence L_{tank} = 84.4 µH and C_{tank} = 0.75 µF. The inductance has been assigned a small resistive element, 1 mΩ, to avoid numerical errors in the simulation.

The mean tank circuit voltage must be sufficiently high in order to control the input current. If the tank voltage is much smaller or insufficiently greater than the instantaneous line voltage then the line currents will increase uncontrollably. If the tank voltage is

sufficiently higher than the instantaneous line voltage then the line currents can be controlled. To satisfy this requirement the mean tank voltage must therefore satisfy the condition:

(27) $\frac{2}{\pi} \times V_{tank\_max} \geq V_s$

(28) $V_{tank\_max} \geq \frac{\pi}{2} V_s$

therefore:

(29) $\frac{V_s}{V_{tank\_max}} \geq \frac{2}{\pi}$

where V_{Tank_max} is the peak voltage between the tank circuit and the supply neutral and V_s is the peak phase voltage of the line-to-line supply voltage. For a three phase supply voltage of 415 v_{rms} line-to-line, the tank voltage must be greater or equal to 921.9 volts peak. 1000 V_{peak} was therefore chosen as the nominal operating point for the converter.

6.2.3 Current ripple

Power quality may be adversely affected by switching power converters connected to it and converter designers usually have to meet a ripple current requirement specification for converters connected to a power supply or network. Line current ripple is caused by the converter switching action and will occur at the tank resonant frequency. As this is quite a high frequency it should be quickly attenuated by the supply capacitance or line filters. From the circuit shown in Figure 15, the current through the input inductors is given by the equation [45]:

(30) $di_s/_{dt} = \frac{1}{L_s}\left(v_s \pm KV_{tank\_max} \sin \omega_1 t\right)$

where i_s is the line current, L_s is the line inductance, ω_1 is the tank circuit resonant frequency, $\underline{v_s}$ is the instantaneous supply phase voltage, K is the switching coefficient (see Table 2) and V_{tank_max} is the peak tank voltage

The peak current occurs when:

(31) $\frac{di_s}{dt} = 0\,, \quad i.e.\ when\ v_s = \pm KV_{tank\_max} \sin \omega_1 t$

Figure 16 shows the waveforms of the 50 Hz line current, *I*, at an arbitrary time when the source voltage is not zero and for the duration of a half cycle of the tank voltage, may be assumed to be a constant. t_1 and t_2 are the times of the maximum/minimum ripple on the line current.

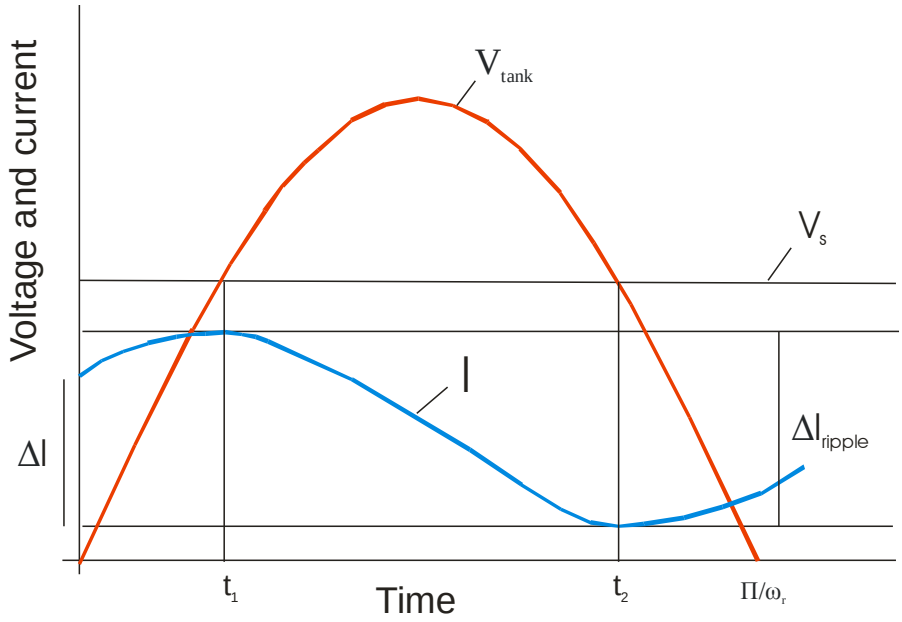

Figure 16 Ripple in line current

For the condition when the switching coefficient is zero, *K=0*, i.e. when the input inductors are shorted together by the switching action, Table 2 switch states 7 and 8, integrating *(30)* over a half cycle, *t*, of the tank circuit voltage, gives the change in line current, Δi_s:

(32) $\Delta i_s = \frac{1}{L_s} \int_0^{\pi/\omega_1} V_s \, dt$

(33) $\Delta i_s = \frac{\pi}{\omega_1 L_s} v_s$

Therefore, evaluating the ripple current for the converter design in [45], for example, with a line voltage of 300 V gives:

(34) $\Delta i_s = 2\,A$

Thus, the line currents will increase at the rate of 80 mA/µs.

For other switch states when $K \neq 0$ the change in line current, Δi_s is given by:

$$(35) \quad \Delta i_s = \frac{-KV_{tank\_max}}{\omega_1 L_s} \left\{ \pi \left({}^{-V_s}/_{KV_{tank\_max}} \right) \left[1 - \frac{2}{\pi} \arcsin\left({}^{-V_s}/_{KV_{tank\_max}} \right) - 2\sqrt{1 - \left({}^{V_s}/_{KV_{tank\_max}} \right)^2} \right] \right\}$$

The results of plotting Δi_s for variations in line voltage are shown in Figure 17. The magnitude of the maximum input current ripple was found to be approximately 2.8 A.

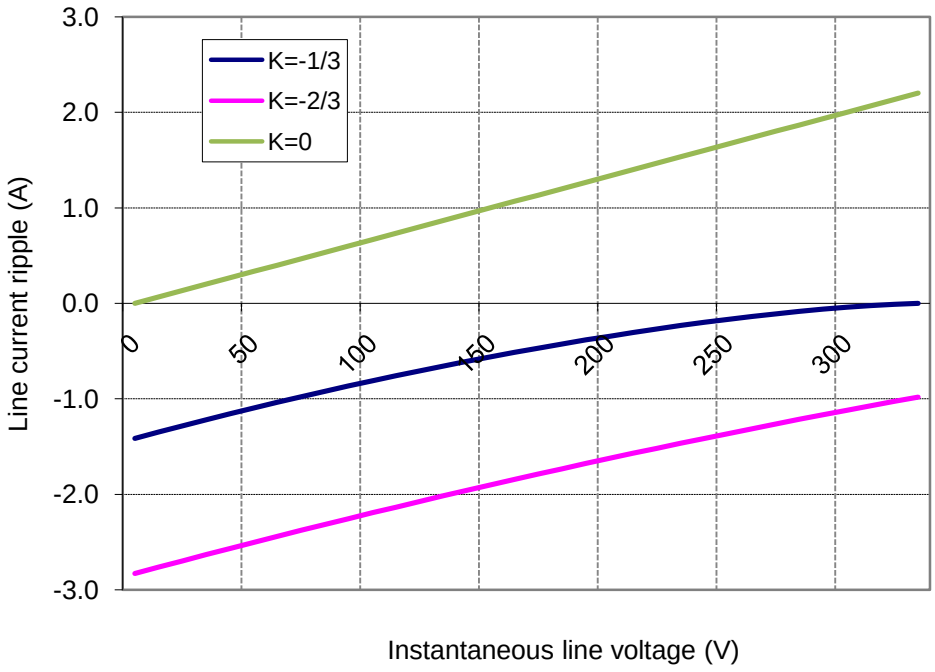

Figure 17 Line ripple current variation with line voltage

6.3. The Simulink® converter model

The Simulink® converter model is shown in Figure 15. It was intended to be quite flexible in its design to facilitate the creation of alternative designs. Considerable use was made of the Simulink® Scope and of other monitoring facilities to verify intended operation of the converter design. The component values and the controller coefficients are derived from

the MATLAB® workspace after the running of an m-file that declares or calculates their values. The central features of the model are:

i) a universal bridge
ii) inductors in the 3-phase supply lines
iii) a resonant circuit at the bridge output
iv) the converter control system.

The converter was current fed and controlled to directly convert the 3-phase 415 V supply to a single phase, 1000 V output at 20 kHz into a resistive load.

The control system model is shown in Figure 18. It consists of four subsystems:

i) voltage maximum detection. This subsystem model detects the time and level of the peak of the 20 kHz converter output voltage.
ii) converter output voltage control. The subsystem provides either PI (discussed in Chapter 5) or $\mathscr{H}_\infty$ control (an alternative controller design discussed in Chapter 7), selectable prior to running a simulation. It produces a reference supply current for the current controller from the mean level of the converter output voltage.
iii) supply current control. This subsystem calculates the supply current at the end of the next half cycle of the converter output for each of the seven possible converter bridge switch combinations. These values are then compared with the current reference produced by the voltage controller to give an error signal. The error signals are weighted by an error squared cost function.
iv) switch vector selector. The selector model finds the switch combination that gives the minimum weighted error and enables the appropriate converter bridge switches ready for the next commutation at a zero crossing of the converter output voltage.

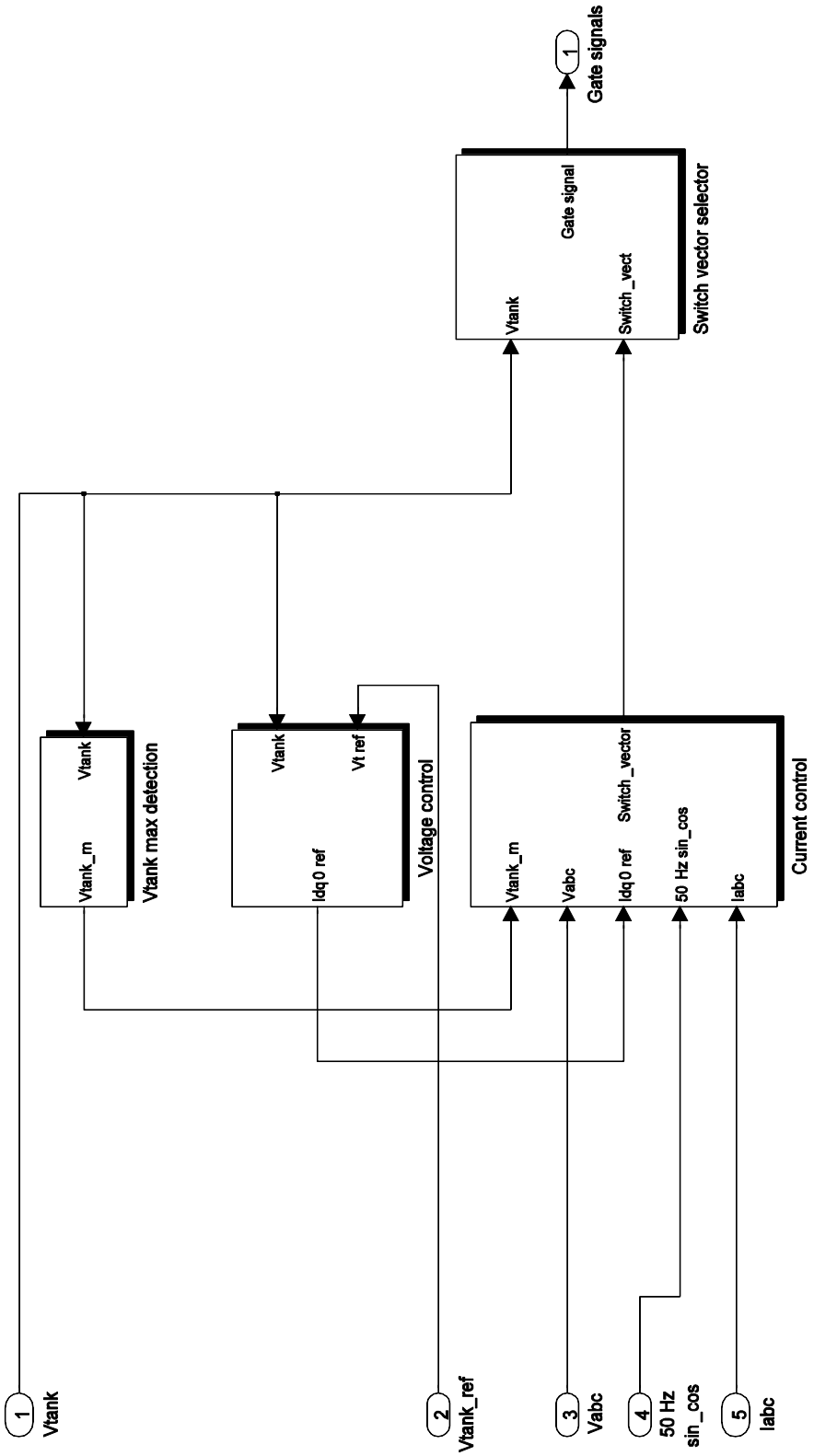

Figure 18 Simulink® control system model

6.3.1 Voltage maximum detection

The voltage maximum detection model is shown in Figure 19. Both positive and negative peaks of the 20 kHz converter output voltage, $V_{tank,}$ are detected by this model by comparing the relative values of consecutive samples of the output voltage. Maximum and minimum running sample measurements are triggered by a zero crossing of the output voltage. When triggered by the appropriate peak detection signal the peak measurements are fixed for half a cycle. A switch and control logic combine the maximum and minimum peak levels to form a composite signal consisting of peak voltages each constant for half a cycle of the converter output.

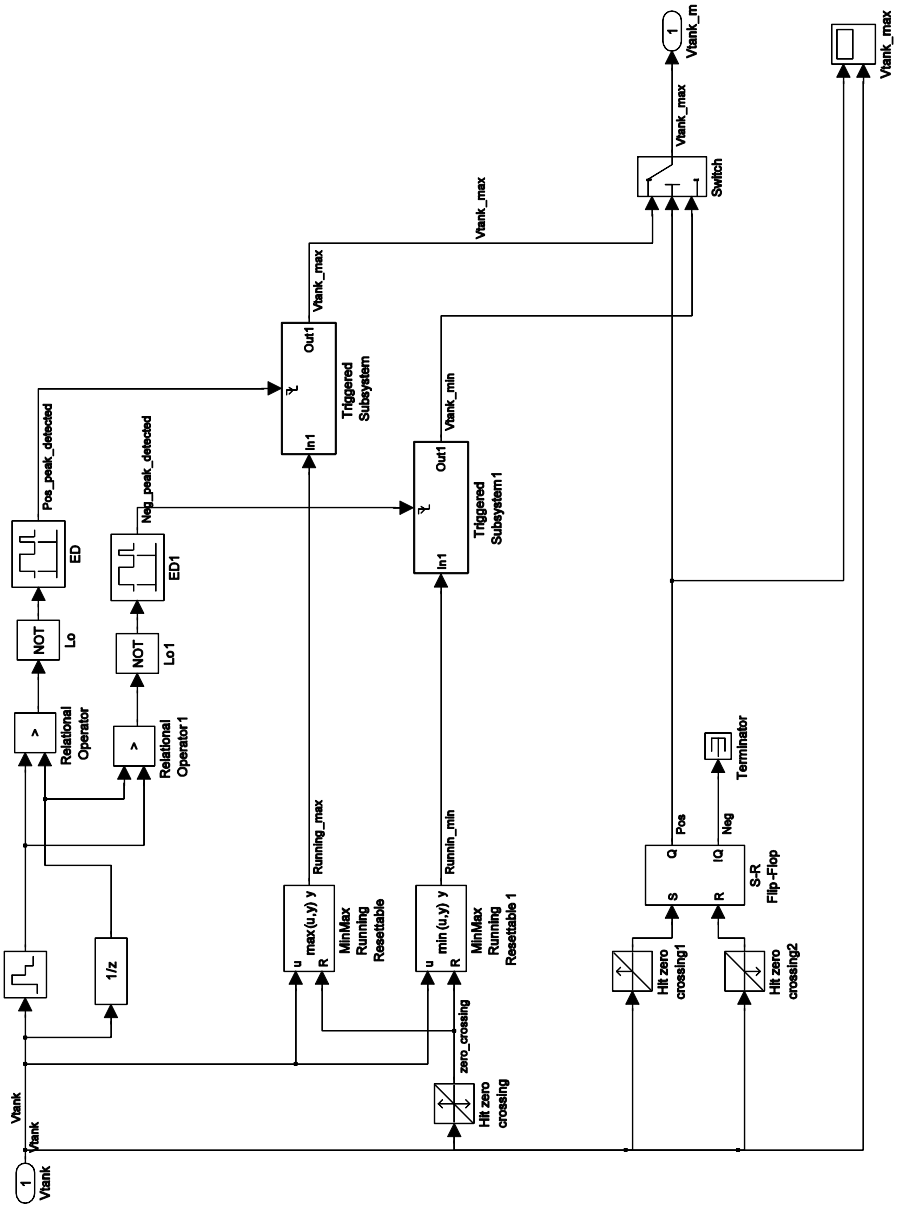

Figure 19 Voltage maximum detection

6.3.2 Voltage control system

The converter output voltage is a 1000 V peak, 20 kHz sinusoid. The voltage control aims to keep the mean of the peak output voltage constant by controlling the value of the reference for direct current i_d and details of the voltage control model are shown in Figure 20. The reference value of I_q and I_0 are set to zero. The I_q reference is intended to control the phase between supply voltage and current in a similar manner to id, but has not been implemented in this work. For a balanced three-phase system I_0 is zero.

The modulus of the converter output, $V_{tank,}$ is passed through a low pass filter to derive the mean level of the output voltage. It is then compared to the reference voltage, V_{tref}, to produce an error signal for input to the PI or $\mathcal{H}_\infty$ controller. The design of these controllers was produced off-line prior to running a simulation.

For convenience of comparing results, the voltage control model allows the manual selection of either PI or $\mathcal{H}_\infty$ control prior to running a simulation. The transfer functions are derived from the MATLAB® workspace. [The PI voltage controller is a Simulink® implementation of the analysis previous shown in section 5.2.2 and the $\mathcal{H}_\infty$ controller is an implementation of the designs developed in Chapter 7].

The output of the voltage control model is replicated seven times to provide an individual reference for each channel in the current controller model.

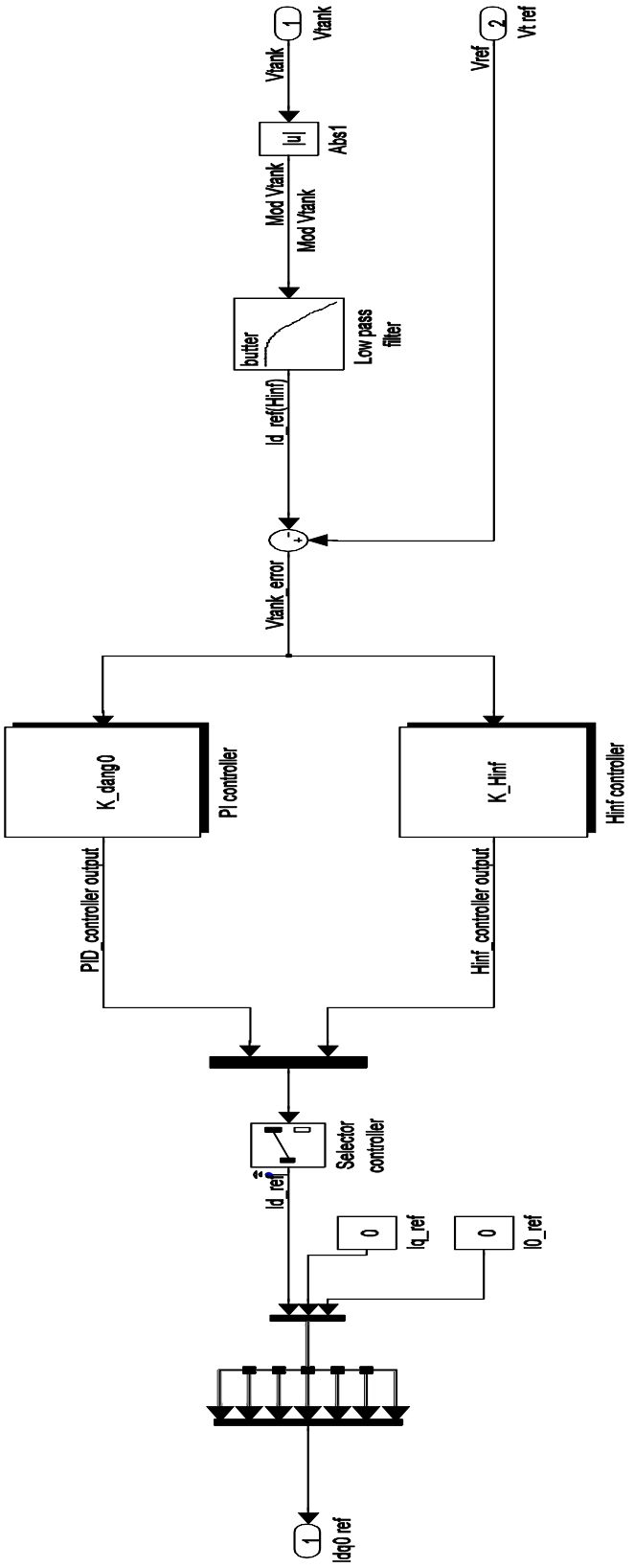

Figure 20 Voltage control model

6.3.3 Predictive current control system

6.3.3.1 Background

Predictive current control as used in the resonant converter is a form of sliding mode control and some further background to this technique is presented. The choice of sliding mode current control for a direct matrix converter is rather an intuitive one. It meets the usual desires for robustness and stability, but because the converter has only seven switch states, choosing the one that takes the controlled variable, in this case, line current, closest to the desired reference value is a very simple control objective to implement. In the design of power converters, simplicity is often a great advantage. However, a disadvantage is the level of ripple in the chosen variable, but this can usually be set at an acceptable level by appropriate design.

The term "geometric" is often related to "sliding mode" in control systems literature [58] as a method of controlling non-linear systems by imposing defined system states by specific switching action. The similarity in power electronic systems can be seen as the way in which the switching interacts with the system states. For example, switch states are changed as voltages or currents cross zero, or when a reference voltage crosses a triangular waveform in pulse width or phase modulation schemes. This action is also referred to as "boundary control" and can be seen in operation in early gunnery control systems, where a system of coarse/fine change-over as tracking errors reach set boundaries was used in naval gun target tracking and stabilisation systems.

Hysteresis control is another form of boundary control and often applied to the control of power converters. In hysteresis control, boundaries are usually expressed in terms of a single state variable or system output, and control effected by maintaining the variable between two, narrowly separated limits by on-off or bang-bang control. In effect, hysteresis control can eliminate output variations other than the ripple caused by the control dead-band and is therefore a robust means of control. Most boundary control systems are robust to system uncertainty and provide an immediate response to a system disturbance.

Hysteresis control is a special case of boundary control employing a single state variable. In general, any number of states or combinations of states and boundaries can be used for control. Boundary control uses the ideas of structures in state space with one less dimension than the number of states. So for a two state system, such as the resonant converter, the peak level of the output voltage is a system boundary. For a system with more than two states, the boundary becomes a switching surface.

When studying boundary control it is useful to consider the state trajectories as they cross a boundary. There are three possibilities:

i) refractive - states evolve in a new direction when they cross the boundary
ii) reflective - states are redirected back to the boundary when they cross the boundary
iii) rejective - on both sides, states evolve away from the boundary.

In the reflective case, the system reverses direction when a boundary is reached. This action leads to "chatter" and the system is constrained to move along the boundary thus defining a "sliding mode" as described in control literature. The reversing action of the direct converter at zero voltage crossing to maintain the tank circuit oscillating and in conjunction with the predictive current control justifies the description of a "sliding mode controller".

Academic groups in the former Soviet Union undertook early work on such systems. Discontinuous feedback control strategies first appeared under the name of variable-structure systems where the control inputs take values from a limited set of defined values. Based on these principles, sliding mode control was developed in a seminal paper by Utkin, [59]. The essential feature of this method is that a switching surface of the state space is chosen to meet the closed loop dynamic requirements. The main advantages are [60]:

i) its robustness against perturbations and uncertainties
ii) less information than classical control techniques

iii) the possibility of stabilising some non-linear systems that are not stabilised by continuous state feedback laws.

An example of converter control is described in [61], showing sliding motion and direct control of a full bridge boost converter. Here, periodic references were tracked and the unstable inductor current was independently regulated at a prescribed level. The results of simulation showed that the system was robust to changes of load.

6.3.3.2 Simulink current controller model

The current controller design is a Simulink® implementation of the analysis shown in Equation (7), which is repeated here for convenience.

$$(36) \quad \Delta I_i = \frac{1}{L_s \omega_r} \left(V_{in}\pi + 2K_i V_{tank\_m} \right); \quad i = A, B, C$$

The change in current through the input inductors, Δ_i, during the next half-cycle of the output voltage was evaluated for each possible switch state of the converter bridge. The results were then used to predict the average supply current for the next half cycle of the output voltage and compared to a reference current generated by the output voltage controller.

The current predictor model is shown in Figure 22. This model has inputs of:

i) Maximum tank voltage V_{tank_max}
ii) A matrix of coefficients derived from Table 2 for K_i
iii) Instantaneous value of the 3-phase supply voltage V_{abc_1}
iv) Instantaneous value of 3-phase supply current I_{abc_1}
v) A 50 Hz reference signal 50 Hz sin_cos

The model consists of seven similar channels that replicate the evaluation of ΔI_i, Equation (36), for each possible combination of the switches in the converter bridge circuit. A sub-matrix is selected providing the appropriate values $2K_iV_{tank\_max}$ for each channel to which is added the value of $V_{abc\_1} \times \pi$. The resulting value is multiplied by a constant derived from circuit component values to give the change in line current, ΔI_i. The change in current is

then added to the present supply current to give the predicted average 3-phase current during the next half cycle of the converter output voltage. The predicted 3-phase current in each channel is then transformed into the d-q plane by the dq-transform. The demanded or reference current in d-q form is subtracted from each channel output to create a predicted error signal, Figure 21. The seven possible predicted error signals are weighted by an error squared cost function Figure 23.

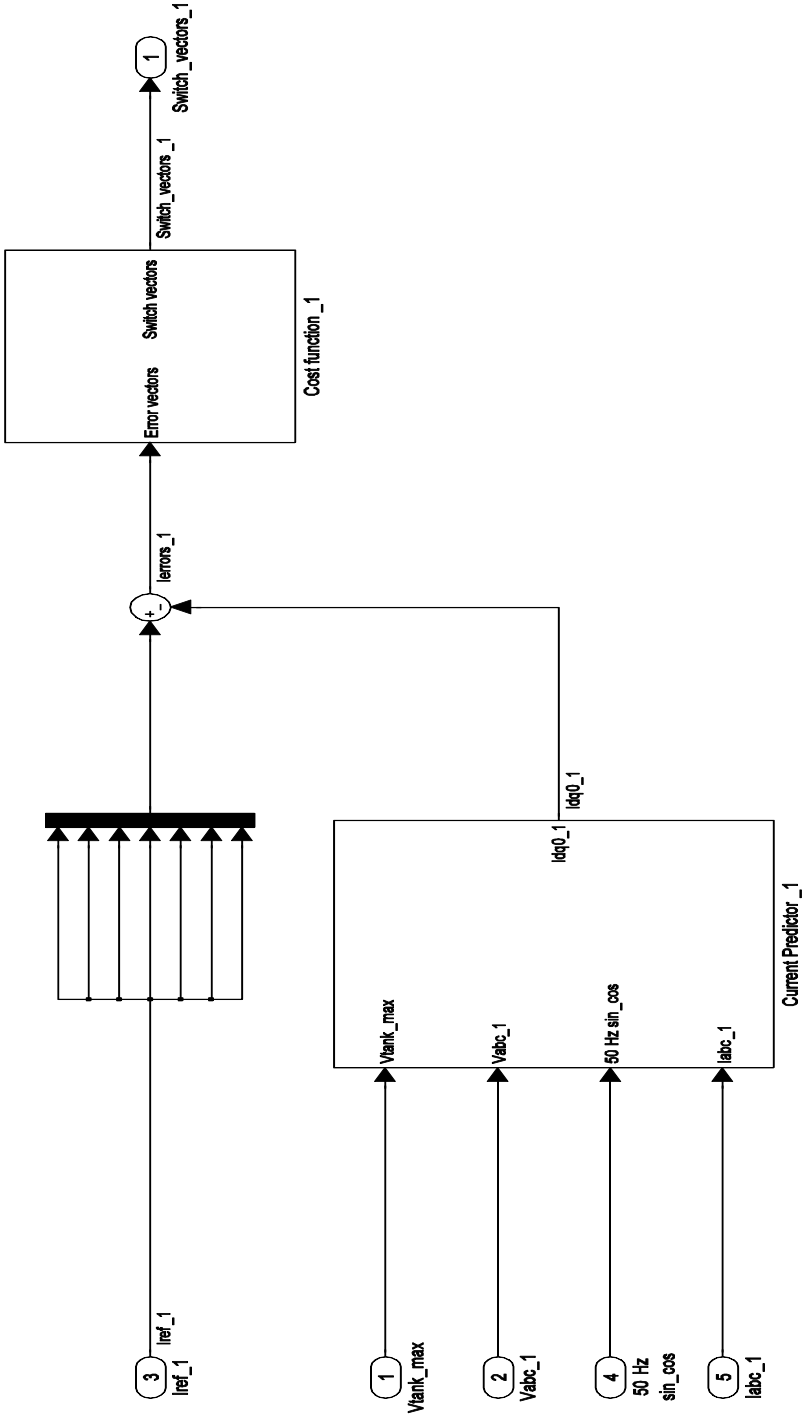

Figure 21 Current control

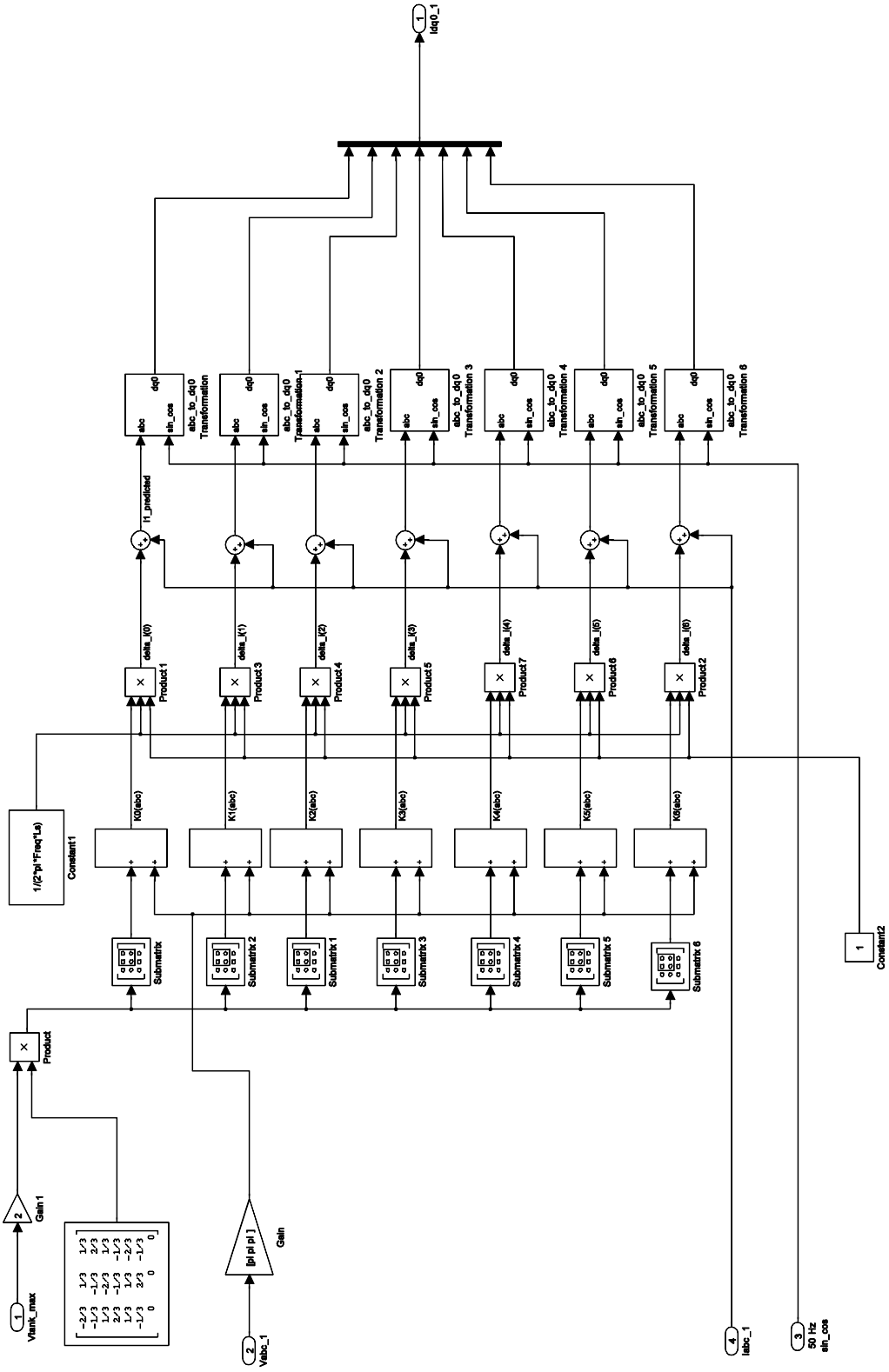

Figure 22 Block diagram of current predictor

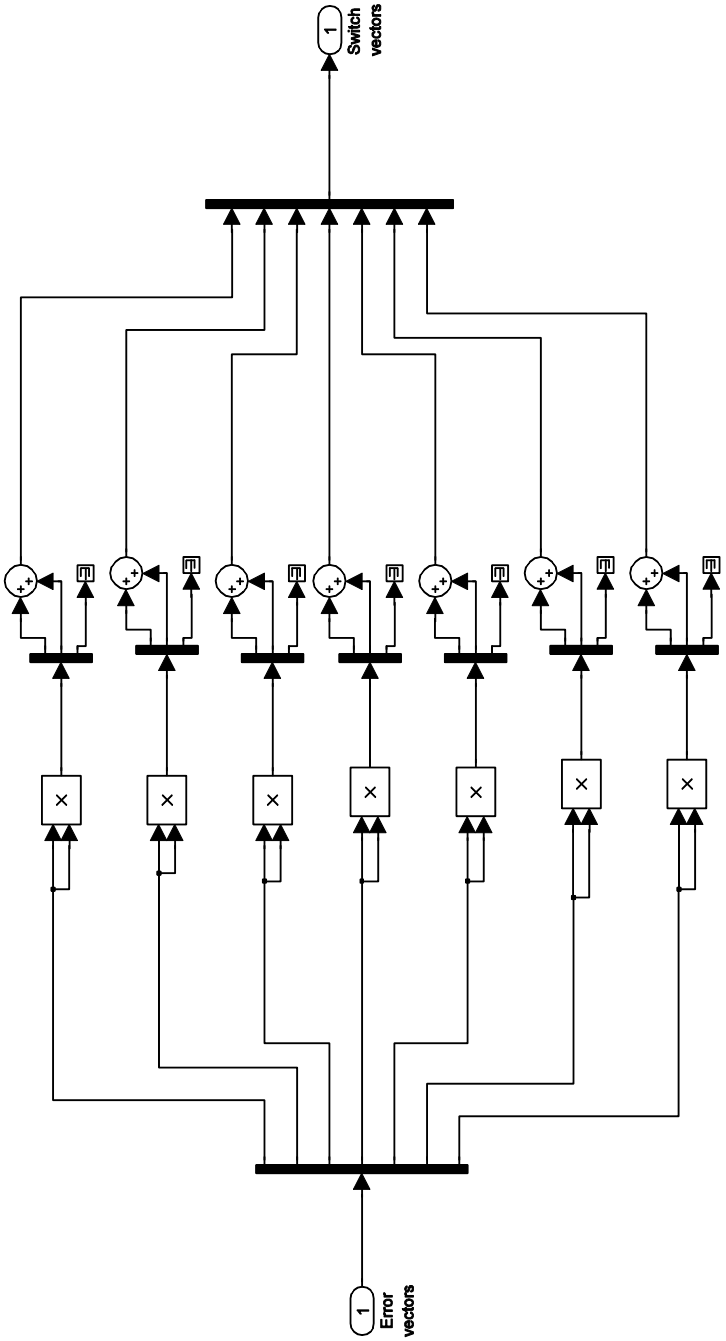

Figure 23 Logic to apply an error-squared cost function

6.3.4 Switch vector selector

The seven weighted error signals are evaluated by the switch selector model, Figure 24, to determine the channel that provides the minimum error. First, the minimum error is determined and fed to seven £relational operators" so that a logical "1" indicates where there is an equivalence of inputs and hence the channel with the minimum error. All other output will remain at a logical "0". The logical "1" output of the channel that has the minimum error is increased by a gain proportional to the channel number. At the next zero crossing of the tank voltage, V_{tank}. this channel number is used to select a pattern of switch states from a look up table that enables the appropriate converter bridge switches.

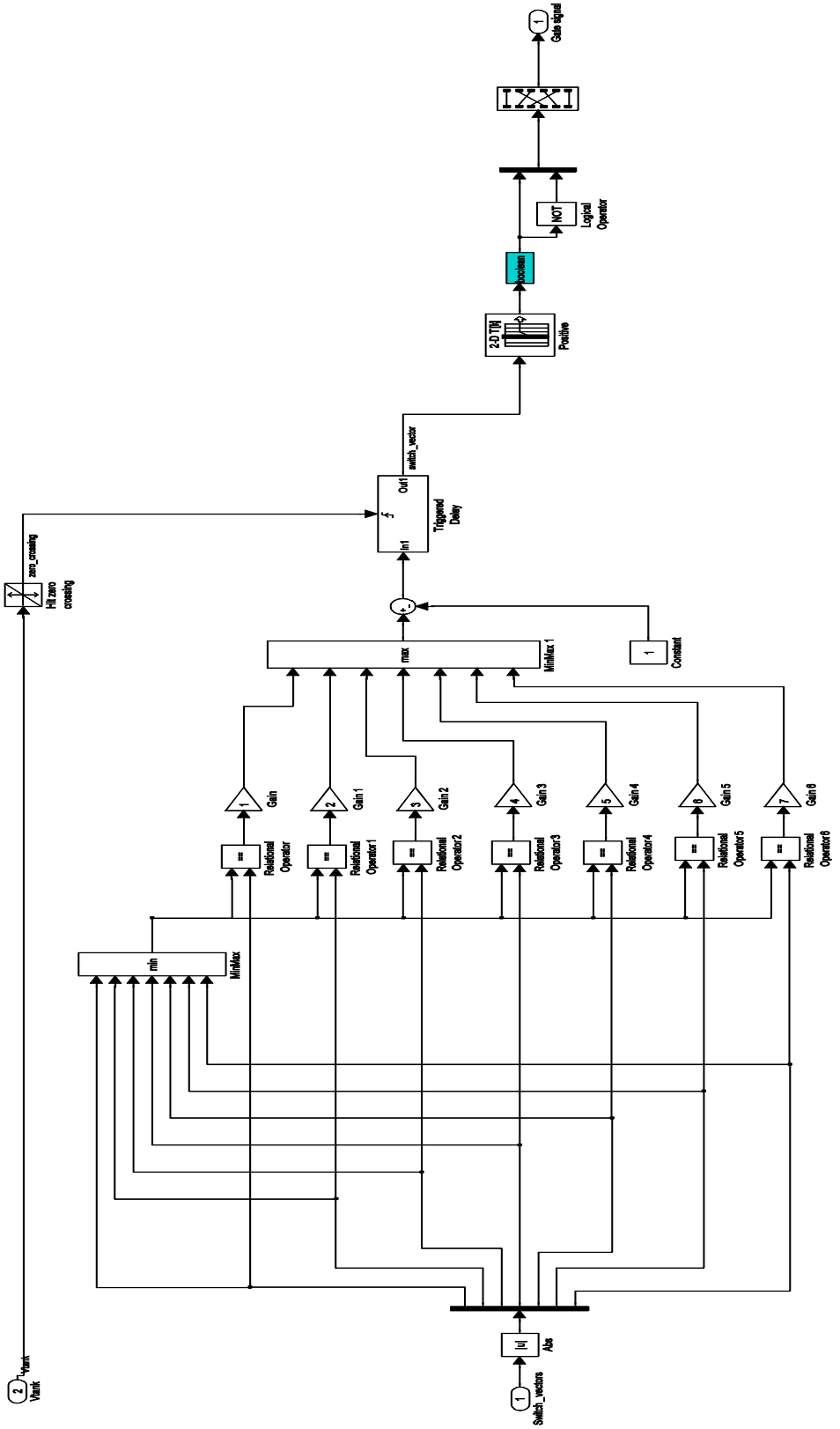

Figure 24 Switch vector selector

6.4. Simulation of converter operation

The aim of verification was to compare and contrast the results of the equivalent Simulink® converter model, using a classical PI controller, with the simulation test results in [45], for similar load and demand changes in configurations for:

i) current control only
ii) both voltage and current control.

The model supply voltage, output voltage demand and simulation parameters were set to:

i) simulation time, T_s, 1.0^{-6} s
ii) solver type Variable step
iii) solver ode23t

6.4.1 Test 1 Current control verification.

The design aim of the converter control is to maintain a steady tank voltage level and the input phase currents at a defined magnitude and phase related to the supply voltage. To verify the current controller operation a simulation without voltage control was first run for 80 ms duration. To facilitate this change the voltage control model, Figure 20, was replaced by a constant for the demanded line current.

The test simulations are described with reference to Figure 15. In this test the converter model is configured for forward mode operation with the following initial conditions set:

i) grid side generator line-line 415 V, 50 Hz
ii) line current demand12 A
iii) fixed load 100 Ω 150 Ω
iv) switched load cct. breaker closed, open at 50 ms
v) switched load 100 Ω 300 Ω

The simulation was run for 80 ms. At 50 ms a step change in load from 100 to 150Ω was introduced by opening the load circuit breaker thus increasing the load resistance to 150 Ω and increasing the load voltage while maintaining the load power. The results, showing the converter output voltage and 3-phase input currents, are shown below in Figure 25. The mean of V_{tank} peak is approximately 1100 volts and is consistent with a peak input current of 12 amps. An expanded view of the output voltage shows a sinusoidal waveform with a small amplitude difference between successive peaks. The variation is more evident in the full view where it appears as a ragged edge to the voltage peaks. It is caused by the errors in the predicted current and the limited options of voltage applied to the tank circuit. At the change of load, the load resistance is increased hence, as the converter current is expected to remain constant, the output voltage must increase to approximately 1300 V. The change in voltage is rapid and with not observable overshoot.

The three-phase grid current waveform also shows a high frequency ripple as a result of the switch of the converter bridge. The grid current signal could have been filtered to provide a cleaner waveform and one that made the measurement of the amplitude more straight forward, but the visibility of the ripple current was considered to be useful indication of the correct operation of the converter, hence retained, and the mean amplitude was estimated as 11.6 A, close to the demanded 12 A. This procedure is used consistently throughout this thesis.

These simulation results show good agreement with those from [45], which are shown in Figure 26 for comparison.

A plot of single phase input voltage and current, Figure 27, shows the voltage and current in phase and good agreement with the results from [45], which are shown in Figure 28 for comparison.

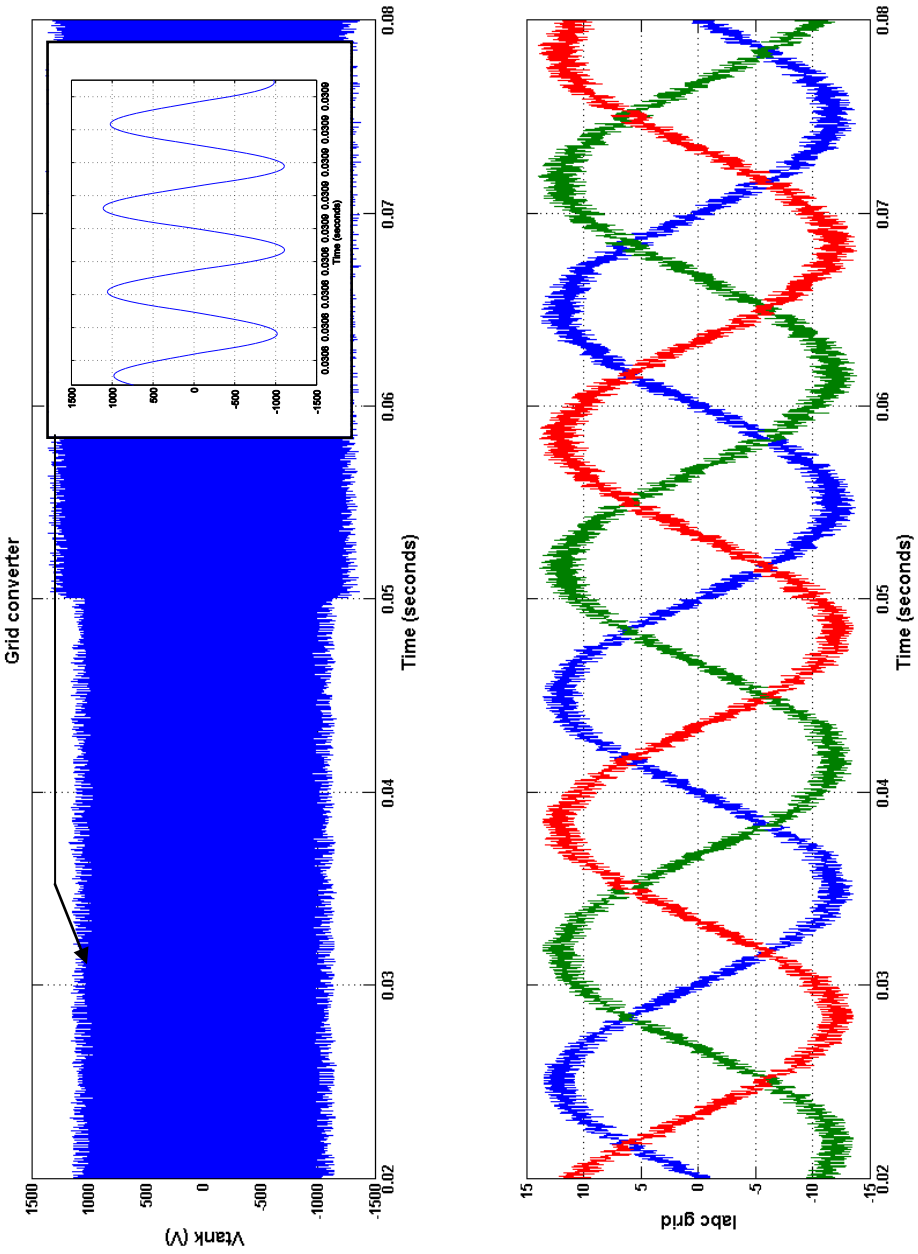

Figure 25 Simulink converter model tank voltage with predictive control only

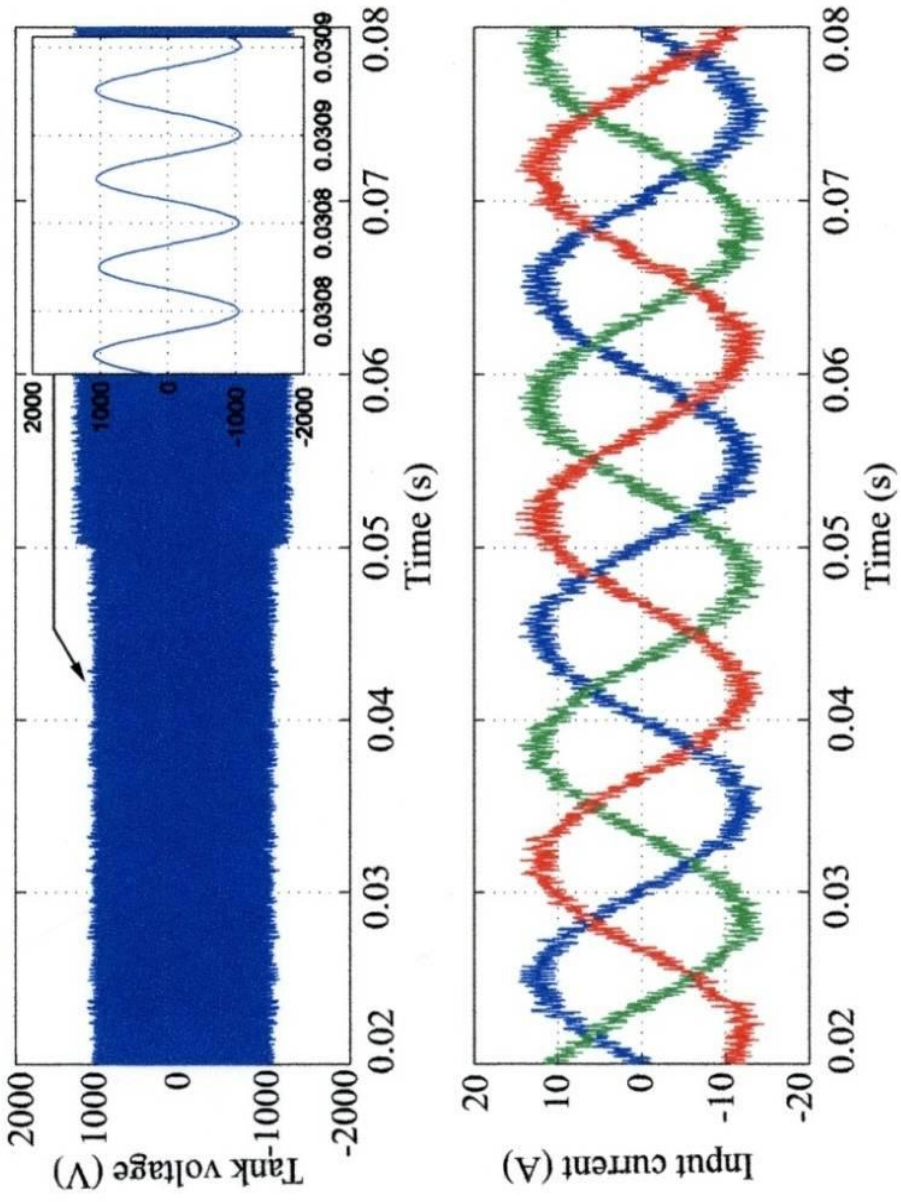

Figure 26 Converter input and output waveforms with predictive current control[6]

[6] [45] Figure 5.8 page 102.

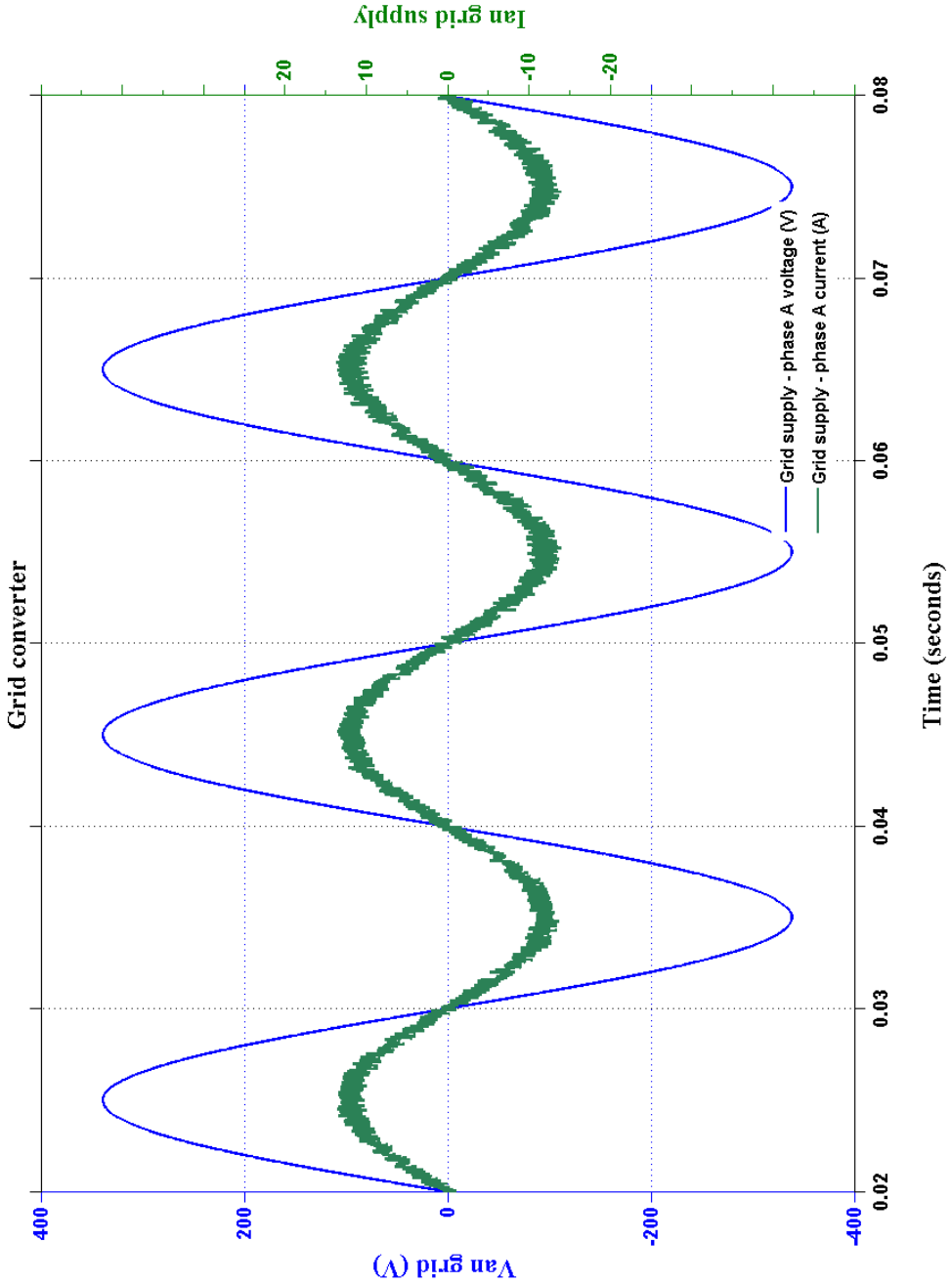

Figure 27 Simulink converter model: Phase A with predictive current control only

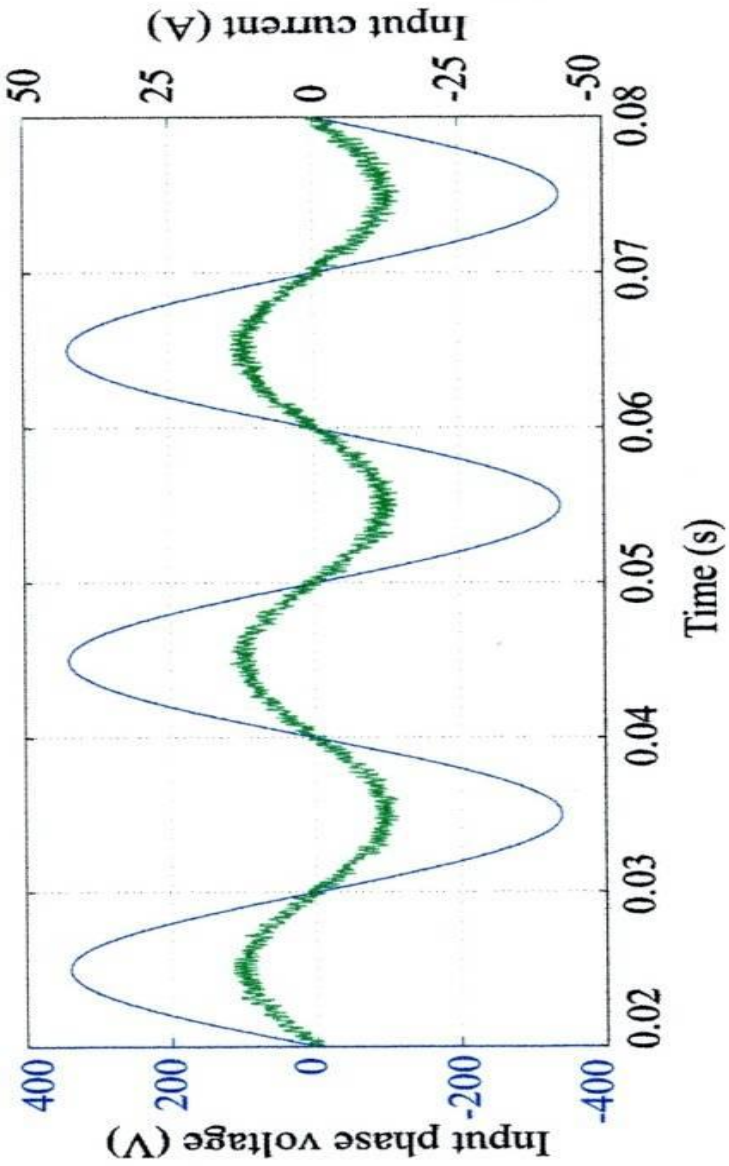

Figure 28 Unity displacement factor between input voltage and input current[7]

[7] [45] Figure 5.9 page 103.

6.4.2 Test 2 Voltage and current control

The second verification simulation used both line current control and output PI voltage control. PI voltage control was selected by "Selector controller " switch shown in the voltage control model, Figure 20. The PI control provides a demand current reference to current control so that the converter output voltage, V_{tank}, is kept close to a constant mean peak level.

The test simulations are described with reference to Figure 15. In this test the converter model is configured for forward mode operation with the following initial conditions set:

i) grid side generator line-line 415 V, 50 Hz
ii) Vtank_ref 636.6 V_{mean}
iii) fixed load 100 Ω 100 Ω
iv) switched load cct. breaker closed, open at 40 ms
v) switched load 100 Ω 100 Ω

First the simulation was run for approximately 40 ms then the load circuit breakers opens resulting in a step change of load, from 100 to 50 ohms. At approximately 80 ms, a manual change to the demanded output voltage, 636.6 to 826.8 V_{mean}, was made.

The results of the simulation are shown in Figure 29. They show good agreement with the results from [45], which are shown in Figure 30 for comparison. It is difficult to make accurate measurements from these traces therefore all measured values are treated as best approximations. The simulation starts from zero initial conditions and therefore the voltage and current variations in the first few mille-seconds of the results are numerical as a result of the start-up transient and are generally ignored. Up to 40 ms the V_{tank} trace shows good voltage control with the amplitude approximately 1069 V, a little higher than the demanded. At 40 ms the voltage trace dips to 930 V and then recovers to 1100 V without significant overshoot. A similar increase in voltage outcome is shown in the reference trace, Figure 29. The reason for this discrepancy is that the PI controller was designed for small perturbations around full load, but the change in load was large and therefore the controller is no longer operating at its design point.

On application of the step change in demand to 1300 V, the output voltage rises and overshoots to approximately 1535 V and recovers to 1488 V whereas the reference trace, Figure 29, is under-damped but has a similar change in final voltage possible due to additional damping introduced for the demonstration model.

However, these responses indicating that the Simulink® model was a reasonable representation of the results from the simulations and demonstration model given in [45] and would be the basis of comparisons for alternative controller designs.

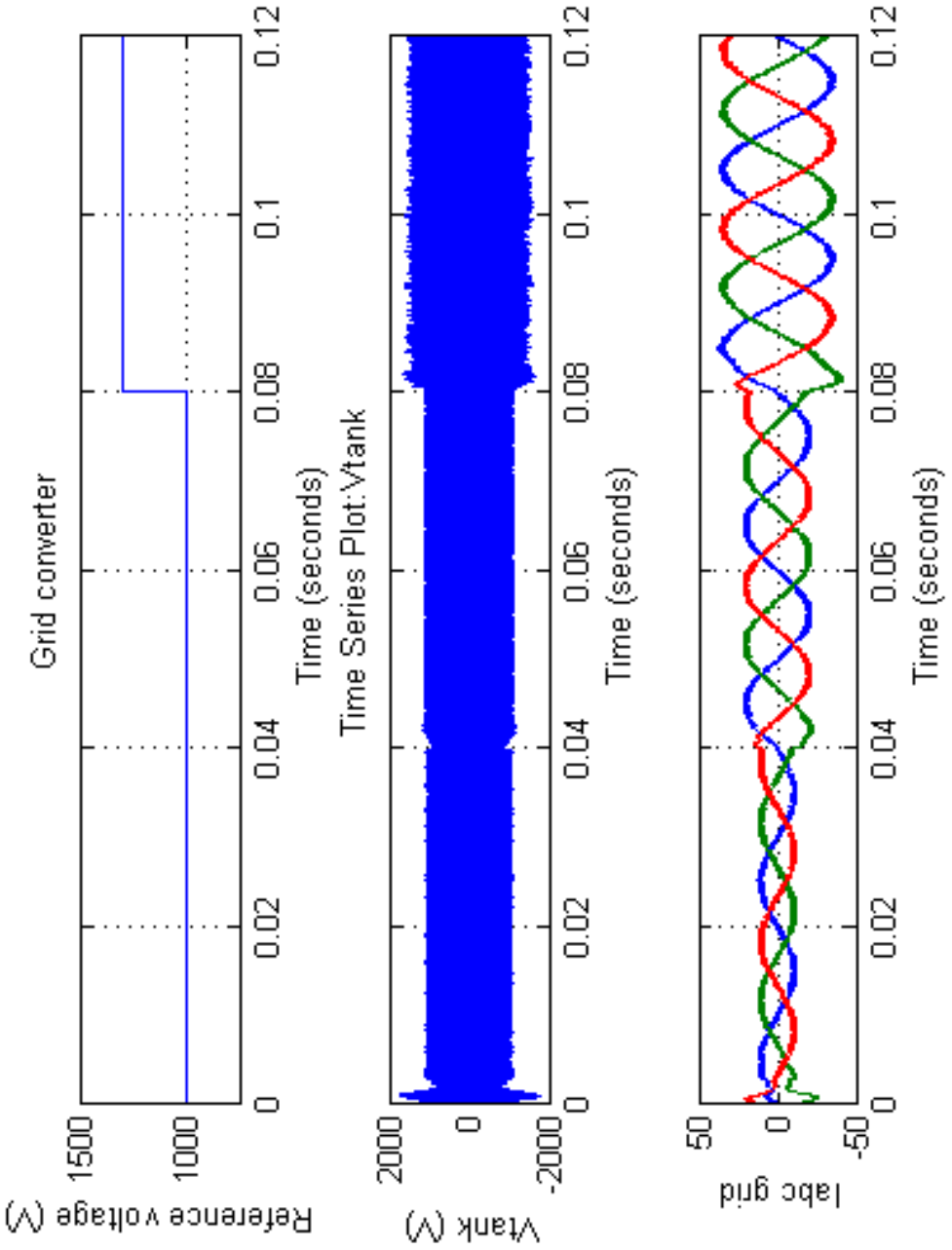

Figure 29 Simulink converter model Tank voltage with current and voltage control

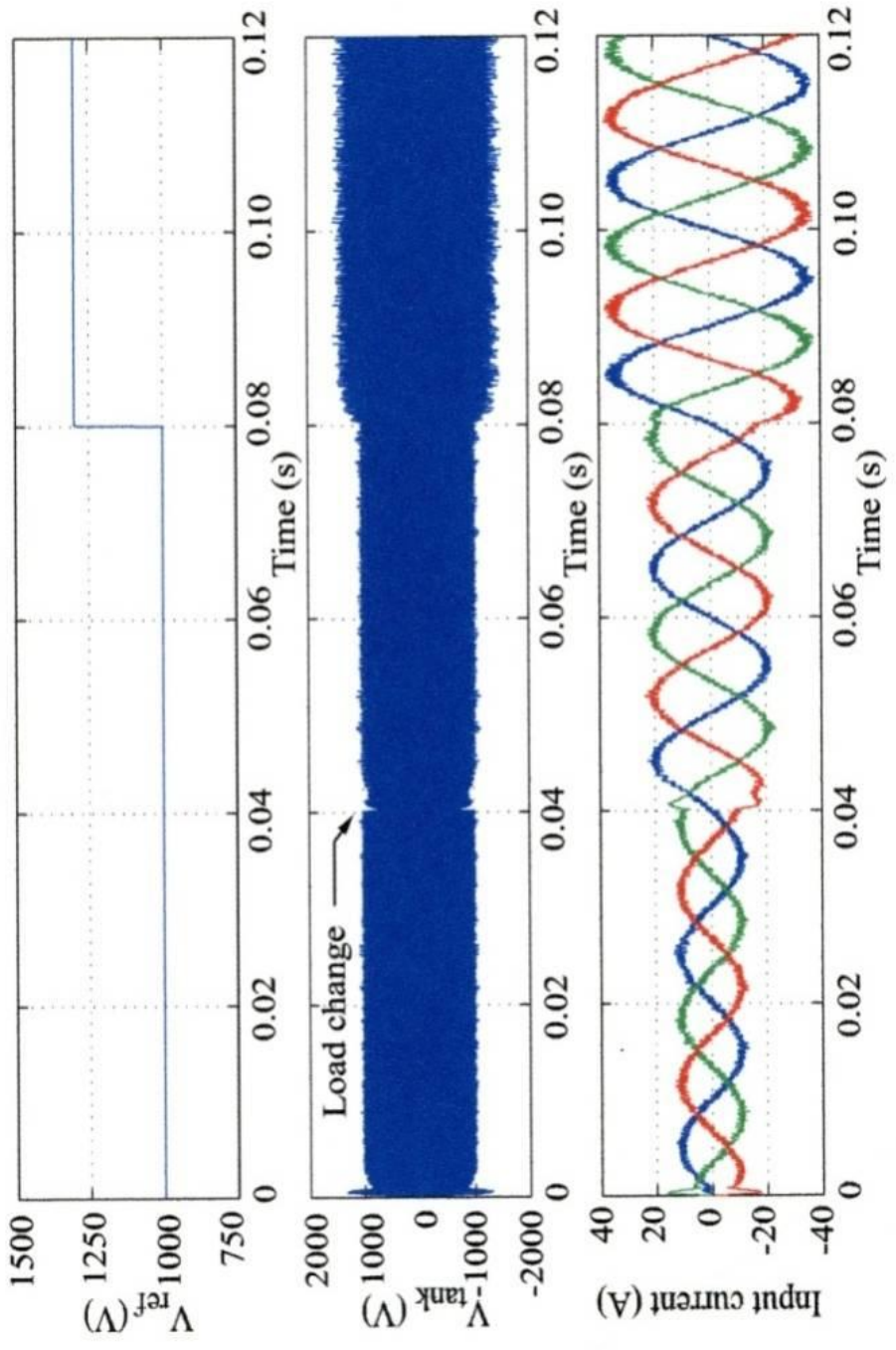

Figure 30 Tank voltage and current when having both controllers[8]

[8] Dang's Thesis [45] Figure 5.14 page 108.

6.5. Summary

The above results gave sufficient confidence in the verification tests that the Simulink® converter model could be used as a test vehicle for advanced controller designs and for building an Active Transformer model for further simulation. The key characteristics required for the converter controllers are summarised as:

i) to maintain strong oscillations, reverse the voltage across the resonant circuit every half cycle

ii) select a switch vector with reference to the state/phase of the supply voltage that minimises input current error with respect to a reference determined by the voltage controller

iii) maintain the peak output voltage within ±10% for loads of 10 – 200%, and for changes of load of 100-200% and 100-10%. These loads changes are very severe. The change from 100 – 200% load would never happen under normal operating conditions but is regarded as a withstand test to demonstrate robustness or survivability of abnormal conditions. The sudden change from 100 to 10% is more likely to occur than the previous conditions as a result of fault clearance or restoration actions on a network.

Chapter 7.

Converter Advanced Control Studies

7.1. Introduction

A number of modern control methods are available in control literature, however this thesis concentrates on the use of an $\mathcal{H}_\infty$ method as applied to the control of the converter output voltage. This chapter describes the application of an alternative controller design method based on the $\mathcal{H}_\infty$ technique and a design procedure described by Skogestad and Postlethwaite [52]. It presents the results of simulations using a resonant converter model and compares the performance of the PI and $\mathcal{H}_\infty$ controllers.

Modern control methods provide an approach where a number of objectives of the control problem can be simultaneously addressed. Classical control can be effectively applied to many SISO control design problems providing robust designs that were proven in many naval gun control applications, but modern control methods address a wider class of control problems including the more complicated structures such as MIMO systems.

Analysis of the classical converter PI voltage controller has shown a potential problem of instability at light converter loads and an alternative controller is the main subject of this chapter. The converter control requirements necessitate a multi-variable control system approach, but to aid an early appreciation of the $\mathcal{H}_\infty$ technique the requirements were restricted to a single-input single-output system and a step-by-step approach was adopted.

The first step was to design a $\mathcal{H}_\infty$ controller using the loop-shaping design procedure in [52] and the original PI controller gains as a weighting function, effectively wrapping the PI design in an $\mathcal{H}_\infty$ controller. The next step was to adjust the weights to improve robust

performance. Uncertainty modelling was used to choose appropriate weights and ensures that the controller was robust and able to deal with the uncertainties of the load that appear in the linearised converter transfer function. The Simulink® converter model was used to verify the new controller's performance and compare it to the performance of the original PI controller.

7.2. $\mathcal{H}_\infty$ controller

7.2.1 Background

The $\mathcal{H}_\infty$ norm of a stable scalar transfer function $f_{(s)}$ is equal by definition as the peak value of the $|f_{(j\omega)}|$:

$$\left\| f_{(s)} \right\|_\infty \stackrel{\Delta}{=} \max_{\omega} \left| f_{(j\omega)} \right|$$

In the early 1980s the poor robustness properties of Linear Quadratic Gaussian (LQG) control [62] led to the further development of $\mathcal{H}_\infty$ optimisation for robust control. Since that time $\mathcal{H}_\infty$ has become a widely used method in the design of control systems generally, but in high power electronic applications, it is only relatively recently that designers are beginning to apply it to robust drive systems [63] and d.c.-a.c. converters [64], perhaps because of its frequency-domain nature and ready inclusion of uncertainty [65].

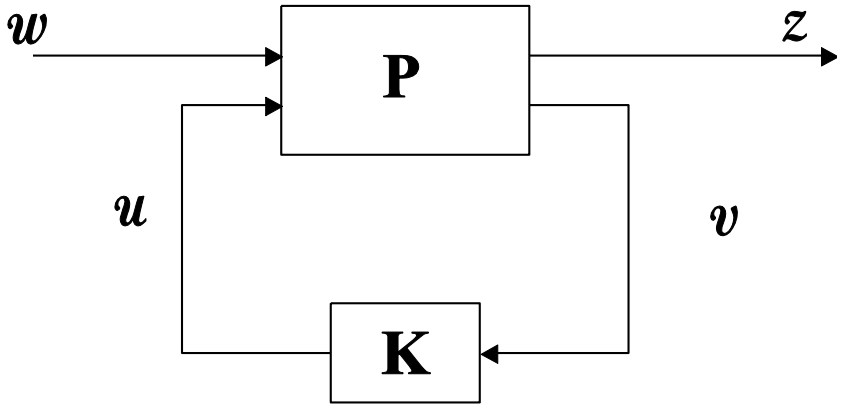

Figure 31 General system control configuration (Generalised regulator)

There are many ways in which the design of feedback controllers can be formulated using $\mathcal{H}_2$ (efficient with stochastic control specifications) or $\mathcal{H}_\infty$ (efficient with deterministic control specifications) optimisation and it is useful to have a systematic way of describing the design problem in which any specific problem may be solved [52]. Such a system may be described by a general system shown in Figure 31.

A system P is described by:

$$(37) \quad \begin{bmatrix} z \\ v \end{bmatrix} = \begin{bmatrix} P_{11}(s) & P_{12}(s) \\ P_{21}(s) & P_{22}(s) \end{bmatrix} \begin{bmatrix} w \\ u \end{bmatrix}$$

$$(38) \quad u = K(s)v$$

with a state-space realisation of the system given by:

$$(39) \quad P \overset{s}{=} \left[\begin{array}{c|cc} A & B_1 & B_2 \\ \hline C_1 & D_{11} & D_{12} \\ C_2 & D_{21} & D_{22} \end{array}\right]$$

i.e
$$\dot{x} = Ax + B_1 w + B_2 u \quad \textit{the state equation}$$
$$z = C_1 x + D_{11} w + D_{12} u \quad \textit{regulated signals}$$
$$v = C_2 x + D_{12} w + D_{22} u \quad \textit{measurements}$$

where the signals are: u the control variables, v the measured variables, w the exogenous signals e.g. disturbances w_d and commands r, and z the so-called "error" signals that are to be minimised to meet the control objectives. The closed loop transfer function from w to z is given by the linear fractional transformation (a way of representing a closed loop system with plant and controller integrated):

$$z = F_l(P,K)w \quad (40)$$

where:

$$F_l = P_{11} + P_{12}K(I - P_{22}K)^{-1}P_{21} \quad (41)$$

$\mathcal{H}_\infty$ control aims to minimise the $\mathcal{H}_\infty$ norms of $F_l(P,K)$.

7.2.2 $\mathcal{H}_\infty$ loop-shaping

Classical loop-shaping shapes the magnitude of the open-loop transfer function and the designer aims to obtain a desired bandwidth, slope etc. It is difficult to apply to complex systems and therefore the step-by-step loop-shaping design procedure, described in Skogestad & Postlethaite's excellent and very readable book, [52], is used in this thesis and which is based originally on the work of McFarlane and Glover [66] "$\mathcal{H}_\infty$ robust stabilisation combined with classical loop-shaping". Readers are referred to these texts for an in-depth understanding. The key mathematical analysis needed to understand the application of robust stabilisation is given in 7.2.4.

The $\mathcal{H}_\infty$ loop-shaping design process has two stages:

i) the open-loop system is augmented by pre- and post-compensators to give the required open-loop frequency response. The pre-compensator or weighting function was initially chosen as the original PI controller transfer function.
ii) the resulting shaped system was robustly stabilised with respect to the general class of coprime factor uncertainty using $\mathcal{H}_\infty$ optimisation.

7.2.3 Loop shaping

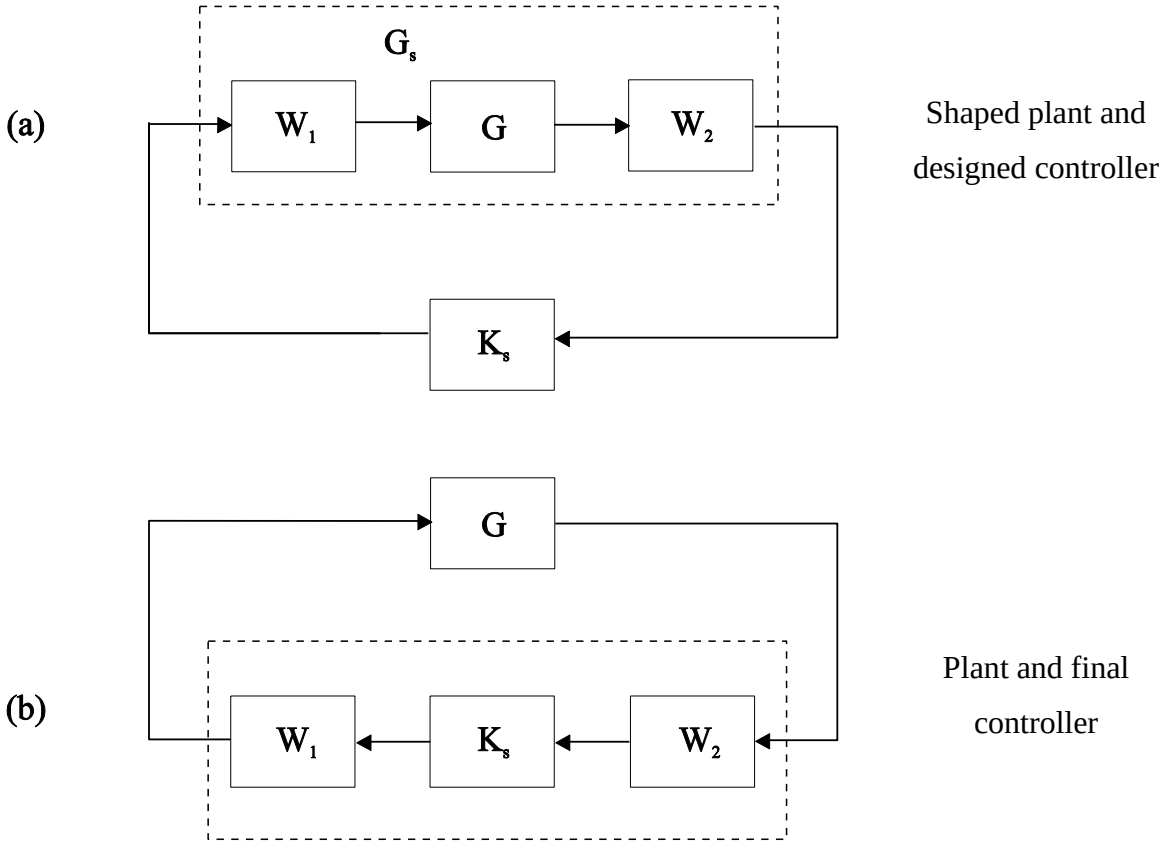

Figure 32 Shaped plant and controller

Shaping of the plant open-loop transfer function, *G*, is achieved with the use of weighting functions W_1 and W_2, or pre and post processors respectively. The "shaped" plant transfer function G_s is shown in Figure 32(a) and the system implementation, with the weighting functions absorbed into the controller, is shown in Figure 32(b). G_s is given by:

$$(42) \quad G_s = W_2 G W_1$$

Omitting the Laplace "*s*" for clarity, the controller, *K*, for the original plant *G* is then:

$$(43) \quad K = W_1 K_s W_2$$

In this analysis it is important to recognise that the system must have stable co-primes. Coprime means having no common factors and is an alternative way to represent a system transfer function. Consider the system transfer function (having an unstable zero):

$$G(s) = \frac{k(s-1)}{s+5}$$

This may be represented in coprime (factors have no common unstable zeros) form by:

$$G(s) = N \times D$$

For example:

$$G(s) = \frac{k(s+1)}{s+5} \times \frac{(s-1)}{s+1}$$

Here both coprimes are first order polynomials, are stable and do not contain any common factors.

In considering the converter, it is clearly non-linear with a resonant circuit at its output. However, the linearised transfer function, equation (9), is stable.

7.2.4 Robust stabilisation

Classical gain and phase margins are unreliable indications of stability in multivariable systems because simultaneous changes may be occurring in each loop. Stability and coprimeness imply that there are no right-hand plane zeros in the co-primes that would result in pole cancellations when describing a transfer function.

The following analysis develops the equations necessary for the design of a stable and robust controller. It is an integral part of the design procedure used in section 7.2.5. The coprime uncertainty description provides a good generic uncertainty model for systems where there is little or no prior information regarding the uncertain parameters.

Consider the stabilisation of a system G(s), Figure 33, which has normalised left coprime factorisation where the subscript *l* has been omitted for clarity:

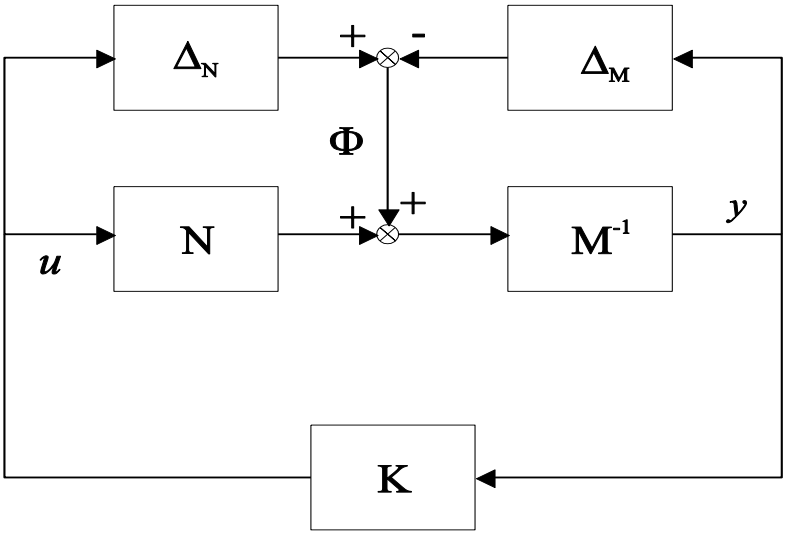

Figure 33 H_∞ robust stabilisation problem

(44) $$G(s) = M^{-1}(s)N(s)$$

where M and N are coprime if and only if they have no common right-hand-plane zeros, including the point s=∞. Therefore, there exists a stable *U(s)* and *V(s)* such that the following Bezout identity is satisfied:

(45) $$NU + MV = I$$

We can therefore describe a perturbed system G_p as:

(46) $$G_p = (M + \Delta_M)^{-1}(N + \Delta_N)$$

where Δ_M and Δ_N are stable unknown transfer functions representing the uncertainty in the system, Figure 33. Here the object is to stabilise the system G_p defined by:

(47) $$G_P = \{(M + \Delta_M)^{-1}(N + \Delta_N) : \| \Delta_N \quad \Delta_M \|_\infty < \varepsilon \}$$

where ε > 0 is then the margin of stability.

To maximise the stability margin is the problem of robust stabilisation of coprime factor systems that was solved by Glover and McFarlane [67]. For the system shown in Figure

33, the stability characteristic is stable "if and only if" (iff) the original feedback system is stable and:

$$(48)\quad \gamma_K \stackrel{\Delta}{=} \left\| \begin{bmatrix} K \\ I \end{bmatrix} (I - GK)^{-1} M^{-1} \right\|_\infty \le \frac{1}{\varepsilon}$$

where γ_K is the $\mathcal{H}_\infty$ norm from Φ to $\begin{bmatrix} u \\ y \end{bmatrix}$ and $(I - GK)^{-1}$ is the sensitivity function for a positive feedback system. The lowest achievable value of γ_K and the corresponding maximum stability margin ε are:

$$(49)\quad \gamma_{\min} = \varepsilon_{\max}^{-1} = \left\{ 1 - \left\| \begin{bmatrix} N & M \end{bmatrix} \right\|_H^2 \right\}^{0.5} = (1 + \rho(XZ))^{0.5}$$

where $\|.\|_H$ represents the Hankel norm [52], ρ denotes the spectral radius (maximum eigenvalue), and for a minimal state-space realisation (A,B,C,D) of G.

Z is the unique positive definite solution to the algebraic Riccati equation:

$$(50)\quad (A - BS^{-1}D^T C)Z + Z(A - BS^{-1}D^T C)^T - ZC^T R^{-1} CZ + BS^{-1}B^T = 0;\ \textit{Filter}$$

where:

$$(51)\quad R = I + DD^T,\ \ S = I + D^T D$$

and is the unique positive definite solution of the following algebraic Riccati equation:

$$(52)\quad (A - BS^{-1}D^T C)^T X + X(A - BS^{-1}D^T C) - XBS^{-1}B^T X + C^T R^{-1} C = 0;\ \textit{Control}$$

For a strictly proper plant (when D=0), the formulae simplify.

A controller, which guarantees that:

$$(53)\quad \left\| \begin{bmatrix} K \\ I \end{bmatrix} (I - GK)^{-1} M^{-1} \right\|_\infty \le \gamma$$

for a specified $\gamma > \gamma_{\min}$ is given by:

$$(54)\quad K = \left[\begin{array}{c|c} A+BF+\gamma^2(L^T)^{-1}ZC^T(C+DF) & \gamma^2(L^T)^{-1}ZC^T \\ \hline B^TX & -D^T \end{array}\right]$$

Which has the general form:

$$\dot{x}_{control} = A_{control}x_{control} + B_{control}U_{control}$$
$$y_{control} = C_{control}x_{control} + D_{control}u_{control}$$

$$(55)\quad F = -S^{-1}(D^TC + B^TX)$$

$$(56)\quad L = (1-\gamma^2)I + XZ$$

MATLAB statements, used in subsequent m-files, for the design of the controller K_s are listed in Appendix C.2.

7.2.5 Systematic $\mathcal{H}_\infty$ loop-shaping controller design procedure

The design approach is rather adhoc in choosing the weighting functions, usually some initial aspects of equivalent classical control is used and further changes applied iteratively. There have been attempts at building a more systematic selection procedure and in this context the following procedure, based on [52] was used for the design of the controller.

i) The converter outputs were scaled using normalisation.

ii) Diagonalisation was recommended but for a SISO system this was unnecessary.

iii) The pre-and post compensators, *W1* and *W2* were chosen for the "shaped plant", $G_s = W2GW1$ where $W1 = W_pW_aW_g$. This involves some trial and error. W2 is usually chosen as a constant to reflect the relative importance of the controlled system outputs, with only one output, *W2* was set to equal one. The pre-compensator, W_p, contains the dynamic shaping, i.e. high-gain integral action for low frequency performance, phase advance or phase lag as for classical control etc. (Some time was spent in this activity and a variety of compensators were initially chosen, including low-pass and band-pass filters with various centre frequencies, to see their effect on performance. However,

most of these were based on trial and error and proved unsatisfactory and later abandoned.)

iv) The PI controller had good robustness near its design point and this seemed to offer a useful starting point for the weight *W1*for the $\mathcal{H}_\infty$ design.

v) The singular values were aligned at a desired bandwidth using a further constant weight contained if W_a. (This optional step was quite useful as it simply adjusted the controller gain.)

vi) W_g was an optional gain introduced to provide control over actuator usage. For the SISO system under consideration.

vii) The shaped plant, $G_S=W_2GW_1$, was robustly stabilised. The maximum stability margin $\varepsilon_{max}=1/\gamma_{min}$. If the margin was too small, <0.25, then modify the weights, otherwise select $\gamma > \gamma_{min}$ by about 10% and synthesise the controller using the procedure given in C.2.

viii) The design was analysed and compared with the performance specification, and weights adjusted for any improvements required.

ix) The controller was implemented in the system model.

Initially, the controller was designed at the full load condition, 100 Ω, without the measurement filter characteristics in order to make a comparison with [45], and subsequently redesigned with the filter characteristics included in the converter model. Finally, the controller was designed at a 10% load, 1000 Ω, condition. Closed loop step response simulations using the MATLAB® model, were compared to those of the original PI controlled system.

7.3. Controller designed at 100% converter load

7.3.1 Converter model without measurement filter

The design procedure requires the controller designer to choose appropriate weighting functions and adjust these for the required system performance. This is a rather arbitrary task. The weight *W1* contains the dynamic shaping. In the classical design the PI controller provided good robustness against small perturbations near the operating point

and this seemed a reasonable starting weight for the H_∞ controller design. The use of the classical PI gains also enabled a comparison to be made with the original system performance. Using the design procedure, the resulting H_∞ controller transfer function at the full load design point was:

$$(57) \quad K = \frac{0.001174s^3 - 229s^3 - 1.833\times10^7 s^2 - 1.957\times10^{11}}{s^3 + 7.516\times10^4 s^2 + 1.882\times10^9 s + 1.882\times10^7}$$

This is in fact a more complex controller than the original PI controller:

$$(58) \quad K_{PI} = \frac{0.002s + 100}{s}$$

The frequency response of each controller is shown in Figure 34. The shapes of the gain responses are very similar but the phase responses are quite different and thus have quite different dynamic effects on the converter. Notably the phase advance of the H_∞ controller occurs at a much lower frequency than in the PI controller and therefore the H_∞ controller is expected to have a faster response time. The additional complexity would be acceptable provided an improved system performance was achieved.

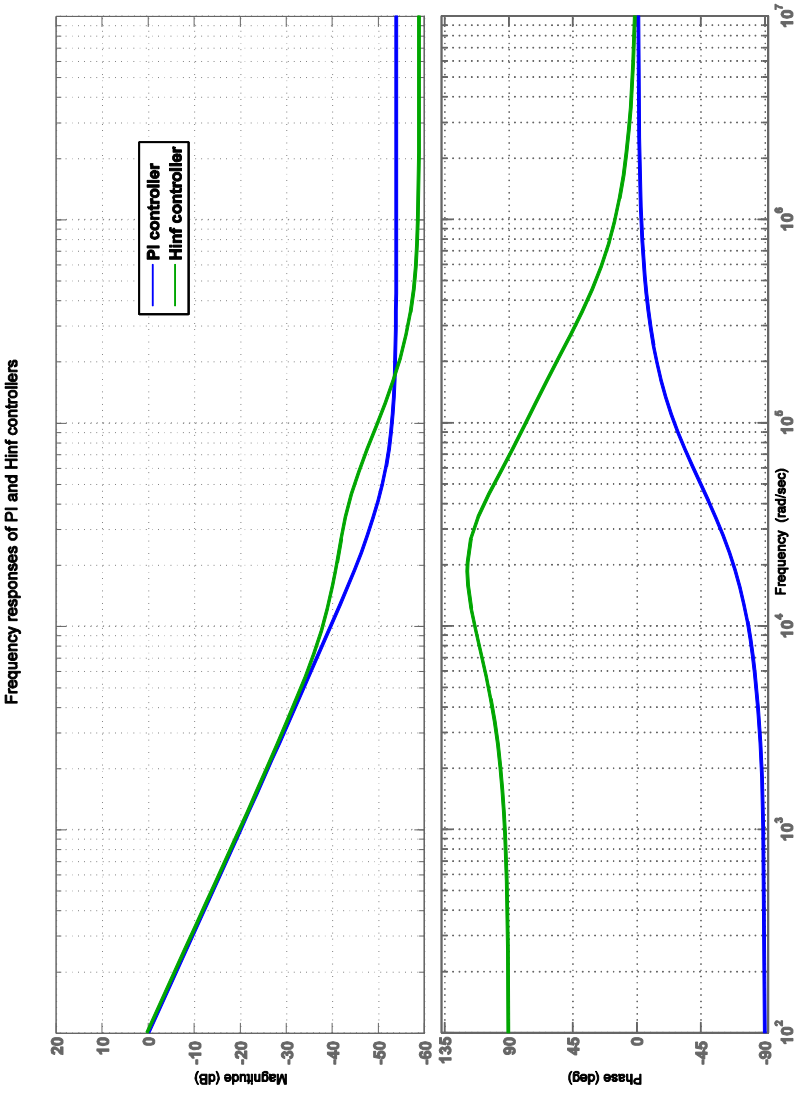

Figure 34 Frequency responses of PI and H_∞ controllers

The $\mathcal{H}_\infty$ controller design aims to improve system robustness without degrading performance. Using the the design procedure, the bandwidth weighting W_a, an element of W_1, Figure 32, was varied to investigate its effect on the overall system performance and the results recorded in Table 3 below.

	Converter model without measurement filter		**Converter model with measurement filter**	
W_a	γ_{min}	Maximum stability margin	γ_{min}	Maximum stability margin
1.5	1.9891	0.5027	2.771	0.361
2.0	2.1869	0.4572	2.851	0.351
2.5	2.3872	0.4189	2.91	0.344
3.0	2.5896	0.3862	2.95	0.339
4.0	3.0003	0.3333	3.01	0.332
6.0	3.8434	0.2602	3.09	0.324

Table 3 Variation of stability margin with bandwidth weighting W_a

All the above results with a stability margin greater than 25% are acceptable designs and an example of the loop shapes resulting from the design procedure are shown in Figure 35. The "H_∞ wrapping" has reduced the loop gain and reduced the cross-over frequency to 3.74 krads/s, but did not significantly alter the overall shape of the response. For step changes in demand, controllers using the lower values of bandwidth weighting produced a sluggish system performance while those using the higher values tended to give an oscillatory response, particularly for high values of R_L (low loads). W_a was therefore chosen as 2.5 to give an acceptable performance and approximately 42% co-prime stability margin.

Figure 36 shows the closed-loop system step responses, from a MATLAB® simulation of the voltage control system described by (9), the original Proportional plus Integral (PI)

controller and the $\mathcal{H}_\infty$ controller for load changes from 50 Ω, (twice full load) to 100 kΩ. Notably, the $\mathcal{H}_\infty$ controller produces significant beneficial improvements, Table 4: a faster response, less overshoot and great damping for light loads. However, the overshoot is still greater than 50% where less than 20% would be a reasonable design aim.

Table 4 Comparison of Time responses – 100 kΩ load

Controller	Maximum overshoot	Rise time	Settling
PI	82%	0.28 ms	>7 ms
$\mathcal{H}_\infty$	64%	0.24 ms	3 ms

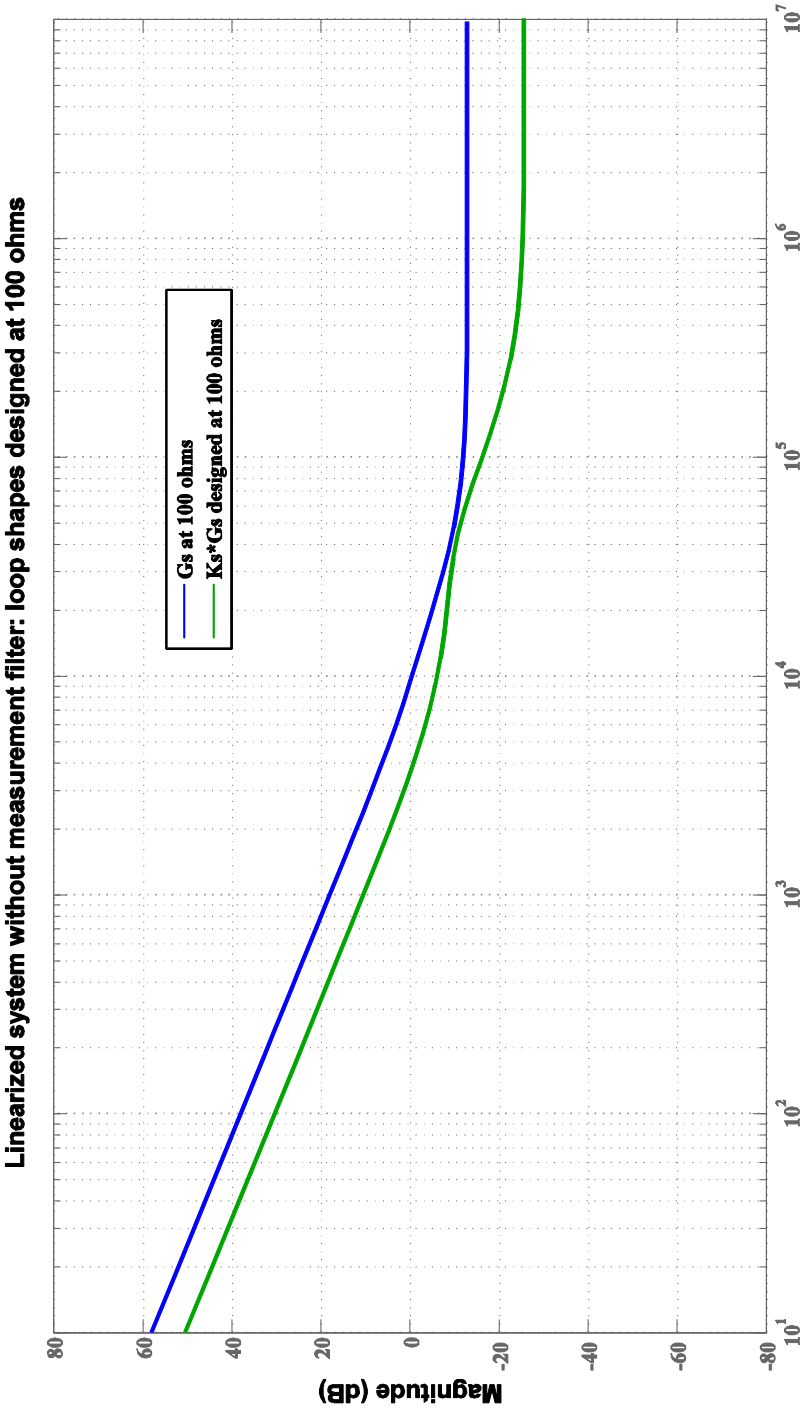

Figure 35 Linearised system loop shapes

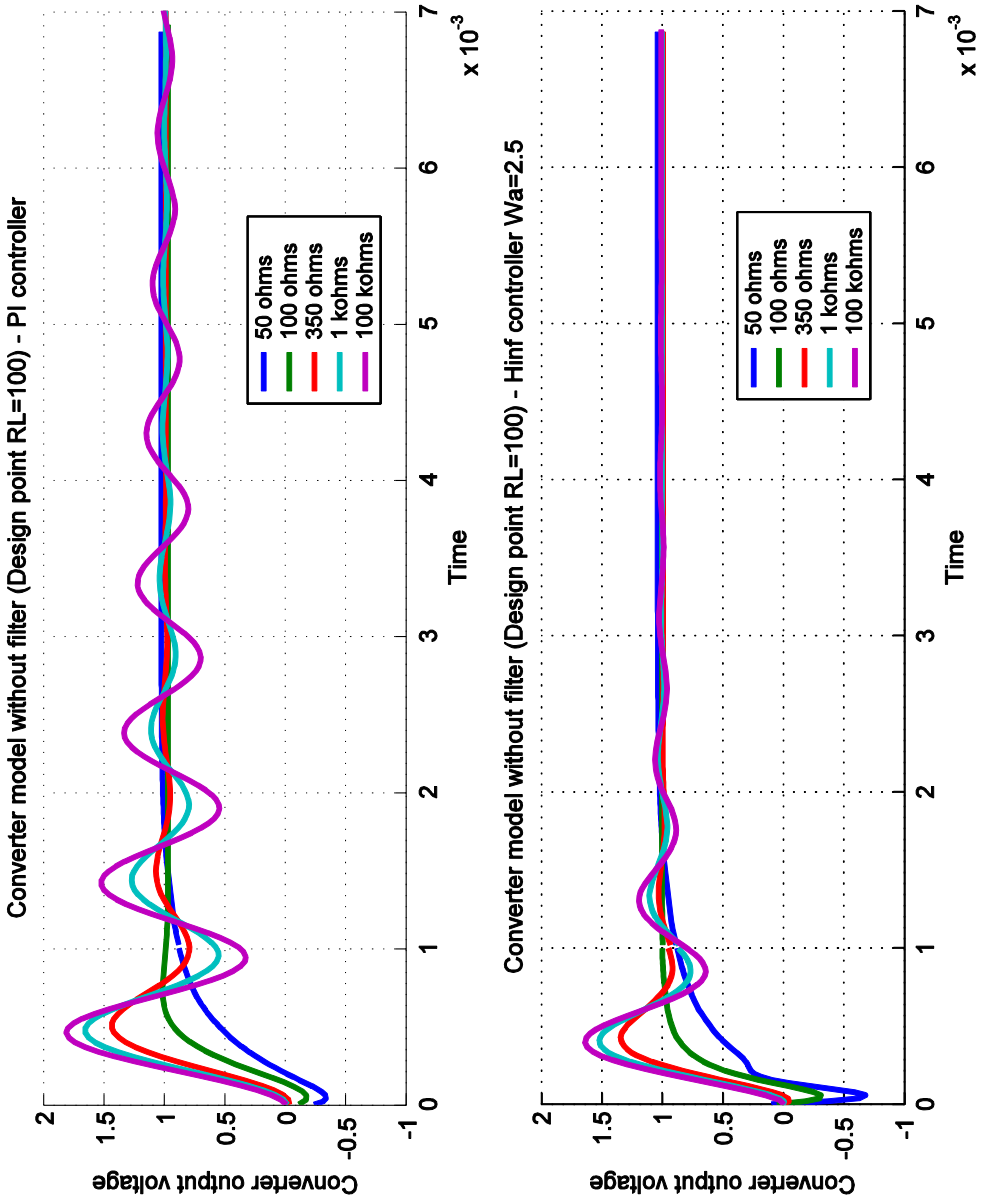

Figure 36 Linearised system PI and H_∞ step responses

Using the non-linear converter model developed in Chapter 6, simulations of step changes in loads, similar to those in Chapter 6.4.2 from 100 Ω to 150 Ω and a change of demand from 1000 V to 1300 V, were made to compare the performance of the PI and $\mathcal{H}_\infty$ controller.

The model simulation parameters used in this chapter were set to:

i) simulation time, T_s, 1.0^{-6} s
ii) solver type Variable step
iii) solver ode23t

In the following controller simulations the converter model, Figure 15, is configured for forward mode operation with the following initial conditions set for the initial step changes:

i) grid side generator line-line 415 V, 50 Hz
ii) Vtank_ref 636.6 V_{mean}
iii) fixed load 100 Ω 100 Ω
iv) switched load cct. breaker closed, open at 40 ms
v) switched load 100 Ω 100 Ω

and, additionally for the load change to 10% simulation:

i) fixed load 100 Ω 1000 Ω
ii) switched load cct. breaker closed, open at 20 ms
iii) switched load 100 Ω 1000/9 Ω

For the PI controller, Figure 37 shows the simulation results of step changes and similarly, Figure 38 shows the results for the $\mathcal{H}_\infty$ controller. These figures show well behaved responses with similar results to those described in Chapter 6.4.2.

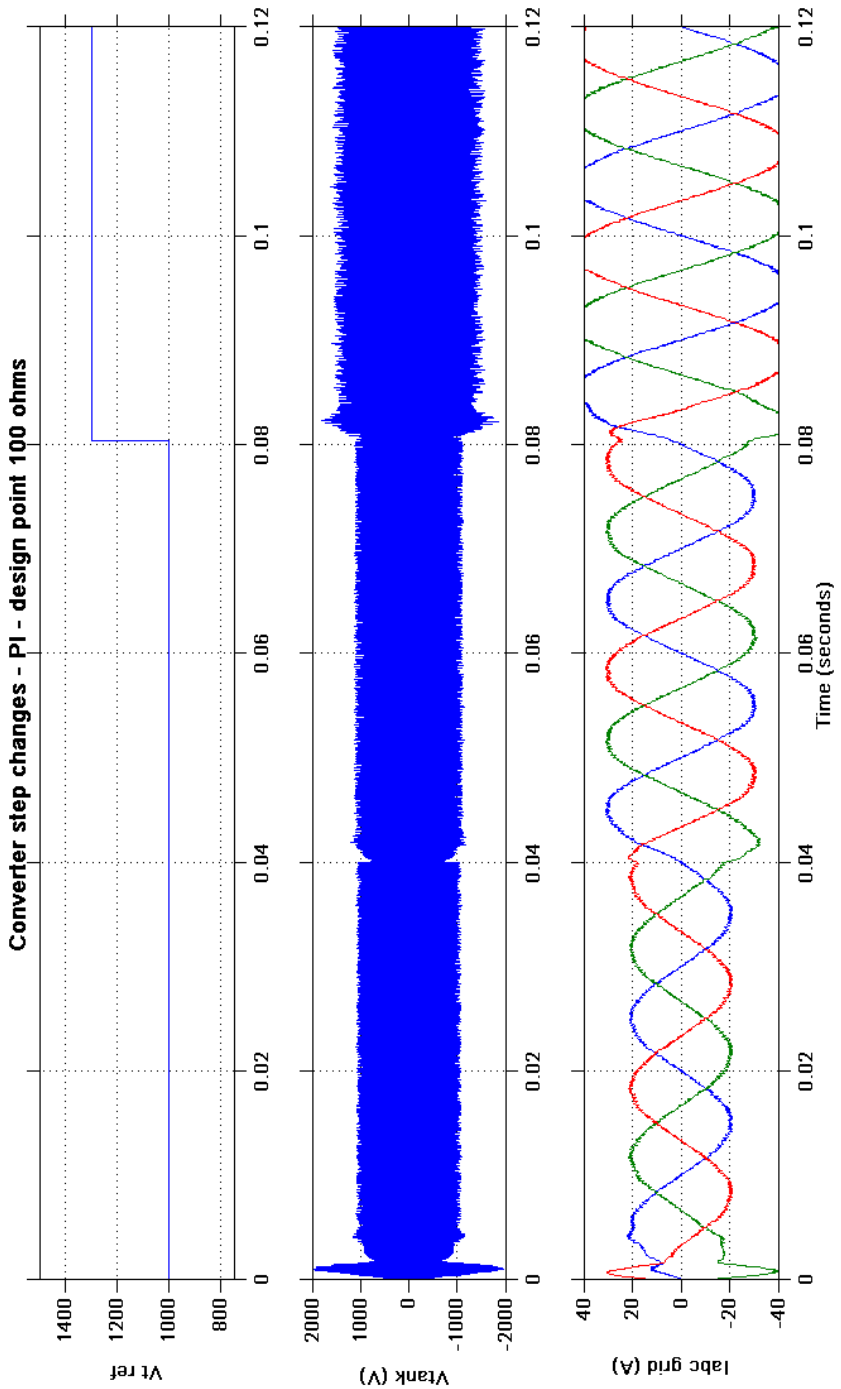

Figure 37 Simulink® system model - PI controller - design point R_L=100Ω

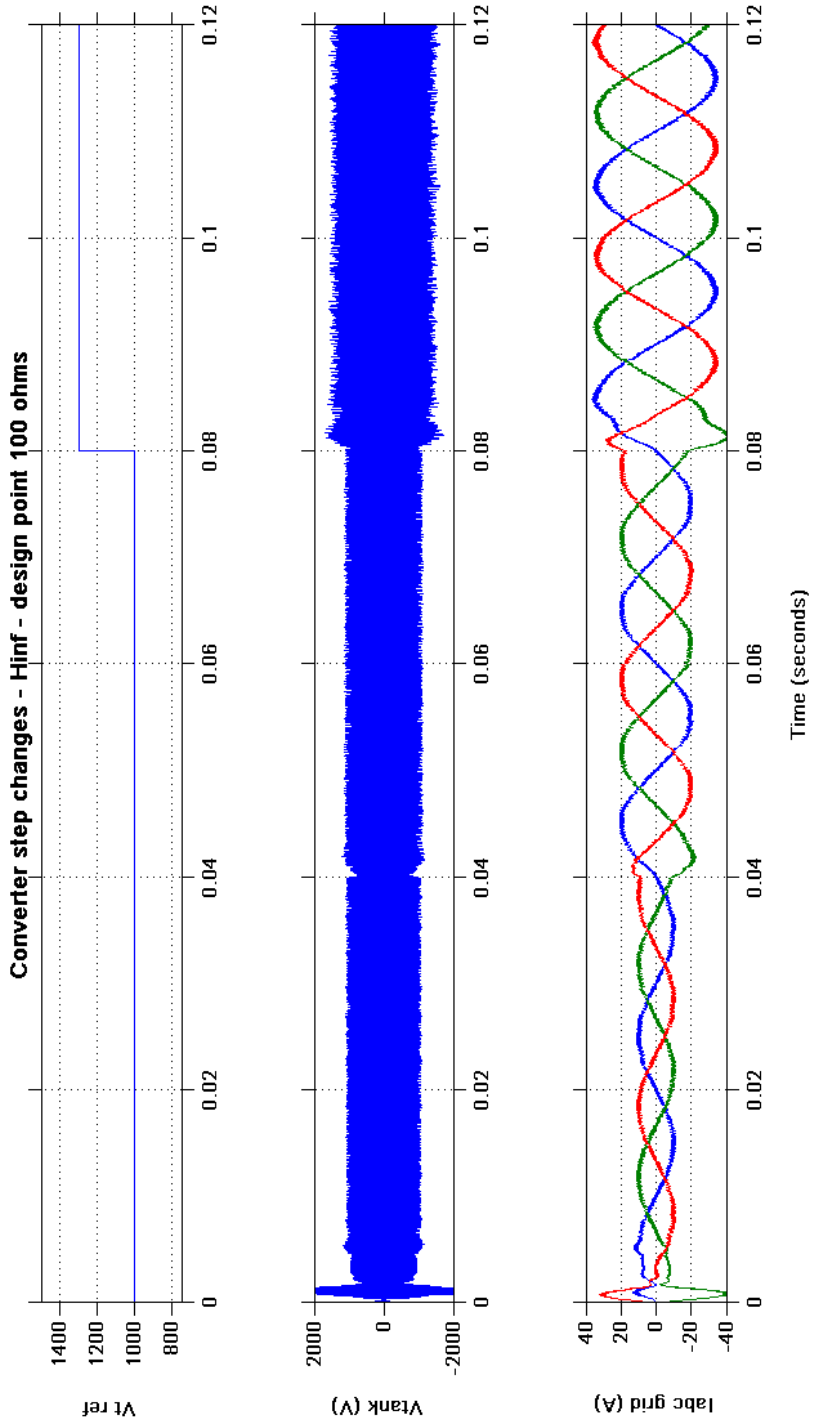

Figure 38 Simulink® system model - H_∞ controllers – design point $R_L = 100\Omega$

Load throwing is a test often applied to converters during development to verify their robustness and response to abnormal conditions. This strategy was also applied to the models developed in this research.

Using the same controller designs as used above, Figure 39 and Figure 40 show the tank voltage and supply currents responses to a larger step change in load, from 100 Ω to 1000 Ω, which is equivalent to a load change from 100 to 10%. The results for the two controllers are similar, but are far from satisfactory responses. Recall that the SISO design model includes a varying RHP zero. Although the $\mathscr{H}_\infty$ controller produces better results than the classical PI approach, being a SISO controller design its performance will still be constrained by the RHP zero characteristics [68]. Further remarks on the above issues are discussed in Chapter 7.4 (uncertainty and choice of design model). Up to 20 ms the responses are as for normal operation at 100% load. On the load change at 20 ms the converter output voltage rises to 2000 V amplitude before recovering into an irregular regime with large variations in amplitude. The line current response shows a similar pattern and clearly this mode of operation does not meet the design expectation for control of the average peak voltage on a half cycle basis.

Both responses are unacceptable and sufficient robustness has not been achieved with either controller design. The converter model used for the design of the voltage control loop is a first order, non-minimum phase model and does not represent the practical converter in sufficient detail, and it should include the feedback measurement dynamics. An alternative converter model was therefore derived that included the measurement low pass filter used in [45].

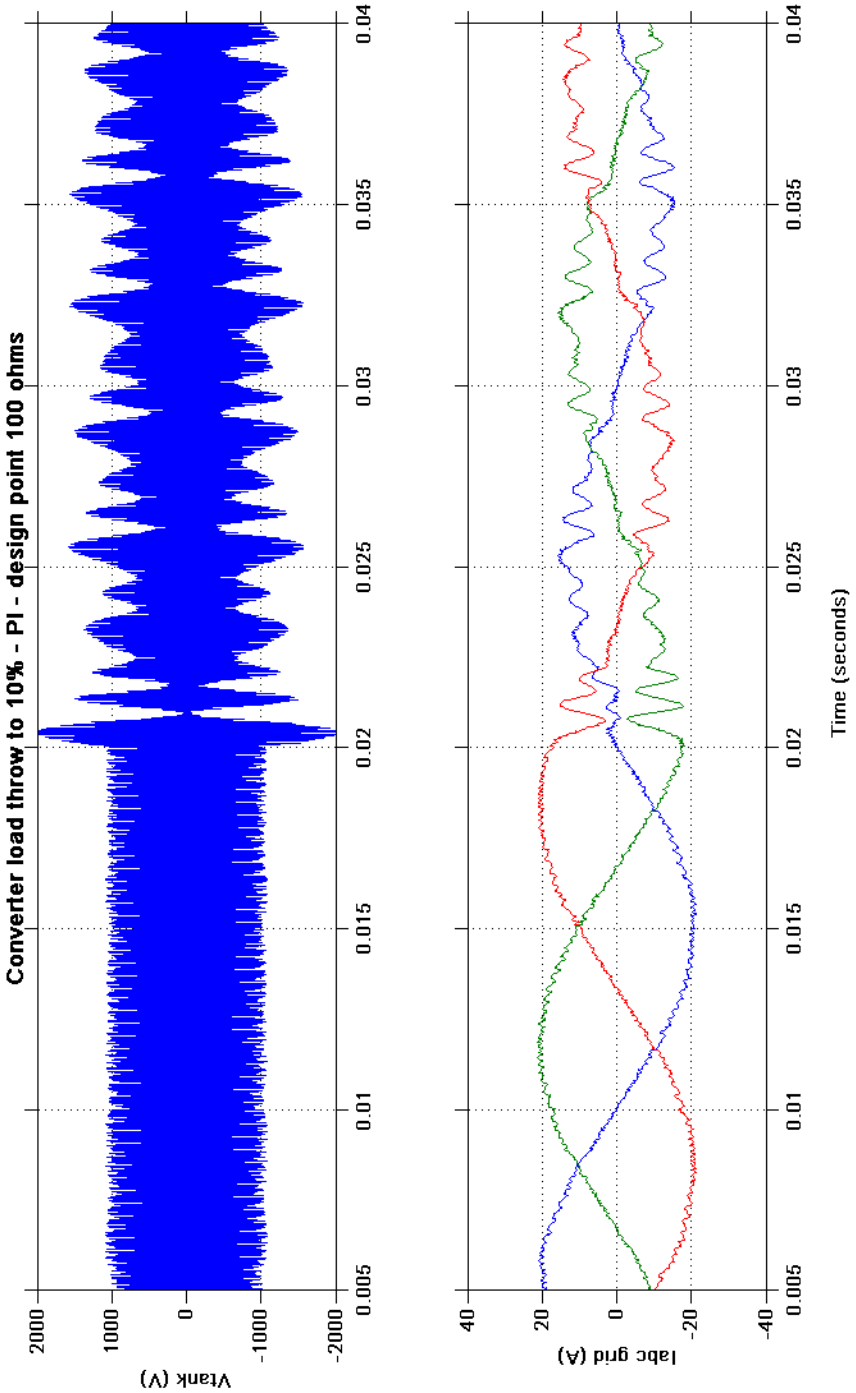

Figure 39 Simulink® converter model - PI controllers - step to R_L 1000Ω

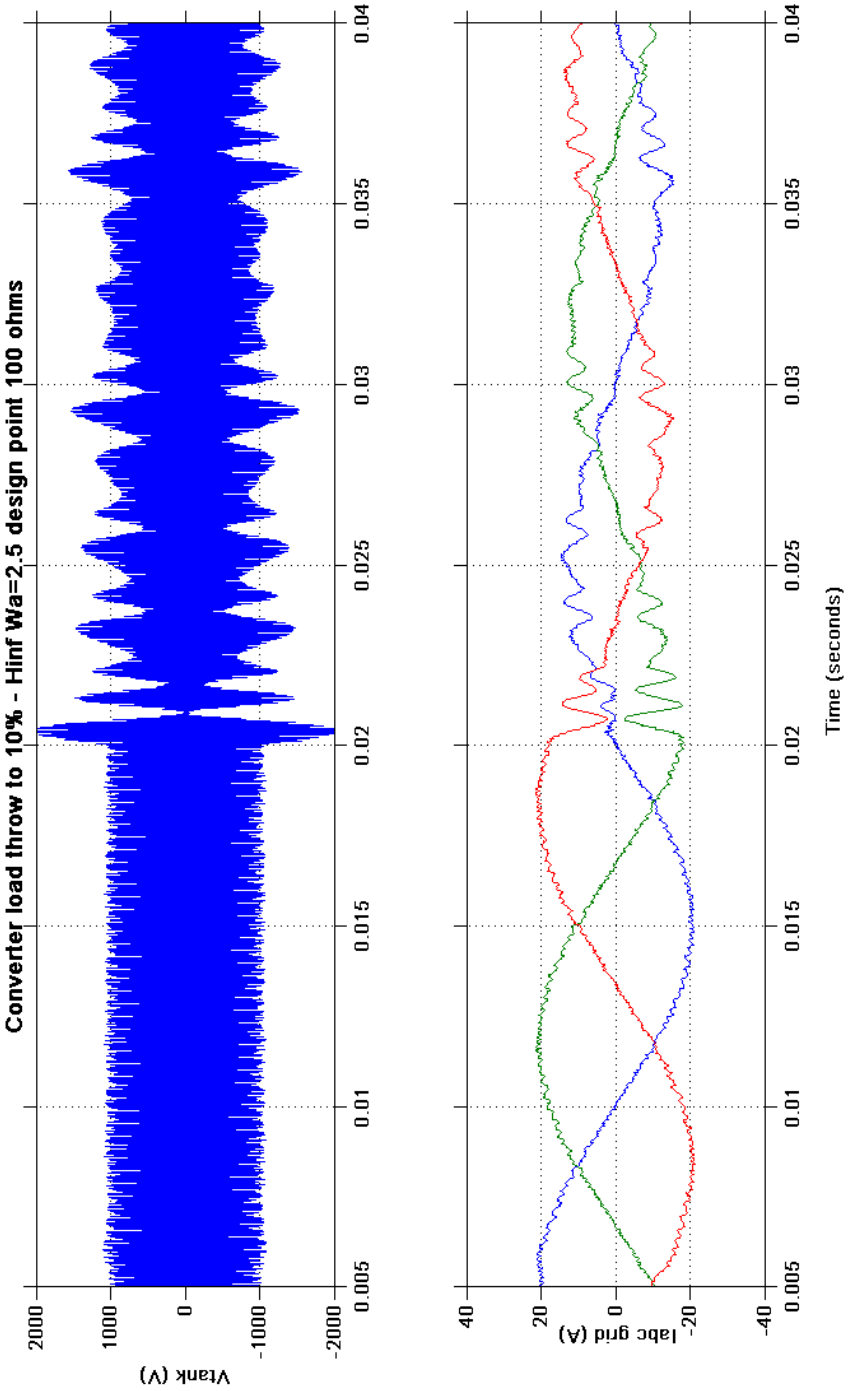

Figure 40 Simulink® converter model - H_∞ controllers - step to R_L 1000Ω

7.3.2 Converter model including measurement filter

In the transfer function (9), the converter output voltage, V_{tank_avg} has no dynamics whereas in practise, it is derived from a measurement of the peak tank voltage and the measurement circuit uses a low-pass filter. The dynamics of the filter should be taken into account as part of the system transfer function in the controller design. A 500 Hz first order low pass filter was therefore used, thus avoiding the addition of further unknown dynamics in the uncertainty of the model:

$$(59) \quad G_f = {}^{3142}/_{s+3142}$$

The PI controller was retuned using MATLAB® Sisotool for this new converter model, which resulted in revised controller gains as shown in Table 5 below.

The design of an H_∞ controller was repeated using the new PI gains and the stability margins recorded in Table 2 above for comparison with the original design. The effect of including the measurement filter in the converter model was to reduce the stability margin. However, within the range of weighting functions used, the results fell well within the limit recommended, gammin < 4.0 and indicated a robust design.

The shaped loop singular values were plotted for the revised converter model, which now included the measurement filter and a revised $\mathscr{H}_\infty$ controller, Figure 41. Because of its low frequency characteristic, the filter now dominates the converter responses, reducing the system gain, particularly at high frequencies. The cross-over frequency is much reduced at 1.5 krads/s but the characteristic has a smaller angle at the cross over frequency, which results in a slow response to changes of load. The slower response of both controllers is clearly shown in the step responses, Figure 42, but this is somewhat academic because for large changes of load large, i.e. to 1 kΩ and 100 kΩ, the system output is increasing with time and therefore unstable.

The non-linear simulations from Chapter 7.2.6 were repeated using the revised controller designs, Figure 43 and Figure 44, and as anticipated also showed a slower system response

to step changes when compared to the results shown in Figure 37 and Figure 38 respectively.

Table 5 PI Controller gains

Gain	PI gains for converter model without measurement filter	PI gains for converter model with measurement filter
K_p – proportional gain	0.002	0.000734
K_i – Integral gain	100	36.7

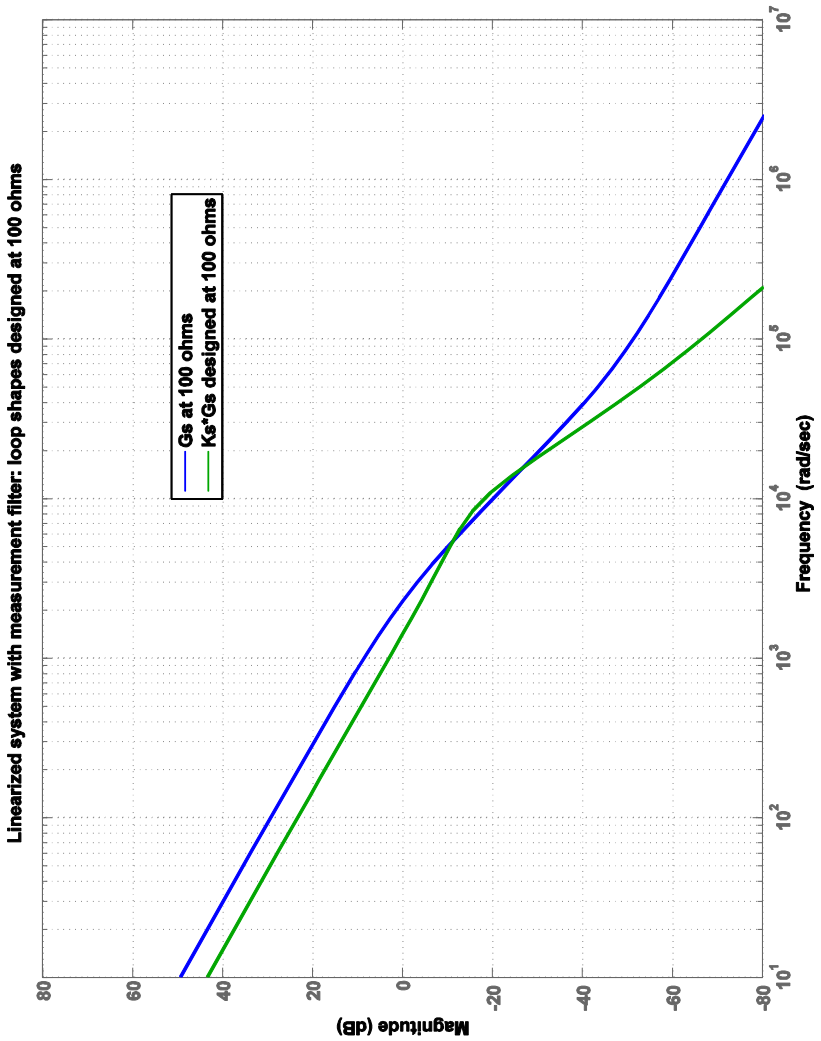

Figure 41 Converter model loop shape

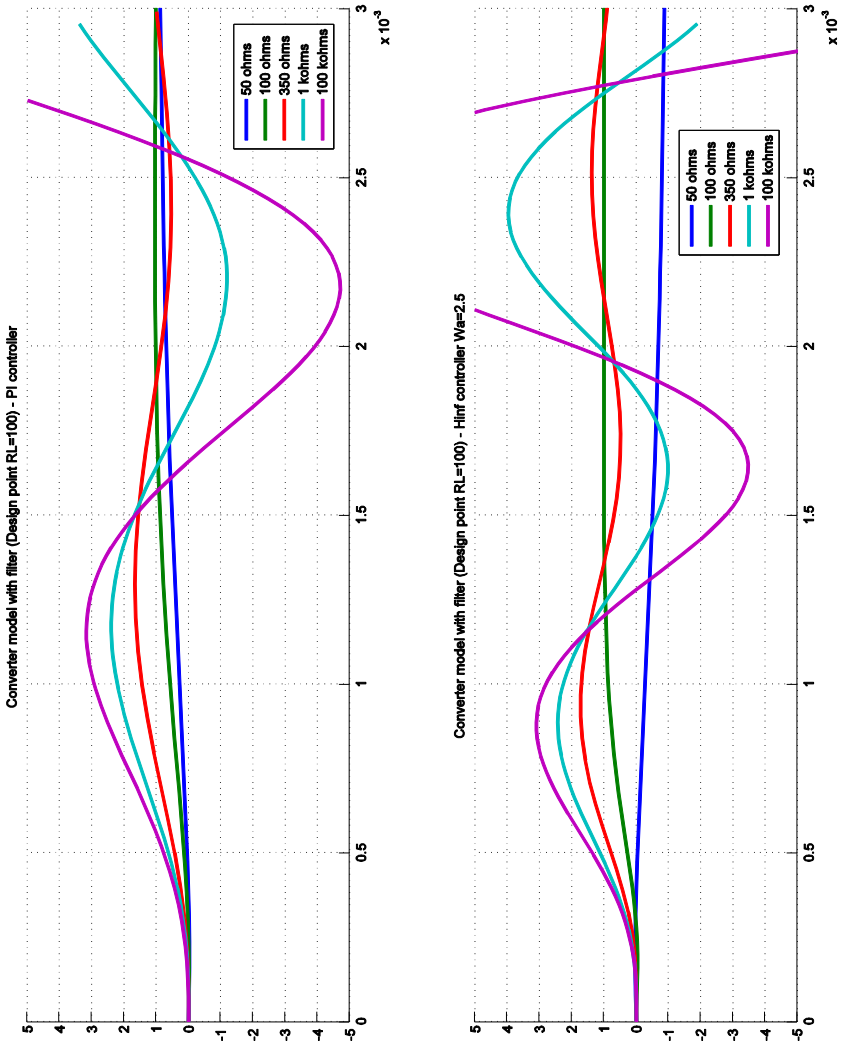

Figure 42 Converter model step responses with measurement filter

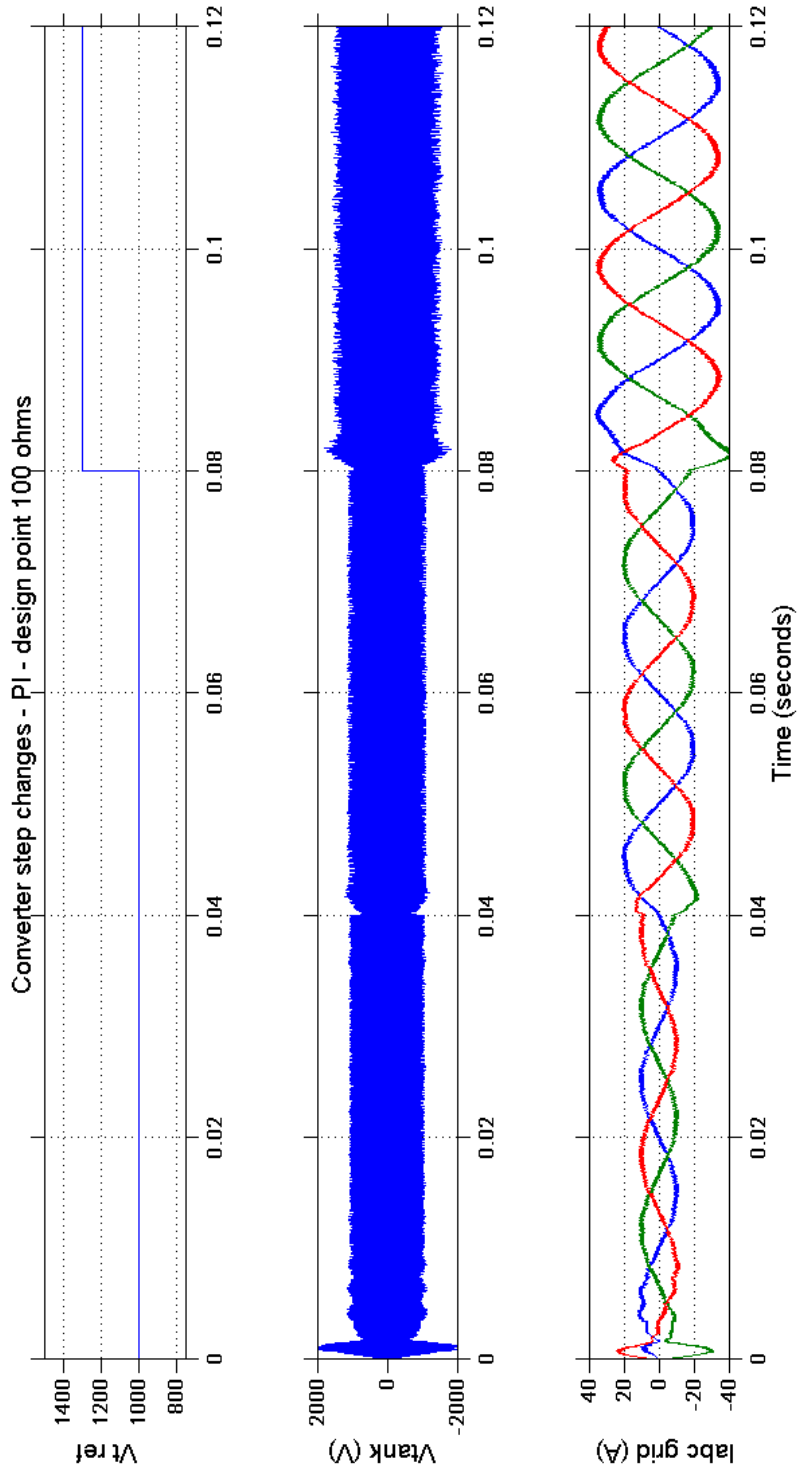

Figure 43 Converter model with measurement filter – PI(100) step changes

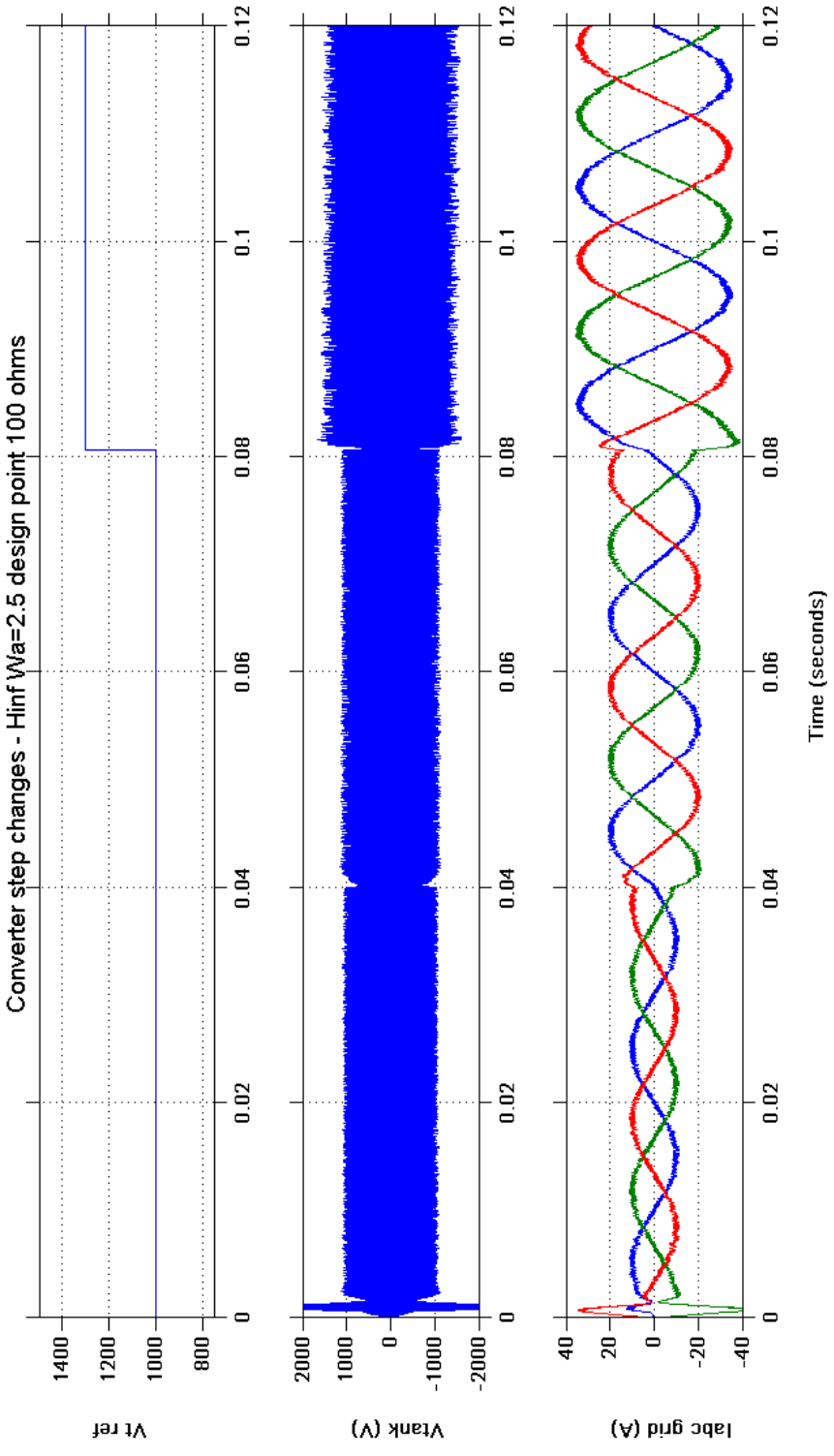

Figure 44 Converter model with measurement filter – $H_\infty(100)$ step changes

7.3.4 Load changes from 100 to 10%

Using the non-linear converter model with the PI and $\mathcal{H}_\infty$ controllers designed at full load (100 Ω) to include the measurement filter, the converter model was again subjected to a large step change of load from full load, equivalent to 100 -10% load change. Figure 45 and Figure 46 show the tank voltage and supply currents responses to the step change in load from 100 Ω to 1000 Ω at 20 ms. Both controllers produce satisfactory steady state control at full load but after the change of load both controllers exhibit large variations in the amplitude of the converter output voltage, which again do not meet with the requirements for control of the average peak voltage and thus the use of classical PI gains in as weighting functions in the design of an $\mathcal{H}_\infty$ controller in this instance did not produce an acceptably robust system design. Some further analysis and refinements of the weighting functions are needed.

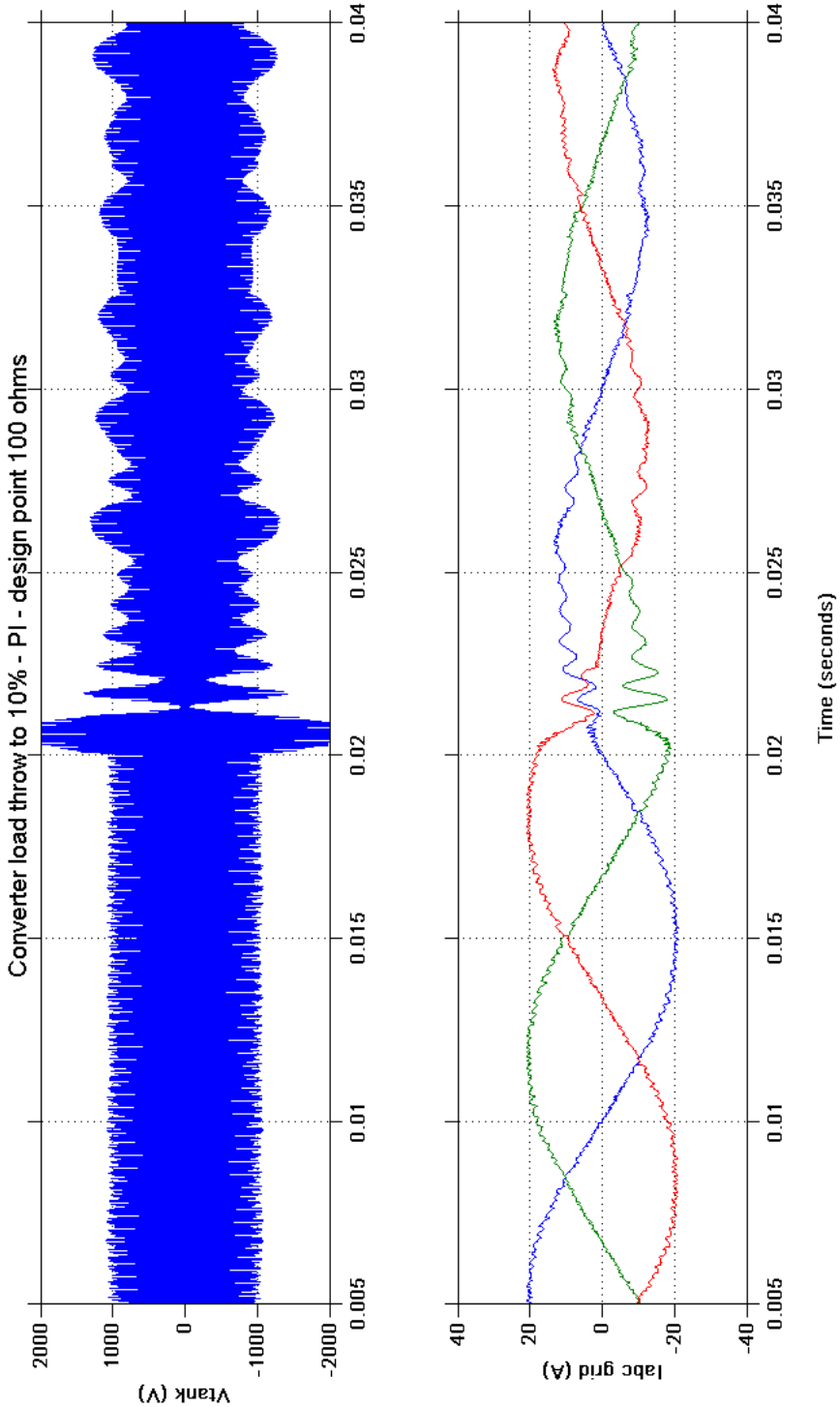

Figure 45 PI Controller – step response to 10% load

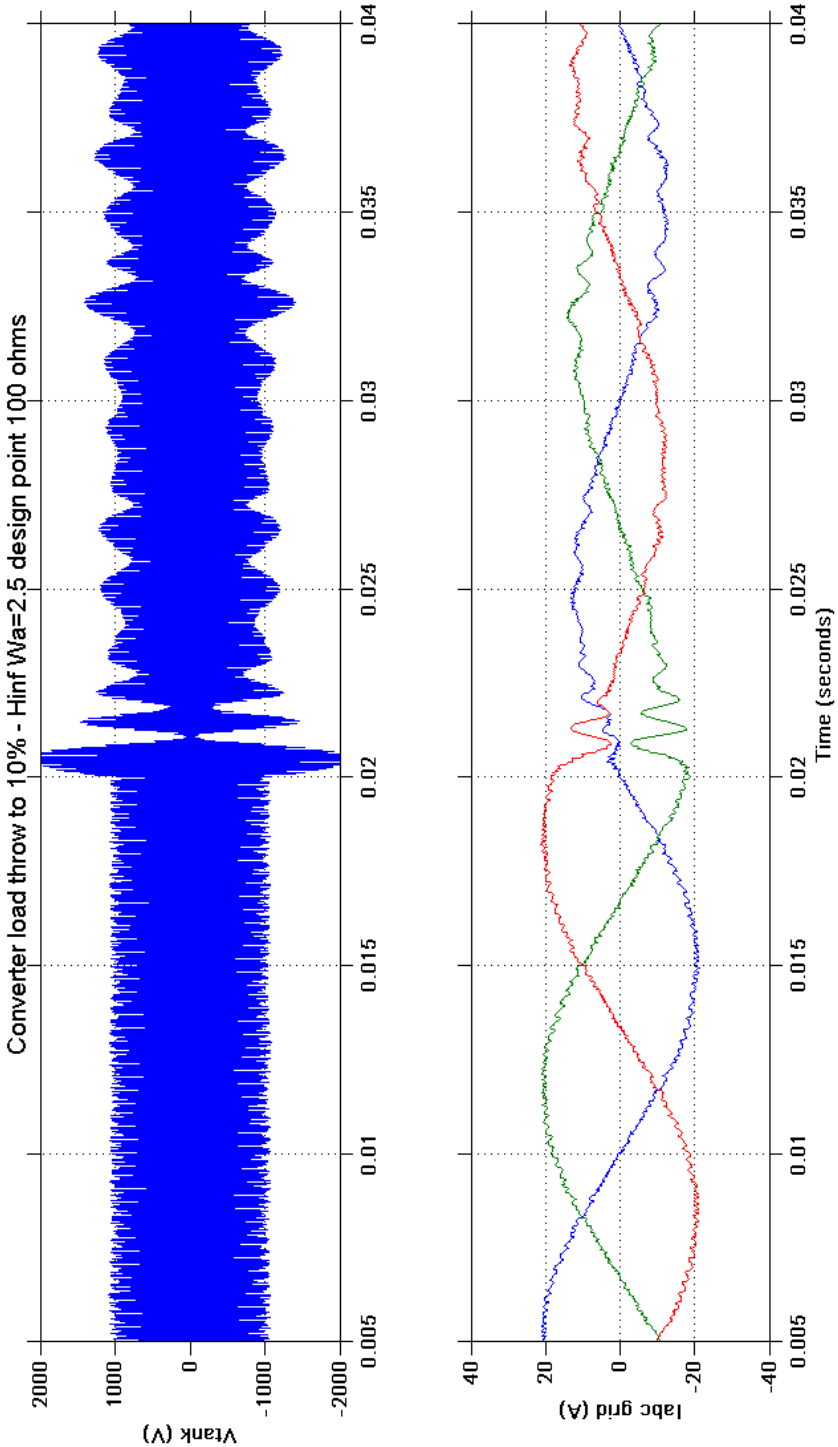

Figure 46 H_∞ Controller – step response to 10% load

7.4. Uncertainty modelling

7.4.1 Controller designed at 10% converter load

To improve performance the controller design point was changed from full load, 100 Ω to 1000 Ω and the PI controller retuned using MATLAB® Sisotool for this new converter model, which resulted in revised controller gains as shown in Table 5. The shaped system singular values were again plotted and are shown in Figure 47.

With this revised controller design the cross-over frequency of the loop is greater than the two previous results at 4.5 krads/s and again close to that of the shaped system. The angle of the response at cross-over is much gentler indicating wider bandwidth, gain and phase margins. The corresponding step response results are shown in, Figure 48, which shows that the $\mathcal{H}_\infty$ controller is less oscillatory with light loads but at the expense of an over-damped response at 50 and 100 Ω loads. The initial rate of change of output voltage (100 kΩ load) was 4.2 V/μs compared to 4.8 V/μs for the original PI controller. The corresponding comparison of time responses in shown in and Table 6, again indicating good improvement in performance, if at the expense of a slower rise time.

Table 6 Comparison of time responses – 100 kΩ load

Controller	Maximum overshoot	Rise time	Settling
PI (original design)	82%	0.28 ms	>7 ms
$\mathcal{H}_\infty$	64%	0.32 ms	2.5 ms

The Simulink® simulations were repeated for step changes from full to 10% load. Figure 50 shows the performance of the revised $\mathcal{H}_\infty$ controller design and compared to the performance of the PI controller, Figure 49, shows a more consistent steady-state level without any pronounced variations. The mean peak tank voltage is a little higher at full load before the load change, estimated as 1015 V peak, but afterwards, is very close to the demanded 1000 V. The rise in tank voltage at the change of load is interesting as its

amplitude seems unaffected by any of the voltage controller designs. Its duration for the $\mathcal{H}_\infty$ controller, however, is 1 ms compared to 3.5 ms for the PI controller and may well be a function of the coarse current control, changes to which are outside the scope of this work.

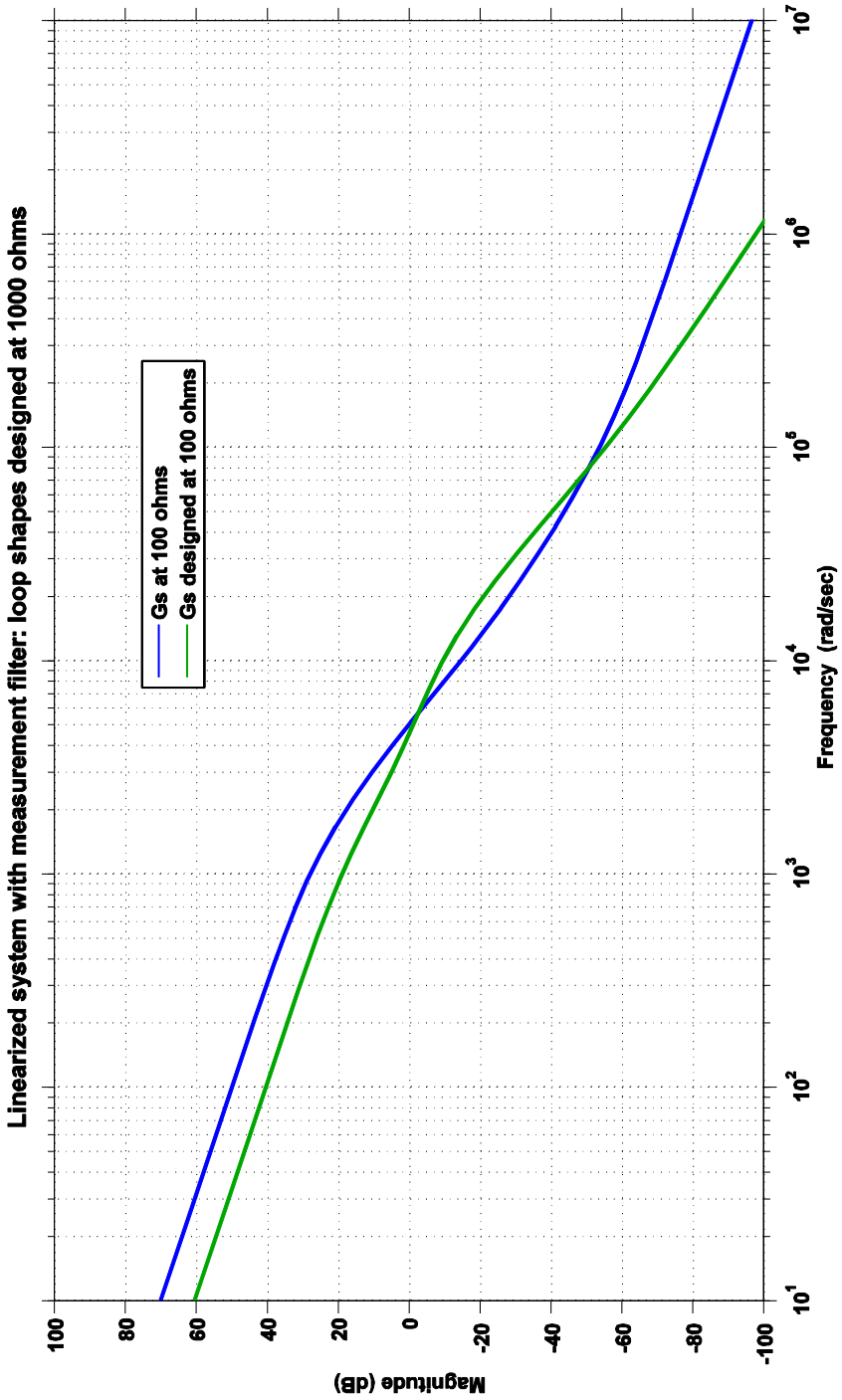

Figure 47 Converter model (design point 1 kΩ) – loop shape

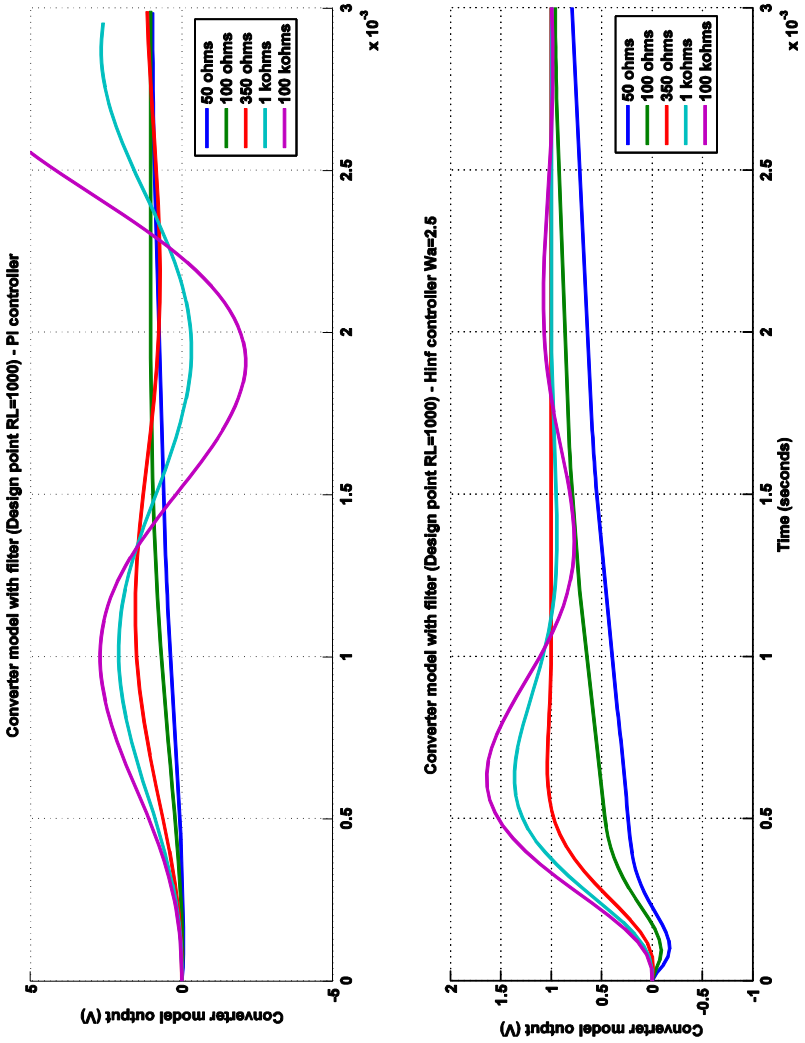

Figure 48 Converter model (design point 1 kΩ) – step responses PI and H_∞ filter

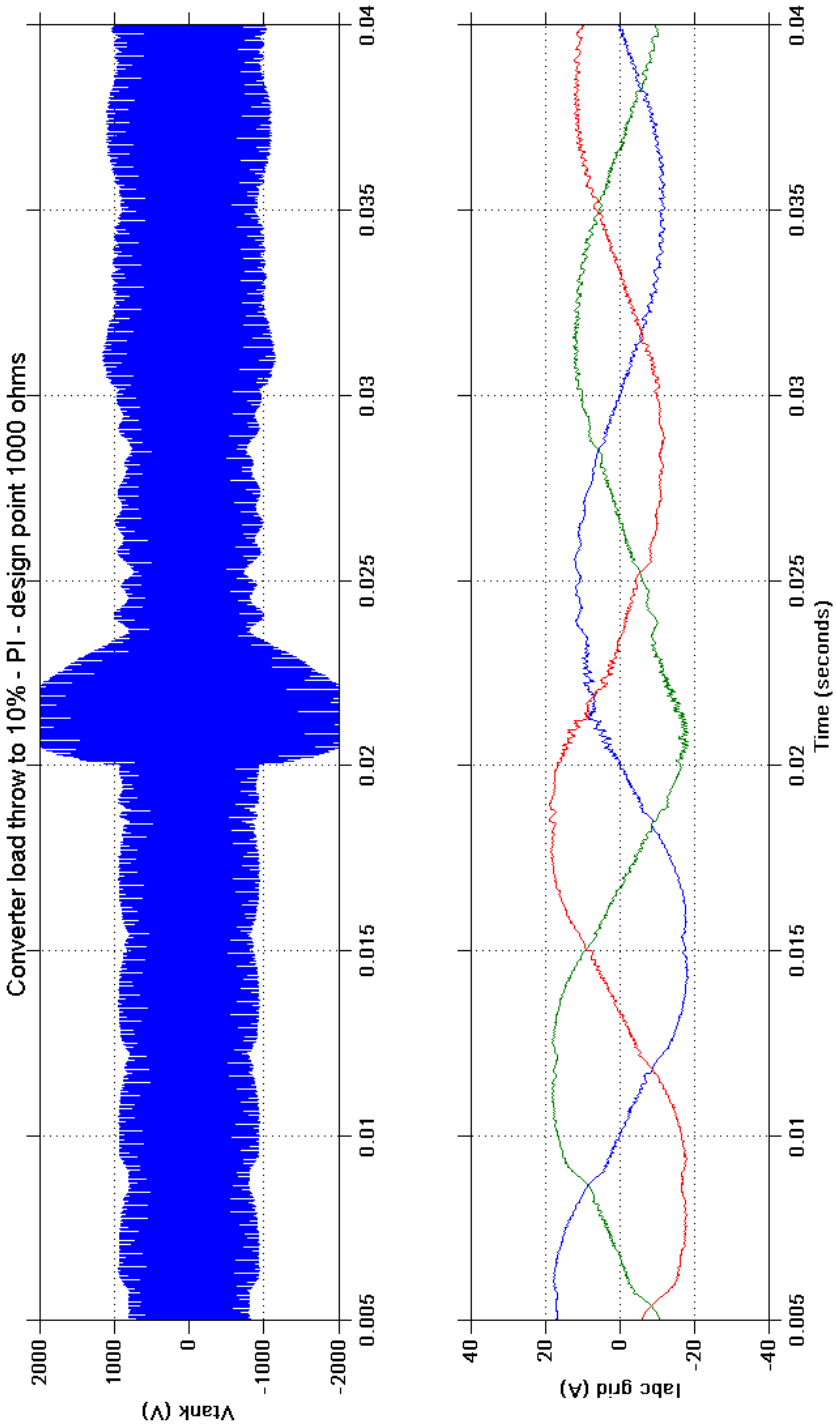

Figure 49 PI controller Design point R_L=1000Ω, step 100 -10% load

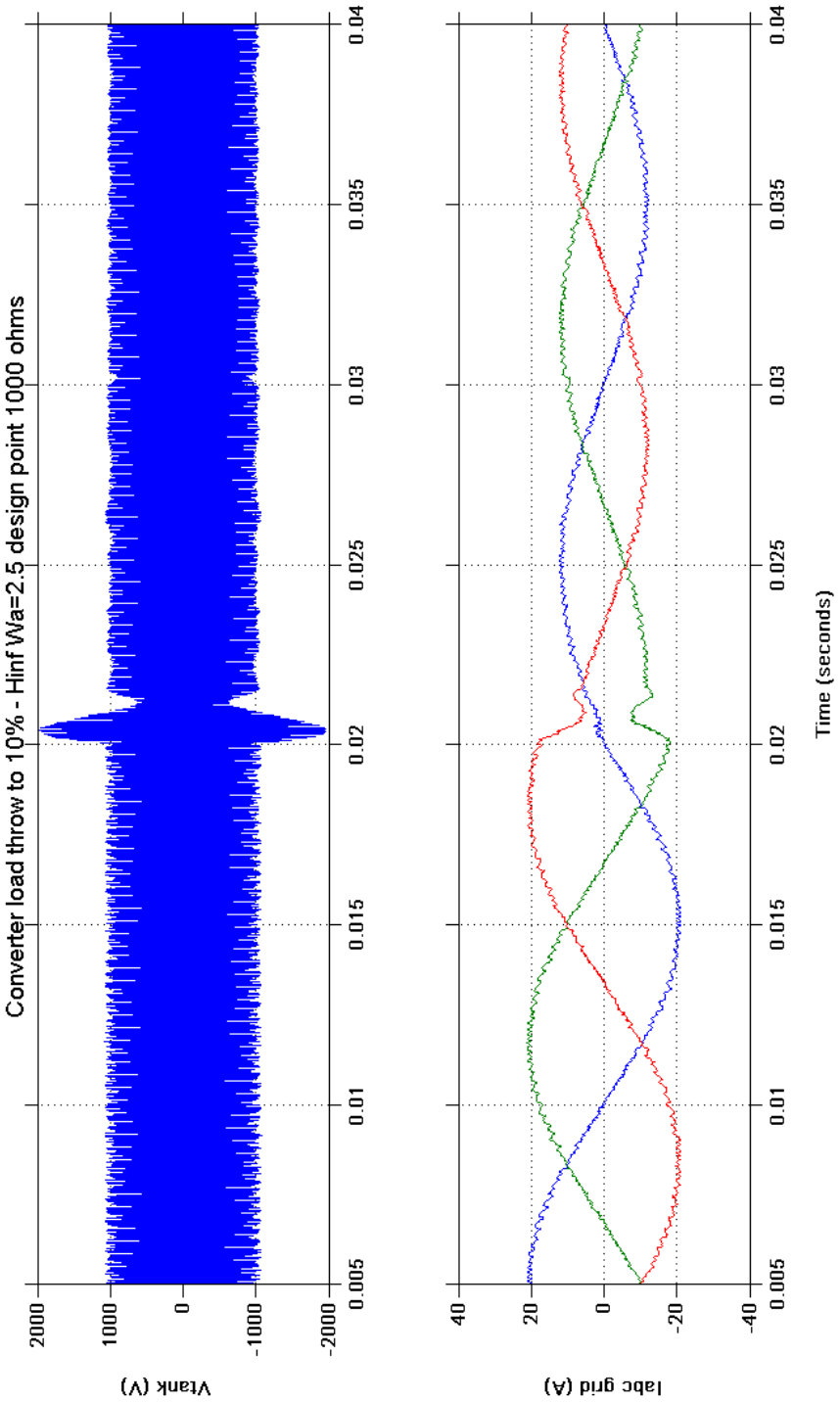

Figure 50 $\mathcal{H}_\infty$.controllers Design point R_L=1000Ω, step 100 -10% load

7.4.2 Multiplicative Uncertainty

An H_∞ controller, designed using Mcfarlane and Glover's loop shaping approach [66], was chosen to provide improved robustness over that provided by a classical PI controller as robust stability is an integral part of this procedure. One measure of the robustness of a control system is its insensitivity to differences between the model used for analysis and control design and the real system, or to paraphrase, its uncertainty model. Its robustness properties, in dealing with the uncertainties of the converter load that appear in the linearised transfer function of the converter, are a key consideration in choosing an appropriate control methodology.

Real systems contain frequency-dependant or dynamic uncertainty where the model lacks unknown system dynamics or lacks a true understanding of the detailed system characteristics. A power converter when connected to an uncertain load is a good example of such a type of model uncertainty. The uncertain load generates an uncertain pole, gain and importantly a right half plane zero in the converter transfer function.

The various sources of uncertainty are often lumped together into Multiplicative uncertainty. Multiplicative (or relative) uncertainty is often preferred and is expressed as:

$$(60) \quad l_I(\omega) = \frac{max}{G_P \in \prod} \left| \frac{G_P(j\omega) - G(j\omega)}{G(j\omega)} \right|$$

With a rational weight:

$$(61) \quad |\omega_I(j\omega)| \geq l_I(\omega), \forall \omega$$

Where l_I is the value of the relative errors of all possible systems as a function of ω, G_p is the transfer function of the perturbed system, G is the transfer function of the original system. Equation (61) then represents a weight, or desired transfer function, that embraces all the family of possible systems due to the uncertainty.

In the design of an $\mathscr{H}_\infty$ controller a family of perturbed system transfer functions is often used for uncertainty modelling, but in this investigation, we have chosen two plant transfer functions at the extremes of expected normal load conditions to represent the system

uncertainty. Understanding the performance differences between the two controller designs is fundamental to good design practice.

Using the Multiplicative Uncertainty model from (60) a frequency response of relative errors was plotted using each model in turn as the nominal plant and the other as the perturb plant and the results are shown in Figure 51. The converter control system was designed using positive feedback and, for the system designed at full load, the uncertainty response lies above 0 dB for low frequencies. This indicates that an integrator in the $\mathcal{H}_\infty$ weighting function, *W1*, is not appropriate, because when closing the control loop, the system would still have positive gain at these frequencies. Alternatively, with the system designed at 10% load, the uncertainty response lies below 0 dB for low frequencies, indicating an integrator in the $\mathcal{H}_\infty$ weighting function, *W1*, is feasible. For the converter controller, integral action is required in order to provide zero error between the tank voltage and reference.

From Figure 51 it was also recognised that there was a threshold design point between stable and unstable operation and this was found to be for a load of approximately 200 Ω, which is much less than 350 Ω indicated by the simple analysis shown in Chapter 5.2.2.

The choice of a design point at 10% load ensured a sufficiently low resistance to demonstrate a large step change in load. In a practical design, an analysis with the real load would be necessary to provide a more optimum design point or a limit to load excursions.

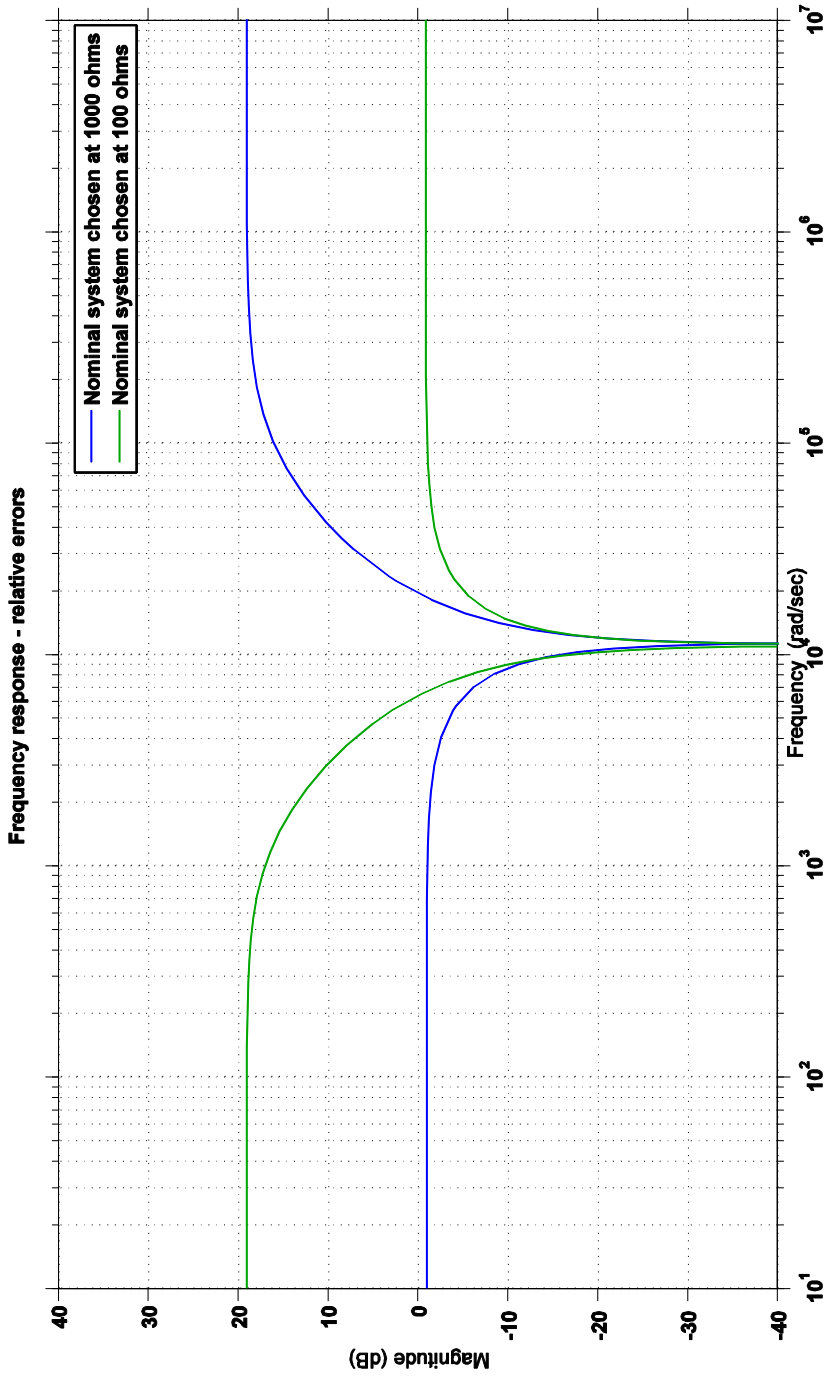

Figure 51 System multiplicative uncertainty responses for 1000 and 100 ohm designs

7.4.3 Inverse Multiplicative Uncertainty

Reference [52] suggests an alternative approach for cases of pole uncertainty, as is the case of the converter, which is well represented by inverse multiplicative uncertainty that can represent complex perturbations. The inverse multiplicative responses for the two systems are shown in Figure 53. These are simply the inverse of those shown in Figure 51. However, the aim of the controller design process is to guarantee robustness and stability in the presence of uncertainty and the necessary conditions for this are derived in the analysis below.

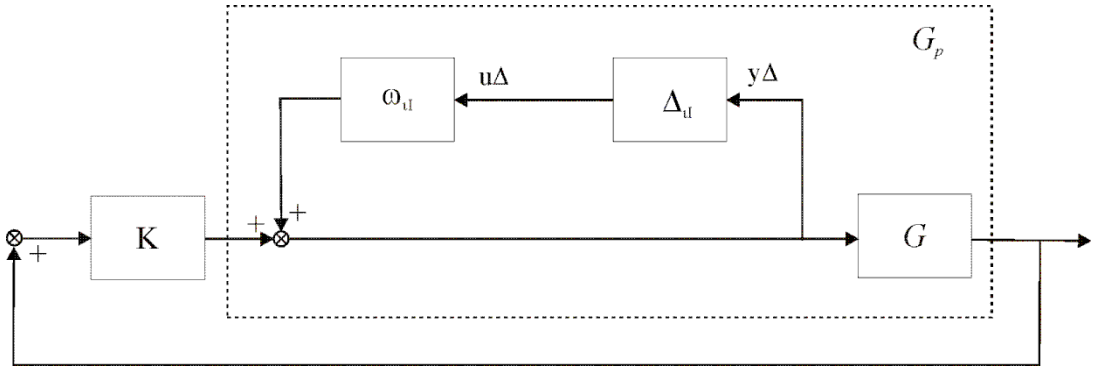

Figure 52 Feedback system with inverse multiplicative uncertainty

A representation of inverse multiplicative uncertainty, Figure 52, is given by:

$$(62)\quad \Pi_{iI} : G_p(s) = G(s)(1+\omega_{iI}(s)\Delta_{iI}(s))^{-1};\ \ |\Delta_{iI}(j\omega)| \le 1\ \forall\omega$$

Where:

Π is a set of possible perturbed system models, (the nominal model) $G(s) \in \Pi$, (the perturb model) $G_p(s) \in \Pi$ and $\Delta_I(s)$ is any stable transfer function where its magnitude at any frequency is ≤ 1. ω_{iI} is the magnitude of the system uncertainty expressed at each frequency, e.g. uncertainty response of relative errors. The subscript *I* denotes "input", but for a SISO system the perturbation may be considered at the system input or output.

Assuming that the perturbed loop transfer function, L_p, is stable, then robust stability is guaranteed if the encirclements by $L_p(j\omega)$ of the point -1 are avoided, hence:

(63) $RS \Leftrightarrow |1 + L_p| > 0, \ \forall L_p, \forall \omega$

(64) $RS \Leftrightarrow |1 + L(1 + \omega_{iI}\Delta_{iI})^{-1}| > 0, \ \forall \Delta_{iI} \leq 1, \forall \omega$

(65) $RS \Leftrightarrow |1 + \omega_{iI}\Delta_{iI} + L| > 0, \ \forall |\Delta_{iI}| \leq 1, \forall \omega$

The worst case for Equation (65) is when $|\Delta_{iI}| = 1$ and when $(1 + L)$ and $\omega_{iI}\Delta_{iI}$ have opposite signs, thus:

(66) $RS \Leftrightarrow |1 + L| - |\omega_{iI}| > 0, \ \forall \omega$

(67) $RS \Leftrightarrow |\omega_{iI} S| < 1, \ \forall \omega$

where S is the sensitivity function. Thus, the condition for robust stability with inverse multiplicative uncertainty gives an upper bound:

(68) $|S| < \frac{1}{|\omega_{iI}|}, \ \forall \omega$

At frequencies where the uncertainty is large and $|\omega_{iI}|$ is greater than 1, the system sensitivity, S, must be made small. For system such as the power converter, this is not always possible because of the right-hand-plane-zero (RHP-zero), which constrains $S = 1$ and therefore requires that: $\frac{1}{|\omega_{iI}|} \geq 1$. The result is that there can not be large pole uncertainty where a system has a RHP-zero.

Figure 54 shows the sensitivity of the closed-loop systems for the $\mathcal{H}_\infty$ controllers designed at 100% and 10% load constrained to 1 at high frequencies and $1/|\omega_{iI}| \geq 1$, thus meeting the robustness requirements. Using the inverse multiplicative uncertainty model, a designer would normally choose a weight closer to the sensitivity function response than is shown in Figure 54 to ensure that the system performance (bandwidth) was not overly degraded. Increasing the gain in the weight by a factor of ten brought the frequency response of the weight closer to the sensitivity responses, and increased the system bandwidth from 3.4 to 8.3 krads/s. However, using the increased gain in the controller

weight was subsequently shown to cause severe fluctuations of the converter output voltage when used in the Simulink® converter model and thus was not used in the final design.

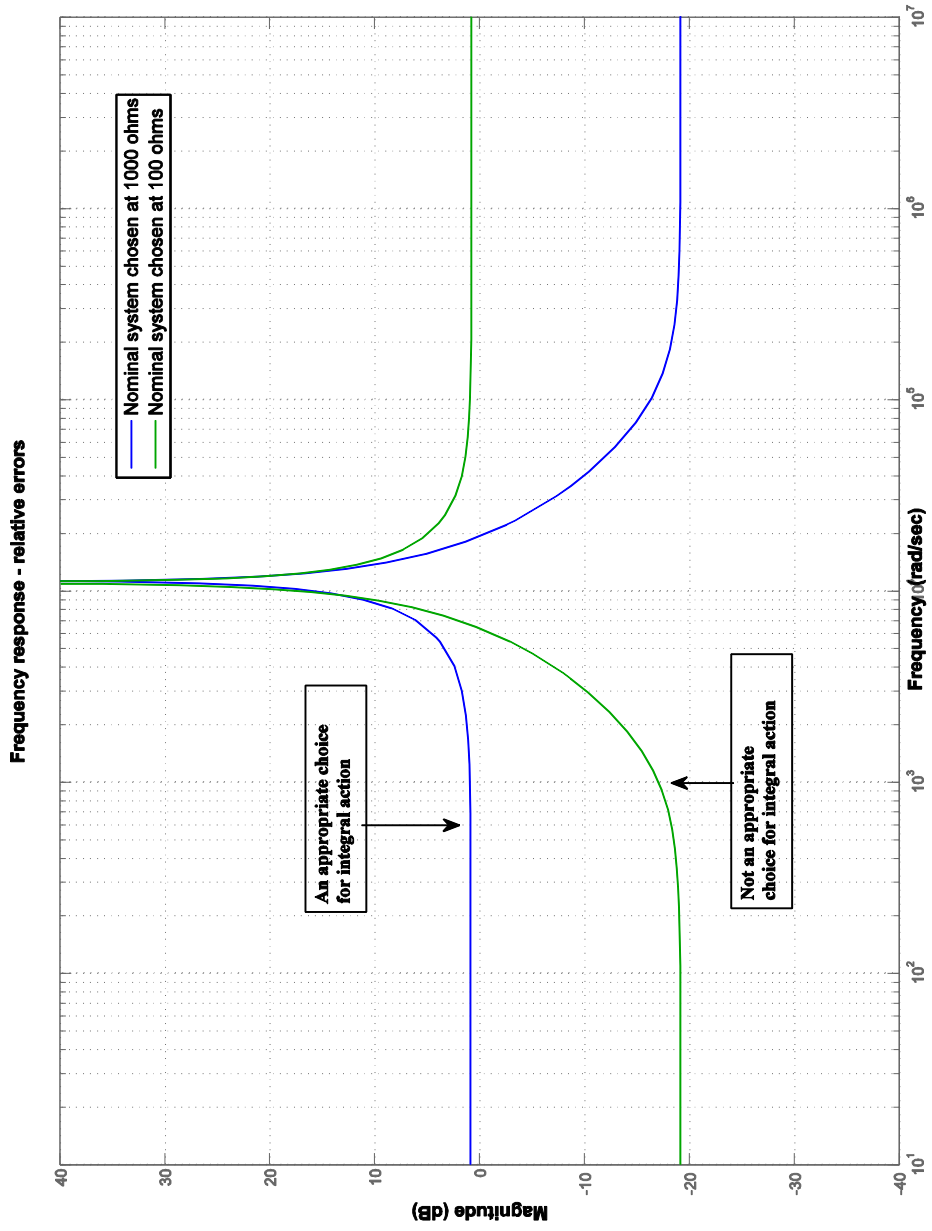

Figure 53 Inverse multiplicative uncertainty responses for 1000 and 100 ohms design

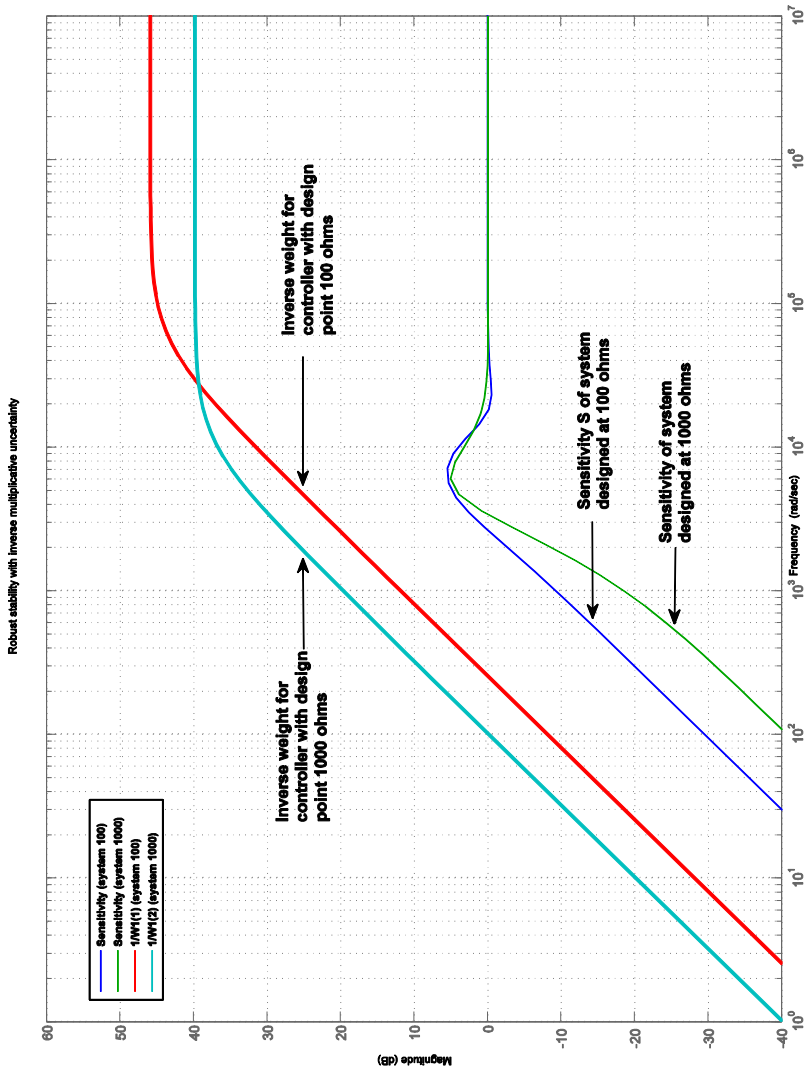

Figure 54 Robust stability with inverse multiplicative uncertainty

7.5. Summary of Advanced Control Studies

The design of a resonant converter controller for application in a power system Active Transformer has been investigated. PI and H_∞ controllers were designed and their performance compared. The results of the comparison showed that the H_∞ controller had an improved performance to a series of step changes in load up to 100 kΩ. These are summarised in Table 7. For a step change to 100 kΩ, the final design of the H_∞ controller produced a slightly slower rise time than the original PI controller, but higher damping of subsequent oscillations. The cost of this improvement was an over damped response at loads of 100% and greater. When used in the non-linear converter model, it provided a similar response to that of the PI controller for a load increase of 100% and for a demanded 30% increase in output voltage.

Table 7 Summary of time responses

Controller	Maximum overshoot	Rise time	Settling
PI (original design)	82%	0.28 ms	>7 ms
$\mathscr{H}_\infty$ (100 Ω design point)	64%	0.24 ms	3.0 ms
$\mathscr{H}_\infty$ (1 kΩ design point)	64%	0.32 ms	2.5 ms

For large load changes, e.g. 100 to 10%, both the PI and the H_∞ controllers, designed at 100% load, were unstable after the load change. The H_∞ controller was redesigned at the 10% load condition resulting in a stable response, both at full load and 10% load. The step response results are again shown in Table 7. The difference in performance between the H_∞ controller designs at the selected design points was reviewed using uncertainty modelling of the system. Using a multiplicative uncertainty model, the system designed at full load had gain positive relative errors at low frequencies and therefore should not be used with integral action in a positive feedback controller as it would produce positive low frequency gain when the loop was closed. Recall that for a tracking system the closed loop transfer function (complementary sensitivity) touches the 0 dB at low frequencies.

However, this is not possible for the above model choice (inverse of the uncertainty bound is below 0 dB). The uncertainty model of the system designed at 10% load had negative relative errors at low frequencies and therefore integral action was appropriate as the inverse of the uncertainty bound was above 0 dB. The threshold design point between stable and unstable operation was found to be a load of approximately 200 Ω, which was much lower than the 350 Ω identified as the threshold of marginal stability by the simple analysis in Chapter 5.2.2.

The choice of a PI function for the weighting in the $\mathcal{H}_\infty$ controller appeared a logical choice, but in fact was rather an arbitrary one and therefore, the "inverse multiplicative" approach recommended in [52] was also used as a design procedure to choose a suitable weight. The PI gains from the original controller design used as the $\mathcal{H}_\infty$ weighting function produced the appropriate frequency response but with a low bandwidth of 3.4 krads/s. Increasing the gain in the weight by 10 produced an inverse weight response closer to the system response as suggested by the approach. Although a bandwidth of 8.3 krads/s was achieved, which may have indicated an improved transient performance, the system actually produced unstable responses when used in the Simulink® converter model indicating too much system gain.

For the resonant converter, the use of a prior PI controller design at full load as the weighting function in an $\mathcal{H}_\infty$ controller design proved to be a successful start and is therefore recommended as an additional step in the general procedure for the design of converter controllers. The subsequent change to a design point less than full load to facilitate the use of integral action was found to be necessary and may well be a more general requirement for power converter designs to avoid poor load throwing performance.

Using the Simulink® converter model a step change of load to 10% load was successfully simulated. Both controller designs produced an initial over-shoot of the converter output voltage to a step change in load, usually in excess of 150%, which, for a practical converter, would prove to be a design limitation. Variations of the voltage controller design appeared to have little effect on the amplitude of the initial overshoot, which is the effect of the varying RHP zero in the system and a further analysis might be required to

quantify these effects. However, the addition of more measurements in the controller could solve the problem and this is suggested as further work.

Chapter 8.

Active Transformer

8.1. Introduction

The principal aim of this research project was to demonstrate, using simulation techniques, the feasibility of the Active Transformer. This chapter contains a description of the development of Active Transformer model and presents the results of simulations including demand and load changes but note that only the $\mathcal{H}_\infty$ controller designed for the 10% load point is used for work in reported in this chapter. A simulation to demonstrate the reversal of power flow is also presented.

The proposed application of the Active Transformer was an interface between the Grid side of a network and a Distribution Network cell as a means of providing improved network management and control in a network with revised architecture. It could also be used to control bi-directional power flow between a power cell and the network, or a large wind farm. In a future network of power cells characterised by high penetration levels of distributed generation, variable cell loads would be satisfied:

i) by the locally connected wind or other renewable energy generation, which is likely to be variable
ii) by power drawn from the network via the active transformer

to automatically achieve a balance between power supply and demand while maintaining cell voltages at supply standards. At times of excess power generation capacity in the cell, and rather than balancing the cell load/generation by generation curtailment, real and/or reactive power could be stored, traded and exported via the active transformer. The Active Transformer may also provide a means of controlling and stabilising distribution network voltages and limiting, or isolating, fault currents in either direction should the need arise.

An "islanded network" control capability may also be achieved although the distribution side converter would use a different method of control from the one described in this research. Whatever the application, the key to the exploitation of the Active Transformer is its versatility and controllability.

An Active Transformer enables the control of power flow, whether it is required to flow from the Grid side (supply side) in the forward direction to the distribution network side (load side) or vice versa in the reverse direction from the distribution network to the transmission network. This implies that the converter design should be symmetrical, and the Grid side and the Distribution side converters should be of similar topology for ease of reverse operation.

The building of an Active Transformer model, simply put, involves connecting two converter models and simplifying their controllers. Firstly, the converter controller model was simplified from that used in Chapter 6 and the controller was then tested for functionality using a Grid side converter model. Secondly, the Grid side converter model was reversed and reconfigured as a Distribution side converter. Finally, the two models were coupled and tested to verify that the desired Active Transformer functionality had been achieved, i.e. to control the flow of current through the Active Transformer in the forward and reverse directions and the ability to control grid and distribution side phase angles independent of current flow. The simplified converter model facilitated this process without many difficulties.

A three-phase switch model was not available in the Simulink® library and therefore a three-phase circuit breaker model was used instead. However, this model did not open all three phases simultaneously, but opened each phase on the next zero crossing of the phase current. Thus, a step change of load used in this chapter effected by opening a breaker was an unbalanced change and although not initially intended to be, was perhaps a more realistic scenario than the sudden event envisaged.

There was one notable lesson learnt from the use of Simulink® library measurement models. Simulink® Sympowersystems provides a model for measuring 3-phase voltages and currents. It is important to recognise that a.c. models, when using measurement

models as part of a control function, the phase of the measurement signal depends upon the direction of the current flowing through the model block. Although this seems a logical conclusion, Simulink® Help does not state this detail clearly and as a result the reversing of the converter proved to be a more lengthy exercise than expected. Therefore, in order to make the measurement of currents consistent and clear in this work, the following convention was adopted:

i) current out of a generator, through a resistance or inductance is measured using A-a connections as positive, and negative if using a-A connection
ii) forward mode is defined as current flowing from the Grid side converter to a Distribution side converter
iii) reverse mode is defined as current flowing from a Distribution side converter to a Grid side converter.

The Active Transformer model simulation parameters used in this chapter were set to:

i) simulation time, T_s, 10^{-6} s
ii) solver type Variable step
iii) solver ode23t

8.2. Grid side converter

8.2.1 Introduction

For power flow control in the forward direction, the grid side converter model controls the line currents sourced from the grid supply, the phase angle between the supply line voltage and current, and the amplitude of the 20 kHz a.c. link voltage.

A Simulink® model of the supply converter was built from a copy of the model used for verification as shown in Chapter 6. Only minor changes were made to the controller model by separating out the voltage and current control in order to facilitate reversal of power flow. The model was used to test the design of the reverse mode operation. A diagram of the Grid side converter model is shown in Figure 55 below. The model consists of five main parts:

i) converter 1
ii) grid network
iii) load circuit
iv) control functions
v) monitoring functions.

8.2.1.1 Converter 1

The converter model consists of a three-phase bridge a resonant circuit connected across its output as described in Chapter 6.3. In the model and subsequent results, the voltages and currents measured at the 3-phase terminals of converter 1 are labelled "*Vabc 1*" and "*Iabc 1* respectively"

8.2.1.2 Grid network

The Grid network in the forward mode is a source of power but in the reverse mode, it is a three-phase load on the converter. The network, in the forward mode, is represented by a fixed 50 Hz frequency, fixed 415 V line-line voltage generator that in the reverse mode sets the grid voltage, as the converter was not designed to control both 3-phase voltage and current simultaneously. A switchable split resistive load (initially 32 Ω) and a series resistance and inductance (1 MΩ and 1 mH) connected in parallel were also included to represent network impedances. The resistive load also helped to identify the phase relationship of the converter and network currents.

8.2.1.3 Converter load circuit

For forward mode operation the output of the converter was connected to a fixed load resistance (shown as 100 Ω) and a variable resistance (also shown as 100 Ω) at its output. For reverse mode operation, the output circuit was replaced by a fixed 1000 V, 20 kHz generator.

8.2.1.4 Control functions

The functions of the controller used in Chapter 6 were split into separate voltage and current controllers.

(a) Voltage control

The functions of voltage control were defined as a subsystem, "Voltage and direction controller", Figure 56, and was modified to enable forward and reverse operation to be easily selected, external to the model, by a change of a constant, Simulink® signal "For_rev", from +1 to -1, as shown in Figure 55. To facilitate comparisons in the forward mode, the output of the voltage controller provided a Grid current reference, for both *Id* and *Iq*, derived from $\mathcal{H}_\infty$ loop-shaping controller and a constant respectively. In the reverse mode, a 3-phase 50 Hz signal was generated and used to provide an *Id* and *Iq* reference for distribution network converter operation.

(b) Current control

The current controller was unchanged from that described in Chapter 6.3.3. The change in current in the converter line inductors was given by Equation (7) for the forward mode of the converter operation. Repeating the analysis for a reverse current flow resulted, logically, in the negative of Equation (7). In the reverse mode of operation, the Grid side converter, converter current was measured at its output as negative current because of the a-A orientation of the current measurement block. When used in the current controller to determine the control error, this measurement of current at the output naturally applies the conditions for operation of the converter in the reverse mode and means that the current controller model was the same for both Grid and Distribution side converters.

8.2.1.5 Monitoring functions

In order to keep the converter diagram uncluttered, the simulation signal and waveform monitoring was confined to a subsystem, "Monitoring". Monitored signals in this subsystem were derived from the model directly using monitoring "scope" functions or indirectly using Simulink® signal recording features.

8.2.2 Initial simulations

To verify that the revised converter model operated as intended, simulations were run firstly, in the forward mode and then in reverse mode.

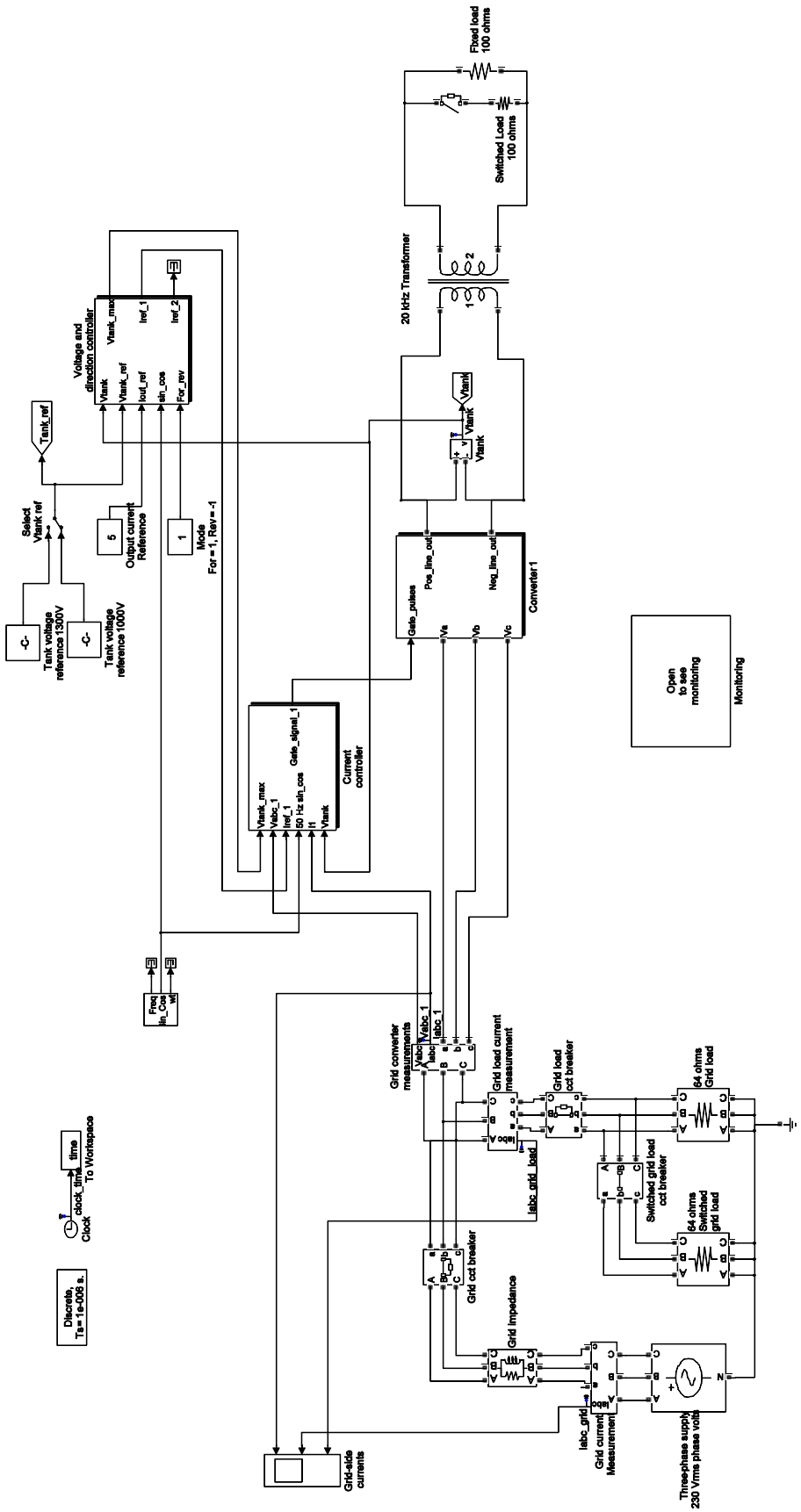

Figure 55 Grid side converter model – forward mode

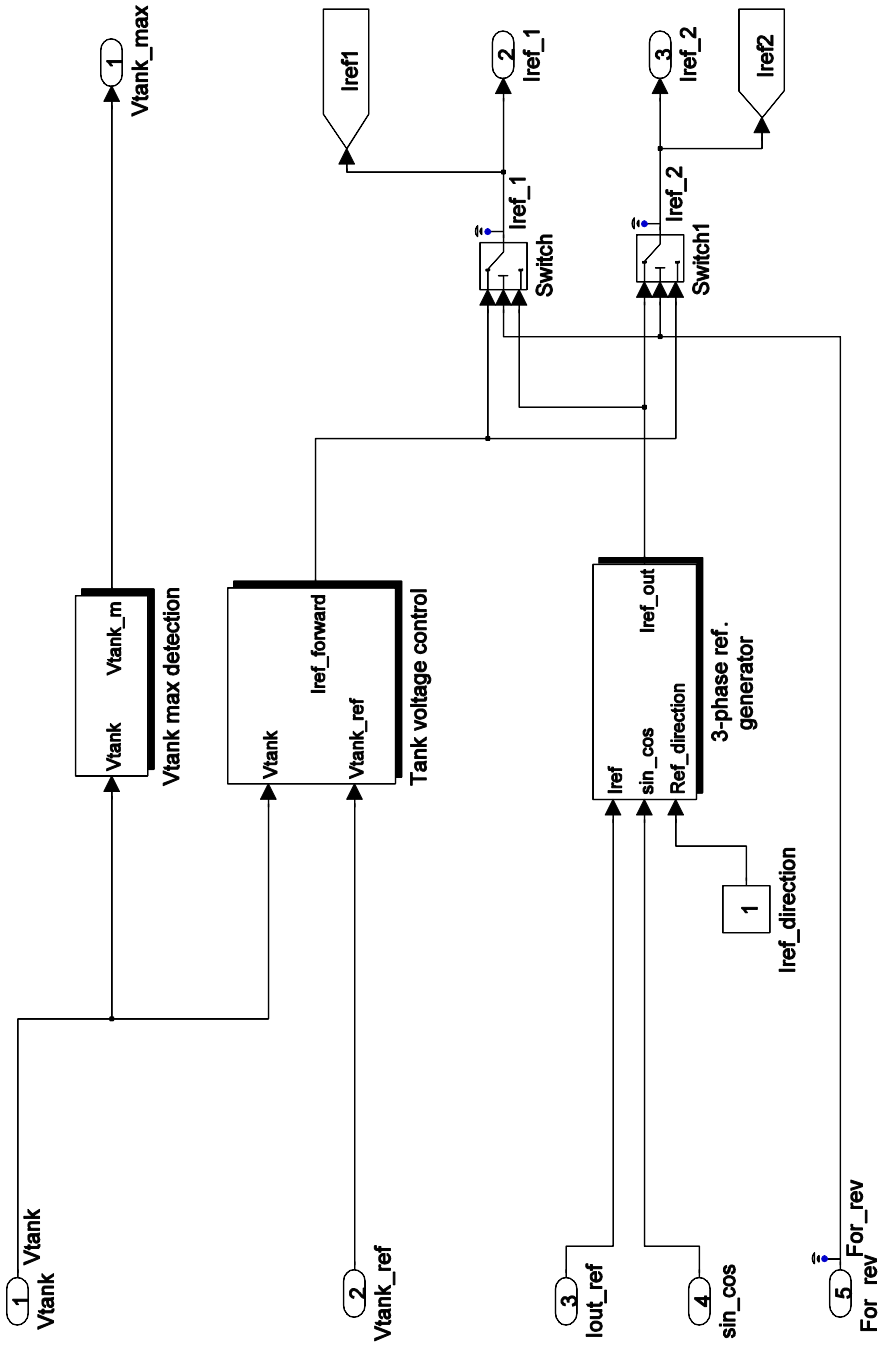

Figure 56 Voltage and mode controller

8.2.3 Forward mode simulation

For the Grid converter, the forward mode is defined as current flowing from the 3-phase terminals to the 2 terminal side of the converter and the input current reference is derived from the voltage feedback loop. The following simulation conditions were set:

i) simulation time 0.06 s
ii) grid side generator line to line 400 Vrms 50 Hz
iii) select Vtank ref Tank voltage ref 1000 V
iv) fixed load 100 Ω 100 Ω
v) grid load cct. breaker closed
vi) grid load 64 Ω
vii) switched grid load cct. breaker closed
viii) switched grid load 64 Ω
ix) mode (forward) 1

The results of this simulation are shown in Figure 57. The three-phase converter line current, I_{abc} 1, signal, shows a high frequency ripple as a result of the switch of the converter bridge. This signal could have been filtered to provide a cleaner waveform and one that made the measurement of the amplitude more straight forward, but the visibility of the ripple current was considered to be a useful indication of the correct operation of the converter, hence retained, and the mean amplitude was therefore estimated. This procedure is used consistently throughout this chapter.

In the forward mode, total current supplied by the Grid is shared between the grid load, 10 A peak, and the converter. The converter portion flows into the converter line inductors and is determined by the converter operation into a load resistance with the demanded output voltage, which were set to 100 Ω and 1000 V peak respectively as the full load condition. For this load the approximate converter line input current I_{abc} 1 was 9.9 A_{peak} and the total Grid current approximately 20 A_{peak}.

8.2.4 Reverse mode simulation

For the Grid converter, the reverse mode is defined as current flowing from the 2-terminal side to the 3-phase terminals and the output current reference is set by a constant value before running the simulation.

It was during the testing of the reverse converter model that the importance of the phasing of the output current measurement referred to in 8.1 was realised. Selection of the wrong phase invariably led to unstable operation of the converter.

For the reverse mode simulation the forward mode load circuit was replaced with a generator and the simulation initial conditions set similar to the forward mode except for:

i) Generator 1000V 20 kHz generator
ii) output current reference 5. For this demand the converter will supply current in anti-phase to the grid supply.
iii) mode (reverse) -1.

The results of this simulation are shown in Figure 58. In the reverse mode, the grid side load and grid voltage determine the grid side load current, $I_{abc\ grid\ load}$, of 10 A peak. The converter current reference was set to give a converter current of 5 A_{peak} in anti-phase to the grid supply, but because the current now flows out of the converter 3-phase terminals, its measurement in Figure 58, I_{abc} 1, is in anti-phase to the actual current, i.e. it appears to be in-phase with the grid load current, $I_{abc\ grid\ load}$. The grid therefore supplies 15 A_{peak} to satisfy the grid side load conditions.

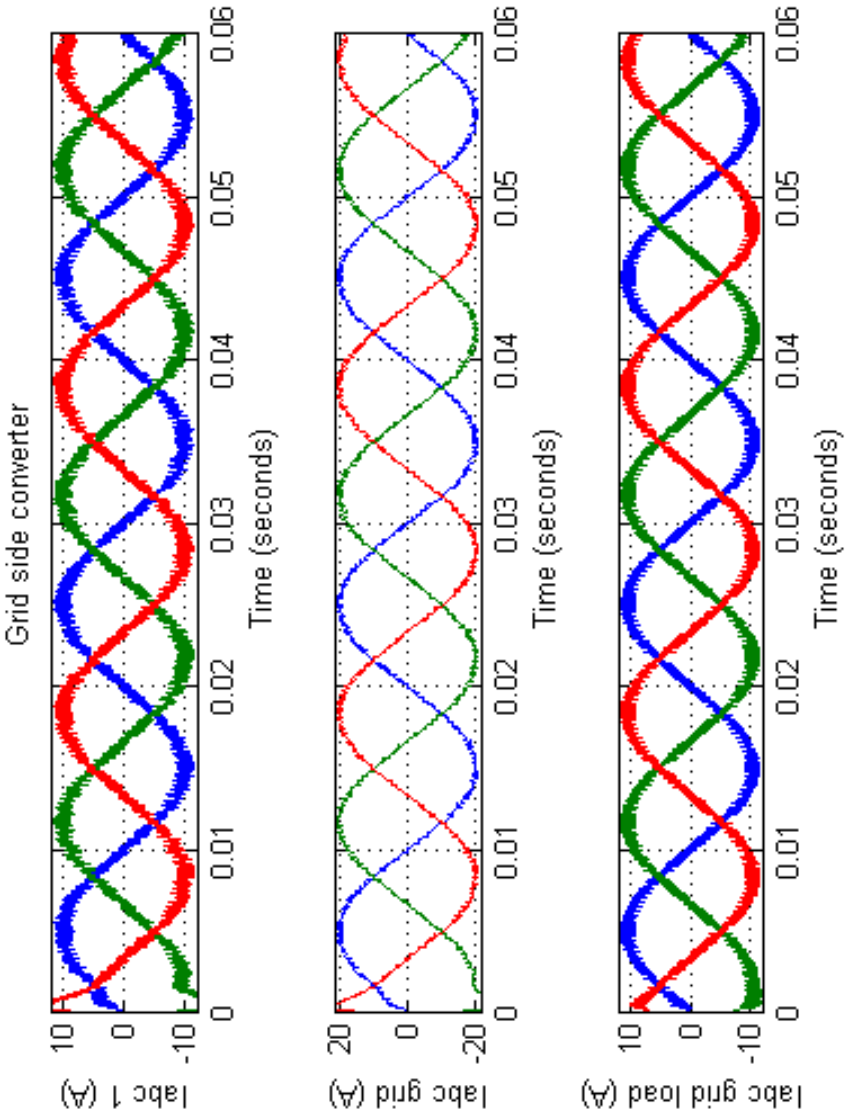

Figure 57 Grid side converter forward mode

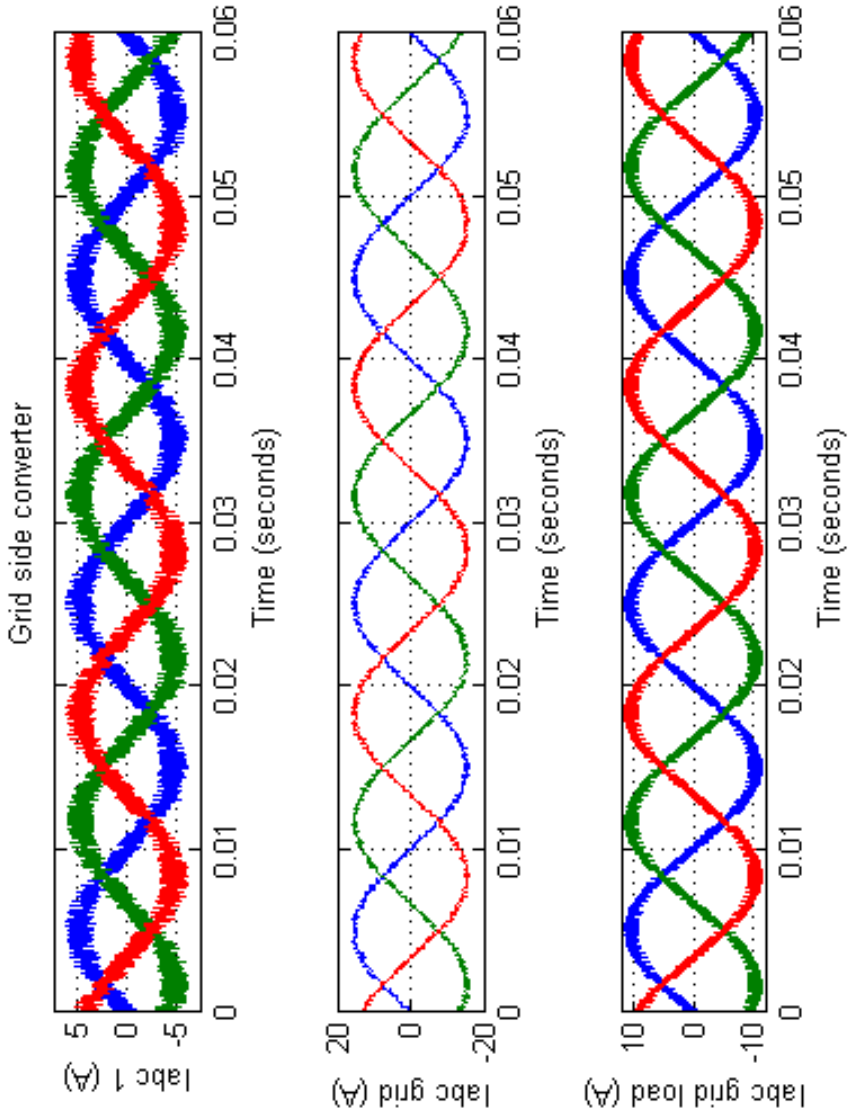

Figure 58 Grid side converter reverse mode

8.3. Distribution side converter model

The Distribution side converter model, Figure 59, was built by reflecting the grid converter design about the high frequency transformer, including, initially, the voltage controller, and altering signal names to make it distinguishable from the grid converter. To distinguish the DN converter measurements from those of the Grid converter, the voltages and currents of the DN converter measured at the 3-phase terminals of the converter have been labelled "*Vabc 2*" and "*Iabc 2* respectively"

In the forward mode the converter controls the current fed (and hence the power) to the distribution network load. In the reverse mode it transfers power from the distribution network and controls the a.c. link voltage. To ensure no errors had been made in the building of the distribution side converter model forward and reverse operation, similar to that applied to the grid side converter, were simulated.

8.3.1 Forward mode simulation

For the Distribution side converter forward mode is the same as the reverse mode in the Grid converter, i.e. current flows from the 2-terminal side to the 3-phase side of the converter.

For the forward mode simulation, the reverse mode load circuit, Figure 59, was replaced with a generator and the following simulation initial conditions set:

i) simulation time 0.06 s
ii) Generator 1000V 20 kHz generator
iii) output current reference -5. For this demand the converter will supply current in phase with the Distribution network supply.
iv) DN side generator line to line 400 Vrms 50 Hz
v) DN load cct. breaker closed
vi) DN load 64 Ω
vii) Switched DN load cct. breaker closed
viii) Switched DN load 64 Ω

ix) mode (forward)1

The results of the forward mode simulation are shown in Figure 60. Although the DN side converter current, I_{abc} 2, is in phase with the DN load current, due to the inversion of the measurement, it is shown as approximately 5 A_{peak} in anti-phase. However, the DN load current is 10 A_{peak}, comprising of 5 A peak converter current and 5 A peak DN grid current.

8.3.2 Reverse mode simulation

For the DN side converter, reverse mode, Figure 59, is the same as the forward mode in the Grid converter, i.e. current flows from the 3-phase side to the 2-terminal side of the converter. The simulation initial conditions were similar to those for the forward mode simulation except for:

i) Select Vtank reference Tank voltage reference 1000 V
ii) fixed load 100 Ω
iii) switched load 100 Ω cct. breaker open
iv) mode (reverse) -1

The results are shown in Figure 61 and are similar to those of the Grid converter in forward mode, Figure 57, noting that the converter current measurement does not have an inversion and is in-phase with the DN supply current.

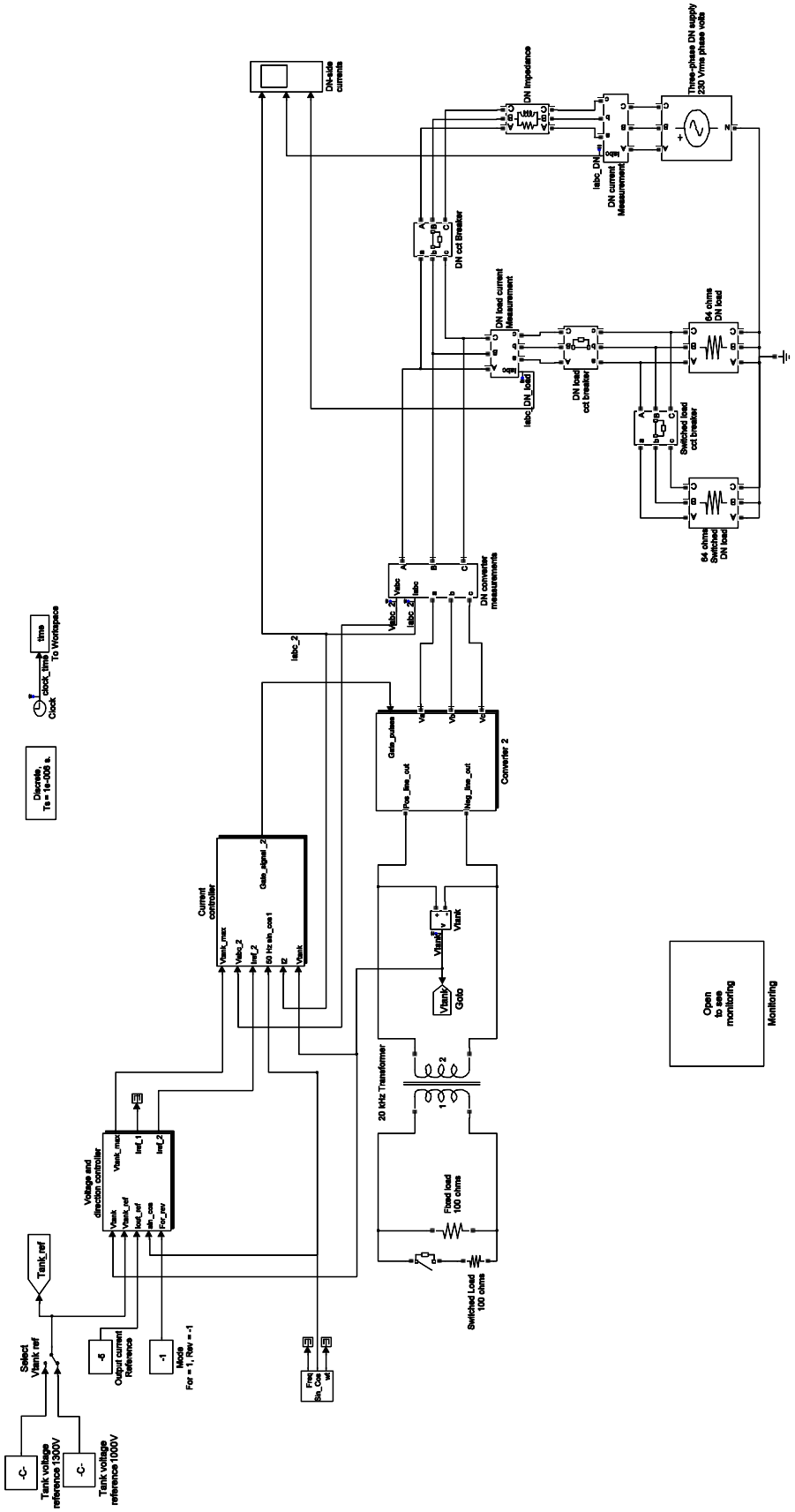

Figure 59 Distribution side converter model – reverse mode

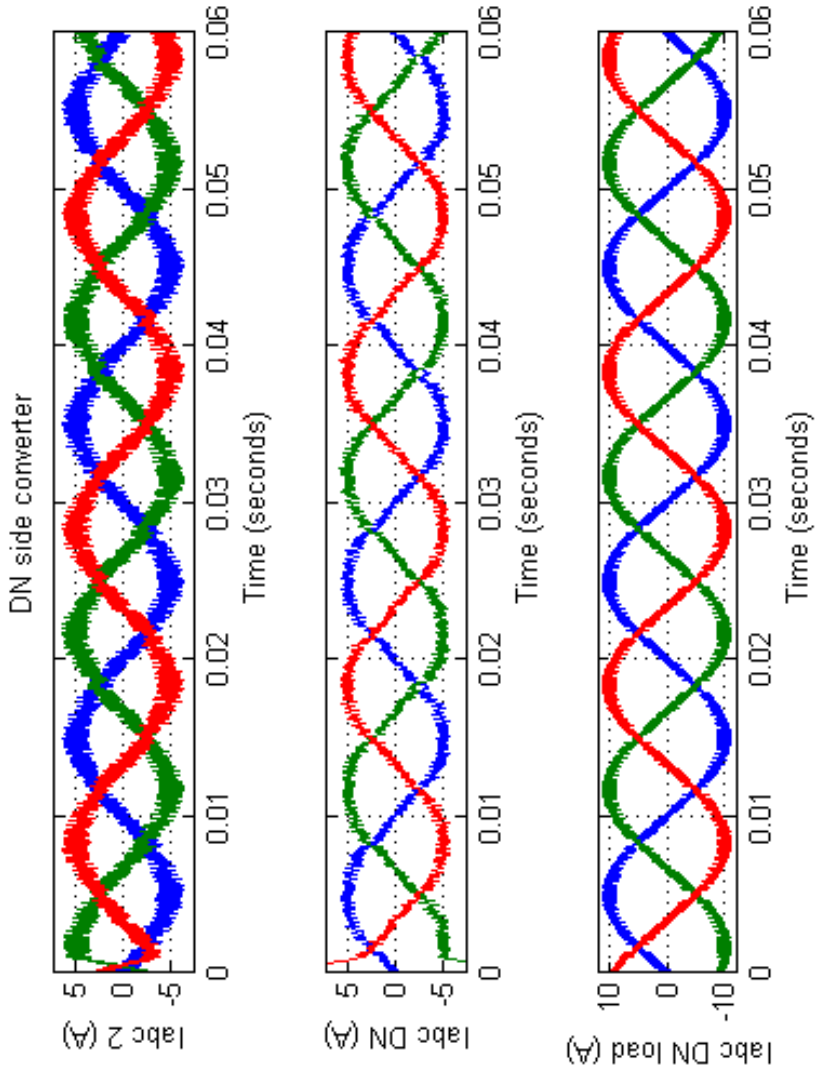

Figure 60 Distribution side converter forward mode

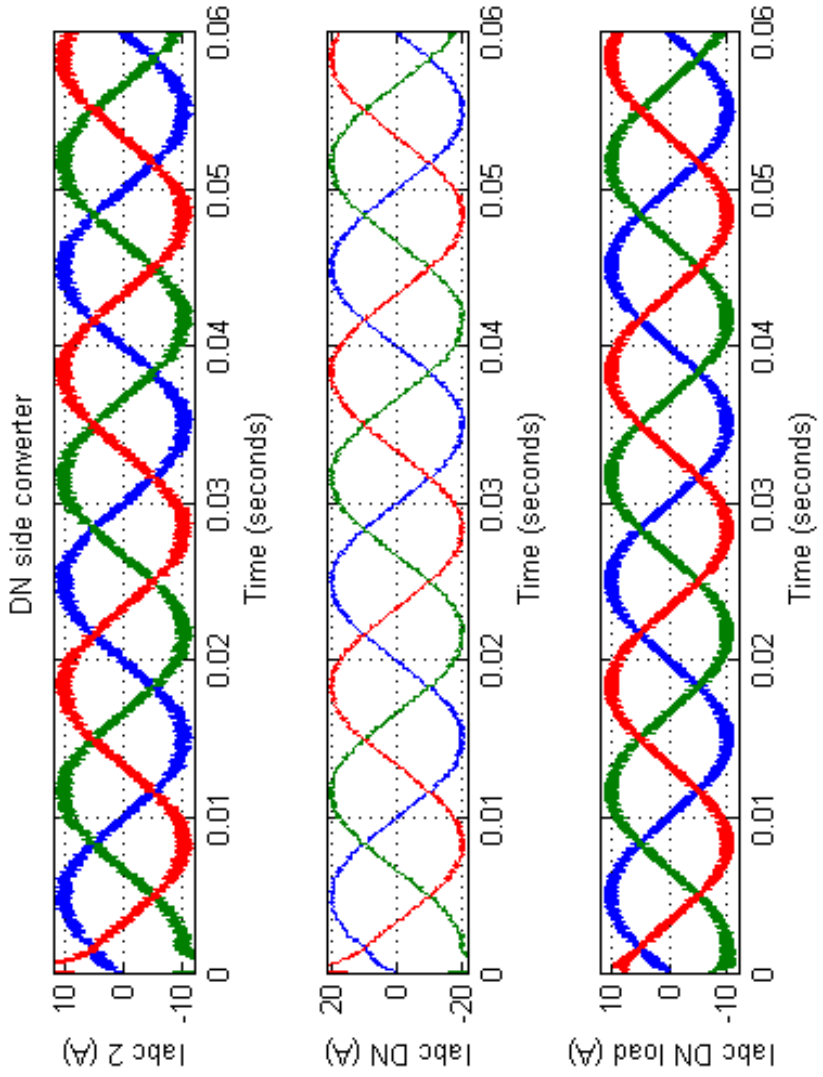

Figure 61 Distribution side converter reverse mode

8.4. Active transformer model

8.4.1 Model outline description

The Grid and Distribution side converter models and their respective network side models were connected to form the Active Transformer model. Duplicate and redundant subsystems and monitoring were removed. Some additional switching was included to facilitate a mode change during simulations and some connections were replaced with "goto" functions to simplify the model schematic diagram. Connecting the converters at their 20 kHz terminals created a high frequency link system. The control of the link voltage was assigned to the Grid converter when the Active Transformer was operating in the forward mode and to the Distribution Network converter during reverse operation. A block diagram of the test arrangement is shown in Figure 62 and the Simulink® model of the Active Transformer is shown in Figure 63. The model was used to simulate the control of power flow from the transmission network side (Grid-side) in the forward direction to the distribution network (DN-side) and, vice versa, in the reverse direction from the distribution network to the transmission network. For power flow control in the forward direction, the Grid converter was used to control the source line currents, the phase angle between the supply line voltage and current, and the a.c. link voltage. Whereas the Distribution Network converter controls the output converter current (and hence the power) fed to the distribution network.

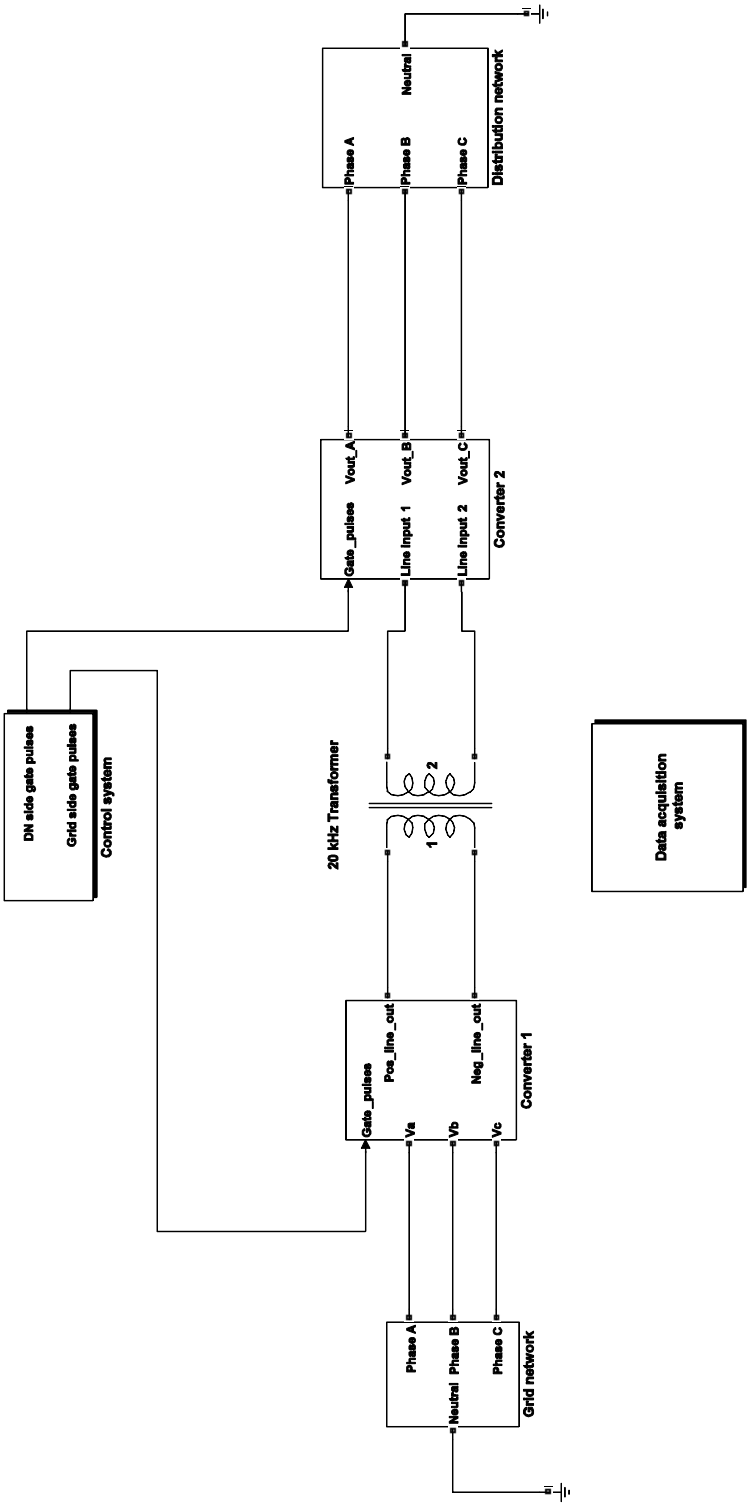

Figure 62 Test arrangement

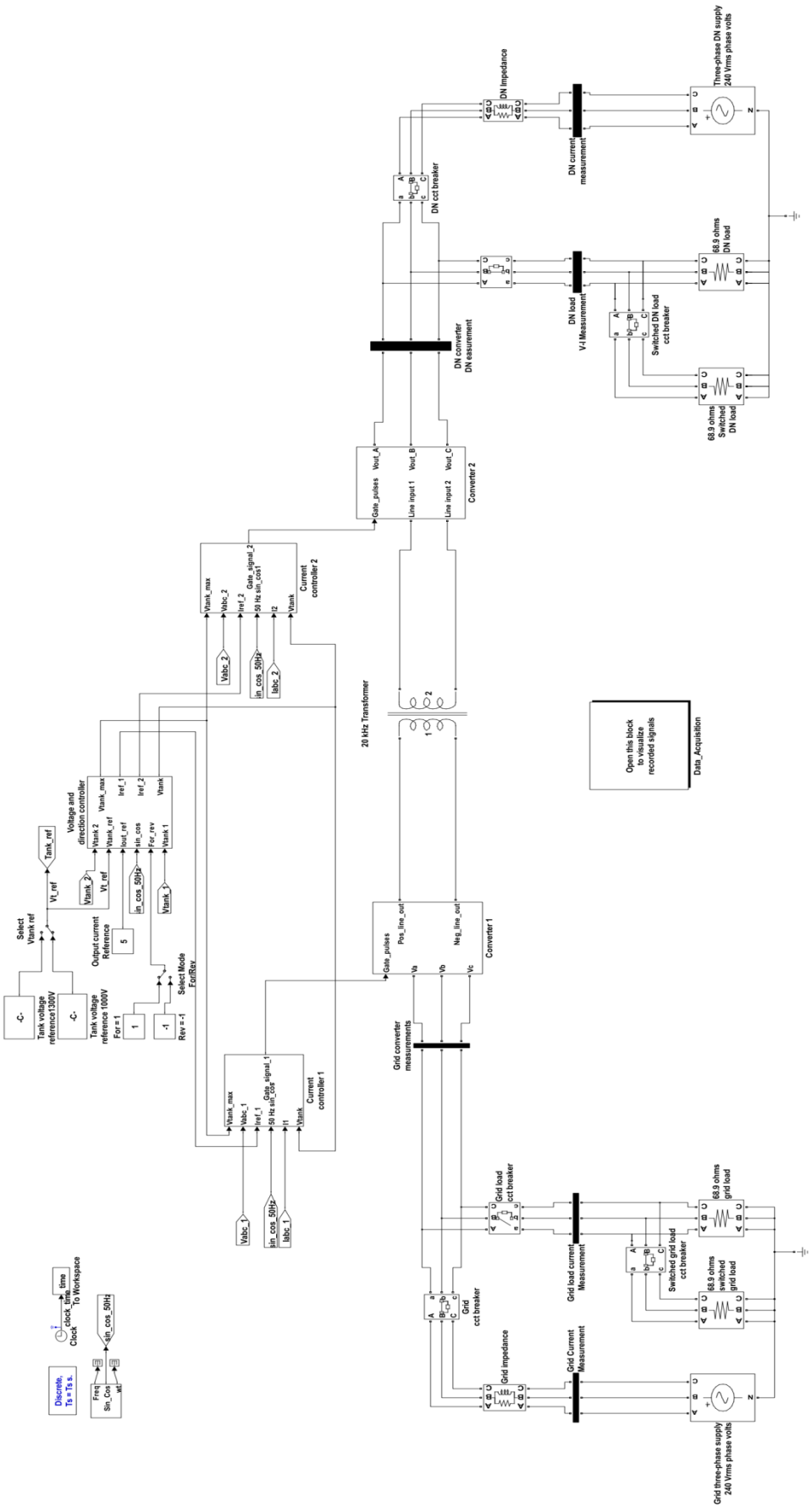

Figure 63 Active transformer Simulink® model

8.5. Simulations and results

8.5.1 Test descriptions

Four test simulations were used to verify the operation of the Active Transformer model. The first two tests repeat the load and demand changes used in the converter simulations, 8.2 and 8.3, to give confidence in the model. The second two tests were sudden reversals of power flow. These tests can be compared to the emergency crash reversal of a ship's propulsion system, which should only be encountered a very few times in the lifetime of the system because of the excessive stress it creates in the system. It is therefore a very harsh operation for a practical implementation of the Active Converter and may cause power semiconductor switch commutation failures unless the transition is designed to happen in a very controlled manner. In the following tests the transitions are sudden in order to identify any underlying control problems.

The test simulations are described with reference to Figure 63 , which is shown with 415 V 50 Hz Grid and DN generators instead of the 400 V generators previously used.

Test 1: In this simulation the Active Transformer model is configured for forward mode operation and step changes in load and demand are made. The following initial conditions were set:

i)	simulation run time	0.12 s
ii)	Grid and DN generators	line-line 415 V, 50 Hz
iii)	mode select (forward)	For = 1
iv)	select Vtank ref switch	Test voltage reference 1000V
v)	output current reference	5, manually changed to 2.5 A at 80 ms
vi)	Grid load cct. breaker	closed
vii)	Grid load	68.9 Ω
viii)	split grid load cct. breaker	closed
ix)	split grid load	68.9 Ω
x)	DN load cct. Breaker	closed
xi)	DN load	68.9 Ω

xii) switched load DN cct. breaker closed, set to open at 50 ms
xiii) switched DN load 68.9 Ω

At 50 ms the DN split load circuit breaker opens reducing the Active Transformer load to 68.9 Ω. At approximately 80 ms, the output current reference is manually changed from 5 to 2.5 A. These actions result in a 100-50% load change and an Active Transformer output current change 5 – 2.5 A.

Test 2: In this simulation the Active Transformer model is configured for forward mode operation at full load and a step change to 20 kW output is made. The initial conditions were similar to those set for Test 1 except:

i) simulation run time 0.08 s
ii) DN load 34.45 Ω
iii) switched DN load cct. breaker open, set to close at 40 ms
iv) DN switched load 11.48 Ω

At 40 ms the DN switched load circuit breaker was closed and the Active Transformer load increased from 5 to 20 kW.

Test 3: In this simulation the Active Transformer model was started in forward mode operation and a sudden mode reversal, forward to reverse, demand was made at 60 ms. The following initial conditions were set:

i) simulation run time 0.12 s
ii) Grid and DN generators line-line 415 V, 50 Hz
iii) mode select (forward) For=1
iv) select Vtank ref switch Test voltage reference 1000V
v) output current reference 5
vi) Grid load cct. breaker closed
vii) Grid load 68.9 Ω
viii) split grid load cct. breaker closed
ix) split grid load 68.9 Ω
x) DN load cct. Breaker closed

xi) DN load 68.9 Ω

xii) switched load DN cct. breaker closed, set to open at 50 ms

xiii) switched DN load 68.9 Ω

Test 4: In this simulation the Active Transformer model was started in reverse mode and a sudden mode reversal, reverse to forward, demand was made at 60 ms. The initial conditions were similar to those for Test 3 except for:

i) mode select (forward) Rev = -1

Test 5: Phase angle changes. There were two parts to this simulation:

i) changes to grid-side phase angle

ii) changes to distribution-side phase angle

These changes were effected by setting a simulation constant representing I_q to ±5 A for the reference demands of the forward and reverse converters. The aim was to verify that the phase angle of the converters could be changed independent of the current amplitude, I_d, which was set to 5 A. The change of phase angle from zero creates reactive power and therefore the power supplied by the Grid and to the Distribution Network was recorded as an indication of phase angle control.

8.5.2 Test 1 results

The main currents resulting from the application of step changes of the resistive load and load-side converter demand are presented in Figure 64 with the start-up variations in the first 20 ms of the traces suppressed for clarity. Although the Active Transformer output current, I_{abc} *2* is sinusoidal, the grid current, I_{abc} *1* contains some distortion that was not present in the individual converter simulations. The cause was likely to be the different loading effects of an active load (the DN converter), often more like a capacitive load than the purely resistive load of previous studies. The ripple was a readily identifiable characteristic of the "importing" converter when reviewing the results of later reversal simulations, and conversely, the undistorted current became the characteristic of the "exporting" converter.

The a.c. link voltage, *Vtank*, shown in Figure 65 is also noticeably more "lumpy" with an amplitude ripple of 200 V peak-peak at 300 Hz. In the resistance loaded converter model this would indicate that the voltage condition, Equation 77, has been violated and the current controller is not operating effectively. The remedy in the case of the converter would be to increase the tank voltage reference. In the case of the Active Transformer, this change was ineffective indicating a more complex loading problem, the investigation of which was assigned to "further work". The a.c. link voltage ripple did not affect the overall operation of the Active Transformer and indicated a good degree of robustness of the control system in dealing with variable link voltage.

8.5.2.1 20 – 50 ms period

During the period 20-50 ms, the DN load is 10 A peak. The Distribution Network generator and the DN converter each supply, in-phase with the generator voltage, 5 A mean-peak into the distribution side load, $I_{DN\ load}$. Note that I_{abc} 2 shown in Figure 64 is in anti-phase to $I_{DN\ load}$ due to the measurement method. As the model is essentially lossless, the DN converter power is drawn from the Grid supply. The Grid converter mean peak current is 5 A, in phase with the Grid supply voltage. The Grid also supplies 10 A peak to the Grid load making a total of 15 A peak drawn from the supply.

8.5.2.2 Step change of load at 50 ms

At 50 ms the DN load was changed from 34.45 to 68.9 Ω and was effected at the next zero crossing of the phase currents. No untoward transient events were seen on the current traces at the zero crossings.

8.5.2.3 50 – 80 ms period

The DN converter was controlled to provide 5 A mean-peak and therefore the reduced load demand was balanced by a reduction of the current supplied by the DN generator. A fall to zero was expected, but due to the 20 kHz ripple on the converter current and the nature of the coarseness of the current control, the DN generator provides a current to maintain balanced load conditions.

8.5.2.4 Step change in demand at 80 ms

The DN converter demand was changed from 5 to 2.5 A mean-peak at 80 ms.

8.5.2.5 80 – 120 ms period

Some variation of the DN converter currents are seen on the *Iabc 2* and *I DN* traces as they change to 2.5 A mean-peak, but it is well controlled and the converter resumes a steady supply within 5 ms. The reduction in current from the DN converter coincides with an increase in the current supplied by the distribution network generator, *I DN*, from zero to 2.5 A mean-peak. The change to the DN converter current is reflected through the Grid converter to the Grid supply, which also reduces from 15 to 12.5 A mean-peak.

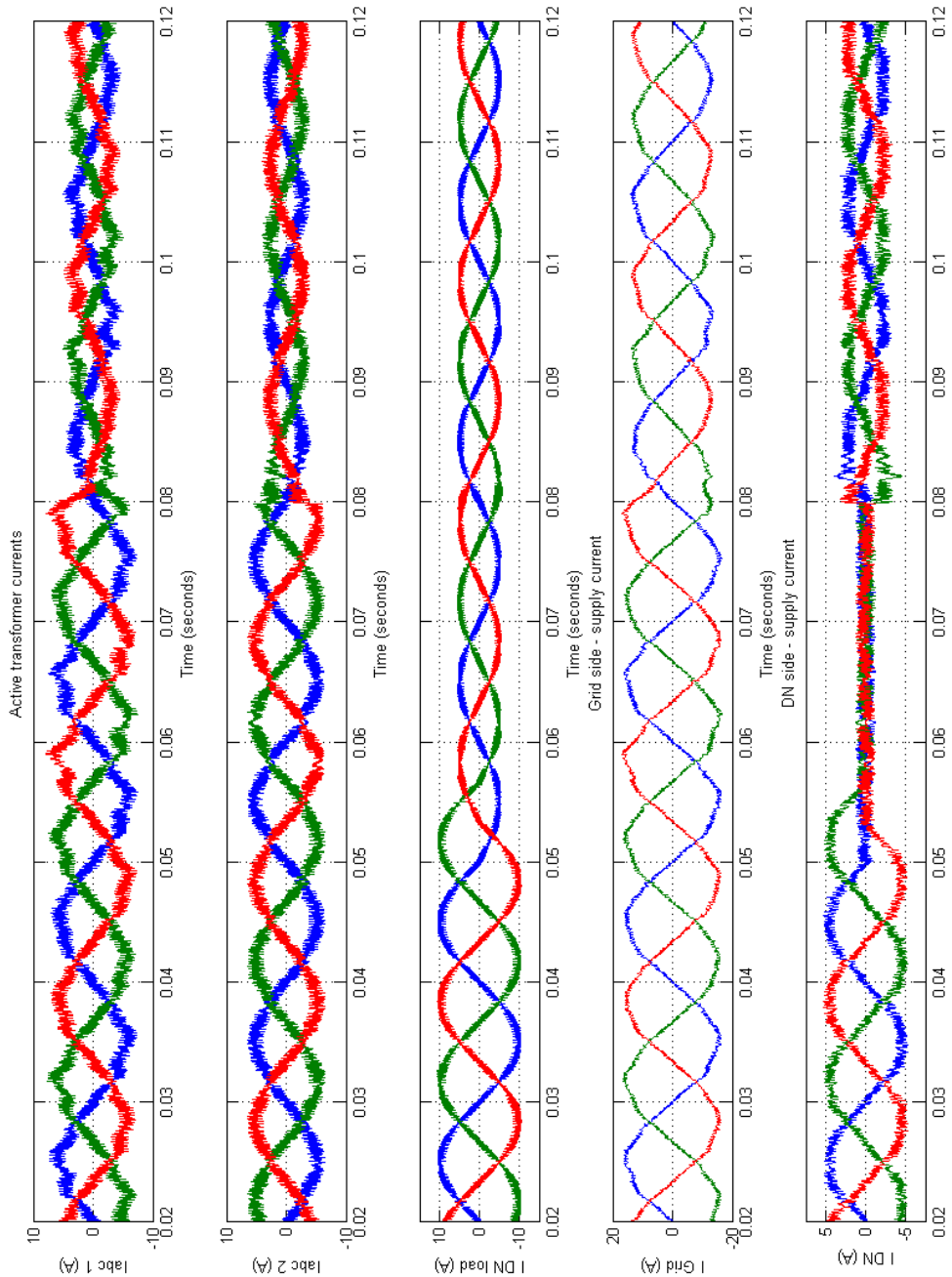

Figure 64 Active transformer: 100-50% load and 5-2.5 A demand changes

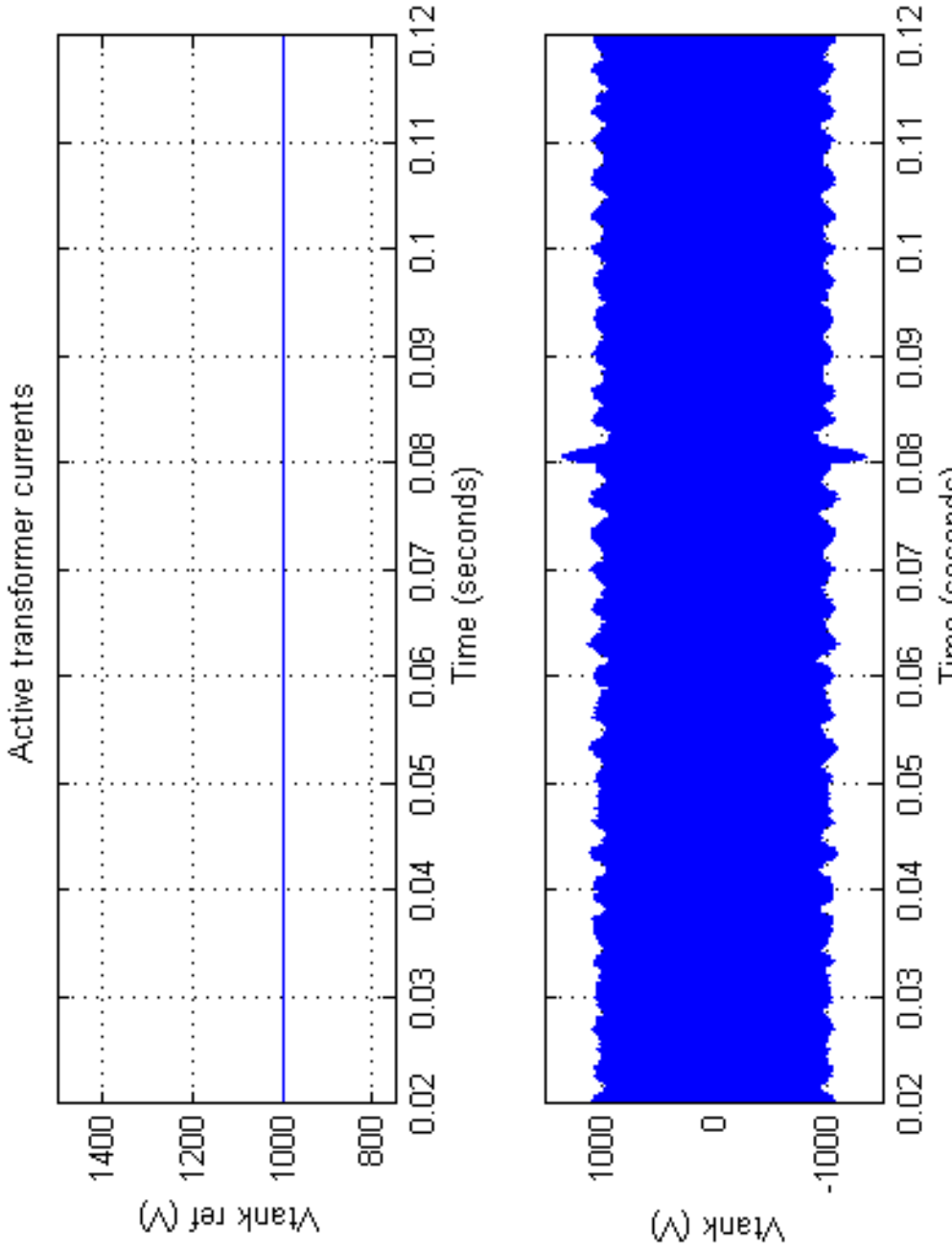

Figure 65 Active transformer tank voltage - 100-50% load and 5-2.5 A demand change

8.5.3 Test 2 results

The results of a large load increase from 5 to 20 kW are shown in Figure 66. The grid converter is in forward mode, recognisable from the distortion in I_{abc} *1* trace. The effects of the load change are seen in the trace I_{DN} load. Up to 50 ms, the Distribution Network load is supplied by 5 A mean-peak from the Active Transformer and 5 A mean-peak from the Distribution side generator. At 50 ms, the load increases suddenly, but the Active Transformer and Grid, I_{abc} *1*, I_{abc} *2* and *I Grid* respectively, currents remain unchanged.

This is not a practical test but serves to demonstrate that the models are well behaved for sudden large changes in demand.

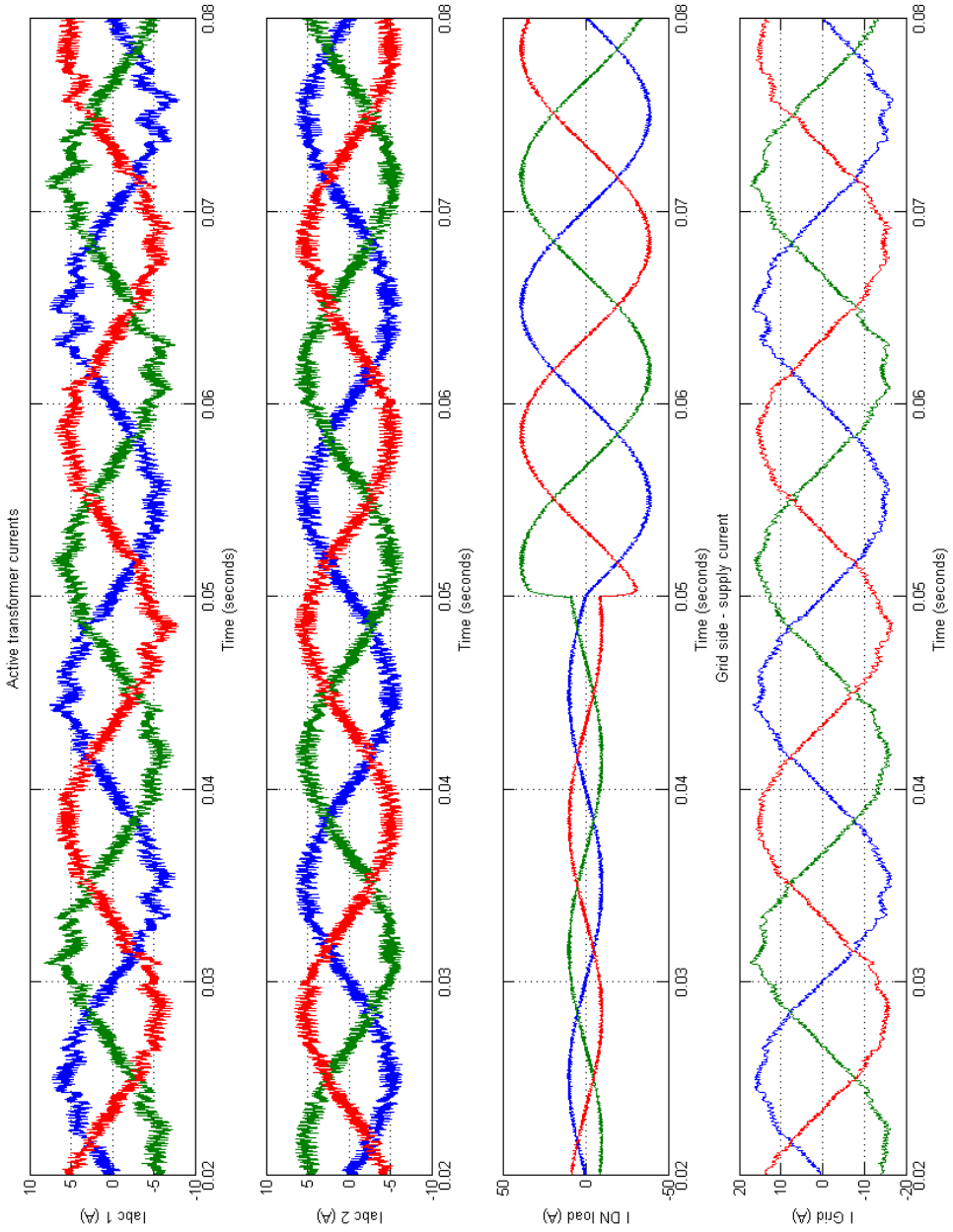

Figure 66 Active transformer: 5-20 kW load change @ 40 ms

8.5.4 Test 3 results

The results of the forward to reverse mode change are shown in Figure 67. The traces are arranged in columns for the Grid and Distribution converters. As with previous results the first 20 ms are suppressed for clarity.

During the period 20 -50 ms the Grid converter is operating in an "forward mode" mode and the characteristic distorted current is seen in I_{abc} *1*. The Grid and Distribution loads are constant at 10 A throughout the simulation. The Grid supplies 15 A mean-peak, 10 A mean-peak to the Grid load and 5 A mean-peak to the grid converter. The DN converter provides current, I_{abc} *2*, 5 A mean-peak, into the Distribution Network load and the distribution generator also provides 5 A mean-peak into the load.

At 60 ms the mode is changed to reverse so that current is now exported from the Grid converter where previously it had been imported. The current remains in phase with the Grid supply voltage but as its measurement is also reversed it appears as sudden change to an anti-phase signal in trace I_{abc} *1*. Note also that now the Grid converter is operating in reverse, its current is undistorted and that the Grid current is reduced from 15 A mean-peak to 5 A mean-peak to maintain balanced conditions at the grid load.

At the mode change, the DN converter current, I_{abc} *2*, changes from forward to reverse mode, and a reversal of phase is evident. The DN generator now has to supply both the DN load and the DN converter so its current increases from 5 A mean-peak to 15 A mean-peak to maintain balanced load conditions.

The mode change used in this simulation was a sudden event, which in practise, may lead to high transient voltages that are clearly unwanted. The solution to this is to profile the mode command first to produce a gradual reduction in the current reference to a zero demand over several cycles, i.e. no power flow through the Active Transformer, and then implement the mode change. The current reference would then be ramped up to the desired level over several cycles.

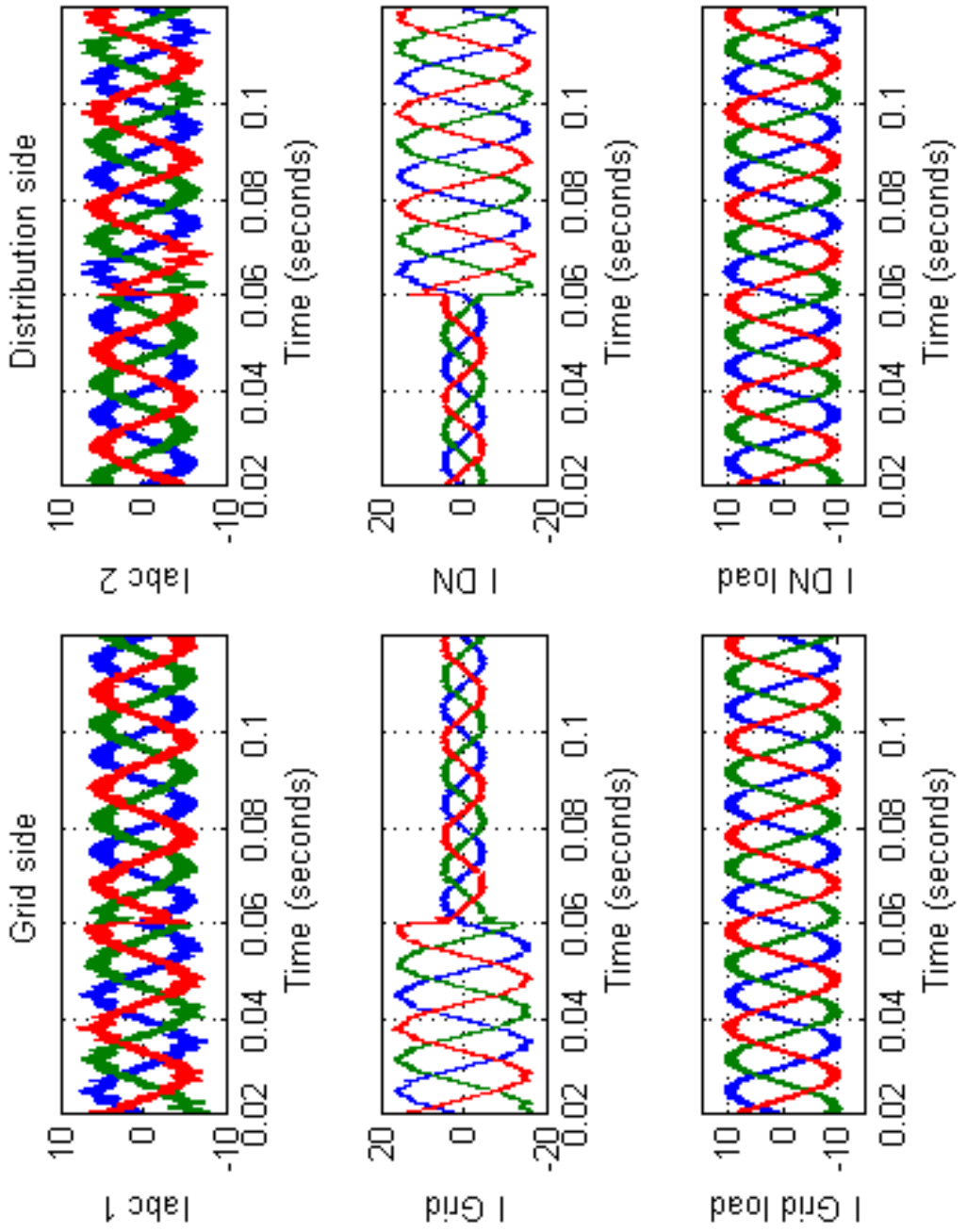

Figure 67 Active Transformer: forward - reverse mode change

8.5.5 Test 4 results

The results of the forward to reverse mode change are shown in Figure 68. The traces are arranged in columns for the Grid and Distribution converters. As with previous results the first 20 ms are suppressed for clarity.

These results are similar to those above except that the Grid and DN converter roles are reversed. The distorted converter currents again indicate the period of "import" operation.

8.5.6 Test 5 Results

(1) Grid supply phase change

Figure 69 shows the results of changing the Grid converter I_q reference when it was operating in forward mode. The amplitude of the DN converter current, $I_{d,}$ was set to 5 A peak, which was equivalent to 2.5 kW real power supplied by the Grid. The first 10 ms of the traces is suppressed to hide the simulation start-up from zero initial conditions. The fourth trace shows the reactive power supplied by the Grid and at 0.3 ms I_q was changed from 0 to +5 A, which was equivalent to a demand of +2.5 kW reactive power supplied by the Grid. After a further 20 ms I_q was changed back to 0 A and at 70 ms I_q was changed from 0 to -5 A, -2.5 kW reactive power. The two conditions, ±5 A, represent the Active Transformer absorbing and exporting reactive power respectively. The third trace shows the real power from the Grid, which remains unaltered throughout the simulation verifying the independence of real and reactive power control. Trace 1 shows the Grid supply phase A voltage V_a and trace 2 shows the Grid supply phase A current I_a.

During the initial 20 ms when I_q is zero, the voltage and currents, trace 1 and 2 respectively, are in phase. The sudden changes in I_q demand are clearly seen as step changes of phase in trace 2. The exact phase change was difficult to measure due to the converter 20 kHz switching action causing several zero crossings. However, it was reasonably clear that each phase shift was approximately 2.5 ms or 45° as was expected from the demands set.

(2) DN converter phase change

Figure 70 shows the results of simulating the changing of the I_q reference of the DN converter in forward mode. The DN converter current amplitude, I_d, is set to -5 A peak, which is equivalent to 2.5 kW real power supplied to the Distribution Network by the converter. Note that the $I_{a\ DN}$ and DN converter real and reactive power traces are inverted due to the method of measurement in the model as previously mentioned. The first 10 ms of the traces is again suppressed to hide the simulation start-up from zero initial conditions. Grid real and reactive mean power remains consistent throughout the simulation at 2.5 and 0 kW respectively. The trace of DN converter reactive power shows the power supplied to the Distribution Network and at 0.3 ms I_q changes from 0 to +5 A, which is equivalent to a demand for +2.5 kW reactive power. After a further 20 ms I_q is changed back to 0 A and at 70 ms I_q is changed from 0 to -5 A, -2.5 kW reactive power. These two conditions represent the Active Transformer exporting and absorbing reactive power respectively. Throughout these changes DN converter mean real power remains constant at 2.5 kW.

During the initial 20 ms when I_q is zero, the voltage and currents are in phase. The sudden changes in I_q demand are clearly seen by the step change of phase in trace 2. The exact phase change was difficult to measure due to the converter 20 kHz switching action causing several zero crossings. However, it was reasonably clear that each phase shift was approximately 2.5 ms or 45°.

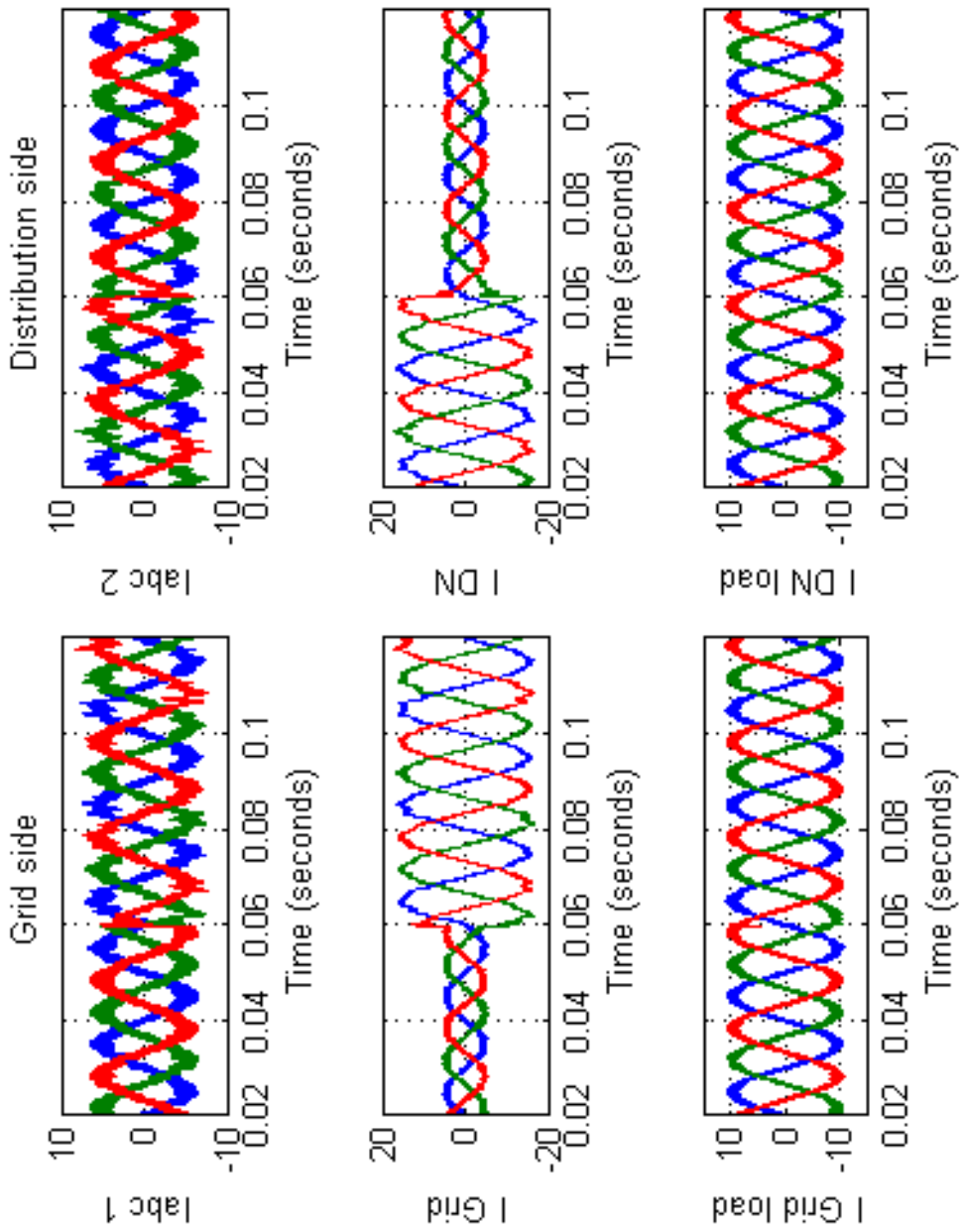

Figure 68 Active Transformer: step change reverse – forward

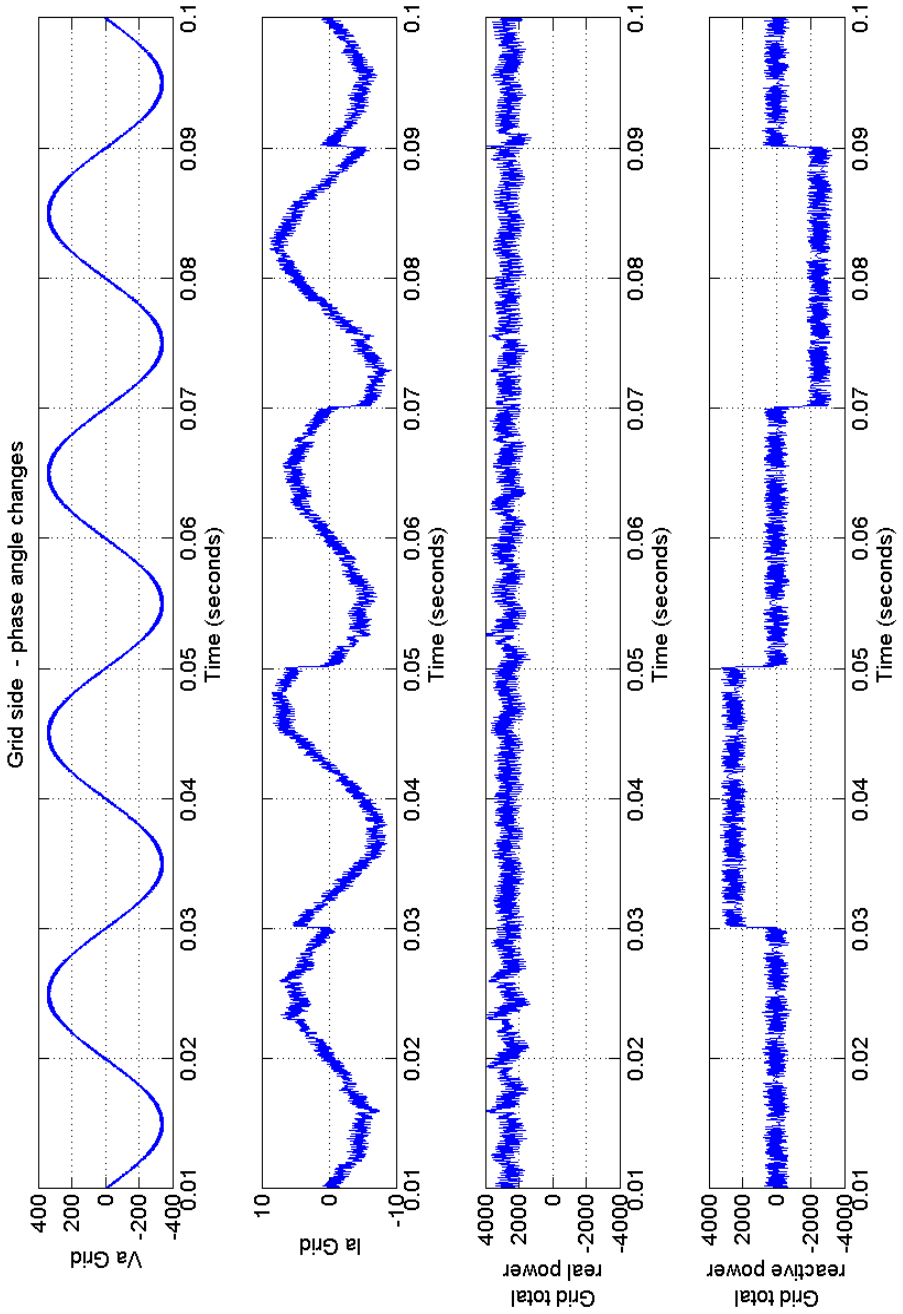

Figure 69 Grid converter phase angle changes

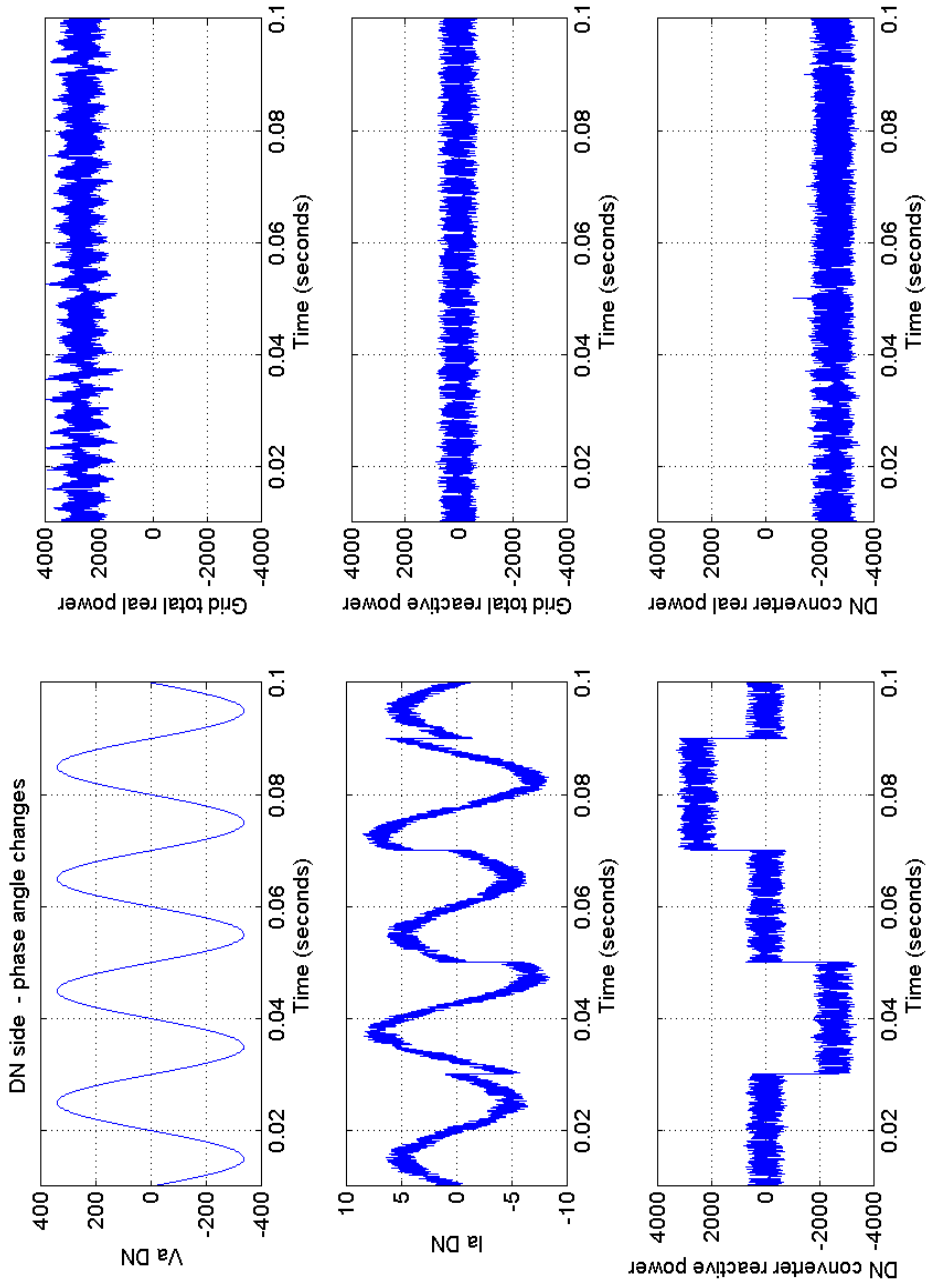

Figure 70 DN converter phase changes

8.6. Summary

Two copies of the converter model were used to create the Grid and Distribution converter models that were first used individually to simulate power flow in the forward and reverse modes of operation. Only the $\mathscr{H}_\infty$ controller designed for the 10% load point was used for work in reported in this chapter. The current waveforms from the initial simulations were much as expected, except for the converter currents I_{abc} *1* in reverse mode and I_{abc} *2* in forward mode. Here the level of ripple current appeared to be greater than that shown I_{abc} *1* in forward mode and I_{abc} *2* in reverse mode. On a closer examination of the waveforms ripple currents in both conditions were similar, varying between 2.7 to 2.9 A, and were similar to the predicted level of 2.8 A in Chapter 6.2.3.

The Grid and Distribution side models were then connected back-to-back arrangement to create the Active Transformer model. For power flow control in the forward direction, the Grid converter controlled the source line currents, the phase angle between the supply line voltage and current, and the a.c. link voltage. The Distribution converter controlled the level of the output current (and hence the power) fed to the distribution network.

Five test simulations were successfully run and demonstrated:

i) 50% load throwing from full load and a 50% reduction in current demand
ii) a sudden load increase to 20 kW
iii) a reversal from forward mode operation
iv) a reversal from reverse mode operation
v) phase angle changes.

The simulations proved successful and importantly demonstrated that there was a power balance between the power supplied by the Grid and that delivered to the DN load. The change of phase simulation successfully demonstrated the independence of controls using the dq0-transform and a means by which the phase angle of the current supplied by the Grid and that of the current supplied to the DN could be varied from net inductive to net capacitive.

The current drawn from the supply by which ever converter was operating in the forward mode contained some distortion that was not present in the individual converter simulations. The cause is likely to be the loading effects of an active load (the DN converter), which are often more like a capacitive load than the purely resistive load of previous studies.

The a.c. link voltage had developed an amplitude ripple of approximately 200 V peak-peak at 300 Hz that had not previously been seen in converter simulations. In the case of the resistance loaded converter model, this ripple would have indicated that the necessary voltage condition had been violated and that the current controller was not operating effectively. The remedy in the case of the converter would be to increase the tank voltage reference, but in the case of the Active Transformer, this change proved ineffective, indicating the presence of a more complex loading problem. The a.c. link voltage ripple did not affect the overall operation of the Active Transformer, the performance of which indicated a good degree of robustness of the control system in dealing with variable link voltage.

Chapter 9.

Conclusions and future work

The historical review of the UK power network provided an overview of the network development and the processes of change that have led to the network that we have today. What became clear very quickly was that the change process was continual, led by technical innovation and development but invariably, particularly in the early years, electrical equipment lagged consumer demand for more electrical power. This historical scenario may be likened to today's demand for more "greener" power and the search for technical solutions.

The first significant architectural change came with the introduction of The Electricity (Supply) Act 1926, which established the Central Electricity Generating Board (CEB) and co-ordinated the integration of the many disparate power systems. It standardised the supply frequency across the whole country and interconnected existing regional systems into a national "Grid" by building a high voltage transmission network. This was the birth of today's network architecture. The network became known as the "National Grid" because of its grid-iron type structure running North-South and East-West and connecting nine areas. The grid like structure or architecture was not initially designed as a long distance transmission system but as an economic means of standardisation and the interconnection of the different regions. The end of the Second World War provided an opportunity for major architectural change that has resulted in today's passive, but highly reliably and robust, network. In the 1950s increasing demand for power led to the construction of a new high voltage "Supergrid" operating at 275 kV and to a bulk-power transfer architecture.

Today's "demand for more electricity" is not so much for more power, but for more "power from renewable energy sources". The growing demand for the use renewable energy is putting the power network under pressure to change again. Many of the potential sources of renewable energy, such as wind, are often intermittent and situated at remote, weak points of the power network and require network support or more cabling to be of most benefit. The initial response from the electricity industry to the pressure for change is usually to seek the lowest cost solution. Hence, there is much interest in "active" networks as these are seen to have a lower cost than new cable or network support systems. What this means in practice, is that the rigid power architecture is unchanged, but a more sophisticated and extensive communications and control architecture overlaid on the existing network. This change is feasible, but only with the introduction of increased level of automation. It is more acceptable to the industry and customers alike than more overhead cables or the high cost of support measures. The conclusion was drawn that active networks will no doubt relieve some of the current pressures, at least for a few years, but, as the penetration levels of distributed generation increase over the next decades, so the pressure to change the rigid power architecture will increase once again and the time will eventually come when an architectural change is not only necessary but unavoidable.

The author concludes that there is a clear need for an architectural solution and has found some support regarding this view in Universities, if not yet in the power companies, in the work at the University of Manchester and ETH in Switzerland. Power electronics technology is used to solve many of today's network control problems but its applications are limited by its high cost. With a successful outcome of current power semiconductor device development, power electronics promises to be an enabling technology for future architectural change.

With this scenario in mind, Sood and Lipo's a.c. link distribution system, [69], and Dang's demonstration of a high-frequency, direct converter [45], when considered together create a novel solution that in this research has been called an "Active Transformer", whose application is intended to replace the large transformers in a power network. Generally, the literature in converter applications for high power systems mainly concentrates on d.c. link type converters that employ classical PI controllers. Contemporary d.c. link

converters require a large number of series devices to achieve high-voltage operation, whereas the direct converter will require less than half the number of devices used in an equivalent d.c. link design. In both cases, the use of silicon semiconductors makes the design uneconomic, except in very specific applications. Thus, it will be the economic demands that dictate the need for fewer devices operating at high voltages, probably greater than 20 kV. Such semiconductor technology, SiC and diamond technology, is in its infancy today and may take 10 or more years to reach the level of maturity, capability and reliability necessary for high power applications.

This thesis focuses on a more novel approach to high-voltage power conversion and studies the use of direct, resonant converters with a modern robust $\mathcal{H}_\infty$ controller. The author has concentrated his research on the control of these converters that are the major part of the Active Transformer concept. The first part of the work created a model of the converter and a basis controller to investigate in a vigorous way its performance and limitations and explore design options. This model was used throughout the work in subsequent chapters. During simulations of the converter operation with a basic PI controller a potential problem with stability and performance of the closed loop at light loads was identified.

A robust loop-shaping $\mathcal{H}_\infty$ controller design for the voltage control loop of a resonant converter has been proposed; in particular, this is based on classical control theory extensions of robustness. Classical loop-shaping procedures shape the magnitude of the open-loop transfer function and the designer aims to obtain a desired bandwidth, slope etc. The key mathematical analysis needed to understand the application of robust stabilisation is given in Chapter 7. The rigorous analysis of robustness issues and the use of uncertainty modelling to identify controller design limitations are an important contribution of this thesis. A rigorous and systematic design procedure of the linear control transfer functions affecting small signal stability can lead to good controller performance and robustness and take less design time. Robust stability and performance was demonstrated for specific variations of load, particular light loads where the decoupling effect resulting from the use of the dq0-transform eliminated interaction between tracking of supply current demand and control of the high-frequency converter output voltage.

Many converter controllers are designed at the full load operating point because at that point the converter is at its most efficient and likely to be operating close to that condition for much of its life. This is not the case with a grid connected converter where the expected load will be varying. The loop-shaping $\mathcal{H}_\infty$ controller design procedure offered an alternative approach, but one which retained the simplicity and physical understanding of classical methods. The procedure was based on what is known as 'coprime factorisation' method, which incorporates the solutions of appropriate control and filtering Riccati equations for the design of the controller and weighting functions.

The weighting function in $\mathcal{H}_\infty$ controllers contains all the controller dynamics and compensation features that determine the overall system performance. The operation and performance of the two converter controller designs were compared using transfer and function and non-linear models and were shown to have similar performance for changes in load around full load. For large changes from full to a light load of 10%, both controller designs produced unstable responses. In the author's experience this was not an unexpected result, particularly for the PI controller, where system gains can change a great deal with operating point. The result brought the design point at 100% load into question. From a control point of view, the general method for dealing with large system gain changes is to schedule changes in the controller gains to maintain stable operating conditions. Although, at first, this seems to be an attractive approach, it is a rigid solution to a very flexible problem, particularly when converter system gains are not well or completely defined. However, the use of the nominal model at full load, with issues of robustness at light loads, proved a burden for the design and in fact, produced some unstable closed loop responses during implementation at light loads. Therefore, a modified design procedure was needed and this was followed via a rigorous uncertainty bound.

The controller design point was changed to the lighter load scenario, 10% load, this being the operating point of minimum load. A reduction of the peak voltage, 82 to 64%, and a reduced settling time, >7 to 3 ms, was achieved for the 100 kΩ load simulation at the expense of over-damping at full load and greater. In the intended application this additional damping may be advantageous, particularly for overload and fault conditions.

The non-linear simulations of load and demand changes were repeated with the revised controller design, and confirmed stable operation at both full and 10% load.

A important contribution of this thesis is the use of an "uncertainty model" of the system to investigate performance differences at full and light loads. The frequency response of the relative errors of the uncertainty model, designed at 100% load, produced positive low frequency gain in the closed loop system and when combined with the integrator in the controller produced an unstable response. The investigation also indicated that the design point where an integrator would not be effective in the control loop, thus avoiding stability problems. This was at a much larger load (50%) than had predicted by an earlier simple stability analysis.

The choice of a PI filter characteristic for the weighting function of the $\mathcal{H}_\infty$ controller appeared logical, but in fact was rather arbitrary and therefore an attempt was made to validate its use by comparison with an "inverse multiplicative" scenario. The PI gains from the original controller design used as the $\mathcal{H}_\infty$ weighting function produced the appropriate frequency response but with a low bandwidth of 3.4 krads/s. Increasing the PI gains by 10 produced a response closer to that suggested by the approach and a bandwidth of 8.3 krads/s, but this produced unstable responses when used in the non-linear converter model and showed the effects of system RHP zeros.

From the results of the uncertainty modelling it was concluded that the design procedure from [52] was not helpful in choosing the $\mathcal{H}_\infty$ controller weights for this class of converter. A modified approach, based on the PI gains from a classical controller design at 10% load, proved to be more successful and produced a stable system design for this class of converter. Further refinement may be possible for specific converter designs by examining a family of systems with differing design points.

A key contribution of this thesis is the concept of an Active Transformer that provides a means of isolating the Grid network from sudden demands that may be balanced at a local level and the control of real and reactive power flows. Control is instantly available and at a distribution network level where, for example, current, and hence power, drawn from the

Grid during periods of high local demand may be kept constant while local demands are reduced, or available local generation (from wind or stored energy) is dispatched to supply an increased load demand or a change of network voltage is accepted. Early control action at a local level should be much more effective than later action taken by a central generator controller to stabilize the network frequency, minimise the effects of faults and meeting performance targets.

An Active Transformer model was built from two converter models connected between a representation of the Grid and Distribution networks. Individual converter operation was first simulated for forward and reverse power flow modes to verify designed operation and control. A series of simulations were run using the Active Transformer model that demonstrated current control and a power balance between the Grid and Distribution networks during load and mode changes.

The simulations proved successful and importantly, demonstrated that there was a power balance between the power supplied by the Grid and that delivered to the DN load. In a fully designed system there will be losses in the converters and transformer, but these were not represented or needed in simulations to demonstrate the functionality of the Active Transformer. Of particular concern will be the currents circulating in the resonant circuits, which, dependent upon the "Q" of the circuit will be of the order of ten times the supply current. Local conductor resistances and stray reactances will need to be made very small by good design and layout of components. The high frequency transformer is a novel device because of the combination of high-voltage, high-power at a high frequency. Its design will be a complex key task and critical to the reliability of the Active Transformer. Stray circuit and component reactances appear in parallel with the converter resonant circuit and will contribute to its designed operating frequency; careful choice of components and layout will be essential.

The change of phase simulation successfully demonstrated the independence of controls using the dq0-transform and a means by which the phase angle of the current supplied by the Grid and that of the current supplied to the DN could be varied from net inductive to net capacitive. This is an important attribute of the Active Transformer and will give

Distribution Network operators a much needed degree of freedom for voltage control that could make the unreliable mechanical tap changers of conventional power transformers redundant.

The Active Transformer a.c. link voltage had an amplitude ripple of approximately 200 V peak-peak at 300 Hz that had not previously been seen in converter simulations and was probably the result of the complex loading effects of back-back converters. The remedy in the case of a single resistance loaded converter would be to increase the tank voltage reference, but in the case of the Active Transformer, this change proved ineffective. The a.c. link voltage ripple did not appear to affect the overall operation of the Active Transformer.

A balance between generated and load power is critical to achieving robust and reliable power network operation. The indicator of this balance is the network frequency. Maintaining a power balance, and hence a stable frequency between very tight limits, is the role of a central control facility where generation is scheduled and dispatched to balance a forecast load. Insufficient generation or an excess of load leads to a low network frequency, whereas an excess of generation or too little load leads to high network frequencies. The UK power network is essentially an "island network" and the maintenance of the system frequency is an obsession in avoiding system collapse, which may be caused very rapidly by an unexpected loss of generation or increase in load. Central controllers have to act very quickly in these circumstances to bring reserve generation on line, but this will take anything from several minutes to several hours to become effective depending on the state of their readiness. The alternative of load shedding is avoided whenever possible and only used in extreme circumstances to avoid total system collapse. A fast and readily available means of balancing network power and load, such as the Active Transformer, will be required to fully integrate high levels of renewable energy generation in the power networks of the future.

Modelling and simulation of the Active Transformer used resistive loads only but the simulated change of phase angle successfully demonstrated the independence of the

control of real and reactive power flow at the input and out of the Active Transformer. The results give initial confidence in the designs but further work is suggested as follows:

i) the models need to be tested against a power network load with varying demands, outages and faults. MATLAB/Simulink is probably not the best tool to undertake these studies and therefore new models will need to be developed in an alternative simulation tool, such as IPSA.

ii) It will be useful to assess the robust controller performance on a laboratory demonstration of the Active Transformer design at 5 kW and an investigation of the tank voltage loading effects in the Active Transformer.

iii) from a control point of view, it would be interesting to follow a structured singular value approach (μ-synthesis) control design, [52]. This includes worst case uncertainty design but unfortunately at the expense of rather high order controllers. In such cases, it is usually unwise to implement these controllers in their original form, and thus a controller reduction approach will be necessary.

Chapter 10.

Bibliography and References

[1] T. Ackermann, G. Andersson b, L. Söder, "Distributed generation: a definition", Elsevier Science, Electric Power Systems Research 57 (2001) 195–204.

[2] A. Collinson, et al., “Solutions for the connection and operation of distributed generation,” K/EL/00303/00/01/REP, DTI New and Renewable Energy Programme, May 2003.

[3] F. Duffy, J. Scott, “Technical Architecture – a framework for tomorrow’s network”, DGCG Paper DGCG01/04.

[4] G. Anderson et al., “Causes of the 2003 major grid blackouts in North America and Europe, and recommended means to improve system dynamic performance”, IEE Transactions on Power Ssytems, vol 20 no. 4, pp 1922 – 1928, November 2005.

[5] V. Akhmatov, H. Knusdsen, “Large penetration of wind and dispersed generation into Danish power grid”, Science direct, Electric Power Research 77 (2007) 1228 – 1238.

[6] K. Zhou, J. C. J. Doyle, K. Glover, “Robust and Optimal Control,” Prentice-Hall Inc., NJ 1996.

[7] Chaudhuri, B. C. Pal, A. C. Zolotas, I. M. Jaimoukha, T. Green, “Mixed-Sensitivity Approach to H-infinity Control of Power System Oscillations Employing Multiple FACTS Devices,” I.E.E.E Transactions on Power Systems, Vol. 18, No. 3, pp. 1149-1156, August, 2003.

[8] Official Journal of the European Union, Council Decision 2002/358/CE of 25 April 2002, OJ L130/1 15/05/2002.

[9] Official Journal of the European Union, Directive 2001/77/EC of the European Parliament and the Council of 27 September 2001, “on the promotion of electricity produced from renewable energy sources in the internal electricity market”, OJ L283/33 27/10/2001.

[10] EU Commission, "R&D needed for Distributed Generation", Europa website, http://europa.eu.int/comm/research/energy/nn/nn_rt/nn_rt_dg/article_1160_en.htm

[11] DTI Energy White Paper: "Our energy future – creating a low carbon economy," published by The Stationery Office, www.tso.co.uk/bookshop, ISBN 0-10-157612-9, Presented to Parliament by the Secretary of State for Trade and Industry by Command of Her Majesty, February 2003.

[12] A. Cooke, P. Baker, "Embedded Generation Co-ordinating Group – Terms of reference," Paper EGCG 1/01.

[13] J. C. Smith, "Winds of change", I.E.E.E Power and Energy, volume 3 number 6 November/December 2005, pp20-25.

[14] D. Botting, "Technical Architecture - A first report", I.E.E., DGCG 3/05, issue 1.4, 04 June 2005.

[15] L. Hannah, "Electricity before Nationalisation",published by The Macmillan Press Ltd., 1979.

[16] Major P. Cardew, "The treatment, regulation, and control of electric supply by the Legislature and the board of Trade," Journal of the IEE, 1890 Volume 19 No: 88 pp425-447.

[17] S. Z. De Ferranti, "Disccussion on the relative advantages of alternating and continuous current for a general supply of electricity, especially with regard to interference with other interests," Journal of the IEE 1900, Vol. 30 No. 147 pp3-26.

[18] E. Eunson, J. Martin, "Public Electricity supply in the United Kingdom the first 120 Years: 1880 - 2000," A contribution to "A History of Electricity," a joint project of AHEF and CIGRE, 2000.

[19] Sir Henry Self, "Electricity Supply in Great Britain", National Board Series, published by George Allen and Unwin Ltd., 1952.

[20] P Good, "Electrical Standardisation, 1926," Journal of the IEE 1927, Vol. 65 No. pp137-142.

[21] National Grid Company, "The Grid Code", issue 3, revision 3, 29 November 2004, http://www.nationalgrid.com/uk/.

[22] Distribution Code Review Panel, "The Distribution Code and the Guide to the Distribution Code of licensed distribution network operators of Great Britain", Issue 8 - November 2006.

[23] P. Kundur, "Power System Stability and Control," 1994 McGraw-Hill, ISBN 0-07-035958-X.

[24] CIGRE, "Development of dispersed generation and consequences for power systems", Electra No. 215-3 August 2004, pages 39-49.

[25] CIGRE, "Changing network conditions and system requirements", TB 335, Working Group A3.13, December 2007.

[26] G. Quinonez-Varela, Keith Bell, Graeme Burt, "Automation to optimise network configuration in real time – to optimise DG contribution and reduce losses", Department for Business, Eneterprise & Regulatory Reform, Contract number: Final Report DG/CG/00096/REP, URN number: 07/1653.

[27] P.Bousseau et al, "Contribution of wind farms to ancillary services", CIGRE Session 2006, paper C6-103, August 2006.

[28] G Strbac, "Electric power systems research on dispersed generation", Science Direct, Electric Power Systems Research 77 (2007) 1143 – 1147.

[29] C. P. Steinmetz, "Power control and stability of electric generating stations", 36th Annual Convention of the American Institute of Electrical Engineers, 1 July 1920.

[30] J. M. Tesseron, S. Corsi, P.H. Ashmole, "Discussion of voltage control schemes by CEGB, ENEL and EDF, CEGB/EDF/ENEL Collaboration on Power System Planning and Operation, paper 2b I.E.E. Colloquium 21 March 1988.

[31] CIGRE, "Distribution systems and dispersed generation", Electra 213-8, April 2004, pp. 17-21.

[32] J. McDonald, "Adaptive intelligent power systems: active distribution networks", Foresight Report, http://www.foresight.gov.uk/Energy/Reports/…, Adaptive intelligent power systems:active distribution networks, version 1.0., downloaded on 26 January 2008.

[33] P. Cartwright, L. Xu, C. Sasse, "Grid integration of large offshore wind farms using hybrid HVDC transmission", Nordic Wind Power conference, 1-2 March 2004, Chalmers University of Technology, Göteborg, Sweden.

[34] N. M. Kirby, L. Xu, M. Lucket, W. Siepmann, "HVDC transmission for large offshore wind farms," I.E.E. Power Engineering Journal, June 2002.

[35] L. Xu, P. Cartwright, "Fault ride through of DFIG based wind turbines", unpublished.

[36] G. Strbac, et al, "Impact of wind generation on the operation and development of the UK electricity systems", Electric Power Systems Research, Volume 77, Issue 9, July 2007, Pages 1214-1227

[37] J.A. Peças Lopes, N Hatzairgyriou, J Mutale, P. Djapic, N Jenkins, "Integrating distributed generation into electric power system: A review of drivers, challenges and opportunities", Science Direct, Electric Power Systems Research, Volume 77, Issue 9, July 2007, Pages 1189-1203.

[38] G. Strbac, S. Grenard, D. Pudjianto, “Why should the distribution systems change?”, I.E.E. Power Systems & Equipment – The Active Network, a Discussion Session at UMIST, 29 June 2004.

[39] M Geidl, “Integrated Modeling and Optimisation of Multi-Carrier Energy Systems”, The Swiss Federal Institute of Technology (ETH) Doctoral Thesis, 2007.

[40] D. A. Roberts, "Network Management Systems for Activie Distribution Networks - A Feasibility Study", DTI, Report No. K/EL/00310/REP, URN 04/1361, 2004.

[41] Kidd, W., McWhirter, E.M. S., “Operational control of electricity supply systems,” and “Discussion before the Transmission Section, 14 March 1945”, The Journal of I.E.E., 1945 Vol. 92 Part 2, pp311-326.

[42] Crary, S.B., “Power System Stability,” Volume 1 – Steady State Stability, John Wily & Sons Inc., copy right 1945, third printing October 1955.

[43] G. Strbac, N. Jenkins, M. Hird, P. Djapic, G Nicholson, "Integration of operation of embedded generation and distribution networks", UMIST, K/EL/00262/REP, May 2002.

[44] CIGRE, "Increased system efficiency by use of new generations of power semiconductors", Technical Brochure TB 337 December 2007, ISBN 978-2-85873-025-4.

[45] Huy Quoc Si Dang, "A new implementation of high frequency, high voltage direct power converter", submitted to the University of Nottingham for the degree of Doctor of Philosophy, February 2006.

[46] P.R. Palmer, A. N. Githiari, "The Series Connection of IGBT’s with Active Voltage Sharing", IEEE Transactions on Power Electronics, VOL. 12, NO. 4, JULY 1997.

[47] L. Zhang, C. Watthanasan, W. Shepherd, "Analysis and comparison of control techniques for ac-ac matrix converters", IEE Proceedings - Electric Power Applications, Volume 145 No.4, July 1998, pp 284-294.

[48] D. G. Holmes, T. A. Lipo, "Pulse Width Modulation for power converters - principles and practice," ISBN 0-471020814-0, I.E.E.E. series on Power Engineering, John Wiley & Sons, Inc.

[49] Z Yu, "Space-Vector PWM With TMS320C24x/F24x Using Hardware and Software Determined Switching Patterns," Texas Instruments Application Report SPRA524, Digital Signal Processing solutions, March 1999.

[50] A. Klönne, F.W. Fuchs, "Multivariable PI control with feedforward control for a current source converter", Proceedings the IEEE Nordic Workshop on Power and Industrial Electronics, NORpie 2000, June 2000.

[51] A. Klönne, F.W. Fuchs, "Optimal State feedback control of a vector controlled current source rectifier", Conference proceedings of EPE 2001, Topic 4a, Graz, 2001.

[52] S. Skogestad, I Postlethwaite, "Multivariable Feedback Control Analysis and Design," Second Edition, ISBN 978-0-470-01168-3.

[53] M. Aten, H. Werner, "Robust multivariable control design for HVDC back to back schemes", IEE Proceedings of Generation, Transmission and Distribution, Vol 150 No.6 November 2003.

[54] D. C. M. Oates, "Electrical substation", United States Patent, Pub. No. US 2002/0176265 A1, 28 November 2002.

[55] D. C. M. Oates, "Converters", United States Patent, Pub. No. US 2003/0095424 A1, 22 May 2003.

[56] E Aldabas, J. L. Romeral, A. Arias, D. Bedford, "A new vector control hysteresis-band current controller for three phase loads," European Power Electronics Conference, Lausanne 1999.

[57] R.C. Dorf, R.H. Bishop, "Modern Control Systems," Tenth Edition, ISBN 0-13—145733-0.

[58] P. T.Krein, "Elements of Power Electronics", Oxford University Press, 1998, ISBN 0-19-511701-8.

[59] V.I. Utkin, "Variable Structure Systems with Sliding Modes", *IEEE TAC*, Vol. AC-22, No. 2, pp. 212-222, 1977.

[60] W. Perruquetti, J-P Bardot, "Sliding Mode Control in Engineering", ISBN 0-8247-0671-4, Published by Marcel Dekker Inc., 2002.

[61] E. Fossas, J.M. Olm, A. Zinober, "Sliding motion and direct control of the output voltage in a full bridge boost converter", 44th IEEE Conference on Decision and Control, 2005 and 2005 European Control Conference. CDC-ECC '05, 12-15 Dec. 2005 Page(s): 4760 – 4765.

[62] A.C. Zolotas, B. Chaudhuri, I.M. Jaimoukha, P. Korba, "A study of LQG/LTR control for damping inter-area oscillations in power systems", IEEE Transactionson control systems technology, Vol. 15, No. 1, January 2007.

[63] Q.-C.,Zhong et al, "Hinf control of the neutral point in four-wire three-phase d.c.-a.c.converters", IEEE Transactions on Industrial Electronics, vol. 53 no. 4, October 2006.

[64] W. Sulkowski, P.-O Nyman, D Samuelson. "PMSM robust drive with H∞ current controller", European Power Electronics conference, Lausanne, 1999.

[65] A.C. Zoloatas, "Advanced Control Strategies for Tiliting Trains", A Doctoral Thesis submitted to Loughborough University, September 2002.

[66] D. McFarlane, K. Glover, "Robust controller design using normalised coprime factor plant descriptions", vol 138 of Lecture notes in Control and Information Sciences, Springer-Verlag, Berlin, 1990.

[67] K. Glover, D. McFarlane, "Robust stabilisation of normalised coprime factor plant descriptions with H_∞-bounded uncertainty", IEEE Transactions on Automatic Control, vol 34 no. 8, August 1989.

[68] J.B. Hoagg, D.S. Bernstein, "Non-minimum phase zeros", IEEE Control Magazine, June 2007.

[69] P. K. Sood, T.A. Lipo, "Power Conversion Distribution System Using a High Frequency AC Link," IEEE-IAS Conference Record, 1986, vol. 1, pp. 533-541.

[70] N. N. Hancock, "Matrix analysis of electrical machinery", Pergamon Press, ISBN 0-08-017898-7, 1974.

[71] F. Milano, "An Open Source Power System Analysis Toolbox", accepted for publication in the I.E.E.E Transactions on Power Systems, March 2005.

[72] M. Castilla, et al, "Sliding-Mode Control of Quantum Series-Parallel Resonant Converters via Input-Output Linearisation", IEEE Transactions on Industrial Electronics, Vol. 52, No. 2, April 2005.

Appendix A.

The d-q transform

A.1. Derivation

Designers of contemporary control systems, particularly of rotating machines driven by power electronic converters, often use a system of artificial variables rather, than the more traditional phase variables, as a means of analysis and control. These artificial variables are derived in analysis from the phase variables by means of a transformation known as the "d-q transform". This methodology may also be applied to the design of three-phase power converter systems. When using the transform, many books and papers dealing with vector control quote only the transform, often with a different system of reference vectors, and do not fully explain the scaling used, describing it as arbitrary, or show how the transform is derived. This tends to leave some gaps in the readers' understanding that may cause some confusion over scaling. This appendix therefore gives a full derivation of the transform and aims to clarify the use of scaling factors.

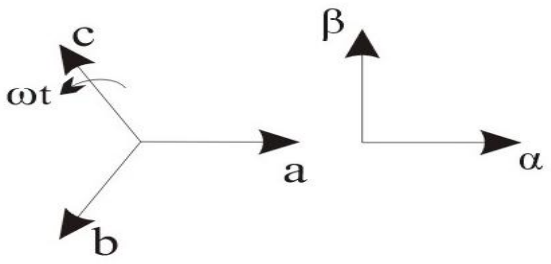

Figure 71 Three-phase and two-phase system phasor diagrams

The analysis is in two stages:

i) transformation from a stationary, three-phase axis to equivalent two-phase stationary axes system

ii) transformation from a two phase stationary axes to a two phase rotating axes system.

For the purpose of this analysis it is assumed that a balanced three-phase supply system can be replaced by an equivalent two-phase system, [70] page 100-102, and that the three-phase currents sum to zero.

The analysis first transforms the three-phase to a two-phase, *abc* to α-β, stationary axis system, phasor diagram Figure 71. This shows a conventional anticlockwise rotation of the phase voltages and where the phases rotate to give a voltage or current sequence of a-b-c.

For an arbitrary, balanced three-phase current source let the phase currents be:

$$\begin{aligned} i_a &= \hat{I}\cos\omega t \\ i_b &= \hat{I}\cos(\omega t - 2\pi/3) \\ i_c &= \hat{I}\cos(\omega t - 4\pi/3) \end{aligned} \qquad (69)$$

Where $\hat{I}$ is the peak value of the phase current and ωt is is the angular frequency of the supply. For the purposes of analysis, these phase currents are assumed to be independent variables. Choosing to let the axis of the a-phase and α-phase be coincident as shown in Figure 71 is an arbitrary, but usual, choice because of the relationship between the a-phase and the α-phase currents and voltages that result under balanced conditions. Resolving the three-phase currents along α and β axes:

$$\begin{aligned} i_\alpha &= N(i_a + i_b\cos(-2\pi/3) + i_c\cos(2\pi/3)) \\ i_\beta &= N(0 + i_b\sin(-2\pi/3) + i_c\sin(2\pi/3)) \end{aligned} \qquad (70)$$

Where *N* is an arbitrary constant. In the analysis of synchronous machines *N* represents the ratio of the effective number of turns of the 3-phase winding and the number of turns of the 2-phase winding and is taken as ⅔ [30].

From a mathematical consideration, a third independent variable is needed. In most three-phase systems the instantaneous currents and voltages sum to zero and this practical consideration defines a third variable, i_0, which, for independence, must be orthogonal to i_α and i_β and is only physically realisable if i_0 is zero as in the balanced three-phase system. Therefore:

$$(71) \quad i_0 = N(ki_a + ki_b + ki_c)$$

where k is an arbitrary constant, giving, in matrix form:

$$(72) \quad \begin{bmatrix} i_\alpha \\ i_\beta \\ i_0 \end{bmatrix} = N \begin{bmatrix} 1 & -1/2 & -1/2 \\ 0 & -\sqrt{3}/2 & \sqrt{3}/2 \\ k & k & k \end{bmatrix} \begin{bmatrix} i_a \\ i_b \\ i_c \end{bmatrix}$$

which may be written as:

$$(73) \quad i_{\alpha\beta} = C^{-1} i_{abc}$$

For invariance of power, [1] page 97, requires:

$$C^{-1} = C^T$$

therefore:

$$(74) \quad (C^{-1})^{-1} = C = \frac{1}{N} * \frac{2}{3} \begin{bmatrix} 1 & 0 & 1/2k \\ -1/2 & -\sqrt{3}/2 & 1/2k \\ -1/2 & \sqrt{3}/2 & 1/2k \end{bmatrix}$$

noting that the scaling factor 2/3 is derived from the inversion of C^{-1}, and therefore:

$$(75) \quad C^T = \frac{1}{N} * \frac{2}{3} \begin{bmatrix} 1 & -1/2 & -1/2 \\ 0 & -\sqrt{3}/2 & \sqrt{3}/2 \\ 1/2k & 1/2k & 1/2k \end{bmatrix}$$

comparing C^T and C^{-1}, then:

$$(76) \quad N = \frac{1}{N} * \frac{2}{3} \ \ and \ \ k = \frac{1}{2k}$$

therefore:

(77) $N = \sqrt{\frac{2}{3}}$

(78) $k = \frac{1}{\sqrt{2}}$

giving:

(79) $$\begin{bmatrix} i_\alpha \\ i_\beta \\ i_0 \end{bmatrix} = \sqrt{\frac{2}{3}} \begin{bmatrix} 1 & -1/2 & -1/2 \\ 0 & -\sqrt{3}/2 & \sqrt{3}/2 \\ \frac{1}{\sqrt{2}} & \frac{1}{\sqrt{2}} & \frac{1}{\sqrt{2}} \end{bmatrix} \begin{bmatrix} i_a \\ i_b \\ i_c \end{bmatrix}$$

or expressed in trigonometric functions:

(80) $$\begin{bmatrix} i_\alpha \\ i_\beta \\ i_0 \end{bmatrix} = \sqrt{\frac{2}{3}} \begin{bmatrix} \cos 0 & \cos(-2\pi/3) & \cos(2\pi/3) \\ \sin 0 & \sin(-2\pi/3) & \sin(2\pi/3) \\ \frac{1}{\sqrt{2}} & \frac{1}{\sqrt{2}} & \frac{1}{\sqrt{2}} \end{bmatrix} \begin{bmatrix} i_a \\ i_b \\ i_c \end{bmatrix}$$

In this analysis the effect of the arbitrary constant N is to increase i_α and i_β by $\sqrt{3/2}$ and hence the total power by 3/2, but because the number of phases is reduced from 3 to 2, the total power remains unchanged. Some authors prefer a direct comparison between the α and a-phases, some omit the factor $\sqrt{3/2}$ and this leads to $i_\alpha = i_a$ but of course, not to the invariance of power. While this may be convenient, this analysis proceeds assuming the invariance of power.

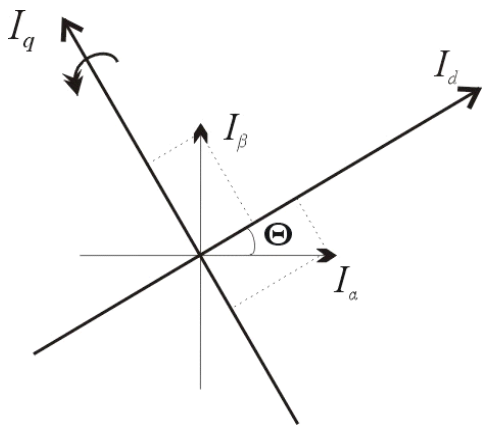

Figure 72 Transforming stationary to rotating axes

The second stage transforms a stationary axes to a rotating axes system ($i_{\alpha\beta0}$- i_{dq0}). The relationship between the axes is shown in Figure 72.

$$i_d = \cos\theta i_\alpha + \sin\theta i_\beta$$

$$i_q = -\sin\theta i_\alpha + \cos\theta i_\beta$$

In matrix form, where $\theta = \omega t$, and extending the matrix to include the orthogonal zero-sequence currents that are not transformed:

$$\begin{bmatrix} i_d \\ i_q \\ i_0 \end{bmatrix} = \begin{bmatrix} \cos\theta & \sin\theta & 0 \\ -\sin\theta & +\cos\theta & 0 \\ 0 & 0 & 1 \end{bmatrix} \begin{bmatrix} i_\alpha \\ i_\beta \\ i_0 \end{bmatrix}$$

therefore:

$$\begin{bmatrix} i_d \\ i_q \\ i_0 \end{bmatrix} = \sqrt{\frac{2}{3}} \begin{bmatrix} \cos\theta & \sin\theta & 0 \\ -\sin\theta & +\cos\theta & 0 \\ 0 & 0 & 1 \end{bmatrix} \begin{bmatrix} \cos 0 & \cos(-2\pi/3) & \cos(2\pi/3) \\ \sin 0 & \sin(-2\pi/3) & \sin(2\pi/3) \\ \frac{1}{\sqrt{2}} & \frac{1}{\sqrt{2}} & \frac{1}{\sqrt{2}} \end{bmatrix} \begin{bmatrix} i_a \\ i_b \\ i_c \end{bmatrix}$$

$$\begin{bmatrix} i_d \\ i_q \\ i_0 \end{bmatrix} = \sqrt{\frac{2}{3}} \begin{bmatrix} \cos\theta & \cos(\theta)Cos(-2\pi/3) + \sin(\theta)\sin(-2\pi/3) & \cos(\theta)Cos(2\pi/3) + \sin(\theta)\sin(2\pi/3) \\ -\sin(\theta) & -\sin(\theta)Cos(-2\pi/3) + Cos(\theta)\sin(-2\pi/3) & -\sin(\theta)Cos(2\pi/3) + Cos(\theta)\sin(2\pi/3) \\ \frac{1}{\sqrt{2}} & \frac{1}{\sqrt{2}} & \frac{1}{\sqrt{2}} \end{bmatrix} \begin{bmatrix} i_a \\ i_b \\ i_0 \end{bmatrix}$$

using trigonometric identities:

$$\cos(A+B) = \cos(A)Cos(B) - \sin(A)\sin(B)$$
$$\cos(A-B) = \cos(A)Cos(B) + \sin(A)\sin(B)$$
$$\sin(A+B) = \sin(A)\cos(B) + \cos(A)\sin(B)$$
$$\sin(A-B) = \sin(A)\cos(B) - \cos(A)\sin(B)$$

$$\begin{bmatrix} i_d \\ i_q \\ i_0 \end{bmatrix} = \sqrt{\frac{2}{3}} \begin{bmatrix} \cos\theta & \cos(\theta+2\pi/3) & \cos(\theta-2\pi/3) \\ \sin(\theta) & \sin(\theta+2\pi/3) & \sin(\theta-2\pi/3) \\ \frac{1}{\sqrt{2}} & \frac{1}{\sqrt{2}} & \frac{1}{\sqrt{2}} \end{bmatrix} \begin{bmatrix} i_a \\ i_b \\ i_0 \end{bmatrix}$$

or $I_{dq0} = TI_{\alpha\beta0}$

where $\theta=\omega t$ is the angular frequency. T is known as "d-q Transform" that maintains the invariance of power.

Appendix B.

Power system modelling

B.1. General

Because of their size and power requirements it is impractical to produce physical models of power networks except under very specific conditions and restrictions. Therefore, it has always been an engineering task to model power networks and systems and over the years many commercial and bespoke methodologies and techniques have been developed, largely aimed at specific problems or scenarios such as load flow, short circuit, electromagnetic transient and stability analysis. Tools used include. PSS/E, PSCAD, and EMTP. Load flow studies tend to be the most significant studies of power system analysis and design. Load flow studies are necessary for planning, operation and network scheduling, but are usually undertaken prior to short circuit and stability studies.

Models for conventional power system components, such as generators and their control systems are well understood. However, the trend towards open competitive electricity markets and infrastructure developments, resulting from the introduction of distributed generation and from the constraints of higher power transfers, demands different, more powerful modelling and simulation tools to support research, development, design and operations. The potential connection of hundreds of 2-5 MW wind turbines, interconnected by a significant medium voltage system, potentially to a weak point in a distribution system, is a significant problem and necessitates a formal analytic assessment of their impact on the network. These turbines exhibit static and dynamic characteristics completely different to those of large steam turbines and as a result do not fit the outline of models of conventional generation.

The size of a network cell model containing a wind farm is likely to be very large and therefore some simplification is necessary. From previous experience, the dynamic

characteristics of a new architecture will be of key importance and a single generator model of a large wind farm will not represent the full dynamic behaviour of the "network cell" for all types of disturbance. Experience of modelling individual wind generators is growing steadily but experience of wind farm or aggregate models is quite limited and not intuitive. When considering the modelling needs for a potentially new network architecture containing an active transformer and a large wind farm, the prime modelling requirement was identified as being the ability to model and control the dynamics of a large complex systems, at a power electronic converter level and at network level. For analytic studies of these power networks the time frames of interest will range from micro-seconds to seconds for steady state. Therefore, power system electrical apparatus models must accurately reflect behaviour over the whole bandwidth. The models need not contain all the characteristics, e.g. those of the mechanical system, but include only those that effect the performance of the electrical system. The tools required should be able to model and simulate power system dynamics, nonlinear systems, power electronics, and have a comprehensive range of control system design facilities.

The conventional methodology of power system modelling cannot guarantee the quality or accuracy of models except where they have been verified for specific conditions on a power network. The process of power system modelling, like that of any other industrial system, consists of physical analysis, mathematical deduction and model construction and scenario testing. Based on a great deal of industry or operational experience, the existing knowledge of many engineering disciplines, a trial and error method is commonly used to develop power system models.

For the purposes of this research project, the aim is to examine the feasibility of a new architecture based around an active transformer and therefore sophisticated models of all the components are not yet required, however, they will be needed for later design stages. This somewhat simplifies the choice of modelling tools to those that are used for control system design.

B.2. Computational tools

B.2.1. MATLAB/Simulink

Simulink is a platform for multi-domain simulation and Model-Based Design for dynamic systems. It provides an interactive graphical environment and a customisable set of block libraries, and can be extended for specialised applications. SimPowerSystems extends Simulink with tools for modelling and simulating basic electrical circuits and detailed electrical power systems. These tools facilitate the modelling of the generation, transmission, distribution, and consumption of electrical power. SimPowerSystems is well suited to the development of complex, self-contained power systems.

Together, SimPowerSystems and Simulink provide an efficient environment for multi-domain modelling and controller design. By connecting the electrical parts of the simulation to other Simulink blocks, circuit topology can be rapidly drawn and simultaneously analyze the circuit's interactions with mechanical, thermal, and control systems.

The latest version of MATLAB/SIMULINK is a powerful simulation tool and the "Simpowersystems" library contains models of the basic elements of the proposed resonant converters and they have been used to build a model of the "active transformer". The block libraries and simulation methods in SimPowerSystems were developed by TransÉnergie Technologies Inc. of Montreal, which tends to give some confidence in the models and their application.

B.2.2. PSAT

PSAT [71] is MATLAB-based and aimed at power flow, optimal power flow, continuation power flow and electromechanical transient problems. Comparing PSAT and Simulink/Simpowersystems, the two software packages realistically have different goals and use different mathematical models. SimPowerSystems has a longer history and has been written by many people and should be generally more reliable than PSAT.

The Simulink environment and its graphical features are used in PSAT only to create a CAD tool able to design power networks, visualise the topology and change the data stored in it, without the need of directly dealing with lists of data. Simulink has been conceived for a control environment with diagrams, outputs and inputs variables. Milano believes that this is not the best way to approach a power system network and, therefore, the time domain routines that come with Simulink and its ability to build control block diagrams are not used. PSAT simply reads the data from the Simulink model and writes down a PSAT data file.

B.3. Modelling simplifications

Power system and network modelling involves many simplifications that aid understanding of basic effects and concepts. Simplified systems help to develop an appreciation of the physical aspects of control and help engineers gain experience with using different analysis techniques and therefore they are able to understand larger and more complex systems.

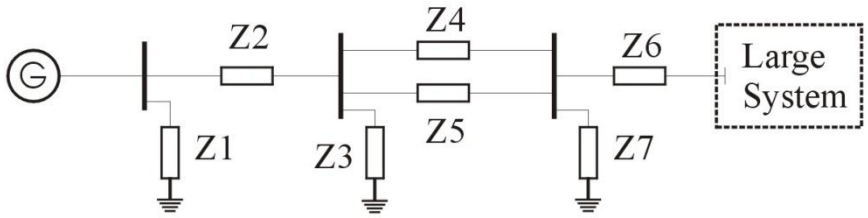

Figure 73 Network diagram

For example, an often used simplification in power system analysis is the infinite bus. Consider the network shown in Figure 73 . For analysis purposes it may be reduced to that shown in Figure 74 by application of Thévenin's theorem. The generator dynamics will cause negligible change to the voltage and frequency, E_b, of the network because of the

relative size of the network compared to the generator that is supply power. Such a voltage source is referred to as “an infinite bus”.

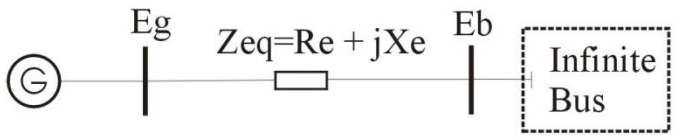

Figure 74 Equivalent system

Appendix C.

MATLAB m-files

C.1. tf_evaluation_dang.m

```
%   Last update:    22 February 2007
%   M file to evaluate closed loop transfer function of Dang's converter.
%   Set system constants
%
clear all;close all;
Vs=415                  %   Vsupply L-L r.m.s.
Ls=3.75e-3              %   Line inductance
Power=5000              %   Design peak power
Vd=Vs*(2^0.5)/(3^0.5)   %
Id=Power/(3*Vd/2)       %   Line current
RL=100                  %    Load resistance
Req=8*RL/pi^2           %   Equivalent load resistance
Q=10                    %
C=7.5e-7                %   Tank capacitance
Ceq=pi^2*C/4
Rs=0                    %   Input resistance
Vtav=636.6              %   Average output voltage
%
%   Calculate system transfer function from [45]
a=-9251.7
p=13333.52
K0=-46.79
G=tf(K0*[1 a],[1 p])
%
%
%
%   Controller PI gains
%
Ki=100
Kp=0.002
%
%   Calculate controller transfer function
%
Gc=tf(Kp*[1 Ki/Kp],[1 0])
Gol=series(Gc,G)
%
%calculate system closed loop transfer function
%
T = feedback(Gol,1)
Tzpk=zpk(T)
%
%   Calculate RLl at marginal stability
```

```
%
p1=-(K0*Ki+K0*Kp*a)
p2=(p+p1)/(1+K0*Kp)
Req1=2/(p1*Ceq)
RL1=Req1*(pi^2)/8
%
%   Sensitivity transfer function
%
S=tf([p 0],[(1+K0*Kp) (p+(K0*Ki)+(K0*Kp*a)) (a*K0*Ki)])
bode(S,T)
%
%   Filter for Robust design
%   T-ideal=Wn^2/(S^2+1.4Wns+Wn^2)
%
zeta=0.7                %   Damping ratio
Ts=100e-6               %   Settling time within 2%
Wn=4/(zeta*Ts)          %   rads/sec
Eq1=1.4*Wn
Eq2=Wn^2
%
%   Comparing T with T-ideal
%   and equating coefficients of s
%   (Eq1-p)=(Ko)Ki + (-Eq1K0+aK0)Kp
%   and contstant
%   Eq2=(aK0)Ki-(Eq2K0)Kp
%   and expressing in matrix form as Ax=B gives:
%
A=[K0 (-(Eq1*K0)+(a*K0));(a*K0) -(Eq2*K0)]
B=[(Eq1-p);Eq2]
%
%   Solving simultaneously
%
x=A\B
Kir=x(1,1)
Kpr=x(2,1)
%
%   Checking by substituting back
%
ck1=(p+(K0*Kir)+(a*K0*Kpr))/(1+(K0*Kpr))
ck2=a*K0*Kir/(1+(K0*Kpr))
%
%   Calculate ITAE compensator transfer function Gi
%
Gci=tf(Kpr*[1 Kir/Kpr],[1 0])
%
%   calculate ITAE system closed loop transfer function Ti
%
Goli=series(Gci,G)
Ti = feedback(Goli,1)
Tiz=zpk(Ti)
[z p k]=zpkdata(Ti,'v')
Gpi=zpk([],[z(1,1) z(2,1)],(Wn^2/k))
%
%   Check transfer function of new system
%   and plot bode diagram in sisotool
%
```

```
ck3=series(Gpi,Ti)
%bode(ck3)
sisotool(G,Gci,1,Gpi)
```

C.2. MATLAB m-code to generate the $\mathcal{H}_\infty$ loop shaping controller

```
AppC_2
%%   Reference MCF Table 9.2 page 367: Matlab function to generate the
Hinf controller in (9.70).
%
gamrel=1.1;
S=eye(size(d'*d))+d'*d;
R=eye(size(d*d'))+d*d';
Rinv=inv(R);Sinv=inv(S);
A1=a-b*Sinv*d'*c;
R1=S;
B1=b;
Qc1=c'*Rinv*c;
[X,XAMP,G]=care(A1,B1,Qc1,R1);
A2=A1';
Qc2=b*Sinv*b';
B2=c';
R2=R;
[Z,ZAMP,G]=care(A2,B2,Qc2,R2);
    %   Optimal gamma
XZ=X*Z;
gammin=sqrt(1+max(eig(XZ)));
    %   Use higher gammin
gam=gamrel*gammin;
gam2=gam*gam;
gamconst=(1-gam2)*eye(size(XZ));
Lc=gamconst+XZ;
Li=inv(Lc');
Fc=-Sinv*(d'*c+b'*X);
Ac=a+b*Fc+gam2*Li*Z*c'*(c+d*Fc);
Bc=gam2*Li*Z*c';
Cc=b'*X;
Dc=-d';
```

Appendix D.

Copies of published papers

i) W.G. Garlick, A.C. Zolotas, "Modelling of a direct converter with H_∞ voltage control," submitted to ICSE 2009 conference, Coventry, 8-10 September 2009.

ii) W. G. Garlick, A. C. Zolotas, D. Grieve, R. M. Goodall, "*The Architecture and Control of Large Power Systems with Distributed Generation*", CIGRE 2008 Session, Paris, 24 – 29 August 2008.

iii) W. G. Garlick, A. C. Zolotas, D Infield, *"A novel architecture for power networks with distributed generation - concept outline"*, UKACC, Control 2006, paper 223, September 2006.